

**MOLECULAR REGULATION OF MATERNAL HEPATIC  
ADAPTATIONS TO PREGNANCY**

by

**Joonyong Lee**

**A Dissertation**

*Submitted to the Faculty of Purdue University*

*In Partial Fulfillment of the Requirements for the degree of*

**Doctor of Philosophy**



Department of Biology at IUPUI

Indianapolis, Indiana

December 2019

**THE PURDUE UNIVERSITY GRADUATE SCHOOL  
STATEMENT OF COMMITTEE APPROVAL**

**Dr. Guoli Dai, Chair**

Department of Biology

**Dr. James Marrs**

Department of Biology

**Dr. Nicolas Berbari**

Department of Biology

**Dr. Jingmei Lin**

Department of Pathology and Laboratory Medicine

**Approved by:**

Dr. Theodore Cummins

## **ACKNOWLEDGMENTS**

I would like to thank Dr. Guoli Dai for his invaluable guidance and mentorship through the completion of my thesis. I would also like to thank my committee members, Dr. James Marrs, Dr. Nicolas Berbari, and Dr. Jingmei Lin, for their advice and knowledge. Furthermore, I would like to extend my thanks to the current and formal laboratory members, Dr. Yuhong Zou, Shashank Nambiar, Dr. Huaizhou Jiang, and especially to Veronica Garcia. Lastly, I wish to thank my parents for their support.

# TABLE OF CONTENTS

|   |    |
|---|----|
| LIST OF TABLES .....  | 7  |
| LIST OF FIGURES .....   | 8  |
| ABBREVIATIONS .....   | 15 |
| ABSTRACT.....   | 17 |
| CHAPTER 1. INTRODUCTION .....                                     | 19 |
| 1.1 Liver.....  | 20 |
| 1.1.1 Development.....  | 20 |
| 1.1.2 Function.....   | 21 |
| 1.1.3 Maternal liver during pregnancy .....                       | 23 |
| 1.1.4 Maternal liver diseases during pregnancy .....              | 23 |
| 1.2 Pregnancy.....  | 24 |
| 1.2.1 Maternal metabolic changes .....                            | 24 |
| 1.2.2 Maternal physiologic changes .....                          | 25 |
| 1.2.2.1 Heart, lung, and blood.....                               | 25 |
| 1.2.2.2 Gastrointestinal tract and gut microbiome .....           | 26 |
| 1.2.2.3 Pancreas .....  | 28 |
| 1.2.2.4 Spleen.....   | 29 |
| 1.2.2.5 Kidney.....   | 29 |
| 1.3 Mammalian achaete-scute homology ( <i>Mash</i> ) family ..... | 30 |
| 1.3.1 <i>Ascl1</i> .....  | 30 |
| 1.3.2 <i>Ascl2</i> .....  | 32 |
| 1.3.3 <i>Ascl3</i> .....  | 34 |
| 1.4 Hypothesis.....   | 35 |
| CHAPTER 2. METHODS .....  | 36 |
| 2.1 Mice .....  | 36 |
| 2.2 Genomic PCR .....   | 37 |
| 2.3 Pregnancy model.....  | 38 |
| 2.4 Tissue collection and histology.....                          | 40 |
| 2.5 Immunohistochemistry .....                                    | 41 |

|                          |  |    |
|--------------------------|--|----|
| 2.6                      | Hepatocyte density .....   | 42 |
| 2.7                      | Oil Red O staining .....   | 42 |
| 2.8                      | Periodic Acid Schiff staining .....  | 42 |
| 2.9                      | $\beta$ -Cell mass .....   | 43 |
| 2.10                     | <i>In situ</i> hybridization.....  | 43 |
| 2.11                     | Western blotting .....   | 43 |
| 2.12                     | Intraperitoneal glucose tolerance tests and insulin measurements .....   | 44 |
| 2.13                     | Quantitative real-time polymerase chain reaction (qRT-PCR) .....   | 45 |
| 2.14                     | RNA sequencing.....  | 46 |
| 2.15                     | Serum biochemistry.....  | 48 |
| 2.16                     | Microbiome 16S sequencing .....  | 48 |
| 2.17                     | Statistics.....  | 49 |
| CHAPTER 3. RESULTS ..... |  | 51 |
| 3.1                      | Maternal liver activates hepatic <i>Ascl1</i> during pregnancy .....   | 51 |
| 3.2                      | Global deletion of <i>Ascl1</i> .....  | 52 |
| 3.2.1                    | Generation of global inducible <i>Ascl1</i> knockout mouse model .....   | 52 |
| 3.2.2                    | Global deletion of <i>Ascl1</i> causes maternal liver abnormalities.....                                       | 53 |
| 3.2.3                    | Global deletion of <i>Ascl1</i> causes alterations in sera.....  | 55 |
| 3.3                      | Cell-specific deletion of <i>Ascl1</i> .....   | 63 |
| 3.3.1                    | Generation of cell-specific inducible <i>Ascl1</i> knockout mouse model.....                                   | 63 |
| 3.3.2                    | Deletion of <i>Ascl1</i> in <i>Ascl1</i> -expressing cells causes maternal liver abnormalities .....           | 67 |
| 3.3.3                    | Deletion of <i>Ascl1</i> in <i>Ascl1</i> -expressing cells causes alterations in maternal hepatic gene profile | 67 |
| 3.4                      | Hepatocyte-specific deletion of <i>Ascl1</i> .....   | 70 |
| 3.4.1                    | Generation of hepatocyte-specific inducible <i>Ascl1</i> knockout mouse model.....                             | 70 |
| 3.4.2                    | Hepatocyte-specific <i>Ascl1</i> knockout results in maternal liver abnormalities .....                        | 73 |
| 3.4.3                    | Hepatocyte-specific <i>Ascl1</i> knockout causes alterations in maternal hepatic gene profile                  | 78 |
| 3.4.4                    | Hepatocyte-specific <i>Ascl1</i> knockout changes hepatocyte identity .....                                    | 79 |
| 3.4.5                    | Hepatocyte-specific <i>Ascl1</i> knockout results in activation of <i>Igf2</i> .....                           | 80 |
| 3.4.6                    | Hepatocyte-Specific <i>Ascl1</i> knockout results in dysregulation of hepatic genes.....                       | 86 |

|                            |   |     |
|----------------------------|---|-----|
| 3.4.7                      | Hepatocyte-specific <i>Ascl1</i> knockout causes alterations in sera.....                               | 87  |
| 3.4.8                      | Hepatocyte-specific <i>Ascl1</i> knockout causes hepatic fat accumulation.....                          | 95  |
| 3.4.9                      | Hepatocyte-Specific <i>Ascl1</i> knockout results in maternal pancreas abnormalities.....               | 96  |
| 3.4.10                     | Hepatocyte-Specific <i>Ascl1</i> knockout results in abnormalities in maternal compartments.....        | 102 |
| 3.4.11                     | Hepatocyte-specific <i>Ascl1</i> knockout results in placental abnormalities .....                      | 103 |
| 3.4.12                     | Hepatocyte-specific <i>Ascl1</i> knockout results in fetal growth abnormalities .....                   | 111 |
| 3.4.13                     | Hepatocyte-Specific <i>Ascl1</i> knockout results in changes in subpopulations of cecal microbiota..... | 111 |
| CHAPTER 4. DISCUSSION..... |   | 117 |
| 4.1                        | Introduction.....   | 117 |
| 4.2                        | Mouse model.....  | 117 |
| 4.3                        | Maternal liver and other organ growth .....   | 119 |
| 4.4                        | Maternal hepatocyte identity.....   | 121 |
| 4.5                        | Fatty liver .....   | 122 |
| 4.6                        | Pancreatic function test.....   | 126 |
| 4.7                        | <i>Ascl1</i> -associated canonical pathway.....   | 127 |
| 4.8                        | Microbiota dysfunction.....   | 127 |
| 4.9                        | Pregnancy outcomes .....  | 128 |
| 4.10                       | Summary of the findings .....   | 130 |
| 4.11                       | Future directions of the study.....   | 131 |
| CHAPTER 5. REFERENCES..... |   | 133 |

## LIST OF TABLES

|   |           |
|---|-----------|
| <b>Table 1. List of Genomic PCR Primers .....</b>   | <b>40</b> |
| <b>Table 2. List of Antibodies for Immunohistochemistry .....</b>                           | <b>42</b> |
| <b>Table 3. List of Antibodies for Western Blotting .....</b>                               | <b>45</b> |
| <b>Table 4. List of TaqMan qRT-PCR Primers.....</b>   | <b>46</b> |
| <b>Table 5 List of SYBR Green qRT-PCR Primers .....</b>                                     | <b>47</b> |
| <b>Table 6 List of Serum Biochemical Profiles in Global <i>Ascl1</i> Gene Knockout.....</b> | <b>64</b> |
| <b>Table 7 Lists of Gene Networks and Functions.....</b>                                    | <b>73</b> |

## LIST OF FIGURES

**Figure 1. Genotyping Gel Image.** DNA was extracted from ear snips and polymerase chain reaction (PCR) was performed with specific primers (**Table 1**) to determine the presence of (A) floxed *Ascl1* allele, (B) *rtTA* allele, (C) *Cre* transgene downstream of *tetO* promoter, (D) *EYFP* allele, and (E) *Cre* allele downstream of *Ascl1* promoter. *Ascl1*, achaete-scute homolog 1; *Cre*, Cre recombinase; *EYFP*, enhanced yellow fluorescent protein; *R26*, *Rosa26* promoter element; *rtTA*, reverse tetracycline-controlled transactivator; *tetO*, tetracycline-responsive promoter element. .... 39

**Figure 2. Activation of maternal hepatic *Ascl1*.** (A) *Ascl1* mRNA expression in the maternal liver. The presence of a copulation plug was designated as gestation day 1. Total RNA was isolated from livers of nonpregnant (NP) and pregnant (gestation days 8, 10, 11, 13, 15, and 18) C57BL6/J mice. Hepatic *Ascl1* mRNA levels were measured using quantitative real-time polymerase chain reaction (qRT-PCR) and expressed as the mean fold changes relative to NP controls ( $\pm$  s.d.;  $n = 3$  for each group). \*\*,  $P < 0.01$ ; \*\*\*,  $P < 0.001$ , compared with NP controls.  $\beta$ -Actin mRNA levels were used as endogenous controls. (B) *Ascl1* mRNA distribution in the maternal liver. Liver sections of NP and gestation day 15 C57BL6/J mice subjected to *Ascl1* *in situ* hybridization using RNAscope 2.5 HD Assay-BROWN kit. The *Ascl1* mRNA is stained dark brown. *Ascl1*, achaete-scute homolog 1. .... 52

**Figure 3. Doxycycline-induced global *Ascl1* knockout mouse model.** (A) The strategy of generating a global inducible *Ascl1* knockout mouse model. In the global inducible *Ascl1* knockout (*Ascl1*<sup>-/-</sup>) (*Ascl1*<sup>fl/fl</sup>; *R26*<sup>rtTA/rtTA</sup>; *tetO*<sup>Cre/-</sup>) mice, the *Rosa26* promoter element (*R26*) ubiquitously expresses the reverse tetracycline-controlled transactivator (*rtTA*). *rtTA* becomes activated by binding with doxycycline and turns on the tetracycline-responsive promoter element (*tetO*) to express *Cre* recombinase. *Cre* recombinase excises out the loxP-flanked *Ascl1*, resulting in the deletion of *Ascl1* in the whole body except in the brain and testis. In the control mice (*Ascl1*<sup>+/+</sup>) (*Ascl1*<sup>+/+</sup>; *R26*<sup>rtTA/rtTA</sup>; *tetO*<sup>Cre/-</sup>), the *Ascl1* lacks the loxP sites and, therefore, remains intact after doxycycline treatment. (B) Doxycycline treatment timeline. The presence of a copulation plug (plug +ve) was designated as gestation day (GD) 1. Doxycycline was administered in drinking water (1 mg/ml) for both *Ascl1*<sup>+/+</sup> and *Ascl1*<sup>-/-</sup> mice from GD6 until maternal samples were collected on GD9, 11, 13, 15, and 18. (C) *Ascl1* mRNA expression in the maternal liver. Total RNA was isolated from livers of nonpregnant (NP) and gestation day 15 *Ascl1*<sup>+/+</sup> and *Ascl1*<sup>-/-</sup> mice. Hepatic *Ascl1* mRNA levels were measured using quantitative real-time polymerase chain reaction (qRT-PCR) and expressed as the mean fold changes relative to NP controls ( $\pm$  s.d.;  $n = 3$  for each group). \*,  $P < 0.05$ , between *Ascl1*<sup>+/+</sup> and *Ascl1*<sup>-/-</sup> mice. *Albumin* mRNA levels were used as endogenous controls. *Ascl1*, achaete-scute homolog 1. .... 54

**Figure 4. Global *Ascl1* ablation phenotypes.** (A-E) Maternal liver changes. Maternal livers were collected and weighed from *Ascl1*<sup>+/+</sup> and *Ascl1*<sup>-/-</sup> mice (described in **Fig. 3**). (A) The maternal liver-to-body weight ratios of *Ascl1*<sup>+/+</sup> and *Ascl1*<sup>-/-</sup> mice are presented. Data are expressed as means  $\pm$  s.d. ( $n = 5-9$ ). \*\*,  $P < 0.01$ , between *Ascl1*<sup>+/+</sup> and *Ascl1*<sup>-/-</sup> mice. (B) Maternal liver histology. Maternal liver sections of *Ascl1*<sup>+/+</sup> and *Ascl1*<sup>-/-</sup> mice were subjected to hematoxylin and eosin (H&E) staining. (C-D) Maternal hepatocyte proliferation. (C) Nonpregnant and maternal liver sections were subjected to Ki67 staining. Ki67-positive cells are stained dark brown in the nucleus.

(D) Nuclear Ki67-positive hepatocytes were counted in five random fields of view (200X magnification) and the data are expressed as the means  $\pm$  s.d. (n = 3-5). \*\*,  $P < 0.01$ , between *Ascl1*<sup>+/+</sup> and *Ascl1*<sup>-/-</sup> mice. (E) Maternal liver lipid deposition. Gestation day 18 maternal liver sections of *Ascl1*<sup>+/+</sup> and *Ascl1*<sup>-/-</sup> mice were subjected to Oil Red O (ORO) staining. The lipid droplets are stained red. (F-G) Fetal outcome. Weight (F) and number (G) of pups born from *Ascl1*<sup>+/+</sup> and *Ascl1*<sup>-/-</sup> dams are presented. Data are expressed as means  $\pm$  s.d. (n = 5-9). *Ascl1*, achaete-scute homolog 1..... 56

**Figure 5. Maternal serum biochemical profile.** Maternal serum was collected from *Ascl1*<sup>+/+</sup> and *Ascl1*<sup>-/-</sup> mice (described in Fig. 3). Maternal serum biochemical profiles from *Ascl1*<sup>+/+</sup> and *Ascl1*<sup>-/-</sup> mice were analyzed by Eli Lilly and Company. Data are expressed as means  $\pm$  s.d. (n = 5). \*,  $P < 0.05$ ; \*\*,  $P < 0.01$ ; \*\*\*,  $P < 0.001$ , between *Ascl1*<sup>+/+</sup> and *Ascl1*<sup>-/-</sup> mice. *Ascl1*, achaete-scute homolog 1; BUN, blood urea nitrogen; Enz Creat, creatinine; ALP, alkaline phosphatase; ALT, alanine aminotransferase; AST, aspartate aminotransferase; CK, creatine kinase; Na, sodium; K, potassium; Cl, chloride; Ca, calcium; IP, inorganic phosphate; Glu, glucose; Chol, cholesterol; HDL Chol, high-density lipoprotein cholesterol; LDL Chol, low-density lipoprotein cholesterol; Trig, triglyceride; Phos Lipid, phospholipid; FFA, free fatty acid; Free Chol, free cholesterol; TP, total protein; Alb, albumin; A/G, albumin/globulin. .... 60

**Figure 6. Tamoxifen-induced cell-specific *Ascl1* knockout mouse model.** (A) The strategy in generating cell-specific inducible *Ascl1* knockout mouse model. In the cell-specific inducible *Ascl1* knockout (cell-*Ascl1*<sup>Cre/-</sup>) (*Ascl1*<sup>Cre/fl</sup>;R26<sup>EYFP/EYFP</sup>) (R26-LoxP-Stop-LoxP-EYFP) mice, the *Ascl1*-expressing cells express *CreERT2*, which is a Cre recombinase fused with a mutant estrogen ligand-binding domain (*ERT2*) that is activated only by tamoxifen, but not naturally occurring estrogen. With the administration of tamoxifen, *Cre-ERT2* fusion protein translocates into the nucleus and excises out the loxP-flanked *Ascl1* and the transcriptional Stop cassette upstream of enhanced yellow fluorescent protein (*EYFP*). As a result, the *Ascl1*-expressing cells delete *Ascl1* and express *EYFP*. In the control mice (cell-*Ascl1*<sup>Cre/+</sup>) (*Ascl1*<sup>Cre/+</sup>;R26<sup>EYFP/EYFP</sup>), *Ascl1* lacks the loxP sites and, therefore, remains intact after tamoxifen treatment while still being labeled with *EYFP*. (B) Tamoxifen treatment timeline. The presence of a copulation plug (plug +ve) was designated as gestation day (GD) 1. Tamoxifen was intraperitoneally injected (i.p., 60 mg/kg) on GD13 and GD14 and maternal samples were collected on GD15 and GD18. (C) *Ascl1* mRNA expression in the maternal liver. Total RNA was isolated from livers of nonpregnant (NP) and gestation day 15 cell-*Ascl1*<sup>Cre/+</sup> and cell-*Ascl1*<sup>Cre/-</sup> mice. Hepatic *Ascl1* mRNA levels were measured using quantitative real-time polymerase chain reaction (qRT-PCR) and expressed as the mean fold changes relative to NP controls ( $\pm$  s.d.; n = 4-5). \*,  $P < 0.05$ ; \*\*\*,  $P < 0.001$ , between cell-*Ascl1*<sup>Cre/+</sup> and cell-*Ascl1*<sup>Cre/-</sup> mice. *18S* ribosomal RNA (rRNA) levels were used as endogenous controls. *Ascl1*, achaete-scute homolog 1..... 65

**Figure 7. Cell-specific *Ascl1* ablation phenotypes.** (A-C) Maternal liver changes. Maternal livers were collected and weighed from cell-*Ascl1*<sup>Cre/+</sup> and cell-*Ascl1*<sup>Cre/-</sup> mice (described in Fig. 6). (A) The maternal liver-to-body weight ratios of cell-*Ascl1*<sup>Cre/+</sup> and cell-*Ascl1*<sup>Cre/-</sup> mice are presented. Data are expressed as means  $\pm$  s.d. (n = 5-9). \*\*,  $P < 0.01$ , between cell-*Ascl1*<sup>Cre/+</sup> and cell-*Ascl1*<sup>Cre/-</sup> mice. (B) Maternal liver histology. Maternal liver sections of cell-*Ascl1*<sup>Cre/+</sup> and cell-*Ascl1*<sup>Cre/-</sup> mice were subjected to hematoxylin and eosin (H&E) staining. (C) Cell lineage tracing. Maternal liver sections on gestation day 18 were subjected to green fluorescent protein (GFP) staining. GFP-positive cells are stained dark brown. (D-E) Pregnancy outcome. Placenta and fetuses were collected and weighed from cell-*Ascl1*<sup>Cre/+</sup> and cell-*Ascl1*<sup>Cre/-</sup> mice. (D) Placental

weight and (E) the number of pups born from cell-*Ascl1*<sup>Cre/+</sup> and cell-*Ascl1*<sup>Cre/-</sup> dams are presented. Data are expressed as means ± s.d. (n = 5-9). \*\*, *P* < 0.01, between cell-*Ascl1*<sup>Cre/+</sup> and cell-*Ascl1*<sup>Cre/-</sup> mice. .... 68

**Figure 8. Differentially expressed genes and canonical pathways affected by *Ascl1* ablation in *Ascl1*-expressing cells.** Maternal livers were collected from cell-*Ascl1*<sup>Cre/+</sup> and cell-*Ascl1*<sup>Cre/-</sup> mice (described in Fig. 6). Total RNA was isolated from livers of cell-*Ascl1*<sup>Cre/+</sup> and cell-*Ascl1*<sup>Cre/-</sup> mice on gestation day (GD) 15 using RNeasy Plus Mini Kit. The isolated RNA was sent to the Center for Medical Genomics Core (Indiana University School of Medicine) for RNA-sequencing. (A) Differentially expressed genes are presented by the volcano plot. Red, significantly up- or downregulated genes; black, green, and blue are non-significant genes. The differentially expressed genes with at least two-fold and *p*-value less than 0.05 were analyzed using the Ingenuity Pathway Analysis (IPA). (B) Top enriched canonical pathways targeted by *Ascl1* are presented. Orange, upregulated; blue, downregulated. *Ascl1*, achaete-scute homolog 1. .... 71

**Figure 9. Virus-induced hepatocyte-specific *Ascl1* knockout mouse model.** (A) The strategy of generating hepatocyte-specific inducible *Ascl1* knockout mouse model. In the hepatocyte-specific inducible *Ascl1* knockout (hep-*Ascl1*<sup>-/-</sup>) (*Ascl1*<sup>fl/fl</sup>;R26<sup>EYFP/EYFP</sup>) (R26-LoxP-Stop-LoxP-EYFP) mice, adeno-associated virus 8 (AAV8)-thyroxine-binding globulin promoter (*TBG*)-*Cre* recombinase (AAV8-TBG-*Cre*) is injected. AAV8 specifically targets the liver and injects the vector that contains *Cre* recombinase driven by the *TBG* promoter, which is expressed only in hepatocytes. Only the hepatocytes express *Cre* recombinase, which excises out the loxP-flanked *Ascl1* and the Stop cassette upstream of enhanced yellow fluorescent protein (*EYFP*), which results in the *Rosa26* promoter element (*R26*) driving *EYFP* expression. Thus, the hepatocytes result in *Ascl1* ablation and *EYFP* expression. In the control mice (*Ascl1*<sup>fl/fl</sup>), a virus with a null gene is introduced (AAV8-TBG-Null), and, therefore, retains the *Ascl1* gene without being labeled with *EYFP*. (B) Virus treatment timeline. The presence of a copulation plug was designated as gestation day (GD) 1. AAV8-TBG-*Cre* or AAV8-TBG-Null was administered by tail vein injection (1x10<sup>12</sup> genomic copies per mouse) to *Ascl1*<sup>fl/fl</sup>;R26<sup>EYFP/EYFP</sup> mice on gestation day (GD) 8 to generate hep-*Ascl1*<sup>-/-</sup> and *Ascl1*<sup>fl/fl</sup>, respectively. Samples were collected on GD15 and GD18. (C) *Ascl1* mRNA expression in the maternal liver. Total RNA was isolated from livers of nonpregnant (NP) and pregnant (GD15 and GD18) *Ascl1*<sup>fl/fl</sup> and hep-*Ascl1*<sup>-/-</sup> mice. Hepatic *Ascl1* mRNA levels were measured using quantitative real-time polymerase chain reaction (qRT-PCR) and expressed as the mean fold changes relative to NP controls (± s.d.; n = 4-5). \*\*\*, *P* < 0.001, between *Ascl1*<sup>fl/fl</sup> and hep-*Ascl1*<sup>-/-</sup> mice. *18S* ribosomal RNA (rRNA) levels were used as endogenous controls. *Ascl1*, achaete-scute homolog 1. .... 74

**Figure 10. Hepatocyte-specific *Ascl1* ablation phenotypes.** Maternal livers were collected and weighed from *Ascl1*<sup>fl/fl</sup> and hep-*Ascl1*<sup>-/-</sup> mice (described in Fig. 9). (A) Morphology of the *Ascl1*<sup>fl/fl</sup> and hep-*Ascl1*<sup>-/-</sup> mice livers on gestation day (GD) 18. (B) The maternal liver-to-body weight ratios of *Ascl1*<sup>fl/fl</sup> and hep-*Ascl1*<sup>-/-</sup> mice are presented. Data are expressed as means ± s.d. (n = 4-6). \*, *P* < 0.05; \*\*, *P* < 0.01, between *Ascl1*<sup>fl/fl</sup> and hep-*Ascl1*<sup>-/-</sup> mice. (C) Maternal liver histology. Maternal liver sections of *Ascl1*<sup>fl/fl</sup> and hep-*Ascl1*<sup>-/-</sup> mice were subjected to hematoxylin and eosin (H&E) staining. (D-E) Maternal hepatocyte proliferation. (D) Maternal liver sections of *Ascl1*<sup>fl/fl</sup> and hep-*Ascl1*<sup>-/-</sup> mice on GD18 were subjected to Ki67 staining. Ki67-positive cells are stained dark brown in the nucleus. (E) The nuclear Ki67-positive hepatocytes were counted in five random fields of view (200X magnification) and the data are expressed as the means ± s.d. (n = 3-6). \*\*\*, *P* < 0.001, between *Ascl1*<sup>fl/fl</sup> and hep-*Ascl1*<sup>-/-</sup> mice. (F-G) Maternal hepatocyte density. (F) Maternal liver

sections of *Ascl1<sup>fl/fl</sup>* and hep-*Ascl1<sup>-/-</sup>* mice on GD18 were subjected to  $\beta$ -Catenin staining.  $\beta$ -Catenin stains the cell membrane dark brown. (G) The maternal hepatocytes were counted (200X magnification) and the data are expressed as the means  $\pm$  s.d. (n = 7 for each group). \*\*\*,  $P < 0.001$ , between *Ascl1<sup>fl/fl</sup>* and hep-*Ascl1<sup>-/-</sup>* mice. *Ascl1*, achaete-scute homolog 1..... 76

**Figure 11. Differentially expressed genes and canonical pathways affected by hepatocyte-specific deletion of *Ascl1* in the maternal liver.** Maternal livers were collected and weighed from *Ascl1<sup>fl/fl</sup>* and hep-*Ascl1<sup>-/-</sup>* mice (described in Fig. 9). Total RNA was isolated from livers of hep-*Ascl1<sup>-/-</sup>* and *Ascl1<sup>fl/fl</sup>* mice on gestation day (GD) 15 using RNeasy Plus Mini Kit. The isolated RNA was sent to the Center for Medical Genomics Core (Indiana University School of Medicine) for RNA-sequencing. (A) Differentially expressed genes are presented by the volcano plot. Red, significantly up- or downregulated genes; black, green, and blue are non-significant genes. The differentially expressed genes with at least two-fold and  $p$ -value less than 0.05 were analyzed using the Ingenuity Pathway Analysis (IPA). (B) Top enriched canonical pathways targeted by hepatic *Ascl1* are presented. Orange, upregulated; blue, downregulated. *Ascl1*, achaete-scute homolog 1; VDR, vitamin D receptor; RXR, retinoid X receptor..... 81

**Figure 12. Changes in maternal hepatocyte phenotypes after hepatic *Ascl1* ablation.** Maternal livers were collected from *Ascl1<sup>fl/fl</sup>* and hep-*Ascl1<sup>-/-</sup>* mice (described in Fig. 9). (A) Hepatic *CD133* mRNA distribution in the maternal liver after hepatic *Ascl1* deletion. Maternal liver sections of *Ascl1<sup>fl/fl</sup>* and hep-*Ascl1<sup>-/-</sup>* mice on gestation day (GD) 18 were subjected to *CD133 in situ* hybridization using RNAscope 2.5 HD Assay-BROWN kit. The *CD133* mRNA is stained dark brown. (B-C) Total RNA was isolated from livers of nonpregnant (NP) and pregnant (GD15 and GD18) *Ascl1<sup>fl/fl</sup>* and hep-*Ascl1<sup>-/-</sup>* mice. Hepatic (B) *CD133* and (C) *EpCAM* mRNA levels were measured using quantitative real-time polymerase chain reaction (qRT-PCR) and expressed as the mean fold changes relative to NP controls ( $\pm$  s.d.; n = 4-5). \*,  $P < 0.05$ ; \*\*,  $P < 0.01$ , between *Ascl1<sup>fl/fl</sup>* and hep-*Ascl1<sup>-/-</sup>* mice. *18S* ribosomal RNA (rRNA) levels were used as endogenous controls. *Ascl1*, achaete-scute homolog 1; *CD133*, prominin-1; *EpCAM*, epithelial cell adhesion molecule..... 83

**Figure 13. Hepatic *Igf2* activation after hepatic *Ascl1* ablation.** Maternal livers were collected from *Ascl1<sup>fl/fl</sup>* and hep-*Ascl1<sup>-/-</sup>* mice (described in Fig. 9). (A) Hepatic *Igf2* mRNA distribution in the maternal liver after hepatic *Ascl1* deletion. Maternal liver sections of *Ascl1<sup>fl/fl</sup>* and hep-*Ascl1<sup>-/-</sup>* mice on gestation day (GD) 18 were subjected to *Igf2 in situ* hybridization using RNAscope 2.5 HD Assay-BROWN kit. The *Igf2* mRNA is stained dark brown. (B-D) Total RNA was isolated from livers of nonpregnant (NP) and pregnant (GD15 and GD18) *Ascl1<sup>fl/fl</sup>* and hep-*Ascl1<sup>-/-</sup>* mice. Hepatic (B) *Igf2*, (C) *Igf2* promoter-specific transcript variants, and (D) *Zfp568* mRNA levels were measured using quantitative real-time polymerase chain reaction (qRT-PCR) and expressed as the mean fold changes relative to NP controls ( $\pm$  s.d.; n = 4-5). \*,  $P < 0.05$ ; \*\*,  $P < 0.01$ ; \*\*\*,  $P < 0.001$ , between *Ascl1<sup>fl/fl</sup>* and hep-*Ascl1<sup>-/-</sup>* mice. *18S* ribosomal RNA (rRNA) levels were used as endogenous controls. *Ascl1*, achaete-scute homolog 1; *Igf2*, insulin-like growth factor 2; *Zfp568*, zinc finger protein 568; P0, placental-specific *Igf2* promoter; P1-3, fetal-specific *Igf2* promoter..... 84

**Figure 14. Hepatic protein expression after hepatic *Ascl1* ablation.** Maternal livers were collected from *Ascl1<sup>fl/fl</sup>* and hep-*Ascl1<sup>-/-</sup>* mice (described in Fig. 9). (A) Maternal protein expression. Western blotting was performed on nonpregnant (NP) and pregnant maternal liver homogenates from *Ascl1<sup>fl/fl</sup>* and hep-*Ascl1<sup>-/-</sup>* mice using antibodies against the proteins listed. GAPDH protein

levels were used as loading controls. **(B)** Quantification of the maternal protein expression. Hepatic maternal protein levels from **Fig. 14A** were measured using ImageJ and expressed as the mean fold changes relative to NP controls ( $\pm$  s.d.;  $n = 3$  for each group). \*,  $P < 0.05$ ; \*\*,  $P < 0.01$ ; \*\*\*,  $P < 0.001$ , between *Ascl1<sup>fl/fl</sup>* and hep-*Ascl1<sup>-/-</sup>* mice. GD, gestation day. *Ascl1*, achaete-scute homolog 1; IGF2, insulin-like growth factor 2; AKT, total protein kinase B; ERK1/2, extracellular signal-regulated kinase 1/2; JAK2, Janus kinase 2; mTOR, mammalian target of rapamycin; 4E-BP1, eukaryotic translation initiation factor 4E-binding protein 1; p70S6K, p70 ribosomal S6 kinase; CD133, prominin-1; HGF, hepatocyte growth factor; FABP4, fatty acid binding protein 4; GAPDH, glyceraldehyde 3-phosphate dehydrogenase. .... 88

**Figure 15. Maternal serum biochemical profile.** Maternal serum was collected from *Ascl1<sup>fl/fl</sup>* and hep-*Ascl1<sup>-/-</sup>* mice (described in **Fig. 9**). Maternal serum biochemical profile from *Ascl1<sup>fl/fl</sup>* and hep-*Ascl1<sup>-/-</sup>* mice was analyzed by Eli Lilly and Company. Data are expressed as means  $\pm$  s.d. ( $n = 5$ ). \*,  $P < 0.05$ ; \*\*,  $P < 0.01$ ; \*\*\*,  $P < 0.001$ , between *Ascl1<sup>fl/fl</sup>* and hep-*Ascl1<sup>-/-</sup>* mice. *Ascl1*, achaete-scute homolog 1; BUN, blood urea nitrogen; Enz Creat, creatinine; ALT, alanine transaminase; AST, aspartate aminotransferase; CK, creatine kinase; Na, sodium; K, potassium; Cl, chloride; Ca, calcium; IP, inorganic phosphate; Chol, cholesterol; HDL Chol, high-density lipoprotein cholesterol; LDL Chol, low-density lipoprotein cholesterol; Trig, triglyceride; Phos Lipid, phospholipid; FFA, free fatty acid; Free Chol, free cholesterol; TP, total protein; Alb, albumin; A/G, albumin/globulin. .... 92

**Figure 16. Hepatic lipid deposition and the expression of lipid-associated genes after hepatic *Ascl1* ablation.** Maternal liver and serum were collected from *Ascl1<sup>fl/fl</sup>* and hep-*Ascl1<sup>-/-</sup>* mice (described in **Fig. 9**). **(A)** Oil Red O (ORO) staining. Gestation day (GD) 15 livers from *Ascl1<sup>fl/fl</sup>* and hep-*Ascl1<sup>-/-</sup>* mice were subjected to ORO staining. The lipid droplets are stained red. **(B-F)** Hepatic lipid gene analysis. Total RNA was isolated from livers of nonpregnant (NP) and pregnant (GD15 and 18) *Ascl1<sup>fl/fl</sup>* and hep-*Ascl1<sup>-/-</sup>* mice. Hepatic **(B)** *Elovl6*, **(C)** *Pnpla3*, **(D)** *Fasn*, **(E)** *Scd1*, and **(F)** *Fitm1* mRNA levels were measured using quantitative real-time polymerase chain reaction (qRT-PCR) and expressed as the mean fold changes relative to NP controls ( $\pm$  s.d.;  $n = 4-5$ ). \*,  $P < 0.05$ , between *Ascl1<sup>fl/fl</sup>* and hep-*Ascl1<sup>-/-</sup>* mice. 18S ribosomal RNA (rRNA) levels were used as endogenous controls. *Ascl1*, achaete-scute homolog 1; *Elovl6*, elongation of very long chain fatty acids protein 6; *Pnpla3*, patatin like phospholipase domain containing 3; *Fasn*, fatty acid synthase; *Scd1*, stearoyl-CoA desaturase; *Fitm1*, fat storage inducing transmembrane protein 1. .... 97

**Figure 17. Hepatocyte-specific *Ascl1* ablation phenotypes in the maternal pancreas.** The maternal pancreas was collected and weighed from *Ascl1<sup>fl/fl</sup>* and hep-*Ascl1<sup>-/-</sup>* mice (described in **Fig. 9**). **(A)** Morphology of the *Ascl1<sup>fl/fl</sup>* and hep-*Ascl1<sup>-/-</sup>* pancreas on gestation day (GD) 18. **(B)** The maternal pancreas-to-body weight ratios of *Ascl1<sup>fl/fl</sup>* and hep-*Ascl1<sup>-/-</sup>* mice are presented. Data are expressed as means  $\pm$  s.d. ( $n = 4-5$ ). \*\*,  $P < 0.01$ , between *Ascl1<sup>fl/fl</sup>* and hep-*Ascl1<sup>-/-</sup>* mice. **(C)** Glucose tolerance test (GTT). Pregnant *Ascl1<sup>fl/fl</sup>* and hep-*Ascl1<sup>-/-</sup>* mice on GD18 were fasted for 6 hrs and injected with glucose (2 g of glucose/kg of body weight) via intraperitoneally. Blood glucose levels were measured using a glucometer (OneTouch Ultra 2) before and 30 min after the glucose injection. **(D-E)** Pancreatic islet analysis. Maternal pancreatic sections of *Ascl1<sup>fl/fl</sup>* and hep-*Ascl1<sup>-/-</sup>* mice on GD19 were subjected to  $\beta$ -Catenin staining. The quantification of percent area insulin staining in **(D)** ventral and **(E)** dorsal pancreas was performed by Eli Lilly and Company. Data are expressed as means  $\pm$  s.d. ( $n = 3-5$ ). \*,  $P < 0.05$ , between *Ascl1<sup>fl/fl</sup>* and hep-*Ascl1<sup>-/-</sup>* mice. **(F-G)** Pancreatic function test. **(F)** Serum glucose was analyzed by Eli Lilly and Company and **(G)** serum insulin was analyzed by the Translation Core at the IU School of Medicine Center for

Diabetes and Metabolic Diseases. Data are expressed as means  $\pm$  s.d. (n = 3-6). **(H)** Maternal pancreatic proliferation. Maternal pancreatic sections of *Ascl1<sup>fl/fl</sup>* and hep-*Ascl1<sup>-/-</sup>* mice on GD18 were subjected to Ki67 staining. Ki67-positive cells are stained dark brown in the nucleus. *Ascl1*, achaete-scute homolog 1; Glu, glucose. .... 100

**Figure 18. Hepatocyte-specific *Ascl1* ablation phenotypes in spleen and kidney.** The maternal spleens and kidneys were collected and weighed from *Ascl1<sup>fl/fl</sup>* and hep-*Ascl1<sup>-/-</sup>* mice (described in **Fig. 9**). **(A)** Morphology of the *Ascl1<sup>fl/fl</sup>* and hep-*Ascl1<sup>-/-</sup>* mouse spleens on gestation day (GD) 18. **(B)** The maternal spleen-to-body weight ratios of *Ascl1<sup>fl/fl</sup>* and hep-*Ascl1<sup>-/-</sup>* mice are presented. Data are expressed as means  $\pm$  s.d. (n = 4-10). \*,  $P < 0.05$ , between *Ascl1<sup>fl/fl</sup>* and hep-*Ascl1<sup>-/-</sup>* mice. **(C)** Maternal splenic histology. Maternal splenic sections of *Ascl1<sup>fl/fl</sup>* and hep-*Ascl1<sup>-/-</sup>* mice on GD15 were subjected to hematoxylin and eosin (H&E) staining. **(D)** The maternal kidney-to-body weight ratios of *Ascl1<sup>fl/fl</sup>* and hep-*Ascl1<sup>-/-</sup>* mice are presented. Data are expressed as means  $\pm$  s.d. (n = 4-5). \*\*\*,  $P < 0.001$ , between *Ascl1<sup>fl/fl</sup>* and hep-*Ascl1<sup>-/-</sup>* mice..... 104

**Figure 19. Hepatocyte-specific *Ascl1* ablation phenotypes in the placenta.** The maternal placenta was collected and weighed from *Ascl1<sup>fl/fl</sup>* and hep-*Ascl1<sup>-/-</sup>* mice (described in **Fig. 9**). **(A)** Placental weights of *Ascl1<sup>fl/fl</sup>* and hep-*Ascl1<sup>-/-</sup>* mice are presented. Data are expressed as means  $\pm$  s.d. (n = 4-9). \*,  $P < 0.05$ ; \*\*,  $P < 0.01$ , between *Ascl1<sup>fl/fl</sup>* and hep-*Ascl1<sup>-/-</sup>* mice. **(B-D)** Maternal placental histology. Placental sections of *Ascl1<sup>fl/fl</sup>* and hep-*Ascl1<sup>-/-</sup>* mice on gestation day (GD) 15 were subjected to **(B)** hematoxylin and eosin (H&E) and **(C)** periodic acid-Schiff (PAS) staining. The glycogen is stained red to purple. **(D)** Placental sections were also subjected to PL-I and PL-II *in situ* hybridization staining using RNAscope 2.5 HD Assay-BROWN kit. The PL-I and PL-II mRNAs are stained dark brown. **(E)** Maternal serum analysis. Maternal serum was collected from *Ascl1<sup>fl/fl</sup>* and hep-*Ascl1<sup>-/-</sup>* mice (described in **Fig. 9**). Maternal serum alkaline phosphatase (ALP) from *Ascl1<sup>fl/fl</sup>* and hep-*Ascl1<sup>-/-</sup>* mice was analyzed by Eli Lilly and Company. **(F)** Placental protein expression. Western blotting was performed on GD15 and GD18 placental homogenates from *Ascl1<sup>fl/fl</sup>* and hep-*Ascl1<sup>-/-</sup>* mice using antibodies against the proteins listed. GAPDH protein levels were used as loading controls. **(G)** Quantification of the placental protein expression. Placental protein levels from **Fig. 19F** were measured using ImageJ and expressed as the mean fold changes relative to GD15 controls ( $\pm$  s.d.; n = 3 for each group). \*,  $P < 0.05$ , between *Ascl1<sup>fl/fl</sup>* and hep-*Ascl1<sup>-/-</sup>* mice. *Ascl1*, achaete-scute homolog 1; IGF2, insulin-like growth factor; ERK1/2, extracellular signal-regulated kinase 1/2; JAK2, Janus kinase 2; PL-II, placental lactogen II; GAPDH, glyceraldehyde 3-phosphate dehydrogenase..... 106

**Figure 20. Hepatocyte-specific *Ascl1* ablation phenotypes in the fetus and postnatal growth.** Fetuses and weaned pups were collected and weighed from *Ascl1<sup>fl/fl</sup>* and hep-*Ascl1<sup>-/-</sup>* dams (described in **Fig. 9**). Fetal weight **(A)** and numbers **(B)** were recorded. **(C-F)** Postnatal pups were weighed after weaning. **(G)** Fetal glucose measurement. Fetal blood glucose was measured using a glucometer (OneTouch Ultra 2) 5 weeks after weaning. ( $\pm$  SEM; n = 13-31). \*,  $P < 0.05$ ; \*\*,  $P < 0.01$ ; \*\*\*,  $P < 0.001$ , between pups born from *Ascl1<sup>fl/fl</sup>* and hep-*Ascl1<sup>-/-</sup>* dams. *Ascl1*, achaete-scute homolog 1. .... 113

**Figure 21. Hepatocyte-specific *Ascl1* ablation phenotypes in maternal cecal microbiota.** The maternal cecal samples were collected from *Ascl1<sup>fl/fl</sup>* and hep-*Ascl1<sup>-/-</sup>* mice on gestation day (GD) 18 (described in **Fig. 9**). **(A)** DNA was isolated from maternal cecal microbiota of *Ascl1<sup>fl/fl</sup>* and hep-*Ascl1<sup>-/-</sup>* mice on GD18 using the PureLink Microbiome DNA Purification Kit. Maternal cecal microbiota changes with  $P < 0.05$  analyzed by Zymo Research Corporation. **(B)** Total RNA was

isolated from livers of nonpregnant (NP) and pregnant (GD15 and GD18) *Ascl1<sup>fl/fl</sup>* and hep-*Ascl1<sup>-/-</sup>* mice. Hepatic hepcidin antimicrobial peptide 2 (*Hamp2*) mRNA levels were measured using quantitative real-time polymerase chain reaction (qRT-PCR) and expressed as the mean fold changes relative to nonpregnant (NP) controls ( $\pm$  s.d.; n = 3-4). \*\*,  $P < 0.01$ ; \*\*\*,  $P < 0.001$ , between *Ascl1<sup>fl/fl</sup>* and hep-*Ascl1<sup>-/-</sup>* mice. *18S* ribosomal RNA (rRNA) levels were used as endogenous controls. *Ascl1*, achaete-scute homolog 1..... 116

**Figure 22. Summary of hepatic *Ascl1* functions during pregnancy.** *Ascl1*, achaete-scute homolog 1; IGF2, insulin-like growth factor 2; *Hamp2*, hepcidin antimicrobial peptide 2; HGF, hepatocyte growth factor..... 131

## ABBREVIATIONS

|              |   |
|--------------|---|
| AFP          | $\alpha$ -Fetoprotein   |
| A/G          | Albumin/globulin  |
| AKT          | Protein kinase B  |
| Alb          | Albumin   |
| ALP          | Alkaline phosphatase  |
| ALT          | Alanine aminotransferase                                      |
| <i>Ascl1</i> | Achaete-scute homolog 1                                       |
| AST          | Aspartate aminotransferase                                    |
| bHLH         | Basic helix-loop-helix  |
| BMP          | Bone morphogenetic protein                                    |
| BUN          | Blood urea nitrogen   |
| CD133        | Cluster of differentiation 133, Prominin-1, PROM1             |
| cDNA         | Complementary deoxyribonucleic acid                           |
| Chol         | Cholesterol   |
| CK           | Creatine kinase   |
| CK8/18       | Cytokeratin 8/18  |
| 4E-BP1       | Eukaryotic translation initiation factor 4E-binding protein 1 |
| Enz Creat    | Creatinine  |
| EpCAM        | Epithelial cell adhesion molecule                             |
| ERK1/2       | Extracellular signal-regulated kinase 1/2                     |
| EYFP         | Enhanced yellow fluorescent protein                           |
| FABP4        | Fatty acid binding protein 4                                  |
| FFA          | Free fatty acid   |
| Free Chol    | Free cholesterol  |
| GAPDH        | Glyceraldehyde 3-phosphate dehydrogenase                      |
| Glu          | Glucose   |
| <i>Hamp2</i> | Hepcidin antimicrobial peptide 2                              |
| HDL Chol     | High-density lipoprotein cholesterol                          |
| HGF          | Hepatocyte growth factor                                      |

|               |  |
|---------------|--|
| HNF4A         | Hepatocyte nuclear factor 4 $\alpha$             |
| <i>Igf2</i>   | Insulin-like growth factor 2                     |
| IP            | Inorganic phosphate                              |
| JAK2          | Janus kinase 2                                   |
| LDL Chol      | Low-density lipoprotein cholesterol              |
| <i>Mash</i>   | Mammalian achaete-scute homolog                  |
| mTOR          | Mammalian target of rapamycin                    |
| p70S6K        | p70 ribosomal S6 kinase                          |
| PCR           | Polymerase chain reaction                        |
| Phos Lipid    | Phospholipid                                     |
| PL-I          | Placental lactogen I                             |
| PL-II         | Placental lactogen II                            |
| qRT-PCR       | Quantitative real-time polymerase chain reaction |
| RNA-seq       | Ribonucleic acid sequencing                      |
| RT-PCR        | Reverse transcript polymerase chain reaction     |
| TP            | Total protein                                    |
| Trig          | Triglyceride                                     |
| TTR           | Transthyretin                                    |
| <i>Zfp568</i> | Zinc finger protein 568                          |

## ABSTRACT

The maternal liver exhibits robust adaptations to pregnancy to accommodate the metabolic needs of developing and growing placenta and fetus by largely unknown mechanisms. We found that achaete-scute homolog 1 (*Ascl1*), a basic helix-loop-helix transcription factor essential for neuronal development, is highly activated in maternal hepatocytes during the second half of gestation in mice. Our aim is to investigate whether and how *Ascl1* plays a pregnancy-dependent role. We deleted the *Ascl1* gene in the maternal liver using three independent mouse models from mid-gestation until term and identified multiple *Ascl1*-dependent phenotypes. When *Ascl1* was deficient in maternal hepatocytes, maternal livers exhibited aberrant hepatocyte histology, fat accumulation, increased hepatocyte cell cycle, and enlarged size, accompanied by reduced albumin production and elevated levels of free fatty acids, ALT, and AST in the maternal blood, indicating maternal liver dysfunction. In the same situation, maternal spleen and pancreas displayed marked enlargement without an overt structural change; the placenta exhibited striking overgrowth with increased ALP production; and the cecal microbiome showed alterations in the relative abundance of several bacterial subpopulations. Moreover, litters born from maternal hepatic *Ascl1* null mutated dam experienced abnormal postnatal growth after weaning. RNA-seq analysis revealed *Ascl1*-regulated genes in the maternal liver associated with *Ascl1*-dependent phenotypes. Of particular interest, we found that, in maternal hepatocytes, *Ascl1* loss-of-function caused the activation of paternally imprinted gene insulin-like growth factor 2 (*Igf2*) encoding a major placental and fetal growth factor. IGF2 is also a known mitogen for hepatocytes and several hematopoietic lineages. Thus, IGF2 is a potential inducer of *Ascl1*-dependent phenotypes including placental overgrowth and maternal organ enlargement. Our studies revealed *Ascl1* as a novel regulator of maternal liver physiology during pregnancy. *Ascl1* activation in maternal

hepatocytes is essential for normal placental growth and appropriate maternal organ adaptations, ensuring the health of both the mother and the fetus.

## CHAPTER 1. INTRODUCTION

The liver is a vital organ that performs many essential physiological processes to maintain the homeostasis of the body (1). Under homeostasis, the liver maintains its liver-to-body weight ratio; however, this ratio can change during pathological conditions and, interestingly, during a physiological condition such as pregnancy. Pregnancy results in dynamic physiological changes, such as an enlarged maternal liver, which alters the mother's homeostasis to accommodate the developing placenta and the growing fetus. However, there is scarce information regarding mechanisms involved in the enlargement and adaptations of the maternal liver to pregnancy. During pregnancy, we found that a proneural transcription factor achaete-scute homolog 1 (*Ascl1*), a mammalian achaete-scute homolog (*Mash*) family member and normally quiescent in the liver, is highly activated in the maternal liver. Therefore, we investigated the function of the maternal hepatic *Ascl1* and its role in pregnancy.

The introduction section provides a summary of the current knowledge of the liver during development, homeostasis, pregnancy, and diseases associated with pregnancy; nonreproductive organs during pregnancy; and the *Mash* family members. The materials and methods section lists important steps of the experiments in collecting the data. The results section presents our findings linking maternal hepatic *Ascl1* to the adaptations of the maternal liver as well as nonreproductive organs and pregnancy outcomes. The discussion section summarizes the important functions of hepatic *Ascl1* and gives novel insights into the vital role of the maternal liver in communicating with other maternal organs, the placenta, and the fetus to ensure a healthy pregnancy.

## 1.1 Liver

### 1.1.1 Development

The fetal liver develops during early embryogenesis and ends after postpartum by undergoing four major stages: competency, commitment, differentiation, and growth (2). During competency at embryonic day (E) 7 in mice, the endoderm forms and specific cells become committed to a hepatic lineage by expressing transcription factors such as forkhead box A (FOXA) 1/2 and GATA binding protein (GATA) 4/6 (3, 4). The commitment stage has three phases: hepatic specification, liver diverticulum, and liver bud initiation. During hepatic specification at E8.5, the septum transversum mesenchyme (STM) expresses bone morphogenetic proteins (BMPs) and cardiac mesoderm expresses fibroblast growth factors (FGFs) to enable the committed cells in the foregut endoderm to become hepatoblasts, the progenitor cells to hepatocytes and cholangiocytes (5-8). During the formation of the liver diverticulum at E9, the hepatoblasts express hepatic genes such as albumin (ALB),  $\alpha$ -fetoprotein (AFP), transthyretin (TTR), hepatocyte nuclear factor 4 $\alpha$  (HNF4A), high expressions of cytokeratin (CK)-8/18, and low expression of CK-19 (8). During the liver bud initiation at E9-9.5, the hepatoblasts proliferate and migrate to the adjacent STM and form an embryonic liver bud (9-11). During differentiation at E10-15, the liver bud grows rapidly from paracrine signals such as FGF, BMP, hepatocyte growth factor (HGF), transforming growth factor beta (TGF- $\beta$ ), retinoic acid (RA), and Wnt from the STM and hepatic mesenchyme. At E14, the hepatoblasts differentiate into either hepatocytes or cholangiocytes. Oncostatin M (OSM), glucocorticoids, HGF, and Wnt promote hepatoblasts to differentiate into hepatocytes by expressing hepatocyte markers such as ALB, CK-8/18, hepatocyte nuclear factor (HNF) 1-4 $\alpha$ , and CCAAT/enhancer-binding protein alpha (C/EBP $\alpha$ ). On the other hand, TGF- $\beta$ , Jagged-Notch, epidermal growth factor (EGF), and HGF promote hepatoblasts to become cholangiocytes by

expressing cholangiocyte markers such as biliary cell surface antigen BDS7, CK-19, onecut [OC]-1/2, and HNF1 $\beta$  (12, 13). Many signaling pathways operating during liver development reactivate during liver regeneration and repair in adults.

### **1.1.2 Function**

The liver is the largest solid organ in the body and performs an essential role in maintaining the homeostasis of the body by synthesizing plasma protein and bile, metabolizing glucose, fatty acid, amino acid, bilirubin, and drugs, and storing glycogen (14, 15). To accomplish these vital functions, the liver contains heterogeneous populations of parenchymal and nonparenchymal cells. The parenchymal cells of the liver are hepatocytes, which make up around 80% of the total liver weight and nearly 70% of the total number of hepatic cells, and performs the majority of the biological functions of the liver such as metabolism, secretion, storage, detoxification, and degradation (16). The nonparenchymal cells of the liver are cholangiocytes (also known as biliary epithelial cells), sinusoidal endothelial cells, Kupffer cells, pit cells, and hepatic stellate cells (17). The cholangiocytes are the ductal cells of the liver and direct bile secreted by the hepatocytes to the gall bladder. The sinusoidal endothelial cells are a highly specialized fenestrated hepatic vasculature that allows an exchange of molecules and proteins between the blood and the hepatocytes. The Kupffer cells are the hepatic macrophages that scavenge for foreign materials, wastes, and bacteria. The pit cells are rare hepatic natural killer cells that play a role in cytotoxicity. The hepatic stellate cells store fat and vitamin A, and maintain the extracellular matrix; however, during liver injury, the hepatic stellate cells are activated to become myofibroblasts, which result in liver fibrosis (12). The liver, therefore, maintains the homeostasis of the body via diverse populations of liver cells.

The liver is made up of basic functional units called the liver lobules, which are a hexagonal arrangement of hepatocytes, the portal triads, and the central vein connected together by the sinusoidal endothelial cells (18). Located at the corners of the hexagonal-shaped liver lobule, the portal triads comprise the portal vein, hepatic artery, and the bile duct (19). Both the portal vein and hepatic artery provide blood to the hepatocytes via the sinusoidal endothelial cells and flows toward the central vein, located at the center of the liver lobule. The portal vein carries deoxygenated and nutrient-rich blood from the intestine while the hepatic artery carries oxygenated and low-in-nutrients blood from the aorta. The bile canaliculus carries bile produced by the hepatocytes towards the bile duct, which lined by cholangiocytes, to be stored in the gall bladder. The central vein passes the blood from the portal vein and hepatic artery to the hepatic vein and then to inferior vena cava (20). Finally, hepatocytes fill the liver lobule radially between the portal triads and the central vein arranged as plates.

The hepatocytes are heterogeneous and perform different biochemical and physiological functions dependent on their location or zonation of the liver lobule (21, 22). There are three zones in the liver: zone 1 is located around the portal triad, zone 3 is located around the central vein, and zone 2 is located between the two zones (23). The zone 1 hepatocytes have high availability of oxygen and have elevated levels of glucose delivery, gluconeogenesis, urea synthesis, fatty acid oxidation, cholesterol synthesis, sulfation, and glutathione and glutathione peroxidase. In contrast, the zone 3 hepatocytes have low availability of oxygen and have elevated levels of glucose uptake, glycolysis, glutamine synthesis, lipogenesis and ketogenesis, bile acid synthesis, glucuronidation, glutathione transferase, and cytochrome P450 enzyme. Finally, zone 2 hepatocytes have intermediate levels of metabolism of both zone 1 and zone 3 hepatocytes (24).

### **1.1.3 Maternal liver during pregnancy**

Very little information is available on the maternal liver growth and adaptations to pregnancy in humans and, therefore, most of the information is on rodent studies. The maternal liver in rodents increases in size proportionally to the maternal body weight gained during midgestation and continues until the end of gestation, which averages to about 20 days, to accommodate the rapid growth of the fetus (25, 26). During the enlargement of the maternal liver, the total hepatic DNA contents increase by the end of pregnancy without changing the hepatocyte ploidy (27, 28). Additionally, the maternal hepatocytes reduce in density due to hepatic hypertrophy and express pregnancy-induced hepatic genes such as genes involved in proliferation, metabolism, and regeneration (27, 28). Furthermore, maternal liver biochemical profile changes markedly during pregnancy (29). In the maternal serum, alkaline phosphatase (ALP) and alpha-fetoprotein (AFP) increases, total protein and albumin decreases, and alanine aminotransferase (ALT), gamma-glutamyl transpeptidase (GGT), and bilirubin do not change during pregnancy (29-31). Moreover, the maternal hepatic enzymes responsible for drug and lipid metabolisms such as cytochrome P450 (CYP) change during pregnancy such as the expression of CYP1A2 decreases whereas CYP2D6 and CYP3A4 increases (32). The maternal liver then returns to its pre-pregnancy size after parturition in ten days without lactation, whereas the maternal liver remains enlarged with lactation (28). Interestingly, we found that, when compared with nonpregnant mice, the highest activated maternal hepatic gene by the end of gestation is *Ascl1*. Our goal is to investigate whether this molecule plays a role in maternal hepatic adaptations to pregnancy.

### **1.1.4 Maternal liver diseases during pregnancy**

Maternal liver diseases during pregnancy are uncommon and affect about 3% of pregnancies; however, they pose a danger to the morbidity and mortality of the mother and the fetus (33, 34).

There are pregnancy-dependent and -independent maternal liver diseases that affect both the mother and the fetus. Pregnancy-dependent maternal liver diseases include hyperemesis gravidarum (HG); intrahepatic cholestasis of pregnancy (ICP); preeclampsia, eclampsia, and HELLP (hemolysis, elevated liver enzymes, and low platelet count) syndrome; and acute fatty liver of pregnancy (AFLP). Pregnancy-independent maternal liver diseases include preexisting liver diseases such as hepatitis B virus (HBV) and hepatitis C virus (HCV) infections, autoimmune hepatitis (AIH), primary biliary cholangitis (PBC), Wilson disease (WD), cirrhosis, and portal hypertension. Currently, there is a lack of research in maternal liver diseases during pregnancy, which, therefore, challenges both hepatologists and gynecologists in diagnosing and treating the affected patients that also guarantees the safety of the growing fetus.

## **1.2 Pregnancy**

### **1.2.1 Maternal metabolic changes**

To provide an energy source for the development of the placenta and fetus, maternal metabolism changes such as lipid anabolism and catabolism (35, 36). The anabolic phase of lipids begins during the first and second trimesters where the maternal tissues synthesize and deposit lipids to be stored as exogenous metabolic energy for the growing fetus (37, 38). By the third trimester, the catabolic phase of lipids activates and begins to breakdown the stored lipids to provide as an energy fuel for the developing fetus (39). Additional energy sources include glucose, which is the major energy source to the growing fetus; fatty acids, which are essential for fetal tissue development and organogenesis; cholesterol, which is essential for cell membrane fluidity as well as cell proliferation and differentiation; and ketone bodies, which are essential as a glucose substitute and embryonic brain development during malnutrition (40-44). Therefore, maternal

metabolic adaptations to pregnancy are necessary and essential to provide energy for the developing fetus and successful pregnancy. However, how these metabolic changes are regulated remains largely unknown.

## **1.2.2 Maternal physiologic changes**

Maternal nonhepatic organs including the heart, lung, blood, gastrointestinal tract, pancreas, spleen, and kidney exhibit a variety of physiological changes during gestation.

### **1.2.2.1 Heart, lung, and blood**

The function of the heart is to pump blood and provide the metabolic needs to organs and tissues of the body. To circulate the blood around the body, the cardiac muscle cells, also known as cardiomyocytes, contract rhythmically at a rate of 60 to 100 beats per minute caused by the electrical impulses from the sinoatrial (SA) node (45). The heart has two chambers, each having an atrium and a ventricle (46). In brief, deoxygenated blood from the vena cava flows into the right atrium and enters the right ventricle (47, 48). The blood then exits the heart and enters the pulmonary circulation via the pulmonary artery where it exchanges carbon dioxide with oxygen from the capillaries in the lungs by diffusion. The oxygenated blood then flows into the pulmonary artery and enters back into the heart in the left atrium and into the left ventricle. The mitral valve shuts preventing the backflow of the blood in the direction of the atrium. Then the blood exits the heart and enters the systemic circulation by flowing into the aorta where organs and tissues take up oxygen and exchanges with carbon dioxide. Finally, the deoxygenated blood flows back into the vena cava.

To deliver nutrients to the increasing metabolic needs of the growing fetus, the maternal blood volume increases from the first trimester and peaks at early third trimester due to an increase

in red and white blood cells, while cardiac output increases due to an increase in stroke volume, which in turn increases the heart rate (49-55). As a consequence, the maternal lung increases oxygen intake by increasing the amount of air inhaled and exhaled while hyperventilating due to the growing fetus pushing up against the maternal diaphragm and causing a decrease in the total lung capacity (51, 56-59). Additionally, the systemic vascular resistance, systolic blood pressure, and diastolic blood pressure decrease during pregnancy (60, 61). Due to the increased hemodynamic stress during pregnancy, the maternal heart results in hypertrophy indicated by increased chamber size and wall thickness, which involves various extracellular matrix (ECM) proteins, signaling pathways, microRNAs, ubiquitin-proteasome system, and hormones (62-64). Nevertheless, pregnancy-induced physiological hypertrophy of the maternal heart requires further mechanistic studies.

### **1.2.2.2 Gastrointestinal tract and gut microbiome**

The function of the gastrointestinal tract, which includes the mouth, pharynx, esophagus, stomach, and small and large intestines, is to digest and absorb food and eliminate wastes (65). During pregnancy, the gastrointestinal tract changes and causes nausea and vomiting during the first trimester; the mechanism for the physiological changes may be due to the hormonal change of progesterone that decreases its motility (66, 67). Additionally, human chorionic gonadotropin (hCG) may play a role in causing nausea and vomiting as the levels of hCG positively correlates to the severity of the symptoms (68).

The gut microbiome plays an important role in human health that includes metabolism of food and drugs, protection against pathogens and epithelial injury, promotion of fat storage and angiogenesis, and modification of the nervous system and the immune system by cross-talking to extraintestinal organs (69, 70). Estimated to have a ratio of 1.3 bacterial cells to one human cell,

the gut microbiome contains the most diverse population of bacteria in the human body (71). Multiple factors, such as the delivery mode, postnatal factors, and diet, shape the infant's microbiome (72). The first microbiome colonization in the human body occurs at birth, which depends on vaginal or cesarean delivery. The vaginally-delivered infants have a microbiome that resembles the maternal vaginal microbiome; however, cesarean-delivered infants have a microbiome that resembles the maternal skin and environmental microbiome (73). For a newborn infant, exposures to antibiotics, breastfeeding or formula, solid foods, host genetics, and environment further changes the infant's microbiome (72). As the toddler grows and consumes an adult diet, the microbiome slowly shifts toward an adult-like microbiome. Dysbiosis of microbiome caused by a bloom of pathogens and a loss of commensal bacteria and diversity results in diseases such as type 1 and 2 diabetes, obesity, colorectal cancer, rheumatoid arthritis (RA), and inflammatory bowel diseases (IBD) (70, 74). Therefore, maintaining a healthy microbiome is crucial to having a healthy life.

The microbiome changes, most prominently in the vagina and gut, to adapt to the physiological and immunological changes of the host during pregnancy (75-77). By the end of the pregnancy, the microbiome diversity and number decrease. The *Lactobacillus* species, which produces lactic acid that prevents the growth of pathogens, becomes the most abundant bacterial species followed by Clostridiales, which is associated with mental health improvement, Bacteroidales, which produces the most abundant capsular polysaccharides for its survival in the gut, and Actinomycetales, which produces antibiotics (77-81). The healthy microbiome during pregnancy is associated with preventing preterm birth due to bacterial vaginosis, gestational diabetes due to decreased diversity of the microbiome, and obesity due to reduced levels of Enterobacteriaceae (76, 82, 83). Furthermore, maternal dysbiosis is associated with the fetus

developing conditions such as obesity, diabetes, allergies, altered brain development, and high blood pressure (84-87). Therefore, a healthy microbiome during pregnancy is essential not only for the health of the mother but also for the fetus during development and postnatal growth.

### **1.2.2.3 Pancreas**

The function of the pancreas, which is composed of dorsal and ventral buds, is to produce digestive enzymes and hormones to break down food and regulate blood glucose levels, respectively (88). The exocrine cells of the pancreas, the acinar cells, account for 98% of the pancreatic mass and produce digestive enzymes such as lipase, protease, and amylase, which travel along the pancreatic duct to the small intestine and aid in the breakdown of foods (89, 90). The endocrine cells, located in the islets of Langerhans of the pancreas, account for 2% of the pancreatic mass and produce hormones such as amylin, C-peptide, and insulin by the  $\beta$ -cells, glucagon by the  $\alpha$ -cells, somatostatin by the  $\delta$ -cells, pancreatic polypeptide (PP) by the  $\gamma$ -cells, and ghrelin by the  $\epsilon$ -cells to regulate blood sugar levels. Therefore, the pancreas regulates digestion and blood glucose homeostasis.

During the first trimester, the fetal blood glucose concentration is lower than the maternal blood glucose, and, therefore, the fetus receives the maternal glucose by passive diffusion using facilitative glucose transporters present in the placenta; however, during late pregnancy, the fetus actively redirects the maternal blood glucose that may result in maternal hypoglycemia (91-94). Additionally, in mice, the maternal  $\beta$ -cells, mostly from preexisting maternal  $\beta$ -cells, proliferate and increase the production of insulin (95, 96). The  $\beta$ -cell expansion in pregnancy may be due to the maternal islets producing serotonin and placenta producing placental lactogen (97, 98). To prevent low maternal blood glucose, the placenta secretes placental hormones, such as placental lactogen, progesterone, prolactin, and cortisol, to increase maternal insulin resistance and

upregulate hepatic gluconeogenesis (99). By the end of pregnancy, prolactin secreted by the maternal pituitary and progesterone secreted by the placenta may block the proliferation of the maternal  $\beta$ -cells and initiates cell death by apoptosis (100-102).

#### **1.2.2.4 Spleen**

The spleen has two compartments called the red pulp, which filters the blood, recycles irons, and produces antibodies, and the white pulp, which contains lymphoid cells for the innate and adaptive immune response (103). The maternal spleen in mice increases in size until midgestation and decreases to the nonpregnant state before parturition (104, 105). Coinciding with the splenic growth, the spleen increases in the erythropoietic activity and upregulates erythroid-associated genes (104, 106). Furthermore, maternal spleen in humans also increases in size throughout pregnancy (107, 108). Therefore, the enlargement of the maternal spleen may represent a normal physiological event.

#### **1.2.2.5 Kidney**

The function of the kidney is to maintain homeostasis of the body by filtering nitrogenous waste products, such as creatinine, urea, and ammonia; reabsorbing essential substances, such as water, glucose, and electrolytes; maintaining acid-base balance; and secreting calcitriol and erythropoietin hormones (109, 110).

The maternal kidney adapts to pregnancy both anatomically and functionally. During pregnancy, the maternal kidney increases in size until parturition due to the increase in the blood flow and fluid retention without increasing the number of nephrons and returns back to its normal size within half a year (111-114). In the maternal kidney, the glomerular filtration rate (GFR) and urinary release and retention increase from the first trimester that may be due to the increase in the

maternal blood volume and human chorionic gonadotropin (hCG) (115, 116). Additionally, changes in the biochemistry of the urine and blood are due to the increase in the clearance of creatinine, uric acid, and urea, which result in the decrease of maternal serum creatinine and blood urea nitrogen (BUN) (50, 117). Consequently, the changes in the filtrations cause an increase in the water volume of the maternal body and provide water to the developing placenta and fetus (117).

### **1.3 Mammalian achaete-scute homology (*Mash*) family**

Currently, there are five mammalian achaete-scute homolog (*Mash*) family members: *Ascl1*, *Ascl2*, *Ascl3*, *Ascl4*, and *Ascl5*. Information regarding the first three members, *Ascl1*, *Ascl2*, and *Ascl3*, are available in the literature; however, studies on the remaining two members, *Ascl4* and *Ascl5*, are lacking. Here, we summarize the current knowledge of *Ascl1*, *Ascl2*, and *Ascl3*.

#### **1.3.1 *Ascl1***

The first member of the mammalian achaete-scute homolog (*Mash*) is achaete-scute homolog 1 (*Ascl1*). Located on chromosome 12q22-q23 in humans and chromosome 10 in mice, *Ascl1* is a basic helix-loop-helix transcription factor that regulates neuronal cell fates in both the central nervous system (CNS) and the peripheral nervous system (PNS) (118-120). During human development, genetic disorders associated with the nervous system due to *Ascl1* mutation include congenital central hypoventilation syndrome (CCHS) and Haddad syndrome, whereas, in rodent, ablation of *Ascl1* results in developmental defects of neuronal lineages and postnatal death (120-122). In the adult, thymus, brain, spinal cord, and B lymphoblasts express *Ascl1* (123). Additionally, *Ascl1* acts as a master regulator to reprogram non-neuronal cells into neuronal

subtypes (124). Therefore, *Ascl1* regulates development, physiological and pathological conditions, and cell fate.

Rodent studies show that the function of *Ascl1* during development is proliferation, cell cycle exit, and/or differentiation in neural stem cells (125). The neural stem cells express *Ascl1* in an oscillatory manner due to its repressor *Hes1* autonomously oscillating via a negative feedback loop every 2 hours (126, 127). Neural stem cells without the expression of *Ascl1* proliferate slowly; however, neural stem cells expressing *Ascl1* in an oscillatory fashion activates proliferation whereas a sustained expression of *Ascl1* results in cell cycle exit and differentiation (125). Therefore, *Ascl1* governs in maintaining neural stem cells.

Before neurogenesis, neural stem cells maintain their undifferentiated state by activating the Notch signaling as a result of a neighboring neuron or another neural stem cell expressing constant or oscillating *Ascl1* and Delta-like 1 (*Dll1*) levels, respectively (128). Neurons constantly express *Ascl1*, which activates the expression of *Dll1* that binds to the transmembrane receptor Notch of their neighboring neural stem cells. The neural stem cells activate the Notch signaling pathway by releasing the Notch intracellular domain (NICD) from the Notch receptor, which translocates to the nucleus, binds with mastermind-like (Maml) and recombining binding protein suppressor of hairless (Rbpj), activates *Hes1* expression that inhibits *Ascl1* expression, and maintain their stem cell properties by a process known as lateral inhibition. Another method in maintaining an undifferentiated neuronal state is ‘salt-and-pepper pattern’ (129). In this method, the neighboring neural stem cells will take turns expressing *Ascl1* and *Dll1* to activate the Notch signaling in their neighboring neural stem cells. As a result, *Ascl1* controls the Notch signaling and the maintenance of the neural stem cell niche.

After neurogenesis, the neural stem cells lose the *Dll1* expression and differentiate into mature neural cells (128). Various cells express *Ascl1* such as the chromaffin cells, glomus cells, oligodendrocytes, olfactory sensory neurons, pulmonary neuroendocrine cells, and parafollicular cells (130-137). During pathological conditions, medullary thyroid cancers and small cell lung cancers highly express *Ascl1* by promoting metastasis and preventing apoptosis (138, 139). Reprogramming studies *in vitro* show that *Ascl1* reprograms postnatal astrocytes into GABAergic neurons; *Ascl1* and *Sox2* reprogram human pericytes also into GABAergic neurons; and *Ascl1*, *Brn2*, and *Myt1l* reprogram hepatocytes into neuronal cells (140-144). Therefore, *Ascl1* influences in maintaining the neural stem cells and controlling neuronal fate, while the upregulation of *Ascl1* expression characterizes subpopulations of cancer cells and overexpression results in reprogramming non-neural cells into neural subtypes.

### **1.3.2 *Ascl2***

The second member of *Mash* is *Ascl2*. Located on chromosome 11p15.5 in humans and chromosome 7 in mice, *Ascl2* is a basic helix-loop-helix transcription factor expressed only in the paternal allele due to genomic imprinting (145). Variety of different organs and cells express *Ascl2* including the placenta, intestine, skeletal muscle, follicular helper T cells, and colon, lung, and gastric carcinoma (146-150).

The ovum transcribes *Ascl2* during oogenesis and, after fertilization, the trophoblast lineage cells express *Ascl2* that continues to the development of the placenta (146). The placenta is a highly specialized temporary organ during pregnancy that helps in the growth of the fetus by exchanging metabolic products and wastes, protecting the fetus against xenobiotics and infections, and releasing hormones between maternal and fetal circulations (151). In the placenta, the spongiotrophoblast cells and subpopulation of the labyrinth trophoblast express *Ascl2*. Ablation of

*Ascl2* in mice yielded in a significantly smaller placenta due to the lack of the spongiotrophoblast layer formation, which results in the death of the embryos around embryonic day (E) 10 (152). Therefore, *Ascl2* influences the development of the placenta and the continuation of the pregnancy.

The *Ascl2* expression is also present in the adult intestinal epithelium, especially in the Lgr5+ stem cells in the crypt base of the intestine (147). The intestine is part of the digestive tract and regulates the absorption of nutrients and water from the food and production of vitamins by the microbiome (153). The turnover rate of the intestinal epithelial cell is about 5 days, and, therefore, intestinal stem cells direct in maintaining homeostasis and structural integrity of the intestinal epithelium (154, 155). Studies show that conditional deletion of *Ascl2* in the mouse intestine results in the loss of the intestinal stem cells due to an increase in cell apoptosis whereas overexpression of *Ascl2* does not induce tumorigenesis (147, 156). Therefore, *Ascl2* is essential in the maintenance and homeostasis of the intestine by sustaining the intestinal stem cells niche.

A recent study links *Ascl2* and muscle stem cells (150). The stem cells of the muscle called satellite cells govern postnatal muscle growth and regeneration of damaged muscle by symmetric and asymmetric divisions (157, 158). In muscle, myogenic regulatory factors activate myogenesis in the satellite cells; however, *Ascl2* inhibits the myogenic regulatory factors, which results in inhibition of proliferation, differentiation, and fusion of myoblasts (150). Additionally, overexpression of *Ascl2* impairs muscle repair from injury. Therefore, *Ascl2* hinders the self-renewal and maintenance of the postnatal satellite cells.

The initiation and development of the follicular helper T cells during an immune response requires *Ascl2* in both humans and mice (159). The follicular helper T cells are essential for the development of the germinal centers where the maturation of B cells and the production of antibodies occur (160). Expression of *Ascl2* induces programming of the follicular helper T cells

by activating *Ascl2*-dependent genes while the ablation of *Ascl2* results in the inhibition of the follicular helper T cells differentiation (159). As a result, *Ascl2* directs in initiating the follicular helper T cell development and function during an immune response to infection.

Recently, multiple studies identify *Ascl2* expression in subpopulations of lung, colon, and stomach cancers. Lung, colon, and stomach cancers are the first, third, and fourth in males and second, third, and fifth in females, respectively, type of cancer-related mortality worldwide (161). A subpopulation of lung squamous cell carcinoma, which is part of a non-small-cell lung carcinoma activates the non-canonical Wnt signaling pathway and express increased levels of *Ascl2* when compared with normal bronchi and lung adenocarcinoma (149, 162). In colon cancer cells, high expression of *Ascl2* associates with tumor malignancy such as proliferation, colony formation, invasion, migration, growth, and epithelial-mesenchymal transition (EMT) (163, 164). Finally, in stomach cancer, overexpression of *Ascl2* promotes cancer development by inducing EMT (165). Therefore, *Ascl2* influences during normal development and tumor metastasis.

### **1.3.3 *Ascl3***

The third member of *Mash* is *Ascl3*. Located on chromosome 11p15.3 in humans and chromosome 7 in mice, *Ascl3* is a basic helix-loop-helix transcription factor expressed in the salivary glands (166, 167). Salivary glands secrete continuous saliva that is essential in the function and health of the oral mucosa such as lubrication of the oral cavity, preventing the growth of microbes, remineralization of the enamel, facilitating soft tissue repair, and digestion (168). During development, subpopulations of the salivary glands progenitor cells of the acinar and ductal cells express *Ascl3* (169, 170). Ablation of *Ascl3* results in smaller development of the salivary glands due to a reduced cell proliferation without affecting the function (171). Therefore, *Ascl3* is necessary, but not essential, in the development of the salivary glands.

A recent study shows that, in addition to the progenitor cells of the salivary glands, the developing olfactory epithelium in the nasal cavity, which is the peripheral organ for sensing smell, also expresses *Ascl3* as early as embryonic day (E) 12.5 (172). During development, *Ascl3* is present in the multipotent horizontal basal cells of the olfactory epithelium, which are the progenitor cells of the microvillar cells and the Bowman's glands. Nevertheless, the ablation of *Ascl3* does not influence the differentiation of the multipotent horizontal basal cells. Furthermore, during injury-induced regeneration of the olfactory epithelium, the horizontal basal cells express *Ascl3* and regenerate the microvillar cells and the Bowman's glands. Therefore, *Ascl3* expression activates in injury and repair of the olfactory epithelium while its involvement in differentiation and homeostasis of the olfactory epithelium requires further research.

#### **1.4 Hypothesis**

While the maternal liver adapts to pregnancy, the hepatic cells activate a proneural gene *Ascl1* during mid to late gestation when the placenta and fetus grow most rapidly. We hypothesize that activation of *Ascl1* in the maternal liver is required to maintain a healthy pregnancy.

## CHAPTER 2. METHODS

### 2.1 Mice

*Ascl1*<sup>-/-</sup> (*Ascl1*<sup>fl/fl</sup>; *R26*<sup>rtTA/rtTA</sup>; *tetO*<sup>Cre/-</sup>) mice delete *Ascl1* in the whole body, except the brain and testes, with the administration of doxycycline. For the generation of *Ascl1*<sup>-/-</sup> mice, *Ascl1*<sup>fl/fl</sup>; *R26*<sup>EYFP/EYFP</sup> mice, a generous gift from Dr. Guillemot (The Francis Crick Institute, Midland Road, London NW 1AT, UK), were crossed with *R26*<sup>rtTA/rtTA</sup> (B6.Cg-*Gt(ROSA)26Sor*<sup>tm1(rtTA\*M2)Jae</sup>/J; Stock No: 006965) mice and *tetO*<sup>Cre/-</sup> (B6.Cg-Tg(tetO-cre)1Jaw/J; Stock No: 006234) mice from the Jackson Laboratory (Bar Harbor, Maine, USA). Selective breeding was required to remove the *EYFP* allele and replace it with the *rtTA* allele. *Ascl1*<sup>+/+</sup> (*Ascl1*<sup>+/+</sup>; *R26*<sup>rtTA/rtTA</sup>; *tetO*<sup>Cre/-</sup>) mice were used as controls.

Cell-*Ascl1*<sup>Cre/-</sup> (*Ascl1*<sup>Cre/fl</sup>; *R26*<sup>EYFP/EYFP</sup>) mice delete *Ascl1* in *Ascl1*-expressing cells with the administration of tamoxifen. For the generation of cell-*Ascl1*<sup>Cre/-</sup> mice, *Ascl1*<sup>fl/fl</sup>; *R26*<sup>EYFP/EYFP</sup> mice were crossed with *Ascl1*<sup>Cre/+</sup> (*Ascl1*<sup>tm1.1(Cre/ERT2)Jejo</sup>/J; Stock No: 012882) mice from Jackson Laboratory. Cell-*Ascl1*<sup>Cre/+</sup> (*Ascl1*<sup>Cre/+</sup>; *R26*<sup>EYFP/EYFP</sup>) mice were used as controls.

For the generation of hep-*Ascl1*<sup>-/-</sup> mice, which delete *Ascl1* in the maternal liver, *Ascl1*<sup>fl/fl</sup>; *R26*<sup>EYFP/EYFP</sup> mice were used as both experimental and control by injecting with a virus containing *Cre* or null vectors, respectively.

All animal studies were performed in accordance with the National Institutes of Health Guide for the Care and Use of Laboratory Animals and with the approval from the Indiana University-Purdue University Indianapolis Animal Care and Use Committee. All mice were maintained on a 12-hour light/12-hour dark cycle (7 AM on and 7 PM off) at 22 ± 1°C. Mice were given a standard rodent chow and water *ad libitum*.

## 2.2 Genomic PCR

Genomic DNA was prepared from mouse ear snips using the modified HotSHOT method (173). In brief, mouse ears were lysed by incubating in a 25 mM NaOH/0.2 mM EDTA solution at 98°C for 1 hour and neutralized with 40 mM Tris-HCl (pH 5.5). All mice were genotyped by polymerase chain reaction (PCR) using KAPA Taq PCR Kits (Kapa Biosystems, Inc., Wilmington, MA, USA). Specific primers purchased from Integrated DNA Technologies (Coralville, IA, USA) were used to detect the wild type and mutant alleles. Genotyping PCR was performed as per directions with modification from the vendor using Mastercycler Pro (Eppendorf, 950030010). The PCR products, after adding ethidium bromide solution (IBI Scientific, IB40075), were separated by agarose gel electrophoresis and visualized using a UV transilluminator.

For *Ascl1*<sup>-/-</sup> (*Ascl1*<sup>fl/fl</sup>; *R26*<sup>rtTA/rtTA</sup>; *tetO*<sup>Cre/-</sup>) mouse line, genotyping was performed with a modification in the PCR conditions (174). Primers *Ascl1* Forward and *Ascl1* Wild type Reverse were used to detect the *Ascl1* wild type allele (342 bp), and primers *Ascl1* Forward and *Ascl1* Mutant Reverse were used to detect floxed *Ascl1* allele (857 bp) (**Fig. 1A**) (**Table 1**). PCR conditions were 35 cycles of 94°C/30 sec; 69°C/30 sec; 72°C/90 sec. Primers oIMR8545 and oIMR8546 were used to detect the *rtTA*-negative allele (650 bp), and primers oIMR8545 and oIMR8052 were used to detect the *rtTA*-positive allele (340 bp) (**Fig. 1B**) (**Table 1**). PCR conditions were 35 cycles of 94°C/30 sec; 65°C/1 min; 72°C/1 min. Primers oIMR7338 and oIMR7339 were used as an internal positive control (324 bp), and primers oIMR1084 and oIMR1085 were used to detect *Cre* transgene (~100 bp) (**Fig. 1C**) (**Table 1**). PCR conditions were 35 cycles of 94°C/30 sec; 70°C/1 min; 72°C/1 min. Primers *EYFP* Forward and *EYFP* Wild type Reverse were used to detect *EYFP*-negative allele (600 bp), and primers *EYFP* Forward and *EYFP* Mutant Reverse were used to detect *EYFP*-positive allele (320 bp) (**Fig. 1D**) (**Table 1**). PCR conditions were 35 cycles of 94°C/30 sec; 69°C/1 min; 72°C/1 min.

For cell-*Ascl1*<sup>Cre/-</sup> (*Ascl1*<sup>Cre/fl</sup>;R26<sup>EYFP/EYFP</sup>) mouse line, primers 10841 and 10842 were used to detect the *Cre*-negative allele (418 bp), and primers 10843 and 10653 were used to detect the *Cre*-positive allele (~300 bp) (**Fig. 1E**) (**Table 1**). PCR conditions were 35 cycles of 94°C/30 sec; 62°C/30 sec; 72°C/30 sec. Identical primers and PCR conditions were used to detect *Ascl1* wild type and floxed alleles, and *EYFP*-negative and -positive alleles as mentioned previously.

For hep-*Ascl1*<sup>-/-</sup> (*Ascl1*<sup>fl/fl</sup>;R26<sup>EYFP/EYFP</sup>) mouse line, identical primers and PCR conditions were used to detect *Ascl1* wild type and floxed alleles, and *EYFP*-negative and -positive alleles as mentioned previously.

### 2.3 Pregnancy model

Timed pregnancy was performed by mating female mice with wild type male mice to ensure that fetuses are heterozygous and have at least one wild type allele. The presence of a copulation plug in the morning was designated as gestation day (GD) 1, and plug-positive female mice were separated from male mice and housed in individual cages.

For *Ascl1*<sup>-/-</sup> (*Ascl1*<sup>fl/fl</sup>;R26<sup>rtTA/rtTA</sup>;tetO<sup>Cre/-</sup>) mice, doxycycline (Alfa Aesar, J60579) was dissolved in Milli-Q water (Millipore Sigma, Z00Q0V0WW) at a concentration of 1 mg/ml in the drinking water bottle on GD6 until the mice were sacrificed. For cell-*Ascl1*<sup>Cre/-</sup> (*Ascl1*<sup>Cre/fl</sup>;R26<sup>EYFP/EYFP</sup>) mice, tamoxifen (Sigma-Aldrich, T5648) was dissolved in 10% ethanol and sesame oil (Sigma-Aldrich, S3547), incubated overnight in a shaker at 37°C, injected intraperitoneally at a dose of 60 mg/kg on GD13-14, and sacrificed on GD15 and GD18. For hep-*Ascl1*<sup>-/-</sup> (*Ascl1*<sup>fl/fl</sup>;R26<sup>EYFP/EYFP</sup>) mice, adeno-associated viruses expressing *Cre* (Addgene, AV-8-PV1091) driven by the thyroxine-binding globulin promoter (*TBG*) promoter were injected via tail

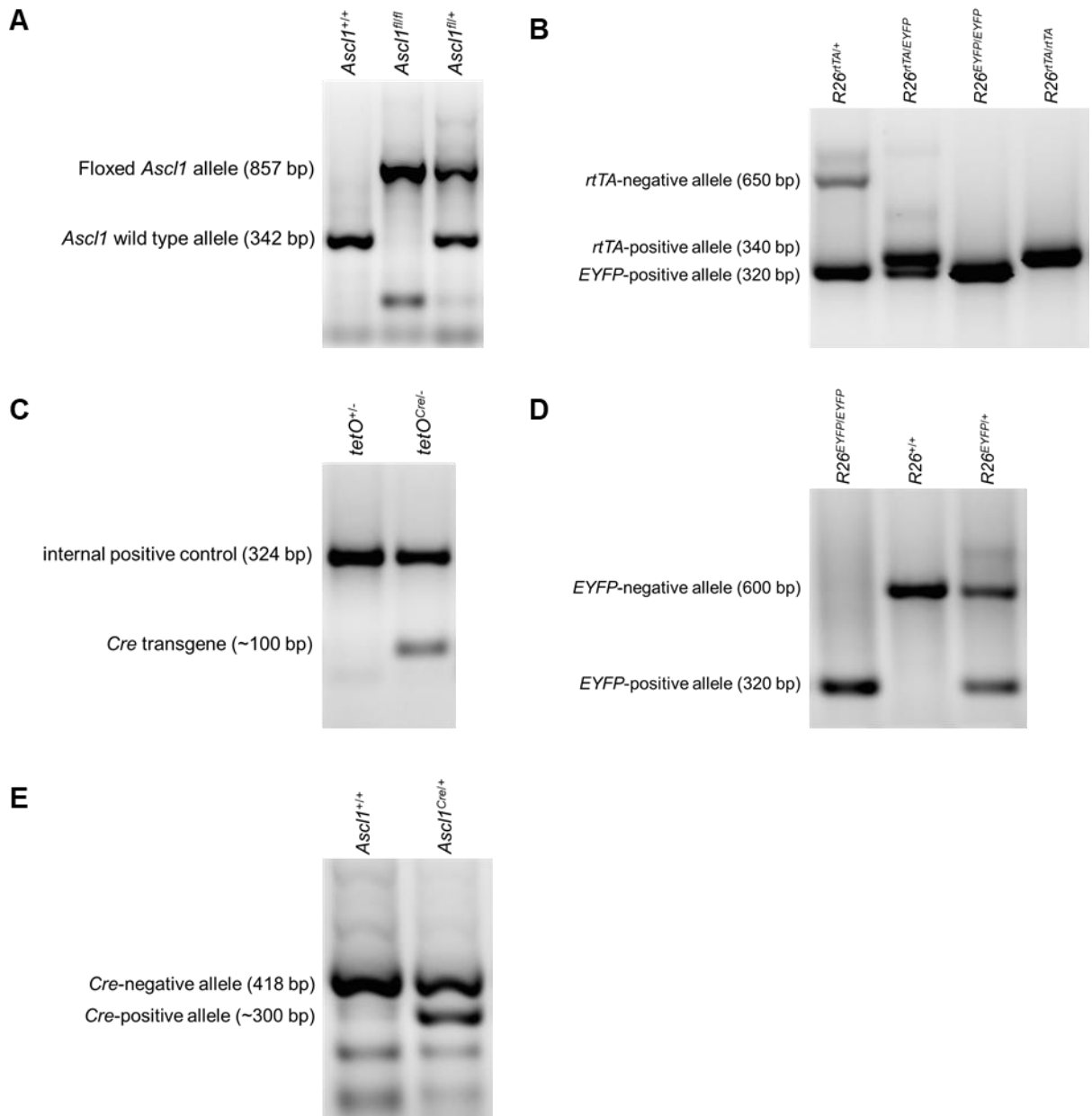


**Figure 1. Genotyping Gel Image.** DNA was extracted from ear snips and polymerase chain reaction (PCR) was performed with specific primers (**Table 1**) to determine the presence of (**A**) floxed *Ascl1* allele, (**B**) *rtTA* allele, (**C**) *Cre* transgene downstream of *tetO* promoter, (**D**) *EYFP* allele, and (**E**) *Cre* allele downstream of *Ascl1* promoter. *Ascl1*, achaete-scute homolog 1; *Cre*, Cre recombinase; *EYFP*, enhanced yellow fluorescent protein; *R26*, *Rosa26* promoter element; *rtTA*, reverse tetracycline-controlled transactivator; *tetO*, tetracycline-responsive promoter element.

**Table 1. List of Genomic PCR Primers**

| Primer Name                   | Primer Type                       | Sequence 5' -> 3'                 |
|-------------------------------|-----------------------------------|-----------------------------------|
| <i>Ascl1</i> Forward          | Common Forward                    | CTA CTG TCC AAA CGC AAA GTG G     |
| <i>Ascl1</i> Wildtype Reverse | Wildtype Reverse                  | GCT CCC ACA ATC CTC GTA AAG A     |
| <i>Ascl1</i> Mutant Reverse   | Mutant Reverse                    | TAG ACG TTG TGG CTG TTG TAG T     |
| <i>EYFP</i> Forward           | Common Forward                    | AAA GTC GCT CTG AGT TGT TAT       |
| <i>EYFP</i> Wild type Reverse | Wildtype Reverse                  | GGA GCG GGA GAA ATG GAT ATG       |
| <i>EYFP</i> Mutant Reverse    | Mutant Reverse                    | AAG ACC GCG AAG AGT TTG TC        |
| oIMR8545                      | Common Forward                    | AAA GTC GCT CTG AGT TGT TAT       |
| oIMR8546                      | Wildtype Reverse                  | GGA GCG GGA GAA ATG GAT ATG       |
| oIMR8052                      | Mutant Reverse                    | GCG AAG AGT TTG TCC TCA ACC       |
| oIMR1084                      | Transgene Forward                 | GCG GTC TGG CAG TAA AAA CTA TC    |
| oIMR1085                      | Transgene Reverse                 | GTG AAA CAG CAT TGC TGT CAC TT    |
| oIMR7338                      | Internal Positive Control Forward | CTA GGC CAC AGA ATT GAA AGA TCT   |
| oIMR7339                      | Internal Positive Control Reverse | GTA GGT GGA AAT TCT AGC ATC ATC C |
| 10841                         | Wildtype Forward                  | TCC AAC GAC TTG AAC TCT ATG G     |
| 10842                         | Wildtype Reverse                  | CCA GGA CTC AAT ACG CAG GG        |
| 10843                         | Mutant Forward                    | AAC TTT CCT CCG GGG CTC GTT TC    |
| 10653                         | Mutant Reverse                    | CGC CTG GCG ATC CCT GAA CAT G     |

vein at a dose of  $1 \times 10^{12}$  genomic copies per mouse on GD8, and mice were sacrificed on GD15, GD18, and GD19. Adeno-associated viruses with a null vector (Addgene, AV-8-PV0148) were used as controls.

#### **2.4 Tissue collection and histology**

Nonpregnant and maternal mouse serum and tissues, such as spleen, kidney, heart, lung, and placenta, were collected and weighed on various gestation days. Tissues were embedded in optimal cutting temperature (OCT) compound (Fisher Scientific, 23-730-571) on heptane cooled in dry ice and stored at  $-80^{\circ}\text{C}$  until processing. Parts of tissues were snap-frozen in liquid nitrogen and stored

at -80°C for protein and RNA extraction. The remaining tissues were fixed in 10% neutral buffered formalin (NBF) for 72 hrs and sent to the Histology Core at the Indiana Center for Musculoskeletal Health (Indiana University School of Medicine) to be embedded in paraffin and sectioned at 5 µm for hematoxylin and eosin (H&E) staining and histological analysis. Maternal pancreatic tissues were fixed in 4% paraformaldehyde (PFA) (Sigma Aldrich, 818715) for 24 hrs, embedded in paraffin, and sectioned at 7 µm for 5 layers at 50 µm apart.

## **2.5 Immunohistochemistry**

Formalin-fixed and paraffin-embedded maternal liver and placental tissue sections were deparaffinized in xylene, hydrated in alcohol gradients, epitope retrieved in citrate buffer (10 mM, pH 6.0) with 0.1% Tween-20 (Fisher Scientific, BP337-100) for 30 min, cooled to room temperature for 3 hrs, and endogenous peroxidase activity blocked using 3% H<sub>2</sub>O<sub>2</sub> for 10 min. The sections were blocked with the appropriate 2% normal serum (Jackson ImmunoResearch) in Dulbecco's phosphate-buffered saline (DPBS) (Quality Biological, 114-059-101) for 1 hr at room temperature. The sections were incubated with the appropriate diluted primary antibody (**Table 2**) in DPBS at 4°C overnight. The next day, the sections were incubated with the appropriate biotinylated secondary antibody (Jackson ImmunoResearch) for 1 hr followed by Vectastain Elite ABC HRP Kit (Vector Laboratories, PK-6100) for 30 min. The signals were developed by incubating the slides with a 3,3'-diaminobenzidine (DAB) solution (Sigma Aldrich, D8001). The sections were counterstained in hematoxylin (Leica, 3801575) for 1 min. Finally, the sections were dehydrated in alcohol gradients, incubated in xylene, and mounted (Vector Laboratories, H-5501).

## 2.6 Hepatocyte density

Liver sections stained with  $\beta$ -Catenin were used to count hepatocytes in five random fields of view at 400x magnification, acquired by Leica DM2000 microscope, using ImageJ (175).

**Table 2. List of Antibodies for Immunohistochemistry**

| <b>Name</b>      | <b>Company</b>           | <b>Catalog No.</b> | <b>Dilution</b> |
|------------------|--------------------------|--------------------|-----------------|
| $\beta$ -Catenin | BD Transduction          | 610153             | 1:100           |
| GFP              | abcam                    | ab6673             | 1:100           |
| HNF4 $\alpha$    | Santa Cruz               | sc-6556            | 1:100           |
| Insulin          | Santa Cruz               | sc-9168            | 1:100           |
| Ki67             | Thermo Fisher Scientific | RM-9106            | 1:100           |

## 2.7 Oil Red O staining

This staining method is used to detect fats such as lipids. Liver tissues were embedded in OCT compound (Fisher Scientific, 23-730-571) on dry-ice cooled heptane, stored at -80°C, and sectioned at 10  $\mu$ m using Leica CM3050 S Research Cryostat (Leica, 14047033518). In brief, the sections were air-dried at 37°C for 15 min, fixed in 10% NBF at room temperature for 10 min, and rinsed in water. Next, the sections were stained in the Oil Red O staining solution (Sigma-Aldrich, O0625) for 15 min, rinsed in 60% isopropanol (Acros Organics, 67-63-0) for 3 min and in water, and mounted (Vector Laboratories, H-5501). The slide images were acquired by the Leica DM2000 microscope and the stained area quantified using ImageJ (175).

## 2.8 Periodic Acid Schiff staining

This staining method is used to detect polysaccharides such as glycogen. Formalin-fixed and paraffin-embedded maternal liver and placental tissue sections were deparaffinized in xylene,

hydrated in alcohol gradients, oxidized in 0.5% periodic acid solution (Santa Cruz, sc-215695, 1:100) for 5 min, and rinsed in water. Next, the sections were incubated in Schiff's reagent solution (Santa Cruz, sc-301793) for 15 min, rinsed in water, and counterstained in hematoxylin (Leica, 3801575) for 1 min. Finally, the sections were dehydrated in alcohol gradients, incubated in xylene, and mounted (Vector Laboratories, H-5501). The slide images were acquired by the Leica DM2000 microscope.

## **2.9 $\beta$ -Cell mass**

Pancreatic sections stained with insulin (Santa Cruz, sc-9168, 1:100) were used to quantify insulin-positive  $\beta$  cell mass by the Eli Lilly and Company (Indianapolis, IN).

## **2.10 *In situ* hybridization**

*In situ* hybridization was performed using the appropriate probes and RNAscope 2.5 HD Assay (Advanced Cell Diagnostics, 322300) as per directions by the manufacturer. The following probes were used: *Ascl1* (Advanced Cell Diagnostics, 476321), *CD133* (Advanced Cell Diagnostics, 412221), *Igf2* (Advanced Cell Diagnostics, 437671), *PL-I* (Advanced Cell Diagnostics, 405521), and *PL-II* (Advanced Cell Diagnostics, 423681). A positive control probe *Ppib* (Advanced Cell Diagnostics, 310043) and a negative control probe *DapB* (Advanced Cell Diagnostics, 313911) were used to determine the efficacy of the protocol. *In situ* hybridization staining images were acquired by Leica DM2000 microscope.

## **2.11 Western blotting**

Tissue homogenates (10-30  $\mu$ g) were prepared from the snap-frozen liver and placental tissues using T-PER Tissue Protein Extraction Reagent (Thermo Fisher Scientific, 78510) and Halt

Protease and Phosphatase Inhibitor Cocktail (Thermo Fisher Scientific, 78443) as per directions by the manufacturer. Protein concentrations were determined by Pierce BSA Protein Assay Standards (Thermo Fisher Scientific, 23208) using NanoDrop 2000 spectrophotometer (Thermo Fisher Scientific, ND-2000). Proteins were separated under reducing conditions on NuPAGE 4-12% Bis-Tris Midi Protein Gels (Invitrogen, NP0336BOX or WG1403BOX) and transferred to PVDF transfer membranes (Thermo Fisher Scientific, 88518). The membranes were then blocked in 5% nonfat milk or BSA (Fisher Scientific, BP1605-100) in Tris-buffered saline (TBS) with 0.1% Tween-20 (Fisher Scientific, BP337-100). The membranes were incubated with the appropriate diluted primary antibody in 5% nonfat milk or BSA (**Table 3**). Immunoreactive proteins were detected by SuperSignal West Pico PLUS Chemiluminescent Substrate (Thermo Fisher Scientific, 34577) according to the manufacturer's protocol and imaged using ImageQuant LAS 4000 Mini (General Electric Life Sciences, 28-9558-15). The relative expression of the protein signals was quantified using ImageJ (175).

## **2.12 Intraperitoneal glucose tolerance tests and insulin measurements**

For the glucose tolerance test, data were collected from two different time points on gestation day (GD) 18 and GD19. On GD18, pregnant hep-*Ascl1*<sup>-/-</sup> mice were fasted for 6 hrs (9 AM to 3 PM) in a clean cage with woodchip bedding and water and injected intraperitoneally (i.p.) with D-glucose (Sigma, G5767) dissolved in Milli-Q water at 2 g of glucose per kg of body weight. Blood glucose levels were measured via tail vein using a glucometer (OneTouch Ultra 2) before glucose injection (T=0) and at 15, 30, 60, 90, and 120 min after glucose injection. On GD19, the hep-*Ascl1*<sup>-/-</sup> mice were fasted for 6 hrs, injected with glucose, and blood samples were collected before injection (T=0) and 30 min after injection, and the blood insulin levels were measured by the

Translation Core at the IU School of Medicine Center for Diabetes and Metabolic Diseases (Indiana University School of Medicine). *Ascl1<sup>fl/fl</sup>* mice were used as controls.

**Table 3. List of Antibodies for Western Blotting**

| <b>Name</b>          | <b>Company</b>       | <b>Catalog No.</b> | <b>Dilution</b> |
|----------------------|----------------------|--------------------|-----------------|
| AKT                  | Epitomics            | 108-1-1            | 1:3,000         |
| P-AKT (T308)         | abcam                | ab76297            | 1:5,000         |
| P-AKT (S473)         | Epitomics            | 2118-1             | 1:2,000         |
| CD133                | Abnova               | PAB12663           | 1:3,000         |
| P-4E-BP1             | Cell Signaling       | 2855               | 1:2,000         |
| ERK1/2               | Cell Signaling       | 9102               | 1:2,000         |
| P-ERK1/2 (T202/Y204) | Cell Signaling       | 4377               | 1:2,000         |
| FABP4                | Cell Signaling       | 3544               | 1:2,000         |
| GAPDH                | Cell Signaling       | 5174               | 1:2,000         |
| HGF                  | abcam                | ab83760            | 1:2,000         |
| IGF2                 | ABclonal             | A2086              | 1:1,000         |
| P-JAK2 (Y1007/1008)  | Cell Signaling       | 3776               | 1:2,000         |
| PL-II                | Gift from Dr. Soares |                    | 1:2,000         |
| P-mTOR (S2448)       | Cell Signaling       | 5536               | 1:2,000         |

### **2.13 Quantitative real-time polymerase chain reaction (qRT-PCR)**

Total RNA was isolated from snap-frozen liver tissue using TRIzol reagent (Invitrogen, 15596018) as per directions by the manufacturer. Complementary DNA (cDNA) was synthesized from 1 µg of total RNA, which was quantified by NanoDrop 2000 spectrophotometer (Thermo Fisher Scientific, ND-2000), using Verso cDNA kit (Thermo Fisher Scientific, AB1453B) and diluted four times with water. qRT-PCR was performed using the diluted cDNA with either

TaqMan Gene Expression Master Mix (Applied Biosystems, 4369016) or PowerUp SYBR Green Master Mix (Applied Biosystems, A25742) with specific TaqMan gene probes (**Tables 4 and 5**) (176). The qRT-PCR was performed using the 7300 Real-Time PCR System (Applied Biosystems, 4351103) and analyzed by the 7300 System SDS RQ Study Software (Applied Biosystems, 4350814). The qRT-PCR conditions using TaqMan Gene Expression Master Mix were UNG incubation (50°C/2 min), polymerase activation (95°C/10 min), and 40 cycles of PCR (95°C/15 sec, 60°C/1 min). The qRT-PCR conditions using PowerUp SYBR Green Master Mix were UDG activation (50°C/2 min), polymerase activation (95°C/2 min), 40 cycles of PCR (95°C/15 sec, 60°C/15 sec, 72°C/1 min), and dissociation curve (95°C/15 sec, 60°C/30 sec, 95°C/15 sec). Relative gene expression was calculated by the comparative CT method ( $\Delta\Delta C_t$ ) and normalized to 18S rRNA.

**Table 4. List of TaqMan qRT-PCR Primers**

| <b>Gene</b> | <b>Assay ID</b> | <b>Catalog No.</b> |
|-------------|-----------------|--------------------|
| Ascl1       | Mm03058063_m1   | 4453320            |
| CD133       | Mm01211402_m1   | 4448892            |
| Epcam       | Mm00493214_m1   | 4453320            |
| Igf2        | Mm00439564_m1   | 4331182            |
| Zfp568      | Mm01169272_m1   | 4448892            |
| 18S         | Mm03928990_g1   | 4453320            |

## **2.14 RNA sequencing**

Total RNA was isolated from snap-frozen liver tissue using the RNeasy Plus Mini Kit (Qiagen, 74134) as per directions by the manufacturer. RNA sequencing (RNA-seq) was performed and analyzed by the Center for Medical Genomics Core (Indiana University School of

Medicine). The concentration and quality of total RNA samples were first assessed using Agilent 2100 Bioanalyzer.

**Table 5 List of SYBR Green qRT-PCR Primers**

| <b>Primer Name</b> | <b>Sequence 5' -&gt; 3'</b>   |
|--------------------|-------------------------------|
| lgf2-all_F         | CGG CTT CTA CTT CAG CAG GC    |
| lgf2-all_R         | GTA TCT GGG GAA GTC GTC CG    |
| lgf2-P0_F          | TTT ATC CAC CGT CCG GGA AC    |
| lgf2-P0_R          | GCA GTC GTC GTA GTC GTT CT    |
| lgf2-P1_F          | CGG CAG CAC AGA TTT TGG AA    |
| lgf2-P1_R          | CAC CAA CAT CGA CTT CCC CA    |
| lgf2-P2_F          | CCC CAG CCC TAA GAT ACC CTA A |
| lgf2-P2_R          | AGC ACC AAC ATC GAC TTC CC    |
| lgf2-P3_F          | CGG CCT CCT TAC CCAACT TC     |
| lgf2-P3_R          | GGG GTG GCA CAG TAT GTC TC    |
| 18S_F              | CTC AAC ACG GGA AAC CTC AC    |
| 18S_R              | CGC TCC ACC AAC TAA GAA CG    |

As stated by the Center for Medical Genomics Core, a RIN (RNA Integrity Number) of five or higher was required to pass the quality control. Then five hundred nanograms of RNA per sample were used to prepare a single-indexed strand-specific cDNA library using TruSeq Stranded mRNA Library Prep Kit (Illumina). The resulting libraries were assessed for its quantity and size distribution using Qubit and Agilent 2100 Bioanalyzer. Two hundred picomolar pooled libraries were utilized per flowcell for clustering amplification on cBot using HiSeq 3000/4000 PE Cluster Kit and sequenced with 2x75 bp paired-end configuration on HiSeq4000 (Illumina) using HiSeq

3000/4000 PE SBS Kit. A Phred quality score (Q score) was used to measure the quality of sequencing. More than 90% of the sequencing reads reached Q30 (99.9% base call accuracy).

The sequencing data were first assessed using FastQC (Babraham Bioinformatics, Cambridge, UK) for quality control. Then all sequenced libraries were mapped to the mouse genome (UCSC mm10) using STAR RNA-seq aligner with the following parameter: “--outSAMmapqUnique 60”. The reads distribution across the genome was assessed using bamutils (from ngsutils). Uniquely mapped sequencing reads were assigned to mm10 refGene genes using featureCounts (from subread) with the following parameters: “-s 2 -p -Q 10”. Quality control of sequencing and mapping results were summarized using MultiQC. Genes with read count per million (CPM) < 0.5 in more than 5 of the samples were removed. The data were normalized using TMM (trimmed mean of M values) method. Differential expression analysis was performed using edgeR and Ingenuity Pathway Analysis (IPA) with +/- 2-fold change and  $P < 0.05$ . False discovery rate (FDR) was computed from p-values using the Benjamini-Hochberg procedure.

### **2.15 Serum biochemistry**

Nonpregnant and pregnant maternal blood were collected on gestation day (GD) 15 and GD18 and left to clot at room temperature for at least 1 hr. After two centrifugations at 3000 RPM and collecting the supernatant, the serum was analyzed by the Eli Lilly and Company (Indianapolis, IN).

### **2.16 Microbiome 16S sequencing**

Total microbial DNA was isolated from the snap-frozen cecal sample using the PureLink Microbiome DNA Purification Kit (Invitrogen, A29789) as per directions by the manufacturer.

Microbiome 16S sequencing was performed and analyzed by the Zymo Research Corporation (Irvine, CA).

As stated by the Zymo Research Corporation, bacterial 16S ribosomal RNA gene targeted sequencing was performed using the Quick-16S NGS Library Preparation Kit (Zymo Research, Irvine, CA). The bacterial 16S primers used amplified the V3-V4 region of the 16S rRNA gene. These primers have been custom-designed by Zymo Research to provide the best coverage of the 16S gene while maintaining high sensitivity. They amplify the V3-V4 region of the 16S rRNA gene. The sequencing library was prepared using an innovative library preparation process in which PCR reactions were performed in real-time PCR machines to control cycles and therefore prevent PCR chimera formation. The final PCR products are quantified with qPCR fluorescence readings and pooled together based on equal molarity. The final pooled library was cleaned up with Select-a-Size DNA Clean & Concentrator (Zymo Research, Irvine, CA), then quantified with TapeStation and Qubit. The final library was sequenced on Illumina MiSeq with a v3 reagent kit (600 cycles). The sequencing was performed with >10% PhiX spike-in.

Amplicon sequences were inferred from raw reads using the Dada2 pipeline. Chimeric sequences were also removed with the Dada2 pipeline. Taxonomy assignment, composition bar charts, alpha-diversity, and beta-diversity analyses were performed with Qiime v.1.9.1. Taxa that have an abundance significantly different among groups were identified by LEfSe with default settings if applicable. Other analyses were performed with in-house scripts. Differential expression analysis was assessed using IPA with +/- 2-fold change and  $P < 0.05$ .

## **2.17 Statistics**

Sample sizes for all data were at least three mice, which were determined by the success rate of pregnancy and a fetal number of at least six pups. To prevent experimental bias in hepatocyte-

specific *Ascl1* deletion, hep-*Ascl1*<sup>-/-</sup> (*Ascl1*<sup>fl/fl</sup>;R26<sup>EYFP/EYFP</sup>) mice were divided randomly into experimental and control groups. Statistical analyses were performed using a two-sided unpaired Student's t-test. All data were shown as mean value ± standard deviation (SD). Significance was defined when  $P < 0.05$ .

## CHAPTER 3. RESULTS

### 3.1 Maternal liver activates hepatic *Ascl1* during pregnancy

During pregnancy, the maternal liver adapts to the rapid growth and development of the placenta and fetus by changing its gene profile (27, 177). We previously reported the pregnancy-dependent activation of maternal hepatic *Ascl1*, a gene associated with neural development in the rat (177). We also observed the same activation of hepatic *Ascl1* in pregnant mice in our unpublished DNA microarray data. To verify our data, we performed a timed-pregnancy experiment on C57BL6/J mice and detected the activation of maternal hepatic *Ascl1* mRNA (**Fig. 2A**). Consistent with the idea that hepatic *Ascl1* expresses during pregnancy, qRT-PCR of hepatic *Ascl1* mRNA expression showed a time-dependence pattern where it remained at a basal level from nonpregnant until gestation day (GD) 10 but began to elevate significantly from GD11 until GD15 and started to decline in GD18. Surprisingly, when compared to the nonpregnant state, the hepatic *Ascl1* mRNA exhibited an up to 26,000-fold increase on GD15. *In situ* hybridization detected the expression of *Ascl1* mRNA localized in the nucleus and cytosol of the *Ascl1*-expressing cells in the maternal liver (**Fig. 2B**). Thus, pregnancy induces the maternal liver to activate the proneural *Ascl1* gene, which peaks during mid to late gestation.

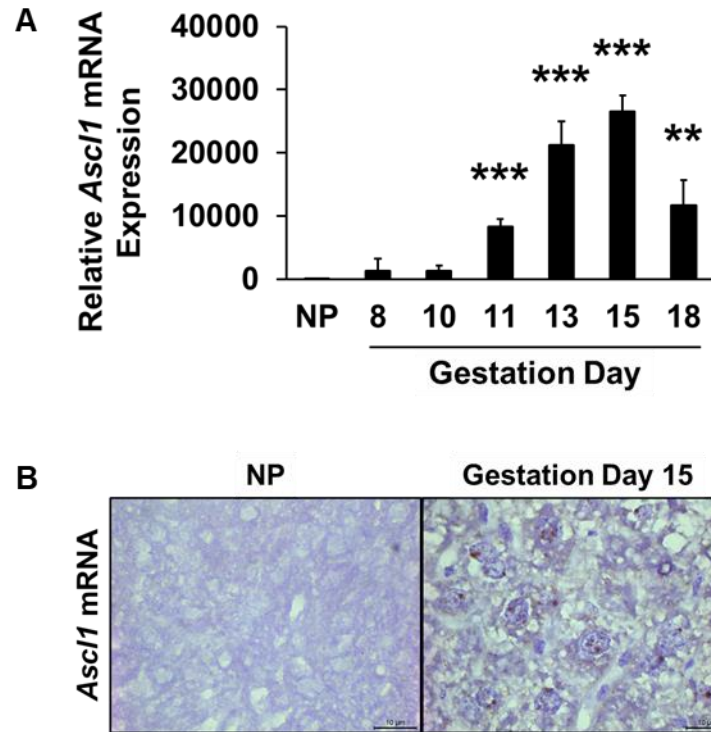


**Figure 2. Activation of maternal hepatic *Ascl1*.** (A) *Ascl1* mRNA expression in the maternal liver. The presence of a copulation plug was designated as gestation day 1. Total RNA was isolated from livers of nonpregnant (NP) and pregnant (gestation days 8, 10, 11, 13, 15, and 18) C57BL6/J mice. Hepatic *Ascl1* mRNA levels were measured using quantitative real-time polymerase chain reaction (qRT-PCR) and expressed as the mean fold changes relative to NP controls ( $\pm$  s.d.;  $n = 3$  for each group). \*\*,  $P < 0.01$ ; \*\*\*,  $P < 0.001$ , compared with NP controls.  $\beta$ -*Actin* mRNA levels were used as endogenous controls. (B) *Ascl1* mRNA distribution in the maternal liver. Liver sections of NP and gestation day 15 C57BL6/J mice subjected to *Ascl1* *in situ* hybridization using RNAscope 2.5 HD Assay-BROWN kit. The *Ascl1* mRNA is stained dark brown. *Ascl1*, achaete-scute homolog 1.

## 3.2 Global deletion of *Ascl1*

### 3.2.1 Generation of global inducible *Ascl1* knockout mouse model

To assess the role of maternal hepatic *Ascl1* in pregnancy, we generated a global inducible *Ascl1* knockout (*Ascl1*<sup>-/-</sup>) (*Ascl1*<sup>fl/fl</sup>; *R26*<sup>rtTA/rtTA</sup>; *tetO*<sup>Cre/-</sup>) mice (Fig. 3A). In this *Ascl1*<sup>-/-</sup> mice, the *Rosa26* promoter element (*R26*) ubiquitously expresses reverse tetracycline-controlled

transactivator (*rtTA*). The *rtTA* activates with the presence of doxycycline and initiates the tetracycline-responsive promoter element (*tetO*) to drive the expression of *Cre* recombinase to delete the loxP-flanked *Ascl1* gene. As a result, with the administration of doxycycline, all the cells in the body, with the exception of the brain and the testis due to the inability of doxycycline to pass the blood-brain barrier and blood-testis barrier, delete *Ascl1* (178). For control mice, we generated the *Ascl1*<sup>+/+</sup> (*Ascl1*<sup>+/+</sup>;*R26*<sup>rtTA/rtTA</sup>;*tetO*<sup>Cre/-</sup>) mice that do not contain the loxP-flanked *Ascl1* gene. After allowing the mice to drink the doxycycline water (1 mg/ml) *ad libitum* from gestation day (GD) 6, we collected maternal livers from both *Ascl1*<sup>+/+</sup> and *Ascl1*<sup>-/-</sup> mice on GD9, 11, 13, 15, and 18 (**Fig. 3B**). qRT-PCR showed, similar to C57BL6/J mice, the basal expression of hepatic *Ascl1* in nonpregnant female mice, and confirmed the activation of the hepatic *Ascl1* mRNA expression in *Ascl1*<sup>+/+</sup> mice and its successful ablation in *Ascl1*<sup>-/-</sup> mice on GD15 by 99.7% (**Fig. 3C**). Therefore, we were able to generate a doxycycline-induced global *Ascl1* knockout mouse model and effectively delete *Ascl1* during pregnancy.

### 3.2.2 Global deletion of *Ascl1* causes maternal liver abnormalities

To determine if the loss of *Ascl1* during pregnancy resulted in *Ascl1*-dependent phenotypes, we collected maternal livers and fetuses. After the *Ascl1* ablation during pregnancy, we observed *Ascl1*-dependent abnormalities in the maternal liver. The *Ascl1*<sup>-/-</sup> mice showed a marked increase in liver-to-body weight ratio on gestation day (GD) 18 by 20% (**Fig. 4A**). Hematoxylin and eosin (H&E) staining showed aberrant staining patterns in the *Ascl1*<sup>-/-</sup> maternal livers, which had a layer of unstained substance and around the nuclei of hepatocytes during mid to late gestation (**Fig. 4B**). Furthermore, a proliferation marker Ki67 staining showed increased numbers of *Ascl1*<sup>-/-</sup> maternal hepatocytes undergoing cell cycle on GD13 by 277% and on GD15 by 204% (**Fig. 4C-D**). Finally, Oil Red O (ORO) staining showed increased lipid accumulation in *Ascl1*<sup>-/-</sup> maternal livers on

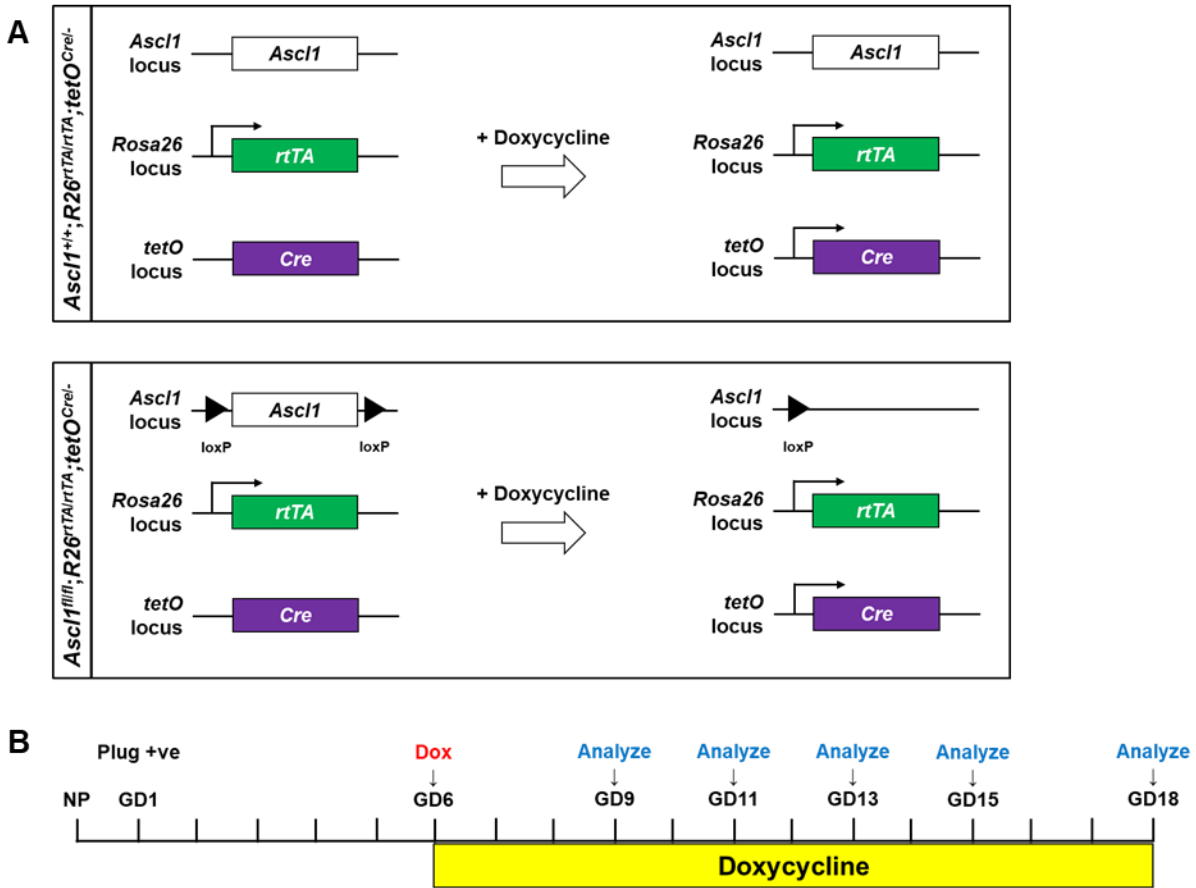
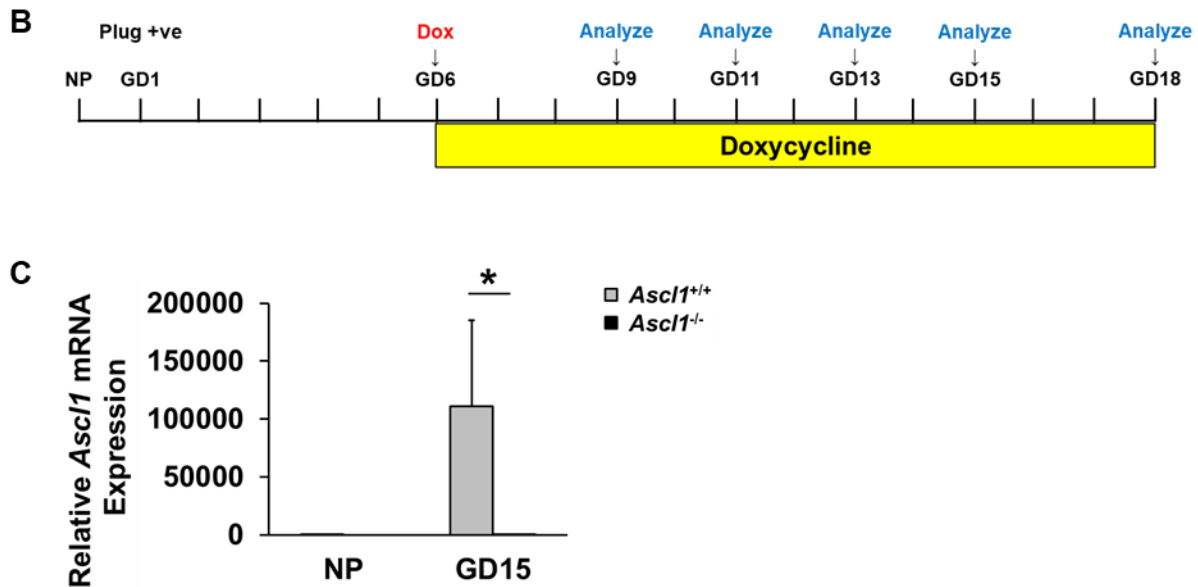


**Figure 3. Doxycycline-induced global *Ascl1* knockout mouse model.** (A) The strategy of generating a global inducible *Ascl1* knockout mouse model. In the global inducible *Ascl1* knockout ( $Ascl1^{-/-}$ ) ( $Ascl1^{fl/fl};R26^{rtTA/rtTA};tetO^{Cre/-}$ ) mice, the *Rosa26* promoter element (*R26*) ubiquitously expresses the reverse tetracycline-controlled transactivator (*rtTA*). *rtTA* becomes activated by binding with doxycycline and turns on the tetracycline-responsive promoter element (*tetO*) to express *Cre* recombinase. *Cre* recombinase excises out the loxP-flanked *Ascl1*, resulting in the deletion of *Ascl1* in the whole body except in the brain and testis. In the control mice ( $Ascl1^{+/+}$ ) ( $Ascl1^{+/+};R26^{rtTA/rtTA};tetO^{Cre/-}$ ), the *Ascl1* lacks the loxP sites and, therefore, remains intact after doxycycline treatment. (B) Doxycycline treatment timeline. The presence of a copulation plug (plug +ve) was designated as gestation day (GD) 1. Doxycycline was administered in drinking water (1 mg/ml) for both  $Ascl1^{+/+}$  and  $Ascl1^{-/-}$  mice from GD6 until maternal samples were collected on GD9, 11, 13, 15, and 18. (C) *Ascl1* mRNA expression in the maternal liver. Total RNA was isolated from livers of nonpregnant (NP) and gestation day 15  $Ascl1^{+/+}$  and  $Ascl1^{-/-}$  mice. Hepatic *Ascl1* mRNA levels were measured using quantitative real-time polymerase chain reaction (qRT-PCR) and expressed as the mean fold changes relative to NP controls ( $\pm$  s.d.;  $n = 3$  for each group). \*,  $P < 0.05$ , between  $Ascl1^{+/+}$  and  $Ascl1^{-/-}$  mice. *Albumin* mRNA levels were used as endogenous controls. *Ascl1*, achaete-scute homolog 1.

Figure 3, continued.



GD18 (**Fig. 4E**). Although maternal liver plays an essential role in the growth of the fetus, maternal liver abnormalities resulted from hepatic *Ascl1* deletion did not affect the fetal weight and number (**Fig. 4F-G**). Taken together, we revealed that *Ascl1* modulates the structure, cell cycle, and lipid metabolism of maternal hepatocytes.

### 3.2.3 Global deletion of *Ascl1* causes alterations in sera

To determine functional alterations in the maternal body resulted from deleting *Ascl1*, we collected nonpregnant and maternal serums from *Ascl1*<sup>+/+</sup> and *Ascl1*<sup>-/-</sup> mice and performed serum analysis. We observed changes in the liver function such as decreased levels of blood urea nitrogen, albumin, globulin, and total protein; lipid metabolism such as increased levels of free fatty acids; and placental secretion such as alkaline phosphatase (**Fig. 5, Table 6**). These data show that the deletion of maternal *Ascl1* during pregnancy causes dysfunctions in the liver, placenta, and lipid metabolism, and results in abnormal maternal biochemical profile.

**Figure 4. Global *Ascl1* ablation phenotypes. (A-E) Maternal liver changes.** Maternal livers were collected and weighed from *Ascl1*<sup>+/+</sup> and *Ascl1*<sup>-/-</sup> mice (described in **Fig. 3**). **(A)** The maternal liver-to-body weight ratios of *Ascl1*<sup>+/+</sup> and *Ascl1*<sup>-/-</sup> mice are presented. Data are expressed as means ± s.d. (n = 5-9). \*\*, *P* < 0.01, between *Ascl1*<sup>+/+</sup> and *Ascl1*<sup>-/-</sup> mice. **(B)** Maternal liver histology. Maternal liver sections of *Ascl1*<sup>+/+</sup> and *Ascl1*<sup>-/-</sup> mice were subjected to hematoxylin and eosin (H&E) staining. **(C-D)** Maternal hepatocyte proliferation. **(C)** Nonpregnant and maternal liver sections were subjected to Ki67 staining. Ki67-positive cells are stained dark brown in the nucleus. **(D)** Nuclear Ki67-positive hepatocytes were counted in five random fields of view (200X magnification) and the data are expressed as the means ± s.d. (n = 3-5). \*\*, *P* < 0.01, between *Ascl1*<sup>+/+</sup> and *Ascl1*<sup>-/-</sup> mice. **(E)** Maternal liver lipid deposition. Gestation day 18 maternal liver sections of *Ascl1*<sup>+/+</sup> and *Ascl1*<sup>-/-</sup> mice were subjected to Oil Red O (ORO) staining. The lipid droplets are stained red. **(F-G)** Fetal outcome. Weight **(F)** and number **(G)** of pups born from *Ascl1*<sup>+/+</sup> and *Ascl1*<sup>-/-</sup> dams are presented. Data are expressed as means ± s.d. (n = 5-9). *Ascl1*, achaete-scute homolog 1.

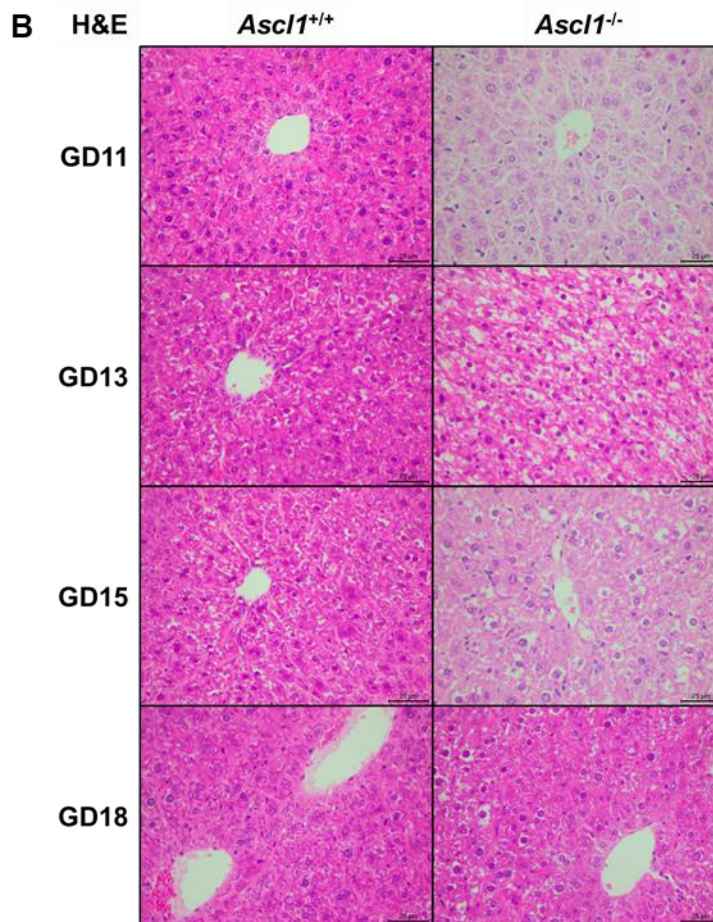
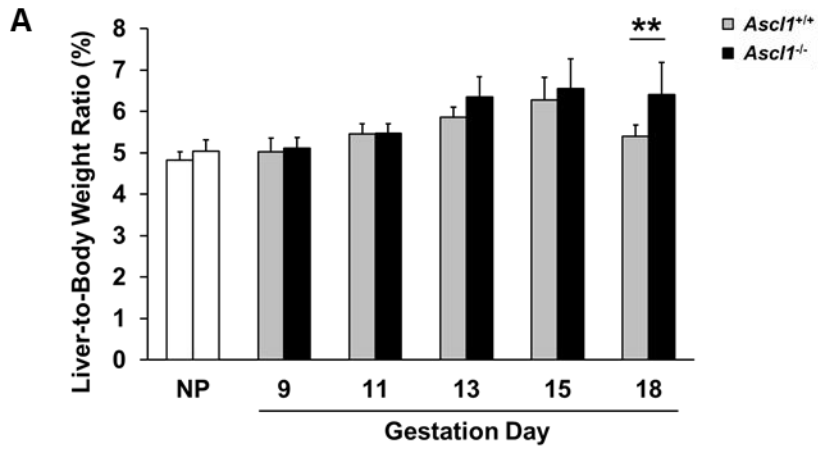


Figure 4, continued.

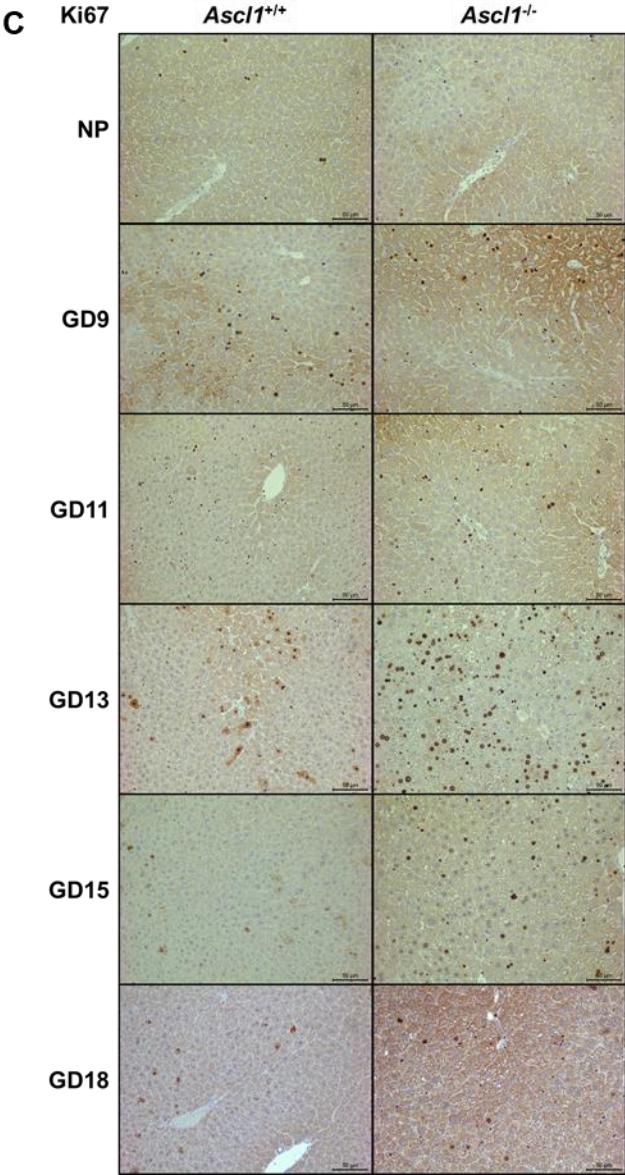
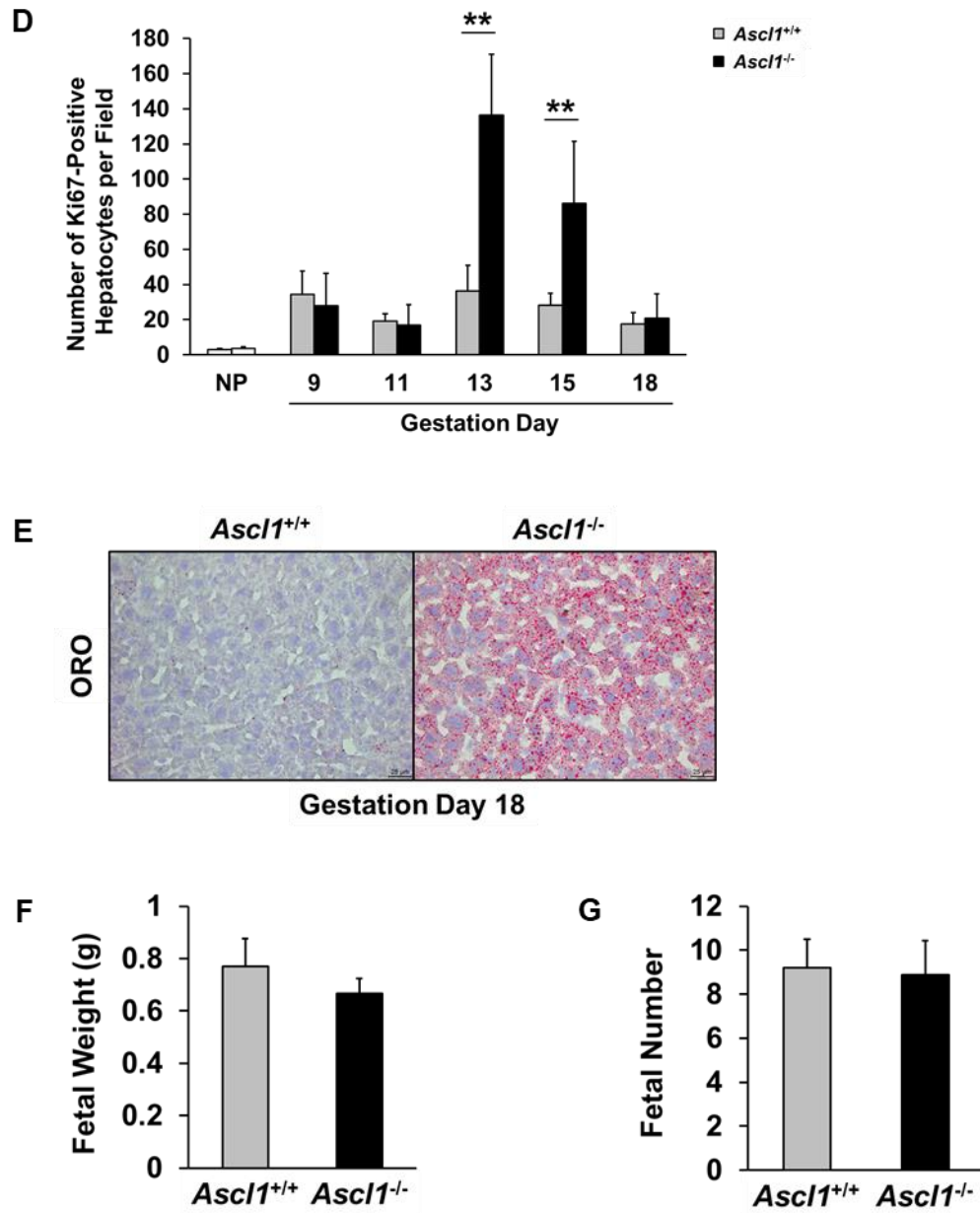


Figure 4, continued.



**Figure 5. Maternal serum biochemical profile.** Maternal serum was collected from *Ascl1*<sup>+/+</sup> and *Ascl1*<sup>-/-</sup> mice (described in **Fig. 3**). Maternal serum biochemical profiles from *Ascl1*<sup>+/+</sup> and *Ascl1*<sup>-/-</sup> mice were analyzed by Eli Lilly and Company. Data are expressed as means  $\pm$  s.d. (n = 5). \*,  $P < 0.05$ ; \*\*,  $P < 0.01$ ; \*\*\*,  $P < 0.001$ , between *Ascl1*<sup>+/+</sup> and *Ascl1*<sup>-/-</sup> mice. *Ascl1*, achaete-scute homolog 1; BUN, blood urea nitrogen; Enz Creat, creatinine; ALP, alkaline phosphatase; ALT, alanine aminotransferase; AST, aspartate aminotransferase; CK, creatine kinase; Na, sodium; K, potassium; Cl, chloride; Ca, calcium; IP, inorganic phosphate; Glu, glucose; Chol, cholesterol; HDL Chol, high-density lipoprotein cholesterol; LDL Chol, low-density lipoprotein cholesterol; Trig, triglyceride; Phos Lipid, phospholipid; FFA, free fatty acid; Free Chol, free cholesterol; TP, total protein; Alb, albumin; A/G, albumin/globulin.

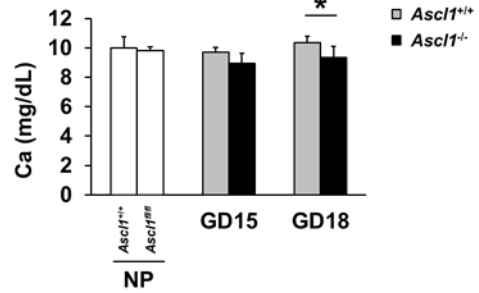
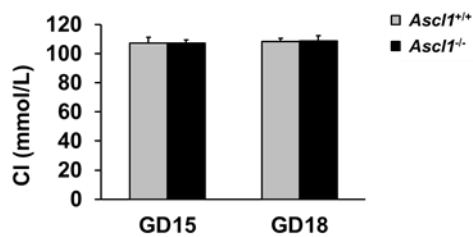
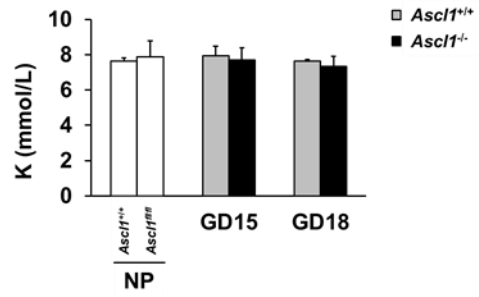
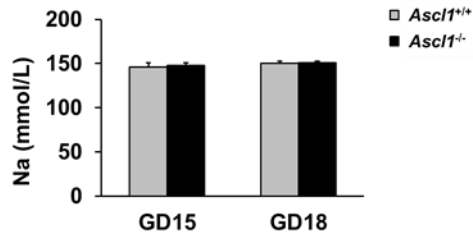
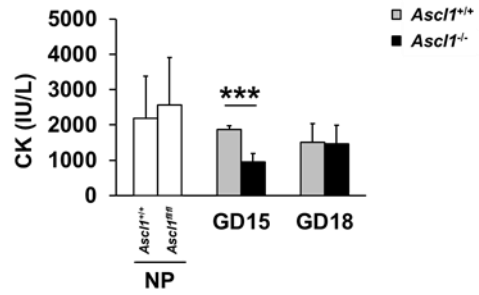
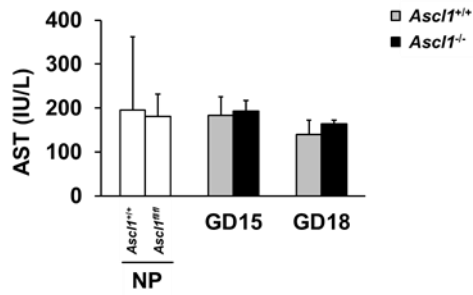
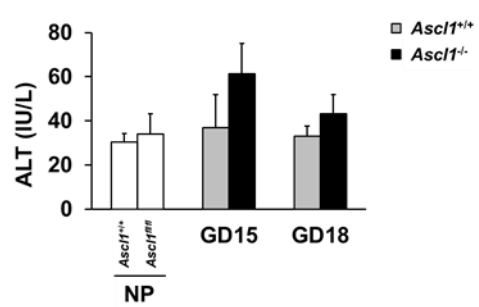
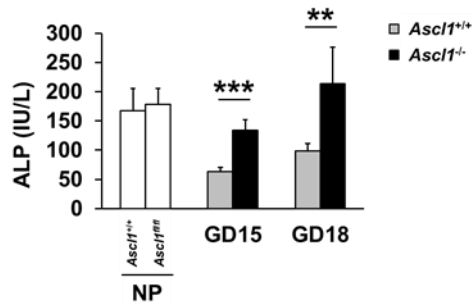
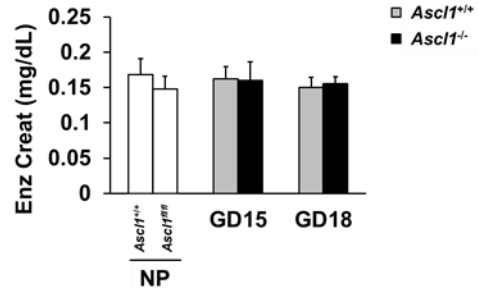
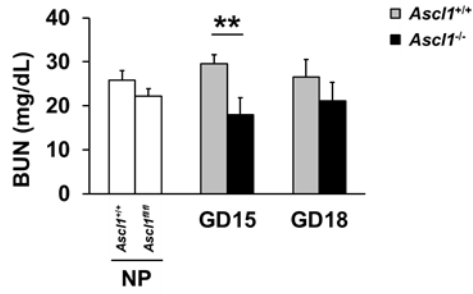


Figure 5, continued.

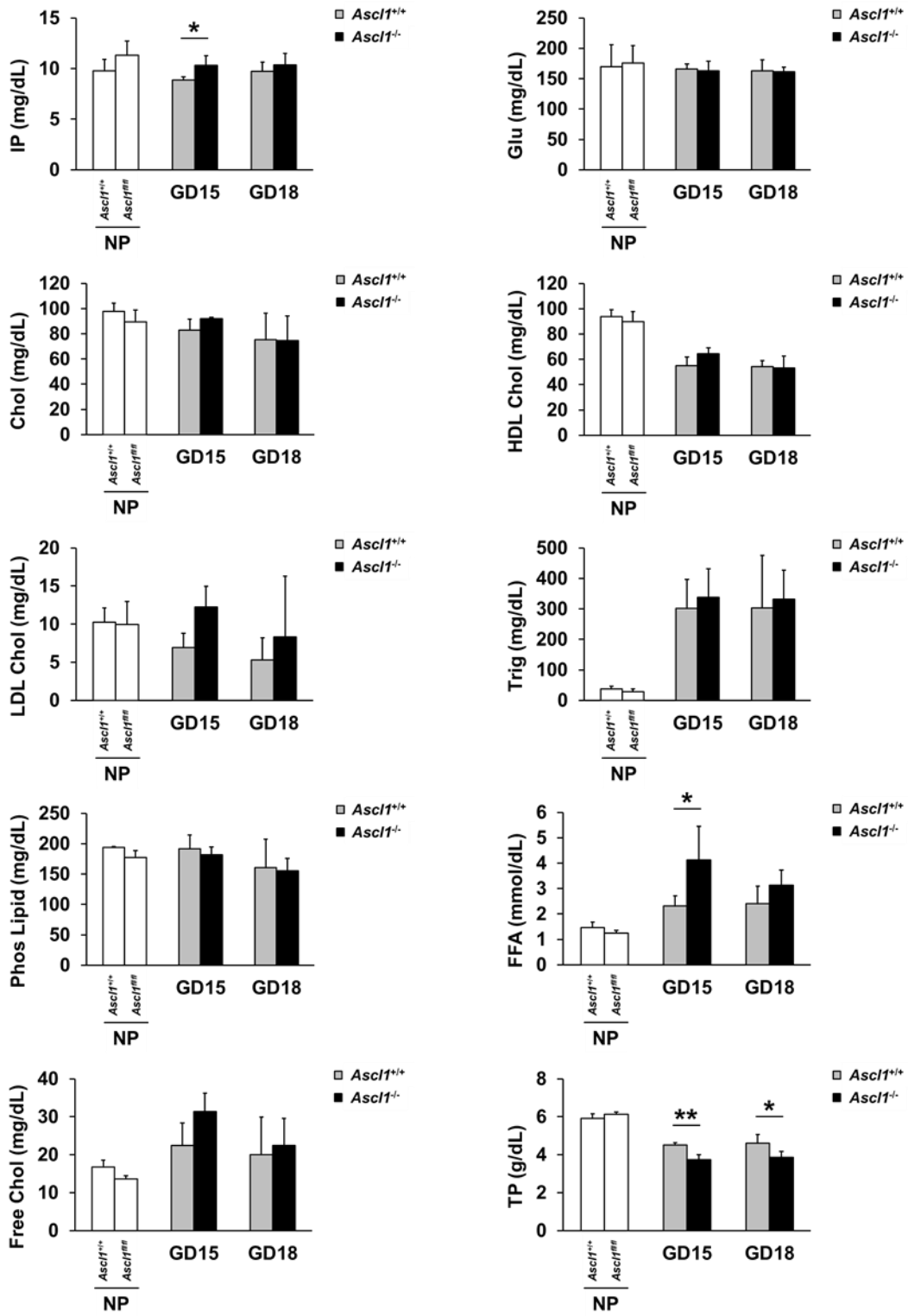
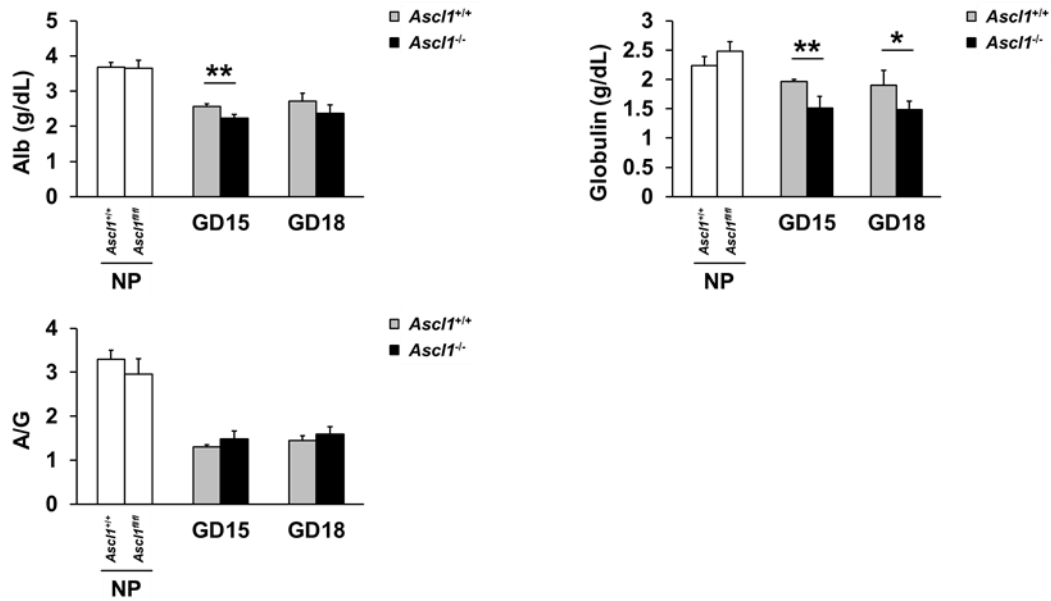


Figure 5, continued.



### 3.3 Cell-specific deletion of *Ascl1*

#### 3.3.1 Generation of cell-specific inducible *Ascl1* knockout mouse model

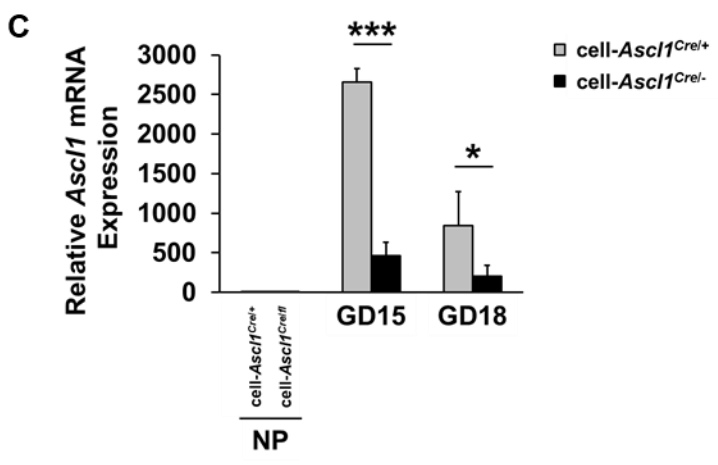
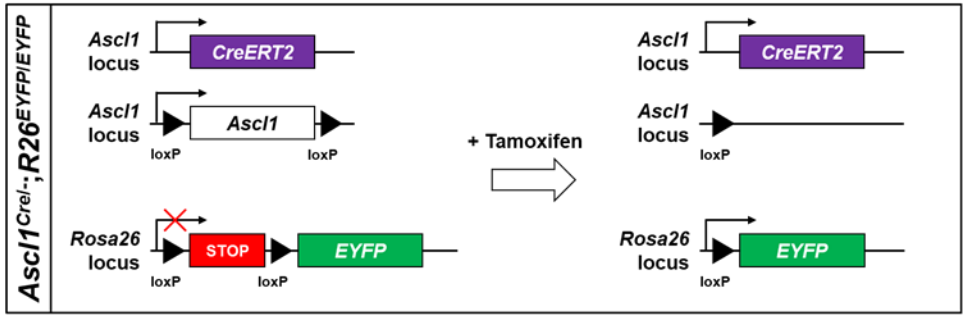
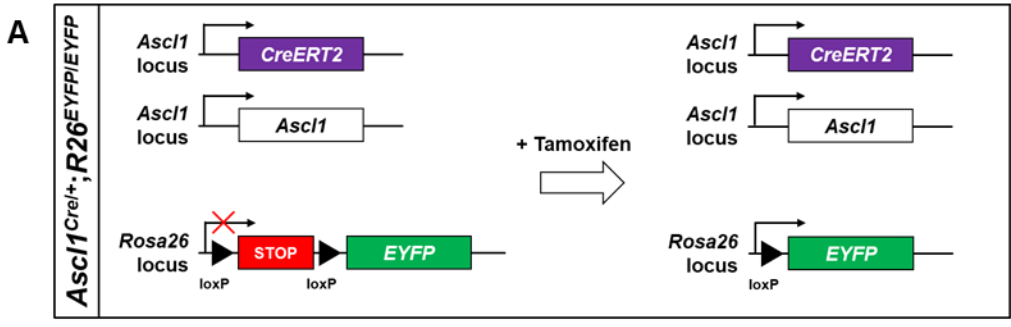
We then tested whether the deletion of *Ascl1* specifically in the *Ascl1*-expressing cells causes similar maternal liver abnormalities, and thus complicates the overall pregnancy. To achieve both the deletion and labeling of *Ascl1* in *Ascl1*-expressing cells, we generated the cell-*Ascl1*<sup>Cre/-</sup> (*Ascl1*<sup>Cre/fl</sup>; *R26*<sup>EYFP/EYFP</sup>) mouse line (Fig. 6A). In this inducible *Ascl1* knockout mouse line, *Ascl1*-expressing cells express *Cre* recombinase fused with tamoxifen-activated mutant estrogen ligand-binding domain (*ERT2*) (*CreERT2*) and, with the administration of tamoxifen, remove the floxed *Ascl1* gene while at the same time delete the transcriptional Stop cassette, which activates the expression of enhanced yellow fluorescent protein (*EYFP*). For control, we generated the cell-*Ascl1*<sup>Cre/+</sup> (*Ascl1*<sup>Cre/+</sup>; *R26*<sup>EYFP/EYFP</sup>) mouse line, which lacked the floxed *Ascl1* allele. The breeding

**Table 6 List of Serum Biochemical Profiles in Global *Ascl1* Gene Knockout**

| Name       | Unit  | NP                          |                             | GD15                        |                             | GD18                        |                             |
|------------|-------|-----------------------------|-----------------------------|-----------------------------|-----------------------------|-----------------------------|-----------------------------|
|            |       | <i>Ascl1</i> <sup>+/+</sup> | <i>Ascl1</i> <sup>-/-</sup> | <i>Ascl1</i> <sup>+/+</sup> | <i>Ascl1</i> <sup>-/-</sup> | <i>Ascl1</i> <sup>+/+</sup> | <i>Ascl1</i> <sup>-/-</sup> |
| BUN        | mg/dL | 25.9 ± 2.1                  | 22.2 ± 1.7                  | 29.6 ± 2.1                  | 18.0 ± 3.9                  | 26.5 ± 4.1                  | 21.2 ± 4.2                  |
| Enz Creat  | mg/dL | 0.17 ± 0.02                 | 0.15 ± 0.02                 | 0.16 ± 0.02                 | 0.16 ± 0.03                 | 0.15 ± 0.01                 | 0.16 ± 0.01                 |
| ALP        | IU/L  | 168 ± 38                    | 178 ± 27                    | 64 ± 7                      | 134 ± 19                    | 99 ± 12                     | 214 ± 62                    |
| ALT        | IU/L  | 30 ± 4                      | 34 ± 9                      | 37 ± 15                     | 61 ± 14                     | 33 ± 5                      | 43 ± 9                      |
| AST        | IU/L  | 195 ± 168                   | 181 ± 51                    | 183 ± 43                    | 193 ± 24                    | 140 ± 32                    | 165 ± 8                     |
| CK         | IU/L  | 2189 ± 1186                 | 2570 ± 1334                 | 1873 ± 97                   | 951 ± 245                   | 1499 ± 528                  | 1467 ± 518                  |
| Na         | mmo/L | N/A                         | N/A                         | 146 ± 5                     | 148 ± 3                     | 150 ± 3                     | 151 ± 2                     |
| K          | mmo/L | 7.6 ± 0.2                   | 7.9 ± 0.9                   | 8.0 ± 0.5                   | 7.7 ± 0.7                   | 7.6 ± 0.1                   | 7.3 ± 0.6                   |
| Cl         | mmo/L | N/A                         | N/A                         | 107 ± 4                     | 107 ± 2                     | 108 ± 2                     | 109 ± 4                     |
| Ca         | mg/dL | 10.0 ± 0.7                  | 9.8 ± 0.3                   | 9.7 ± 0.3                   | 8.9 ± 0.7                   | 10.4 ± 0.5                  | 9.4 ± 0.8                   |
| IP         | mg/dL | 9.76 ± 1.13                 | 11.32 ± 1.40                | 8.88 ± 0.33                 | 10.30 ± 0.96                | 9.74 ± 0.90                 | 10.35 ± 1.17                |
| Glu        | mg/dL | 169.9 ± 35.9                | 176.0 ± 28.1                | 165.7 ± 8.2                 | 162.6 ± 16.5                | 163.1 ± 17.9                | 161.1 ± 7.9                 |
| Chol       | mg/dL | 98 ± 7                      | 90 ± 9                      | 83 ± 8                      | 92 ± 1                      | 75 ± 21                     | 75 ± 20                     |
| HDL Chol   | mg/dL | 93.9 ± 5.3                  | 89.6 ± 8.0                  | 54.9 ± 7.2                  | 64.4 ± 4.9                  | 54.2 ± 4.9                  | 53.1 ± 9.5                  |
| LDL Chol   | mg/dL | 10.2 ± 1.9                  | 10.0 ± 3.0                  | 6.9 ± 1.9                   | 12.2 ± 2.8                  | 5.3 ± 2.9                   | 8.3 ± 8.0                   |
| Trig       | mg/dL | 38.0 ± 8.7                  | 28.8 ± 7.9                  | 301.7 ± 95.8                | 337.4 ± 94.3                | 303.8 ± 171.7               | 331.6 ± 95.1                |
| Phos Lipid | mg/dL | 194 ± 1                     | 177 ± 12                    | 192 ± 23                    | 182 ± 13                    | 161 ± 46                    | 156 ± 20                    |
| FFA        | mmo/L | 1.47 ± 0.21                 | 1.25 ± 0.11                 | 2.31 ± 0.40                 | 4.14 ± 1.31                 | 2.41 ± 0.69                 | 3.14 ± 0.60                 |
| Free Chol  | mg/dL | 17 ± 2                      | 14 ± 1                      | 23 ± 6                      | 31 ± 5                      | 20 ± 10                     | 23 ± 7                      |
| TP         | g/dL  | 5.92 ± 0.23                 | 6.13 ± 0.13                 | 4.52 ± 0.11                 | 3.74 ± 0.26                 | 4.61 ± 0.46                 | 3.85 ± 0.32                 |
| Alb        | g/dL  | 3.68 ± 0.13                 | 3.64 ± 0.24                 | 2.56 ± 0.09                 | 2.23 ± 0.11                 | 2.72 ± 0.23                 | 2.37 ± 0.24                 |
| Globulin   | g/dL  | 2.24 ± 0.15                 | 2.48 ± 0.16                 | 1.96 ± 0.04                 | 1.51 ± 0.20                 | 1.90 ± 0.25                 | 1.49 ± 0.14                 |
| A/G        |       | 3.30 ± 0.20                 | 2.95 ± 0.35                 | 1.31 ± 0.05                 | 1.49 ± 0.17                 | 1.44 ± 0.11                 | 1.60 ± 0.17                 |

strategy was such that both genotypes were present among the littermates. After injecting tamoxifen on gestation days (GD) 13 and 14, we collected maternal livers from both genotypes on GD15 and GD18 for analysis (**Fig. 6B**). qRT-PCR showed that the nonpregnant livers from both genotypes had a similar basal expression of *Ascl1* mRNA, whereas the *Ascl1*<sup>Cre/-</sup> mouse livers had 82.5% and 75.9% reduction in *Ascl1* mRNA expression when compared with the controls on GD15 and GD18, respectively (**Fig. 6C**). Thus, we were able to generate a cell-specific *Ascl1* knockout mouse model and delete *Ascl1* in hepatic *Ascl1*-expressing cells.

**Figure 6. Tamoxifen-induced cell-specific *Ascl1* knockout mouse model.** (A) The strategy in generating cell-specific inducible *Ascl1* knockout mouse model. In the cell-specific inducible *Ascl1* knockout (cell-*Ascl1*<sup>Cre/-</sup>) (*Ascl1*<sup>Cre/fl</sup>;R26<sup>EYFP/EYFP</sup>) (R26-LoxP-Stop-LoxP-EYFP) mice, the *Ascl1*-expressing cells express *CreERT2*, which is a Cre recombinase fused with a mutant estrogen ligand-binding domain (*ERT2*) that is activated only by tamoxifen, but not naturally occurring estrogen. With the administration of tamoxifen, *Cre-ERT2* fusion protein translocates into the nucleus and excises out the loxP-flanked *Ascl1* and the transcriptional Stop cassette upstream of enhanced yellow fluorescent protein (*EYFP*). As a result, the *Ascl1*-expressing cells delete *Ascl1* and express *EYFP*. In the control mice (cell-*Ascl1*<sup>Cre/+</sup>) (*Ascl1*<sup>Cre/+</sup>;R26<sup>EYFP/EYFP</sup>), *Ascl1* lacks the loxP sites and, therefore, remains intact after tamoxifen treatment while still being labeled with *EYFP*. (B) Tamoxifen treatment timeline. The presence of a copulation plug (plug +ve) was designated as gestation day (GD) 1. Tamoxifen was intraperitoneally injected (i.p., 60 mg/kg) on GD13 and GD14 and maternal samples were collected on GD15 and GD18. (C) *Ascl1* mRNA expression in the maternal liver. Total RNA was isolated from livers of nonpregnant (NP) and gestation day 15 cell-*Ascl1*<sup>Cre/+</sup> and cell-*Ascl1*<sup>Cre/-</sup> mice. Hepatic *Ascl1* mRNA levels were measured using quantitative real-time polymerase chain reaction (qRT-PCR) and expressed as the mean fold changes relative to NP controls ( $\pm$  s.d.; n = 4-5). \*,  $P < 0.05$ ; \*\*\*,  $P < 0.001$ , between cell-*Ascl1*<sup>Cre/+</sup> and cell-*Ascl1*<sup>Cre/-</sup> mice. *18S* ribosomal RNA (rRNA) levels were used as endogenous controls. *Ascl1*, achaete-scute homolog 1.



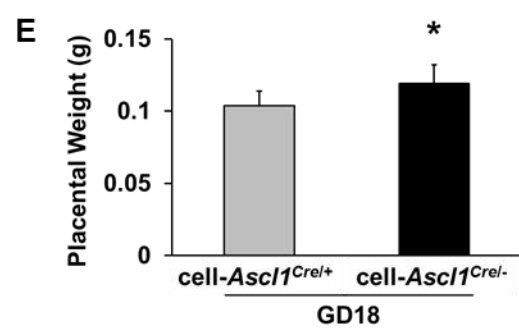
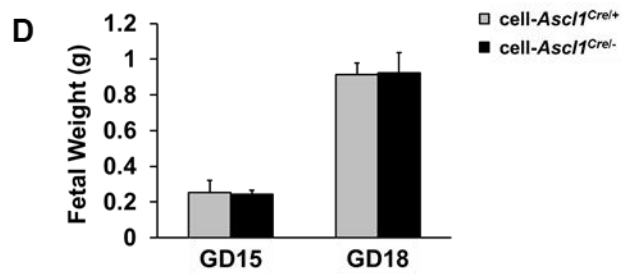
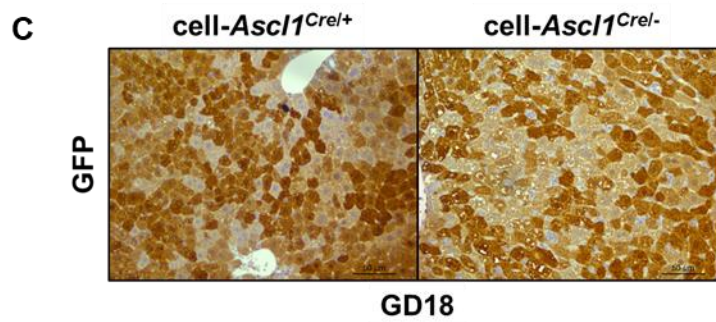
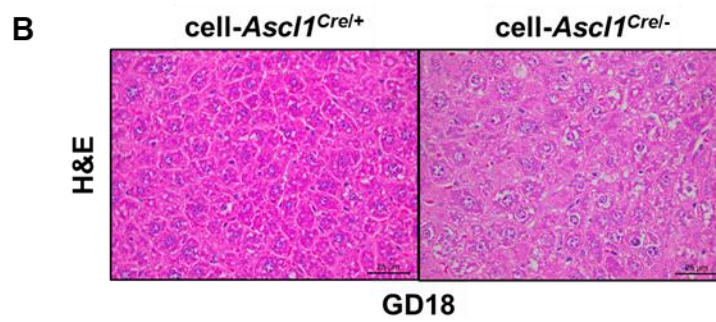
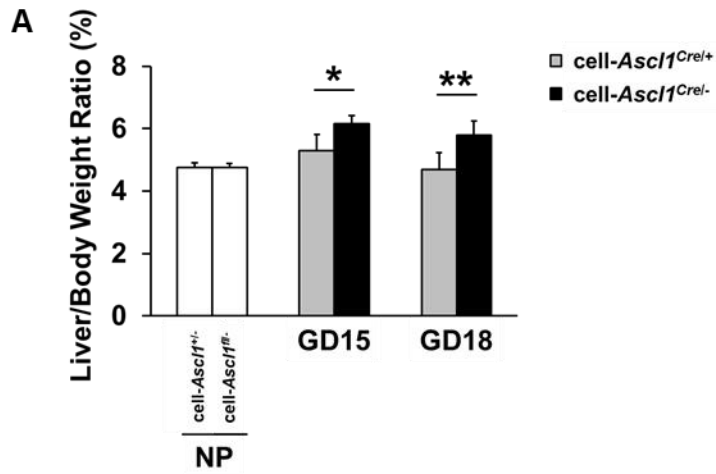
### 3.3.2 Deletion of *Ascl1* in *Ascl1*-expressing cells causes maternal liver abnormalities

We evaluated whether cell-specific deletion of *Ascl1* resulted in similar maternal liver phenotypes as the global *Ascl1* knockout. The lack of *Ascl1* in cell-*Ascl1*<sup>Cre/-</sup> pregnant mice resulted in an increased liver-to-body weight ratio on GD15 and GD18 by 16% and 24%, respectively (**Fig. 7A**). Hematoxylin and eosin staining on cell-*Ascl1*<sup>Cre/-</sup> maternal liver sections revealed abnormalities such as an overall reduction of eosin staining in the liver and a lack of staining around the nucleus of the hepatocyte on GD18 (**Fig. 7B**). Tracing the *Ascl1*-expressing cells by immunostaining both cell-*Ascl1*<sup>Cre/+</sup> and cell-*Ascl1*<sup>Cre/-</sup> maternal livers showed a similar number and random distribution of YFP+ cells (*Ascl1*-expressing cells) (**Fig. 7C**). Cell-*Ascl1*<sup>Cre/-</sup> mice also had 15% larger placental weight on GD18 (**Fig. 7D**) but had similar fetal weight on both GD15 and GD18 (**Fig. 7E**). Thus, we were able to successfully generate a cell-specific *Ascl1* knockout mouse model and observe similar maternal hepatic abnormalities as the *Ascl1* global knockout. Most importantly, using this model, we demonstrated that *Ascl1* absence does not result in the reduction of maternal hepatocyte number or hepatocyte death.

### 3.3.3 Deletion of *Ascl1* in *Ascl1*-expressing cells causes alterations in maternal hepatic gene profile

To investigate the *Ascl1* target genes in *Ascl1*-expressing cells, we isolated total RNA from both cell-*Ascl1*<sup>Cre/+</sup> and cell-*Ascl1*<sup>Cre/-</sup> mice on gestation day (GD) 15 and performed the RNA-sequencing (RNA-seq) analysis. Using the Ingenuity Pathway Analysis (IPA), we detected 362 genes up/downregulated by at least two-fold with an FDR value less than 0.05 in cell-*Ascl1*<sup>Cre/-</sup> maternal livers when compared with the controls (**Fig. 8A**). IPA displayed the top enriched canonical pathways affected by the *Ascl1* ablation (**Fig. 8B**). In cell-*Ascl1*<sup>Cre/-</sup> maternal livers, signaling pathway categories involved in cell death, cell cycle, and cancer were upregulated where-

**Figure 7. Cell-specific *Ascl1* ablation phenotypes.** (A-C) Maternal liver changes. Maternal livers were collected and weighed from cell-*Ascl1*<sup>Cre/+</sup> and cell-*Ascl1*<sup>Cre/-</sup> mice (described in **Fig. 6**). (A) The maternal liver-to-body weight ratios of cell-*Ascl1*<sup>Cre/+</sup> and cell-*Ascl1*<sup>Cre/-</sup> mice are presented. Data are expressed as means  $\pm$  s.d. (n = 5-9). \*\*,  $P < 0.01$ , between cell-*Ascl1*<sup>Cre/+</sup> and cell-*Ascl1*<sup>Cre/-</sup> mice. (B) Maternal liver histology. Maternal liver sections of cell-*Ascl1*<sup>Cre/+</sup> and cell-*Ascl1*<sup>Cre/-</sup> mice were subjected to hematoxylin and eosin (H&E) staining. (C) Cell lineage tracing. Maternal liver sections on gestation day 18 were subjected to green fluorescent protein (GFP) staining. GFP-positive cells are stained dark brown. (D-E) Pregnancy outcome. Placenta and fetuses were collected and weighed from cell-*Ascl1*<sup>Cre/+</sup> and cell-*Ascl1*<sup>Cre/-</sup> mice. (D) Placental weight and (E) the number of pups born from cell-*Ascl1*<sup>Cre/+</sup> and cell-*Ascl1*<sup>Cre/-</sup> dams are presented. Data are expressed as means  $\pm$  s.d. (n = 5-9). \*\*,  $P < 0.01$ , between cell-*Ascl1*<sup>Cre/+</sup> and cell-*Ascl1*<sup>Cre/-</sup> mice.



as coagulation and metabolism were downregulated. We documented the full lists of canonical pathways, *p*-values, *z*-scores, and the associated genes affected by *Ascl1* deletion. Furthermore, IPA associated the differentially expressed genes targeted by *Ascl1* to network categories grouped together based on known diseases and functions such as cell cycle, lipid metabolism, and development (**Table 7**). We documented the categorized lists of the *Ascl1*-associated networks. Therefore, *Ascl1* has a wide range of effects in molecular networks and pathways of the maternal liver that deviates from a normal pregnancy.

### **3.4 Hepatocyte-specific deletion of *Ascl1***

#### **3.4.1 Generation of hepatocyte-specific inducible *Ascl1* knockout mouse model**

The previous data showed that deletion of *Ascl1* in *Ascl1*-expressing cells caused overt maternal liver and placental phenotypes; nevertheless, we further examined whether deletion of *Ascl1* specifically in the liver resulted in similar pregnancy outcomes, as tamoxifen is associated with developmental abnormalities of the fetus, spontaneous abortions, pregnancy terminations, and stillbirths (179). To delete *Ascl1* specifically in the maternal hepatocytes, we generated *Ascl1<sup>fl/fl</sup>;R26<sup>EYFP/EYFP</sup>* (*R26-LoxP-Stop-LoxP-EYFP*) mouse line (**Fig. 9A**). In this inducible and hepatocyte-specific *Ascl1* knockout mouse line (hep-*Ascl1*<sup>-/-</sup>), injecting AAV8-TBG-Cre, where adeno-associated virus (AAV) 8 specifically targets the liver and thyroxine-binding globulin promoter (TBG) expresses only in the hepatocytes, into the animal causes the removal of the floxed *Ascl1* gene and the Stop cassette upstream of enhanced yellow fluorescent protein (*EYFP*). Therefore, the maternal hepatocytes ablate *Ascl1* while, at the same time, being labeled with *EYFP*. For control (*Ascl1<sup>fl/fl</sup>*), we introduced a null gene using the AAV8 virus to the same mouse model, which results in an intact *Ascl1* gene and inexpression of *EYFP* in the maternal liver.

**Figure 8. Differentially expressed genes and canonical pathways affected by *Ascl1* ablation in *Ascl1*-expressing cells.** Maternal livers were collected from cell-*Ascl1*<sup>Cre/+</sup> and cell-*Ascl1*<sup>Cre/-</sup> mice (described in **Fig. 6**). Total RNA was isolated from livers of cell-*Ascl1*<sup>Cre/+</sup> and cell-*Ascl1*<sup>Cre/-</sup> mice on gestation day (GD) 15 using RNeasy Plus Mini Kit. The isolated RNA was sent to the Center for Medical Genomics Core (Indiana University School of Medicine) for RNA-sequencing. **(A)** Differentially expressed genes are presented by the volcano plot. Red, significantly up- or downregulated genes; black, green, and blue are non-significant genes. The differentially expressed genes with at least two-fold and *p*-value less than 0.05 were analyzed using the Ingenuity Pathway Analysis (IPA). **(B)** Top enriched canonical pathways targeted by *Ascl1* are presented. Orange, upregulated; blue, downregulated. *Ascl1*, achaete-scute homolog 1.

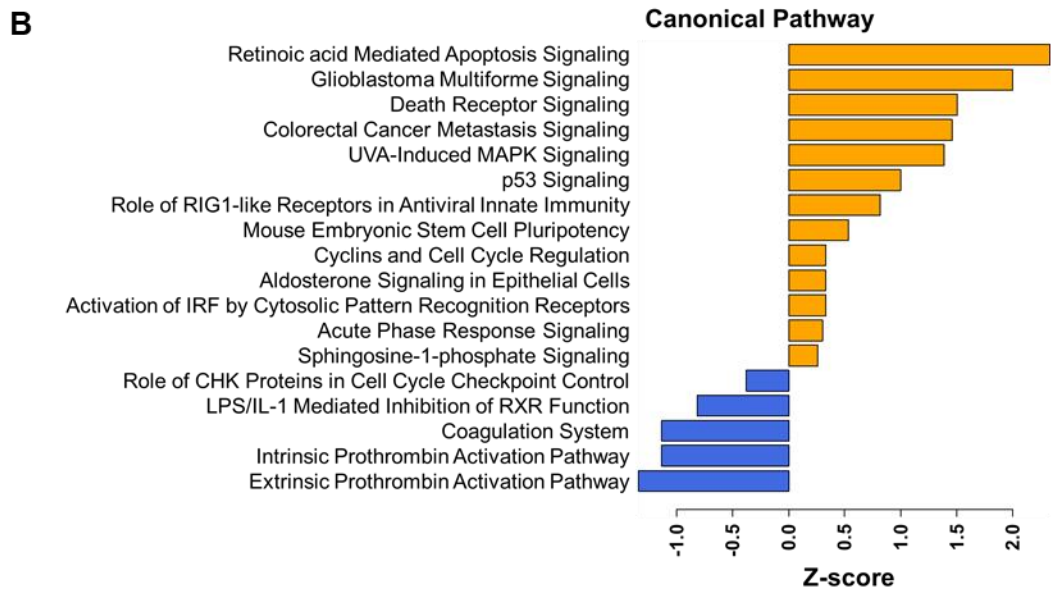
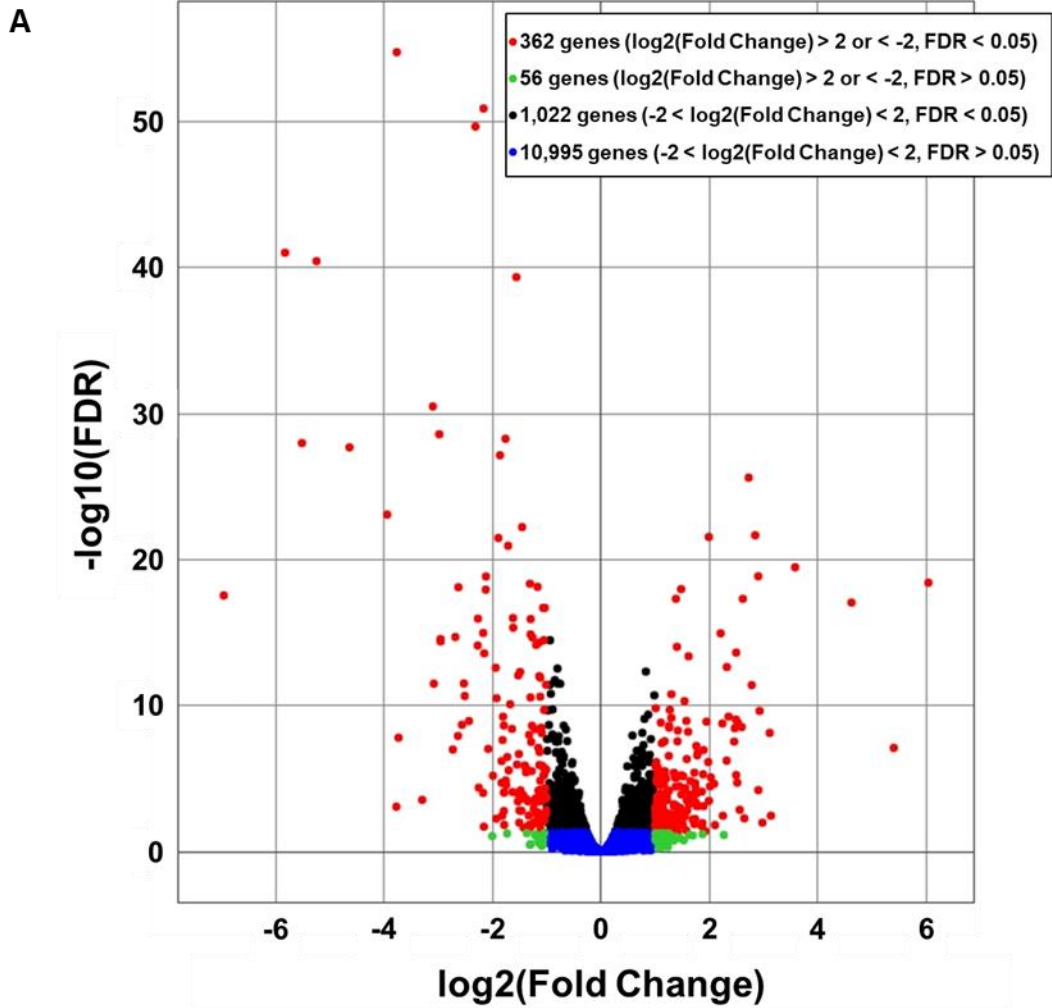


**Table 7 Lists of Gene Networks and Functions**

| No. | Associated Network Functions   |
|-----|--|
| 1   | Gene Expression, Cellular Assembly and Organization, Cell Cycle              |
| 2   | Lipid Metabolism , Molecular Transport, Small Molecule Biochemistry          |
| 3   | Cellular Development, Tissue Development, Organ Morphology                   |
| 4   | Lipid Metabolism, Small Molecule Biochemistry, Carbohydrate Metabolism       |
| 5   | Infectious Diseases, Cellular Development, Cellular Growth and Proliferation |

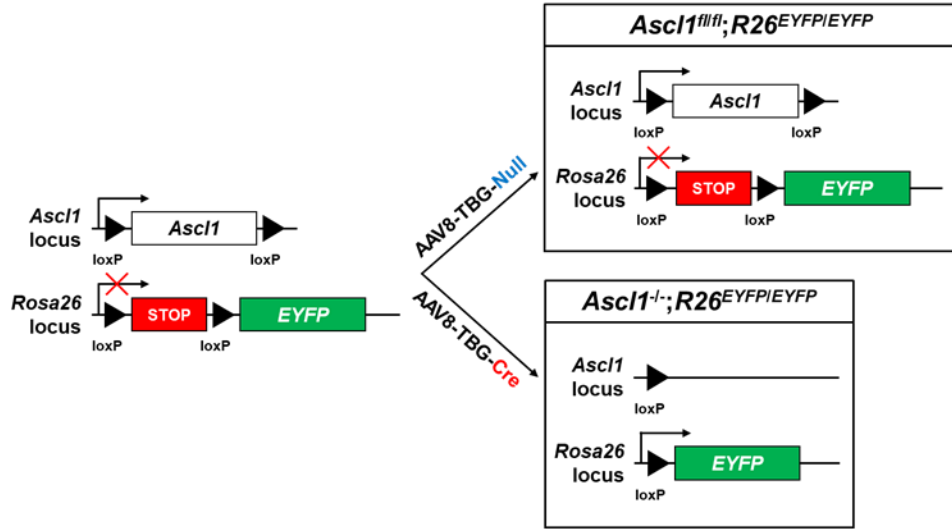
After injecting AAV8 virus on gestation day (GD) 8, we collected maternal organs from both genotypes on GD15 and GD18 for analysis (**Fig. 9B**). By qRT-PCR, we confirmed the successful knockout of hepatic *Ascl1* by AAV8-TBG-Cre on GD15 by 96.9% and GD18 by 99.7% in the hep-*Ascl1*<sup>-/-</sup> mice when compared with the control mice (**Fig. 9C**). Therefore, we successfully generated a hepatocyte-specific conditional *Ascl1* knockout mouse model.

### **3.4.2 Hepatocyte-specific *Ascl1* knockout results in maternal liver abnormalities**

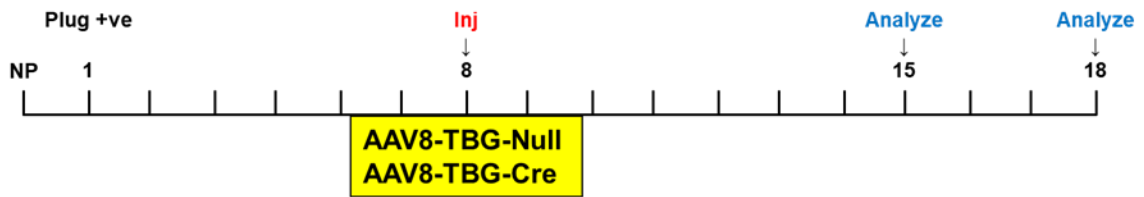
Among the most apparent *Ascl1* null phenotypes were increases of liver-to-body weight ratios on GD15 by 9% and on GD18 by 14% (**Fig. 10A-B**). By hematoxylin and eosin staining, similar to the cell-*Ascl1*<sup>Crel-</sup> mice using tamoxifen, we observed reduced staining patterns in the hep-*Ascl1*<sup>-/-</sup> maternal livers (**Fig. 10C**). By immunostaining with the cell proliferation marker Ki67, we found an increased number of Ki67+ hepatocytes in the maternal liver on GD18 by 114% when compared with the controls (**Fig. 10D-E**); however, we were unable to find hepatocytes undergoing mitosis.  $\beta$ -Catenin staining showed hypertrophy of maternal hepatocytes by 20% in the hep-*Ascl1*<sup>-/-</sup> mice (**Fig. 10F-G**). Thus, hep-*Ascl1*<sup>-/-</sup> maternal livers respond to pregnancy by increased liver weight and cell size.

**Figure 9. Virus-induced hepatocyte-specific *Ascl1* knockout mouse model.** (A) The strategy of generating hepatocyte-specific inducible *Ascl1* knockout mouse model. In the hepatocyte-specific inducible *Ascl1* knockout (hep-*Ascl1*<sup>-/-</sup>) (*Ascl1*<sup>fl/fl</sup>;R26<sup>EYFP/EYFP</sup>) (R26-*LoxP*-*Stop*-*LoxP*-*EYFP*) mice, adeno-associated virus 8 (AAV8)-thyroxine-binding globulin promoter (*TBG*)-*Cre* recombinase (AAV8-*TBG*-*Cre*) is injected. AAV8 specifically targets the liver and injects the vector that contains *Cre* recombinase driven by the *TBG* promoter, which is expressed only in hepatocytes. Only the hepatocytes express *Cre* recombinase, which excises out the loxP-flanked *Ascl1* and the *Stop* cassette upstream of enhanced yellow fluorescent protein (*EYFP*), which results in the *Rosa26* promoter element (*R26*) driving *EYFP* expression. Thus, the hepatocytes result in *Ascl1* ablation and *EYFP* expression. In the control mice (*Ascl1*<sup>fl/fl</sup>), a virus with a null gene is introduced (AAV8-*TBG*-Null), and, therefore, retains the *Ascl1* gene without being labeled with *EYFP*. (B) Virus treatment timeline. The presence of a copulation plug was designated as gestation day (GD) 1. AAV8-*TBG*-*Cre* or AAV8-*TBG*-Null was administered by tail vein injection (1x10<sup>12</sup> genomic copies per mouse) to *Ascl1*<sup>fl/fl</sup>;R26<sup>EYFP/EYFP</sup> mice on gestation day (GD) 8 to generate hep-*Ascl1*<sup>-/-</sup> and *Ascl1*<sup>fl/fl</sup>, respectively. Samples were collected on GD15 and GD18. (C) *Ascl1* mRNA expression in the maternal liver. Total RNA was isolated from livers of nonpregnant (NP) and pregnant (GD15 and GD18) *Ascl1*<sup>fl/fl</sup> and hep-*Ascl1*<sup>-/-</sup> mice. Hepatic *Ascl1* mRNA levels were measured using quantitative real-time polymerase chain reaction (qRT-PCR) and expressed as the mean fold changes relative to NP controls (± s.d.; n = 4-5). \*\*\*, *P* < 0.001, between *Ascl1*<sup>fl/fl</sup> and hep-*Ascl1*<sup>-/-</sup> mice. *18S* ribosomal RNA (rRNA) levels were used as endogenous controls. *Ascl1*, achaete-scute homolog 1.

**A**



**B**



**C**

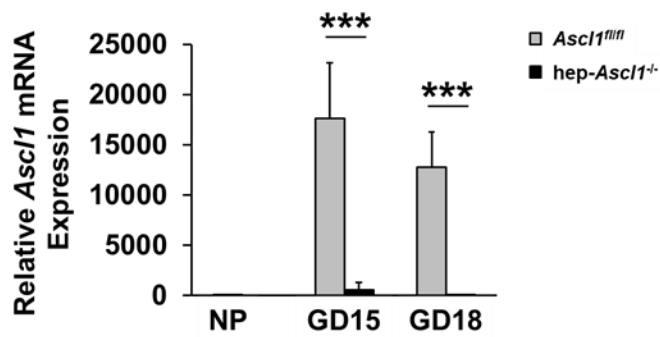


**Figure 10. Hepatocyte-specific *Ascl1* ablation phenotypes.** Maternal livers were collected and weighed from *Ascl1<sup>fl/fl</sup>* and hep-*Ascl1<sup>-/-</sup>* mice (described in **Fig. 9**). **(A)** Morphology of the *Ascl1<sup>fl/fl</sup>* and hep-*Ascl1<sup>-/-</sup>* mice livers on gestation day (GD) 18. **(B)** The maternal liver-to-body weight ratios of *Ascl1<sup>fl/fl</sup>* and hep-*Ascl1<sup>-/-</sup>* mice are presented. Data are expressed as means  $\pm$  s.d. (n = 4-6). \*,  $P < 0.05$ ; \*\*,  $P < 0.01$ , between *Ascl1<sup>fl/fl</sup>* and hep-*Ascl1<sup>-/-</sup>* mice. **(C)** Maternal liver histology. Maternal liver sections of *Ascl1<sup>fl/fl</sup>* and hep-*Ascl1<sup>-/-</sup>* mice were subjected to hematoxylin and eosin (H&E) staining. **(D-E)** Maternal hepatocyte proliferation. **(D)** Maternal liver sections of *Ascl1<sup>fl/fl</sup>* and hep-*Ascl1<sup>-/-</sup>* mice on GD18 were subjected to Ki67 staining. Ki67-positive cells are stained dark brown in the nucleus. **(E)** The nuclear Ki67-positive hepatocytes were counted in five random fields of view (200X magnification) and the data are expressed as the means  $\pm$  s.d. (n = 3-6). \*\*\*,  $P < 0.001$ , between *Ascl1<sup>fl/fl</sup>* and hep-*Ascl1<sup>-/-</sup>* mice. **(F-G)** Maternal hepatocyte density. **(F)** Maternal liver sections of *Ascl1<sup>fl/fl</sup>* and hep-*Ascl1<sup>-/-</sup>* mice on GD18 were subjected to  $\beta$ -Catenin staining.  $\beta$ -Catenin stains the cell membrane dark brown. **(G)** The maternal hepatocytes were counted (200X magnification) and the data are expressed as the means  $\pm$  s.d. (n = 7 for each group). \*\*\*,  $P < 0.001$ , between *Ascl1<sup>fl/fl</sup>* and hep-*Ascl1<sup>-/-</sup>* mice. *Ascl1*, achaete-scute homolog 1.

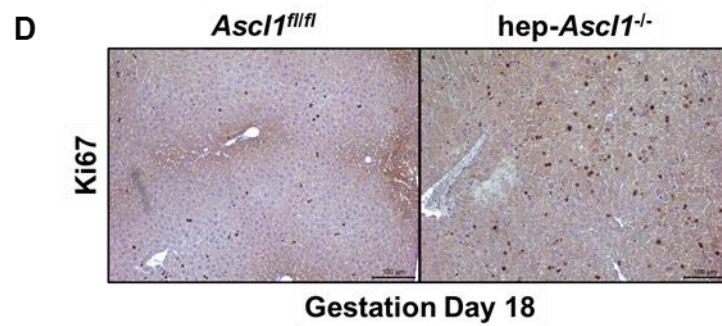
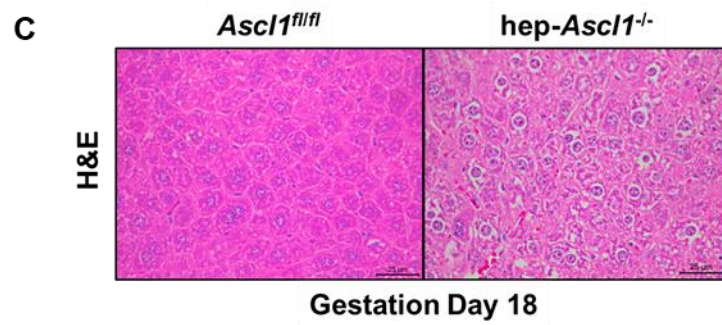
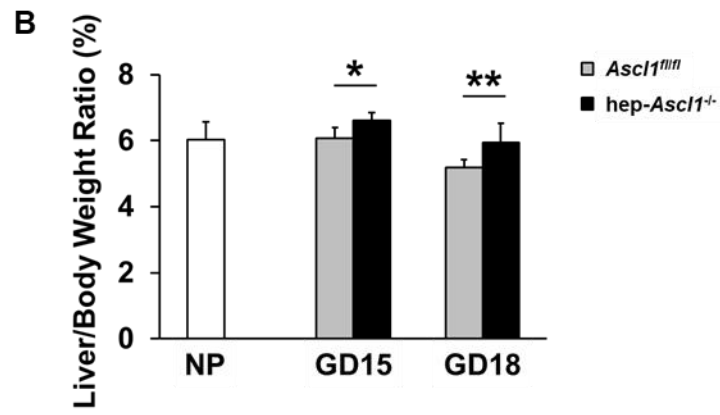
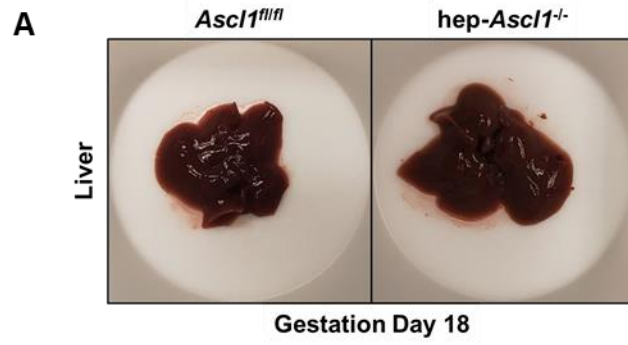
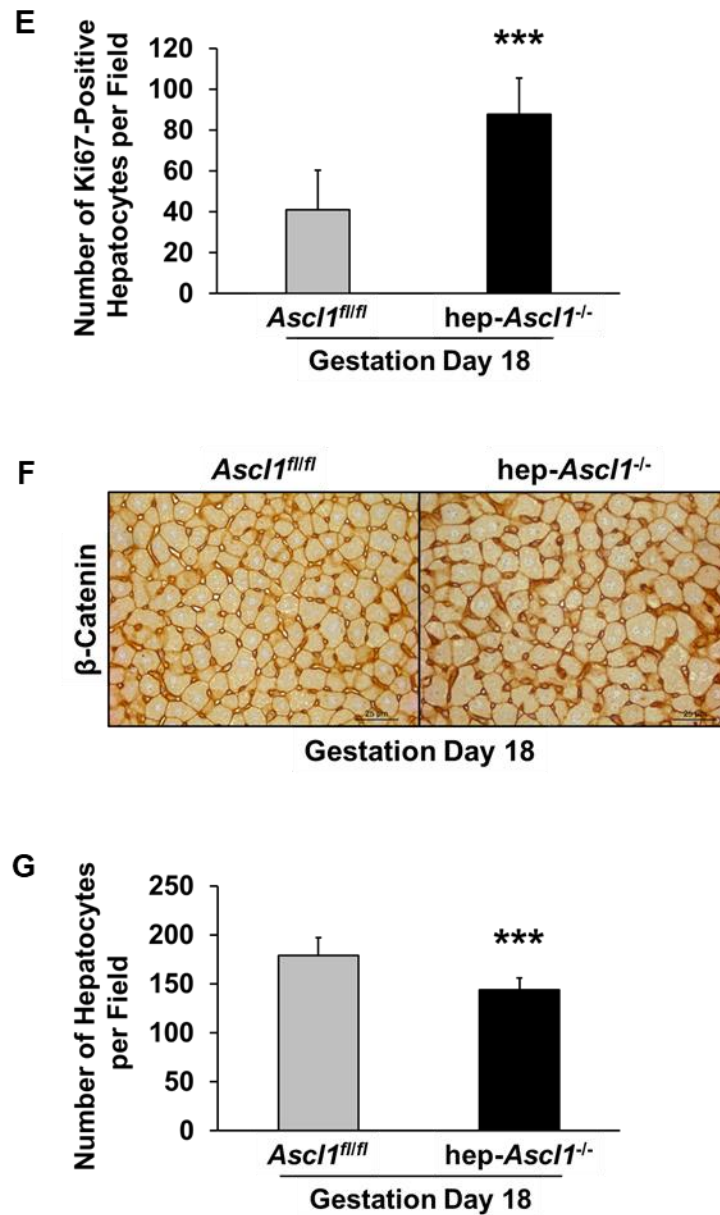


Figure 10, continued.



### 3.4.3 Hepatocyte-specific *Ascl1* knockout causes alterations in maternal hepatic gene profile

To determine the *Ascl1* target genes in the maternal liver, we isolated total RNA from both *hep-Ascl1<sup>-/-</sup>* and *Ascl1<sup>fl/fl</sup>* mice on gestation day (GD15) and performed RNA-sequencing (RNA-

Seq) analysis. Using the IPA, we observed 1,274 genes differentially expressed by at least two-fold with an FDR value less than 0.05 in hep-*Ascl1*<sup>-/-</sup> maternal livers when compared with the controls. IPA summarized the top canonical pathways affected by hepatic *Ascl1* ablation (**Fig. 11**). In hep-*Ascl1*<sup>-/-</sup> maternal livers, signaling pathways affected include downregulation of melatonin, nicotine, and dopamine degradations and upregulation of amyotrophic lateral sclerosis (ALS), pancreatic cancer, and interferon signaling. We documented the complete lists of canonical pathways, with *p*-values, *z*-scores, and associated genes. In addition, IPA analyzed and assigned the *Ascl1* target genes to network categories of diseases and functions such as metabolisms of carbohydrate, nucleic acid, amino acid, disruptions in the cell cycle, and disorders of cellular function and development in the auditory and skin (**Table 8**). We documented the complete lists of networks and the associated genes. Hence, the ablation of maternal hepatic *Ascl1* during pregnancy results in a wide range of gene expression changes.

#### 3.4.4 Hepatocyte-specific *Ascl1* knockout changes hepatocyte identity

*CD133* (also referred to as *PROM1*) and epithelial cell adhesion molecule (*EpCAM*) are hepatocyte stem/progenitor cell markers that are also expressed in cancer stem cells (180). By RNA sequencing (RNA-Seq), we observed that *Ascl1* deficiency affected the expression of hepatic *CD133* mRNA on gestation day (GD) 15. *In situ* hybridization on GD18 showed comparable *CD133* mRNA signals in both genotypes; however, while the *CD133* mRNA remained in the hepatocyte nucleus in the *Ascl1*<sup>fl/fl</sup> hepatocytes, *CD133* mRNA in the hep-*Ascl1*<sup>-/-</sup> hepatocytes showed the presence in both the nucleus and cytosol (**Fig. 12A**). qRT-PCR showed that the hep-*Ascl1*<sup>-/-</sup> mice increased the expression of *CD133* mRNA in the maternal liver on GD15 by 3.37-folds and GD18 by 12.43-folds (**Fig. 12B**). In addition, we observed that the expression of hepatic *EpCAM* mRNA in hep-*Ascl1*<sup>-/-</sup> mice remained the same as nonpregnant; however, *Ascl1*<sup>fl/fl</sup> mice

decreased its expression on GD15 by 73% (**Fig. 12C**). Therefore, the ablation of *Ascl1* influences the phenotypes of the hepatocytes by means of *CD133* and *EpCAM* expression during pregnancy.

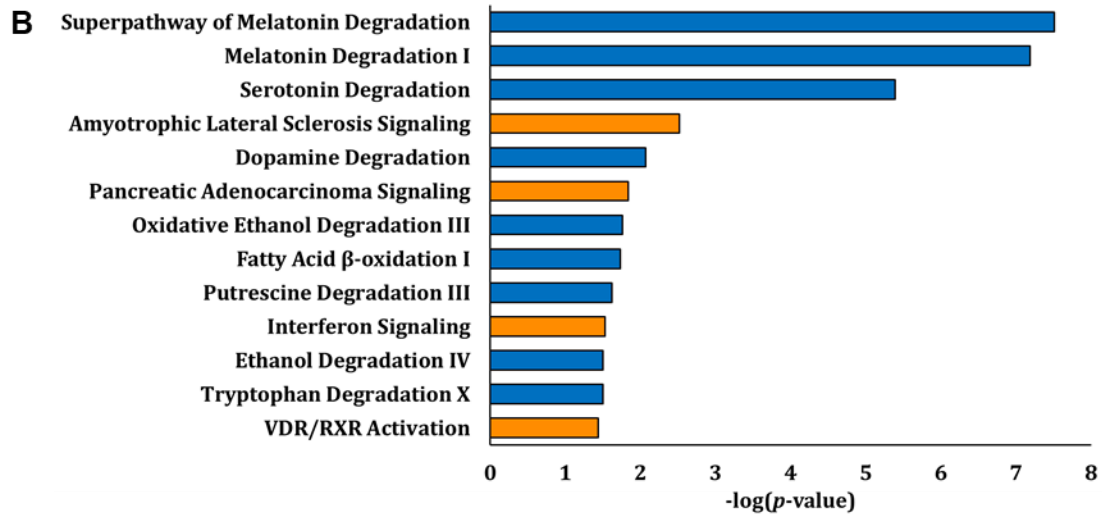
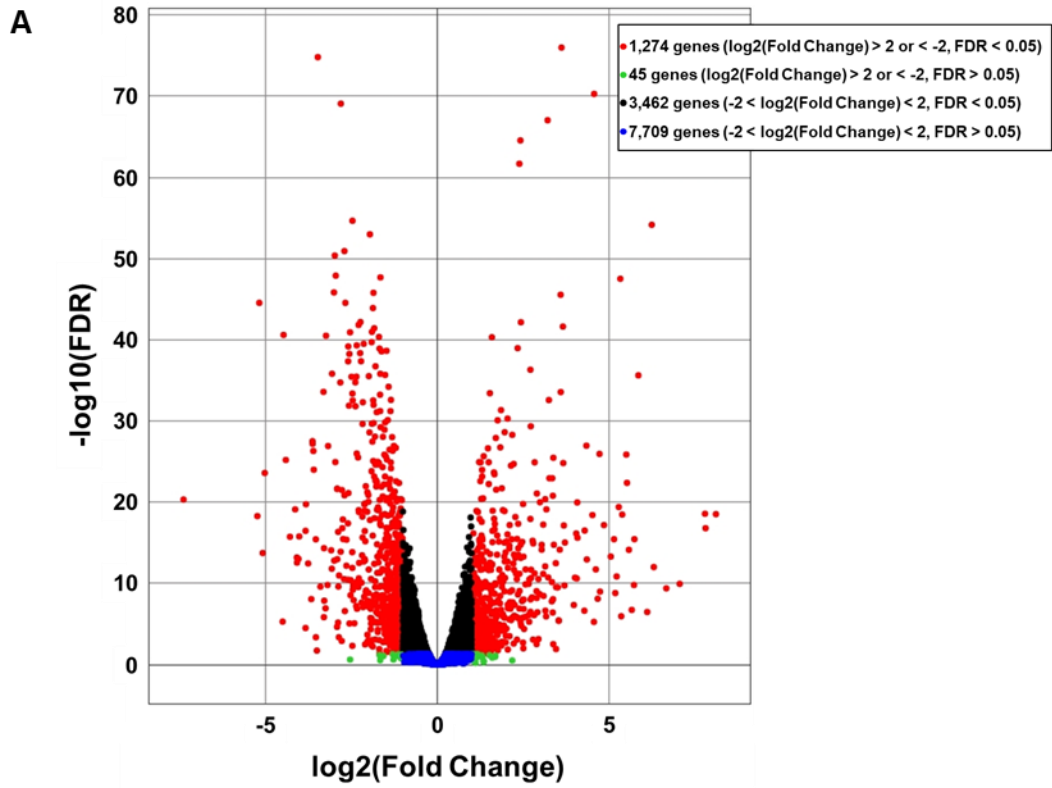
### 3.4.5 Hepatocyte-specific *Ascl1* knockout results in activation of *Igf2*

Another surprising gene activated by removing *Ascl1* in the maternal liver was the insulin-like growth factor 2 (*Igf2*). *Igf2* is an essential growth factor for fetal development but down-regulated in adult tissues (181). *In situ* hybridization on GD 18 livers showed abundant *Igf2* mRNA in hep-*Ascl1*<sup>-/-</sup> mice (**Fig. 13A**). qRT-PCR showed a 350-fold increase in the *Igf2* mRNA level on GD18 (**Fig. 13B**). To determine which promoters of *Igf2* are activated, we performed qRT-PCR to analyze promoter-specific *Igf2* transcripts and observed that activity of the promoter (P) 0, a placenta-specific *Igf2* promoter, was silent due to the loss of *Ascl1* whereas fetal-specific P1, P2, and P3 promoters were activated on GD15 and GD18 (**Fig. 13C**). By qRT-PCR, we did not observe any differential expression of zinc finger protein 568 (*Zfp568*), which is known to silence the placental promoter of *Igf2* in the placenta (**Fig. 13D**). This suggests that *Zfp568* may not be involved in the regulation of P0 in maternal hepatocytes. Together, we found that the deletion of *Ascl1* in maternal hepatocytes results in the activation of hepatic *Igf2* via P1, 2, and 3.

**Table 8. Lists of Gene Networks and Functions**

| No. | Associated Network Functions  |
|-----|---|
| 1   | Carbohydrate Metabolism, Nucleic Acid Metabolism, Small Molecule Biochemistry                               |
| 2   | Nutritional Disease, Psychological Disorders, Cellular Function and Maintenance                             |
| 3   | Auditory and Vestibular System Development and Function, Amino Acid Metabolism, Small Molecule Biochemistry |
| 4   | Cancer, Cell Cycle, Organismal Injury and Abnormalities   |
| 5   | Dermatological Diseases and Conditions, Hair and Skin Development and Function, Organ Morphology            |

**Figure 11. Differentially expressed genes and canonical pathways affected by hepatocyte-specific deletion of *Ascl1* in the maternal liver.** Maternal livers were collected and weighed from *Ascl1<sup>fl/fl</sup>* and hep-*Ascl1<sup>-/-</sup>* mice (described in **Fig. 9**). Total RNA was isolated from livers of hep-*Ascl1<sup>-/-</sup>* and *Ascl1<sup>fl/fl</sup>* mice on gestation day (GD) 15 using RNeasy Plus Mini Kit. The isolated RNA was sent to the Center for Medical Genomics Core (Indiana University School of Medicine) for RNA-sequencing. **(A)** Differentially expressed genes are presented by the volcano plot. Red, significantly up- or downregulated genes; black, green, and blue are non-significant genes. The differentially expressed genes with at least two-fold and *p*-value less than 0.05 were analyzed using the Ingenuity Pathway Analysis (IPA). **(B)** Top enriched canonical pathways targeted by hepatic *Ascl1* are presented. Orange, upregulated; blue, downregulated. *Ascl1*, achaete-scute homolog 1; VDR, vitamin D receptor; RXR, retinoid X receptor.



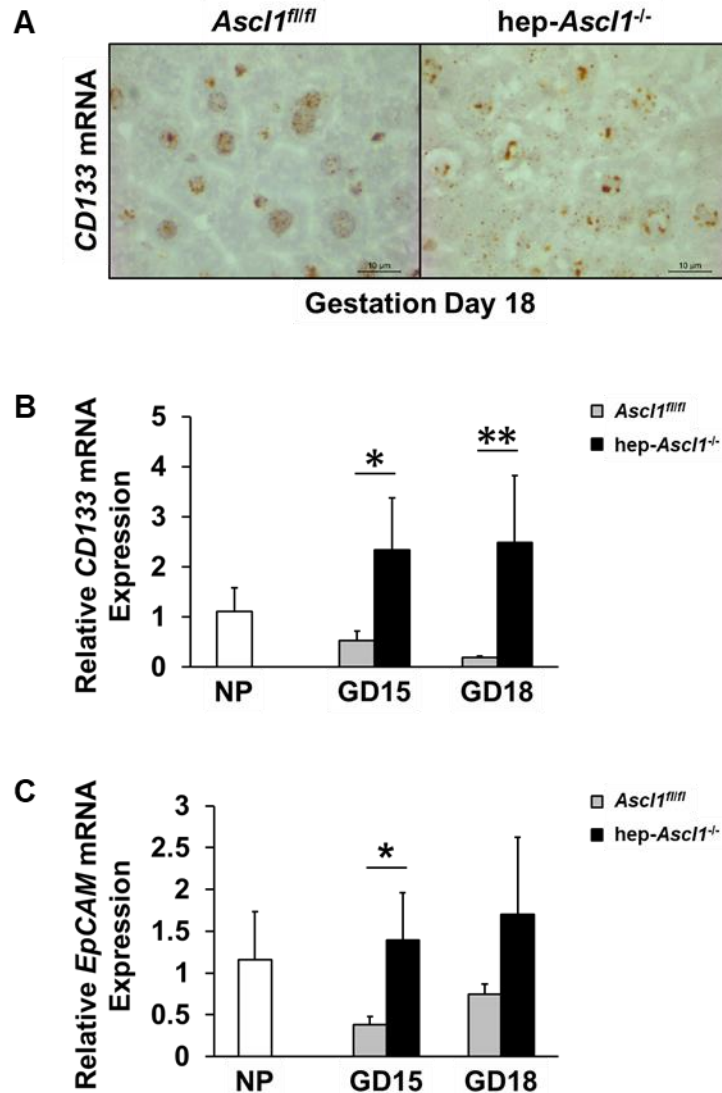


**Figure 12. Changes in maternal hepatocyte phenotypes after hepatic *Ascl1* ablation.** Maternal livers were collected from *Ascl1<sup>fl/fl</sup>* and hep-*Ascl1<sup>-/-</sup>* mice (described in Fig. 9). (A) Hepatic *CD133* mRNA distribution in the maternal liver after hepatic *Ascl1* deletion. Maternal liver sections of *Ascl1<sup>fl/fl</sup>* and hep-*Ascl1<sup>-/-</sup>* mice on gestation day (GD) 18 were subjected to *CD133 in situ* hybridization using RNAscope 2.5 HD Assay-BROWN kit. The *CD133* mRNA is stained dark brown. (B-C) Total RNA was isolated from livers of nonpregnant (NP) and pregnant (GD15 and GD18) *Ascl1<sup>fl/fl</sup>* and hep-*Ascl1<sup>-/-</sup>* mice. Hepatic (B) *CD133* and (C) *EpCAM* mRNA levels were measured using quantitative real-time polymerase chain reaction (qRT-PCR) and expressed as the mean fold changes relative to NP controls ( $\pm$  s.d.;  $n = 4-5$ ). \*,  $P < 0.05$ ; \*\*,  $P < 0.01$ , between *Ascl1<sup>fl/fl</sup>* and hep-*Ascl1<sup>-/-</sup>* mice. *18S* ribosomal RNA (rRNA) levels were used as endogenous controls. *Ascl1*, achaete-scute homolog 1; *CD133*, prominin-1; *EpCAM*, epithelial cell adhesion molecule.

**Figure 13. Hepatic *Igf2* activation after hepatic *Ascl1* ablation.** Maternal livers were collected from *Ascl1<sup>fl/fl</sup>* and hep-*Ascl1<sup>-/-</sup>* mice (described in **Fig. 9**). **(A)** Hepatic *Igf2* mRNA distribution in the maternal liver after hepatic *Ascl1* deletion. Maternal liver sections of *Ascl1<sup>fl/fl</sup>* and hep-*Ascl1<sup>-/-</sup>* mice on gestation day (GD) 18 were subjected to *Igf2 in situ* hybridization using RNAscope 2.5 HD Assay-BROWN kit. The *Igf2* mRNA is stained dark brown. **(B-D)** Total RNA was isolated from livers of nonpregnant (NP) and pregnant (GD15 and GD18) *Ascl1<sup>fl/fl</sup>* and hep-*Ascl1<sup>-/-</sup>* mice. Hepatic **(B)** *Igf2*, **(C)** *Igf2* promoter-specific transcript variants, and **(D)** *Zfp568* mRNA levels were measured using quantitative real-time polymerase chain reaction (qRT-PCR) and expressed as the mean fold changes relative to NP controls ( $\pm$  s.d.; n = 4-5). \*,  $P < 0.05$ ; \*\*,  $P < 0.01$ ; \*\*\*,  $P < 0.001$ , between *Ascl1<sup>fl/fl</sup>* and hep-*Ascl1<sup>-/-</sup>* mice. *18S* ribosomal RNA (rRNA) levels were used as endogenous controls. *Ascl1*, achaete-scute homolog 1; *Igf2*, insulin-like growth factor 2; *Zfp568*, zinc finger protein 568; P0, placental-specific *Igf2* promoter; P1-3, fetal-specific *Igf2* promoter.

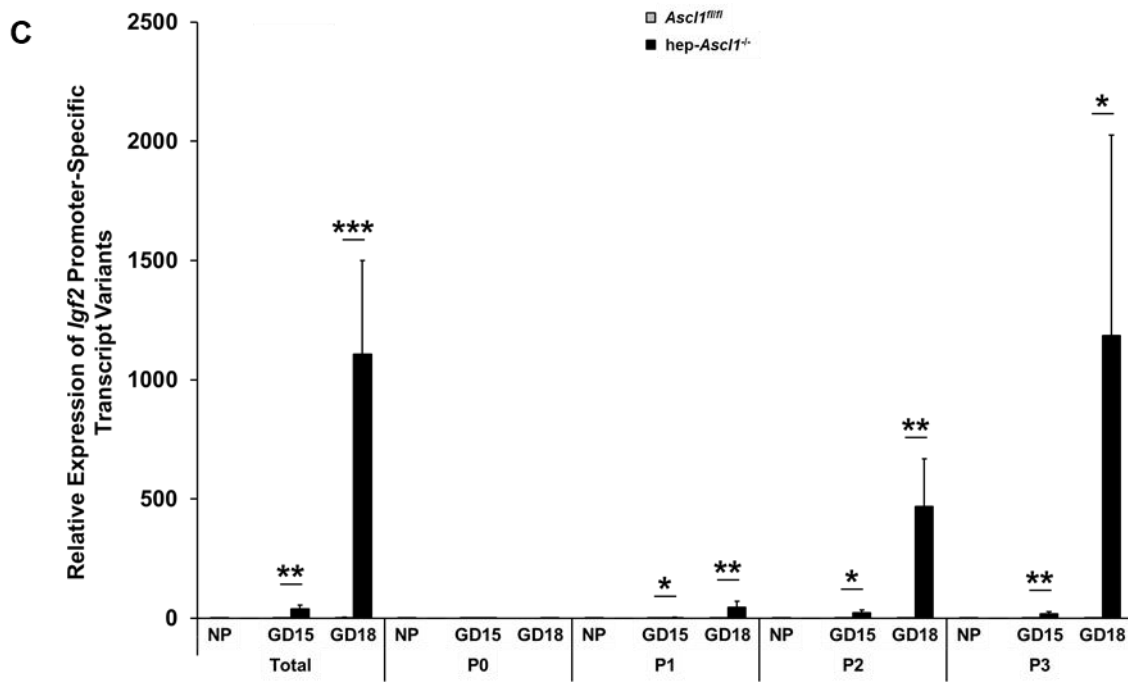
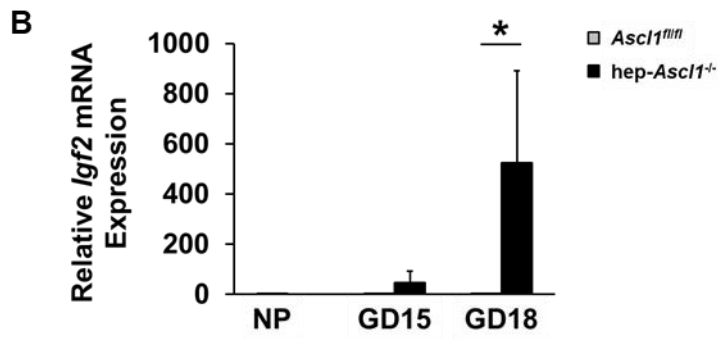
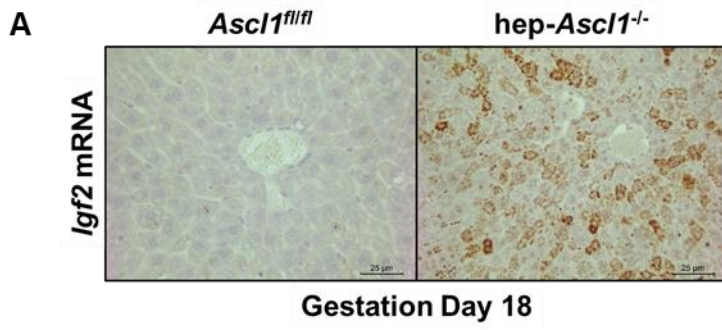
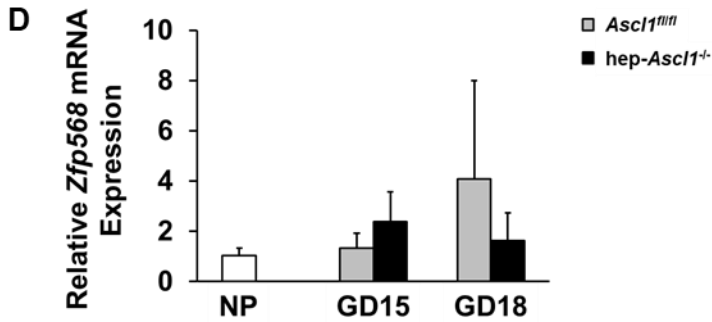


Figure 13, continued.



### 3.4.6 Hepatocyte-Specific *Ascl1* knockout results in dysregulation of hepatic genes

We next analyzed protein expression in hep-*Ascl1*<sup>-/-</sup> maternal liver. The maternal liver without *Ascl1* activated hepatic insulin-like growth factor 2 (IGF2) on gestation day (GD) 18 (**Fig. 14A-B**). However, we were unable to observe changes in the expression and activity of IGF2 upstream regulator protein kinase B (AKT). Mammalian target of rapamycin (mTOR), which can be activated by AKT, decreased on GD15 by 44% whereas phosphorylated mTOR (p-mTOR) decreased on GD18 by 67%. Phosphorylated eukaryotic translation initiation factor 4E-binding protein 1 (P-4E-BP1) at T37/46, which can be activated by mTOR, increased on GD15 by 45% and on GD18 by 69%. Phosphorylated p70 ribosomal S6 kinase (p-p70S6K) at T389, which can also be activated by mTOR, did not show *Ascl1*-dependent change. We were unable to observe changes in the expression of total or phosphorylated extracellular signal-regulated kinase 1 and 2 (ERK1/2), which play a role in cell proliferation and survival. Hep-*Ascl1*<sup>-/-</sup> liver had reduced expression of phosphorylated Janus kinase 2 (JAK2) at T1007/1008, which is involved in cell proliferation, on GD18 by 43%. CD133 increased on GD18 by 535%. Fatty acid binding protein 4 (FABP4), which is involved in lipid transportation, increased on GD15 by 107% and on GD18 by 179%. Hepatocyte growth factor (HGF), a potential hepatocyte mitogen, increased on GD18

by 212%. Taken together, we found that hepatic *Ascl1* regulates the expression of a wide range of proteins in the maternal liver, which is associated with cell proliferation, growth, and metabolism.

### **3.4.7 Hepatocyte-specific *Ascl1* knockout causes alterations in sera**

We next examined the maternal liver function by collecting and analyzing the maternal sera of nonpregnant, GD15, and GD18 mice (**Fig. 15**) (**Table 9**). We observed changes in the liver function such as decreased levels of blood urea nitrogen, creatinine, creatine kinase, and total protein, and increased levels of alanine transaminase and aspartate aminotransferase. We also observed changes in lipid metabolism such as decreased levels of cholesterol, high- and low-density cholesterol, and phospholipid, and increased levels of free fatty acid. These data show that hepatic *Ascl1* absence causes liver and lipid metabolism dysfunctions, and results in abnormal maternal biochemical profile.

**Figure 14. Hepatic protein expression after hepatic *Ascl1* ablation.** Maternal livers were collected from *Ascl1<sup>fl/fl</sup>* and hep-*Ascl1<sup>-/-</sup>* mice (described in **Fig. 9**). **(A)** Maternal protein expression. Western blotting was performed on nonpregnant (NP) and pregnant maternal liver homogenates from *Ascl1<sup>fl/fl</sup>* and hep-*Ascl1<sup>-/-</sup>* mice using antibodies against the proteins listed. GAPDH protein levels were used as loading controls. **(B)** Quantification of the maternal protein expression. Hepatic maternal protein levels from **Fig. 14A** were measured using ImageJ and expressed as the mean fold changes relative to NP controls ( $\pm$  s.d.; n = 3 for each group). \*,  $P < 0.05$ ; \*\*,  $P < 0.01$ ; \*\*\*,  $P < 0.001$ , between *Ascl1<sup>fl/fl</sup>* and hep-*Ascl1<sup>-/-</sup>* mice. GD, gestation day. *Ascl1*, achaete-scute homolog 1; IGF2, insulin-like growth factor 2; AKT, total protein kinase B; ERK1/2, extracellular signal-regulated kinase 1/2; JAK2, Janus kinase 2; mTOR, mammalian target of rapamycin; 4E-BP1, eukaryotic translation initiation factor 4E-binding protein 1; p70S6K, p70 ribosomal S6 kinase; CD133, prominin-1; HGF, hepatocyte growth factor; FABP4, fatty acid binding protein 4; GAPDH, glyceraldehyde 3-phosphate dehydrogenase.

A

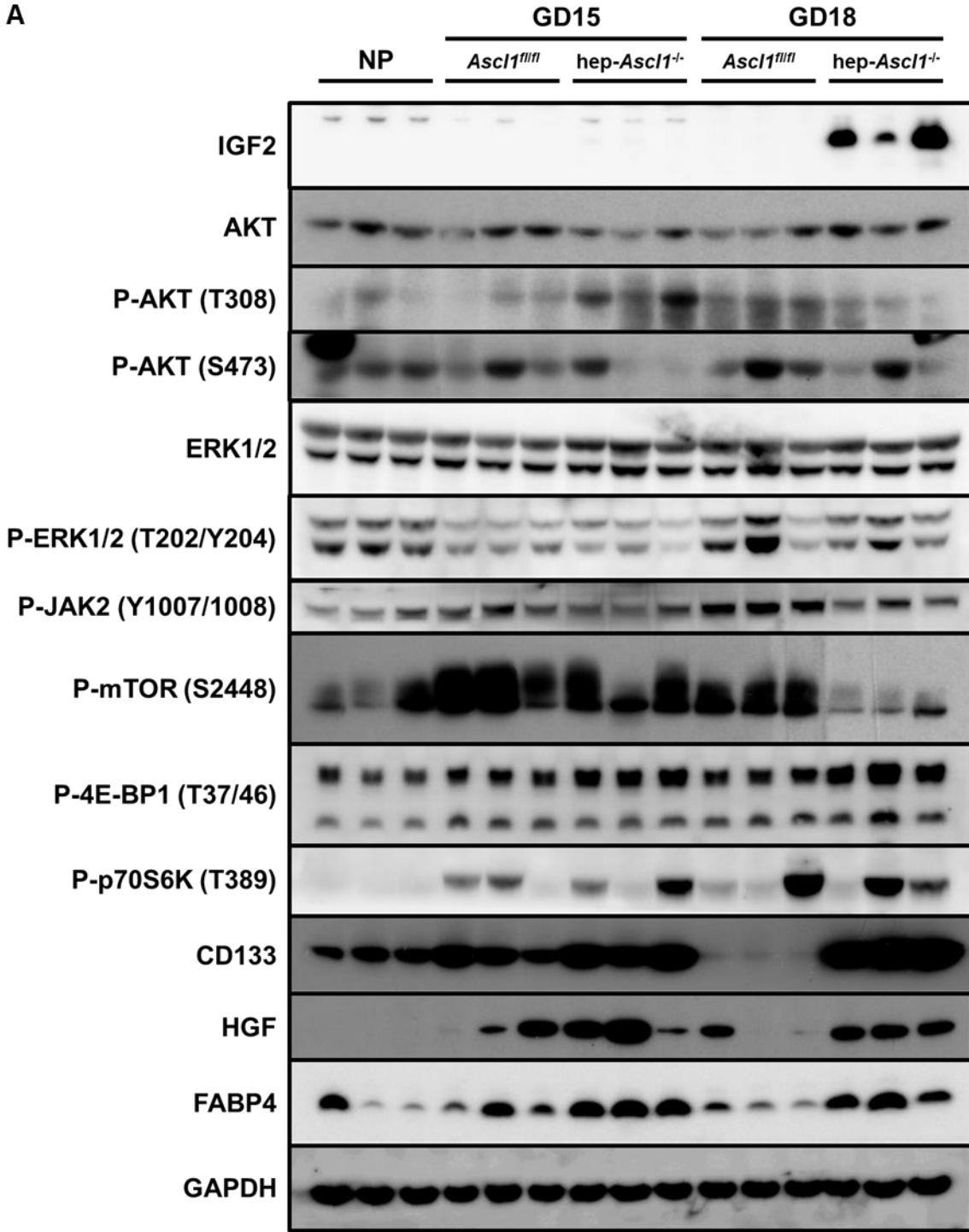


Figure 14, continued.

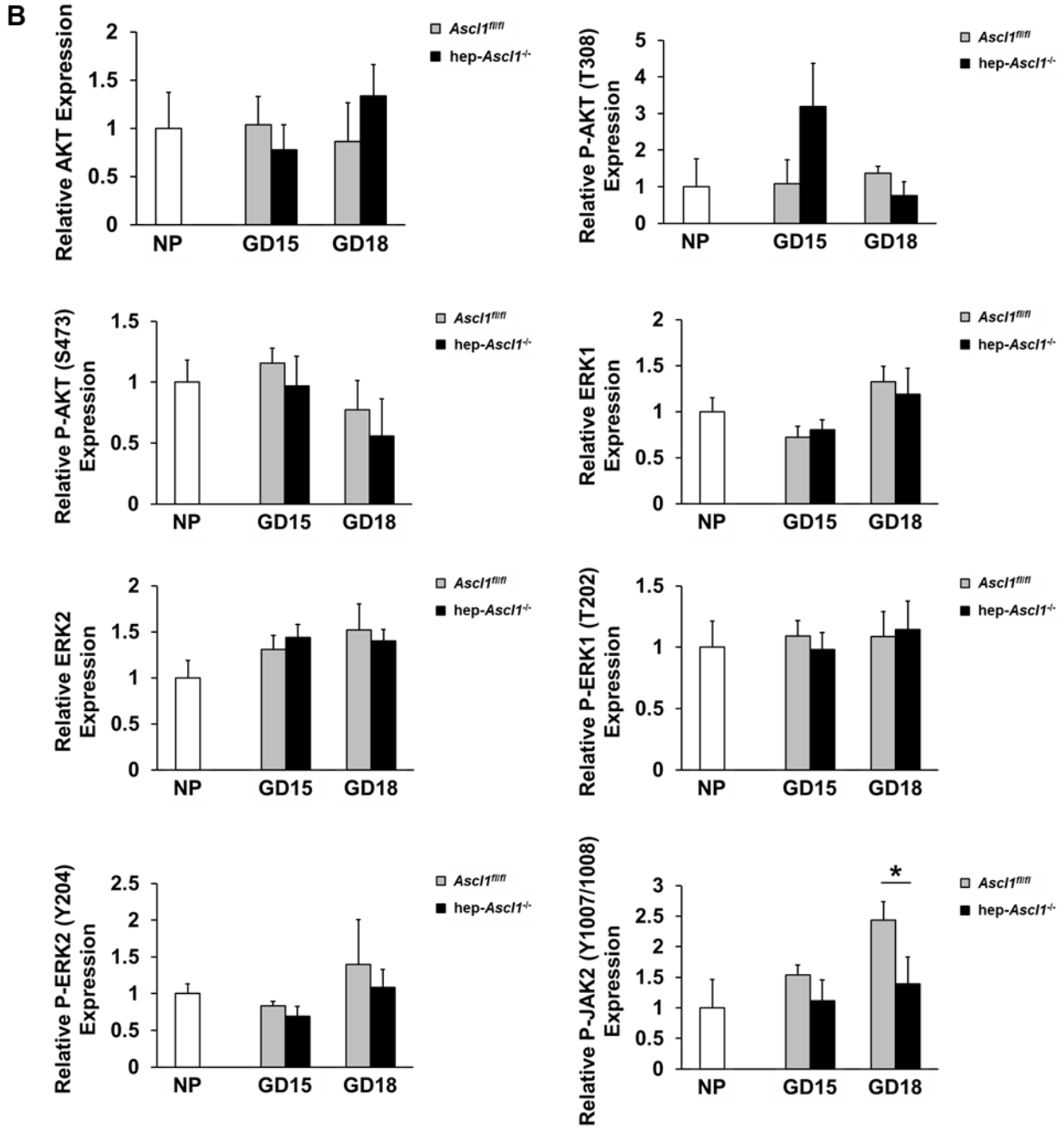
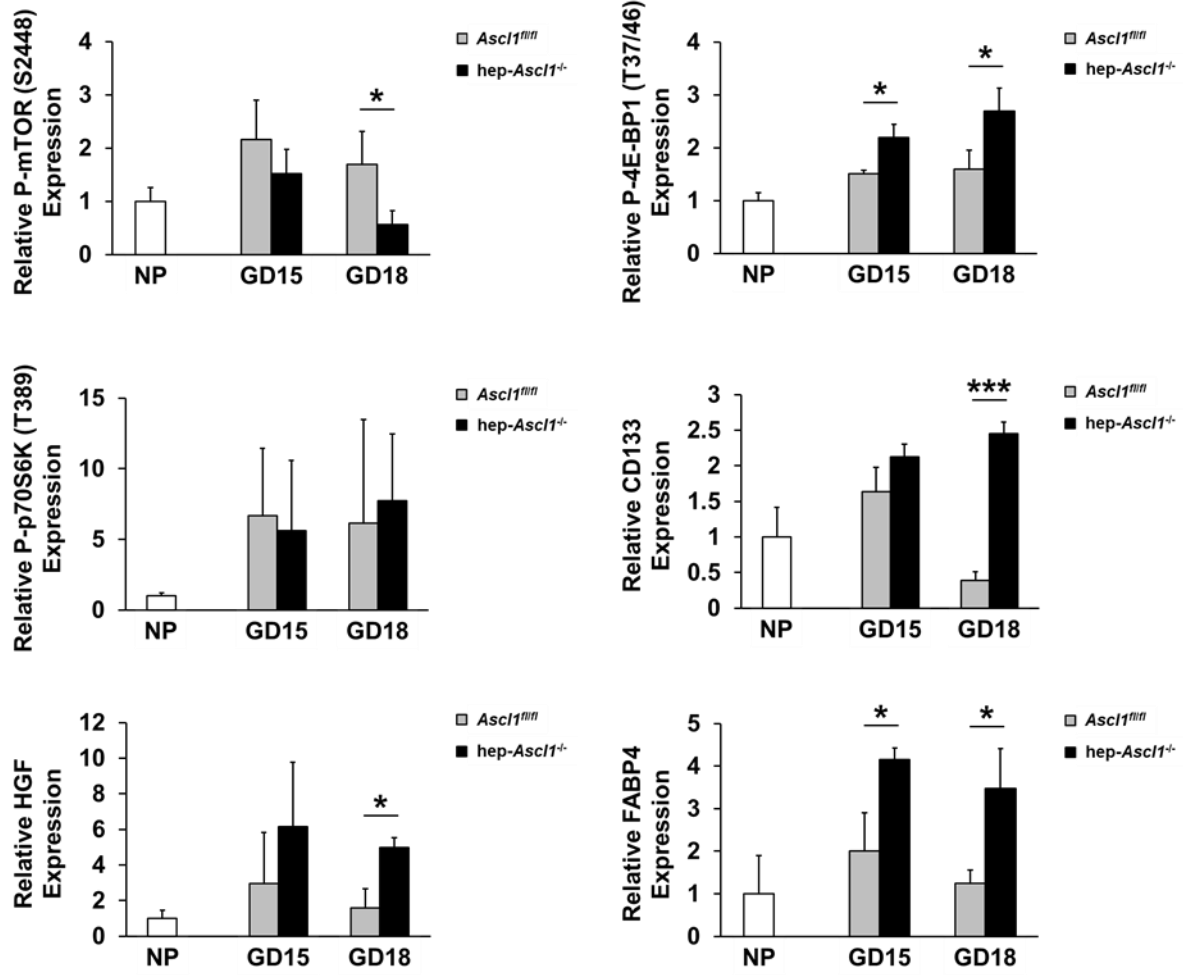


Figure 14, continued.



**Figure 15. Maternal serum biochemical profile.** Maternal serum was collected from *Ascl1<sup>fl/fl</sup>* and hep-*Ascl1<sup>-/-</sup>* mice (described in **Fig. 9**). Maternal serum biochemical profile from *Ascl1<sup>fl/fl</sup>* and hep-*Ascl1<sup>-/-</sup>* mice was analyzed by Eli Lilly and Company. Data are expressed as means  $\pm$  s.d. (n = 5). \*,  $P < 0.05$ ; \*\*,  $P < 0.01$ ; \*\*\*,  $P < 0.001$ , between *Ascl1<sup>fl/fl</sup>* and hep-*Ascl1<sup>-/-</sup>* mice. *Ascl1*, achaete-scute homolog 1; BUN, blood urea nitrogen; Enz Creat, creatinine; ALT, alanine transaminase; AST, aspartate aminotransferase; CK, creatine kinase; Na, sodium; K, potassium; Cl, chloride; Ca, calcium; IP, inorganic phosphate; Chol, cholesterol; HDL Chol, high-density lipoprotein cholesterol; LDL Chol, low-density lipoprotein cholesterol; Trig, triglyceride; Phos Lipid, phospholipid; FFA, free fatty acid; Free Chol, free cholesterol; TP, total protein; Alb, albumin; A/G, albumin/globulin.

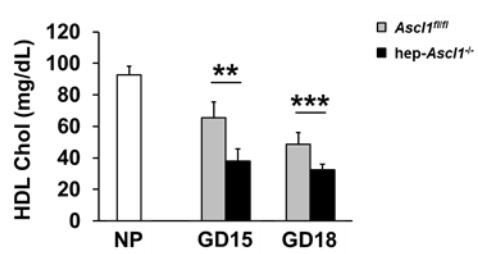
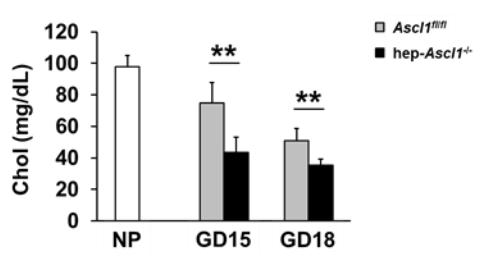
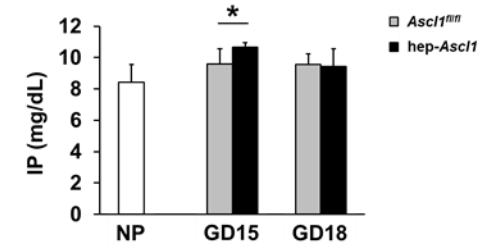
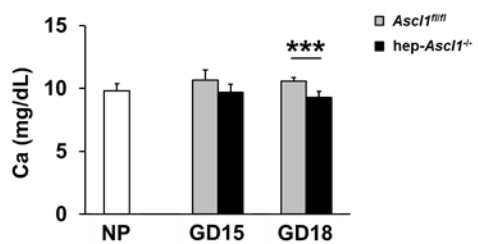
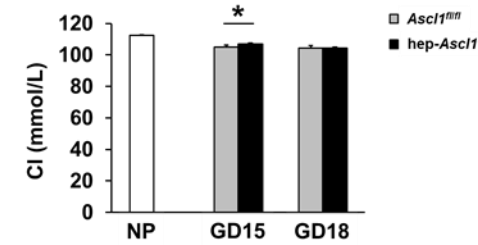
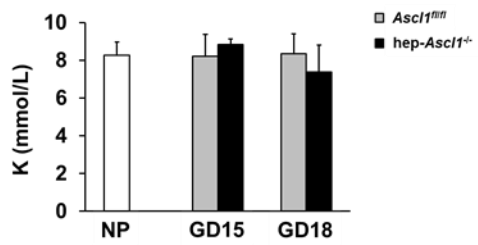
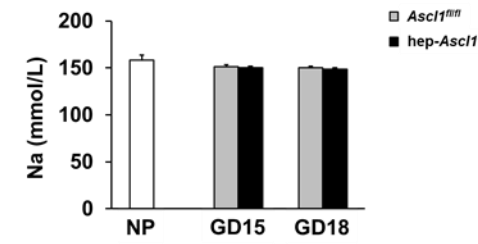
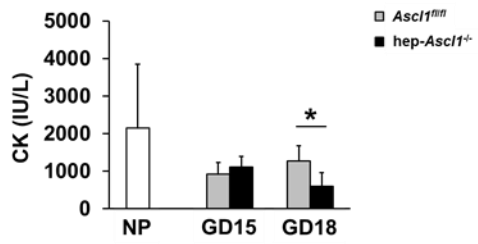
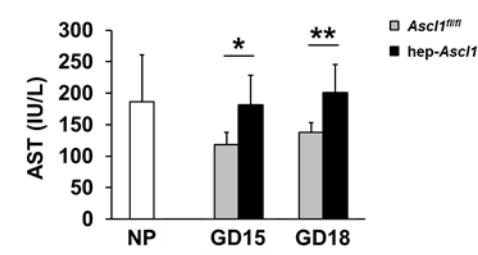
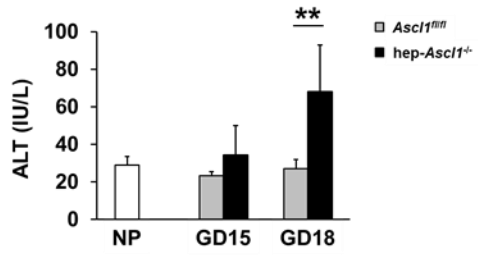
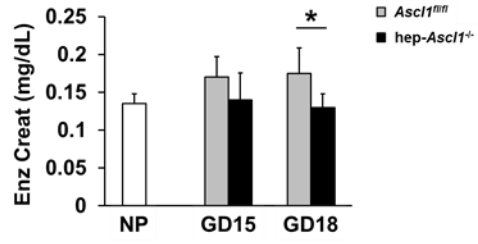
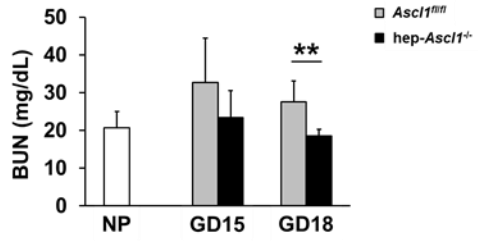
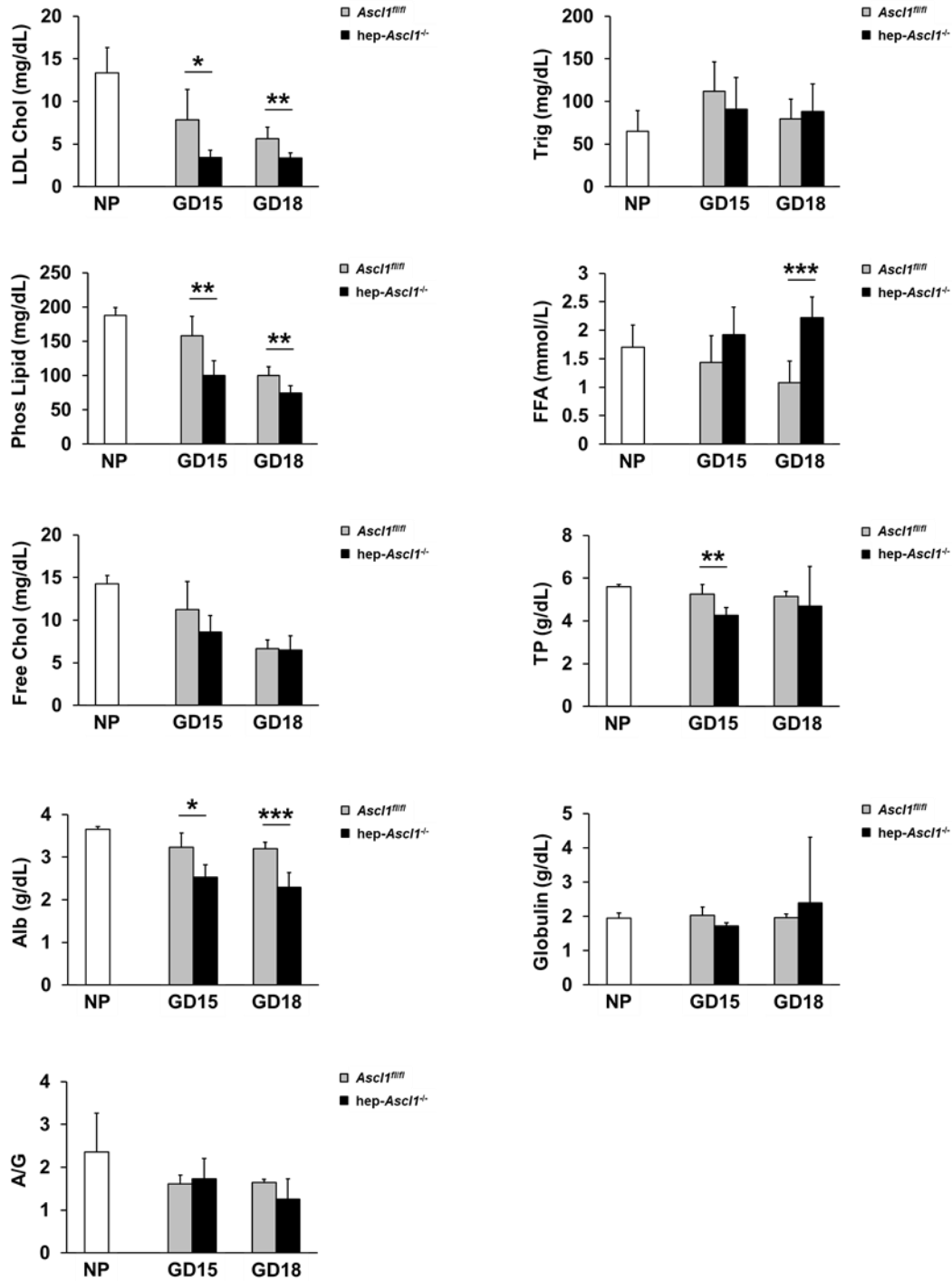


Figure 15, continued.



**Table 9. List of Serum Biochemical Profiles in Hepatocyte-Specific *Ascl1* Gene Knockout**

| Name       | Unit   | NP                           | GD15                         |                                | GD18                         |                                |
|------------|--------|------------------------------|------------------------------|--------------------------------|------------------------------|--------------------------------|
|            |        | <i>Ascl1<sup>fl/fl</sup></i> | <i>Ascl1<sup>fl/fl</sup></i> | <i>hep-Ascl1<sup>-/-</sup></i> | <i>Ascl1<sup>fl/fl</sup></i> | <i>hep-Ascl1<sup>-/-</sup></i> |
| BUN        | mg/dL  | 20.7 ± 4.3                   | 32.7 ± 11.6                  | 23.4 ± 7.1                     | 27.6 ± 5.5                   | 18.5 ± 1.8                     |
| Enz Creat  | mg/dL  | 0.14 ± 0.01                  | 0.17 ± 0.03                  | 0.14 ± 0.04                    | 0.18 ± 0.03                  | 0.13 ± 0.02                    |
| ALP        | IU/L   | 170 ± 31                     | 78 ± 11                      | 152 ± 15                       | 96 ± 4                       | 317 ± 44                       |
| ALT        | IU/L   | 29 ± 5                       | 23 ± 2                       | 34 ± 16                        | 27 ± 5                       | 68 ± 25                        |
| AST        | IU/L   | 186 ± 75                     | 119 ± 20                     | 181 ± 47                       | 138 ± 15                     | 201 ± 45                       |
| CK         | IU/L   | 2142 ± 1701                  | 914 ± 322                    | 1109 ± 279                     | 1269 ± 405                   | 594 ± 368                      |
| Na         | mmol/L | 159 ± 5                      | 151 ± 2                      | 150 ± 2                        | 150 ± 2                      | 148 ± 2                        |
| K          | mmol/L | 8.3 ± 0.7                    | 8.2 ± 1.2                    | 8.8 ± 0.3                      | 8.3 ± 1.1                    | 7.4 ± 1.4                      |
| Cl         | mmol/L | 112 ± 1                      | 105 ± 1                      | 107 ± 1                        | 104 ± 2                      | 104 ± 0                        |
| Ca         | mg/dL  | 9.8 ± 0.6                    | 10.7 ± 0.8                   | 9.7 ± 0.7                      | 10.6 ± 0.3                   | 9.3 ± 0.5                      |
| IP         | mg/dL  | 8.43 ± 1.12                  | 9.60 ± 0.95                  | 10.66 ± 0.29                   | 9.55 ± 0.69                  | 9.42 ± 1.14                    |
| Glu        | mg/dL  | 190.3 ± 34.1                 | 153.7 ± 15.3                 | 147.8 ± 13.1                   | 163.9 ± 18.7                 | 145.1 ± 19.0                   |
| Chol       | mg/dL  | 98 ± 7                       | 75 ± 13                      | 44 ± 10                        | 51 ± 8                       | 36 ± 4                         |
| HDL Chol   | mg/dL  | 92.6 ± 5.7                   | 65.5 ± 10.1                  | 37.9 ± 7.8                     | 48.6 ± 7.7                   | 32.6 ± 3.4                     |
| LDL Chol   | mg/dL  | 13.4 ± 3.0                   | 7.8 ± 3.6                    | 3.4 ± 0.8                      | 5.6 ± 1.3                    | 3.4 ± 0.6                      |
| Trig       | mg/dL  | 65.0 ± 24.4                  | 111.7 ± 34.9                 | 91.0 ± 36.9                    | 79.3 ± 23.5                  | 88.2 ± 32.2                    |
| Phos Lipid | mg/dL  | 188 ± 12                     | 158 ± 28                     | 100 ± 22                       | 100 ± 12                     | 74 ± 11                        |
| FFA        | mmol/L | 1.71 ± 0.38                  | 1.44 ± 0.47                  | 1.92 ± 0.49                    | 1.08 ± 0.38                  | 2.22 ± 0.36                    |
| Free Chol  | mg/dL  | 14 ± 1                       | 11 ± 3                       | 9 ± 2                          | 7 ± 1                        | 7 ± 2                          |
| TP         | g/dL   | 5.59 ± 0.12                  | 5.25 ± 0.44                  | 4.25 ± 0.37                    | 5.15 ± 0.23                  | 4.68 ± 1.86                    |
| Alb        | g/dL   | 3.65 ± 0.07                  | 3.23 ± 0.33                  | 2.53 ± 0.29                    | 3.20 ± 0.15                  | 2.29 ± 0.35                    |
| Globulin   | g/dL   | 1.94 ± 0.15                  | 2.02 ± 0.24                  | 1.72 ± 0.09                    | 1.95 ± 0.11                  | 2.39 ± 1.91                    |
| A/G        |        | 2.36 ± 0.91                  | 1.61 ± 0.21                  | 1.73 ± 0.48                    | 1.64 ± 0.08                  | 1.26 ± 0.47                    |

### 3.4.8 Hepatocyte-specific *Ascl1* knockout causes hepatic fat accumulation

To determine whether the maternal liver without *Ascl1* accumulates fat, we performed the Oil Red O (ORO) staining. The results showed that the *hep-Ascl1<sup>-/-</sup>* maternal liver displayed a 4-fold increase in lipid contents on GD15 when compared to the control mice (**Fig. 16A**). However, hepatic lipid content was not different between the two genotypes on GD18. qRT-PCR showed that the elongation of very long chain fatty acids protein 6 (*Elovl6*), which adds carbons to increase the length of fatty acids, in *Ascl1<sup>fl/fl</sup>* mice decreased on GD15 by 9% and on GD18 by 67% (**Fig. 16B**). Patatin like phospholipase domain containing 3 (*Pnpla3*), which hydrolysis triacylglycerol,

in hep-*Ascl1*<sup>-/-</sup> mice decreased on GD15 by 82% (**Fig. 16C**). We observed no differential expression between genotype groups for fatty acid synthase (*Fasn*), which synthesizes long-chain saturated fatty acids, stearoyl-CoA desaturase (*Scd1*), which synthesizes oleic acid, and fat storage inducing transmembrane protein 1 (*Fitm1*), which involves in fat storage (**Fig. 16D-F**). Thus, these data suggest that *Ascl1* regulates fat metabolism during pregnancy by modulating the expression of a subset of genes involved in lipid synthesis and breakdown.

### 3.4.9 Hepatocyte-Specific *Ascl1* knockout results in maternal pancreas abnormalities

The maternal pancreas responds to pregnancy by the proliferation of maternal  $\beta$ -cells to increase insulin secretion and balance glucose homeostasis between the mother and the fetus (96). To determine whether the deletion of *Ascl1* in the maternal hepatocytes caused changes to the liver-pancreas axis, we collected the maternal pancreas in *Ascl1*<sup>-/-</sup> mice on GD 18 and 19. We observed a 62% increase in the pancreas-to-body weight ratio in the *Ascl1*<sup>-/-</sup> mice when compared with the controls (**Fig. 17A-B**). We performed a glucose tolerance test by injecting 2 g of glucose per kg of body weight on GD18 and measured the blood glucose in 0, 15, 30, 60, 90, and 120 min after the administration. However, we were unable to observe differences in glucose tolerance between genotype groups (**Fig. 17C**). Furthermore, we stained the maternal pancreas on GD19 for insulin and found that the hep-*Ascl1*<sup>-/-</sup> pancreas had a reduction in insulin staining area by 50% in the ventral pancreas and 56% in the dorsal pancreas (**Fig. 17D-E**). By serum biochemistry analysis, we found that the serum glucose and insulin levels did not differ between genotypes on GD15 and GD18 (**Fig. 17F-G**). Both genotypes had similar Ki67 staining in both endocrine and exocrine cells (**Fig. 17H**). Therefore, in the absence of hepatic *Ascl1*, the maternal pancreas increases in size possibly via acinar cell proliferation without disturbing  $\beta$ -cell function.

**Figure 16. Hepatic lipid deposition and the expression of lipid-associated genes after hepatic *Ascl1* ablation.** Maternal liver and serum were collected from *Ascl1<sup>fl/fl</sup>* and hep-*Ascl1<sup>-/-</sup>* mice (described in **Fig. 9**). **(A)** Oil Red O (ORO) staining. Gestation day (GD) 15 livers from *Ascl1<sup>fl/fl</sup>* and hep-*Ascl1<sup>-/-</sup>* mice were subjected to ORO staining. The lipid droplets are stained red. **(B-F)** Hepatic lipid gene analysis. Total RNA was isolated from livers of nonpregnant (NP) and pregnant (GD15 and 18) *Ascl1<sup>fl/fl</sup>* and hep-*Ascl1<sup>-/-</sup>* mice. Hepatic **(B)** *Elovl6*, **(C)** *Pnpla3*, **(D)** *Fasn*, **(E)** *Scd1*, and **(F)** *Fitm1* mRNA levels were measured using quantitative real-time polymerase chain reaction (qRT-PCR) and expressed as the mean fold changes relative to NP controls ( $\pm$  s.d.; n = 4-5). \*,  $P < 0.05$ , between *Ascl1<sup>fl/fl</sup>* and hep-*Ascl1<sup>-/-</sup>* mice. *18S* ribosomal RNA (rRNA) levels were used as endogenous controls. *Ascl1*, achaete-scute homolog 1; *Elovl6*, elongation of very long chain fatty acids protein 6; *Pnpla3*, patatin like phospholipase domain containing 3; *Fasn*, fatty acid synthase; *Scd1*, stearoyl-CoA desaturase; *Fitm1*, fat storage inducing transmembrane protein 1.

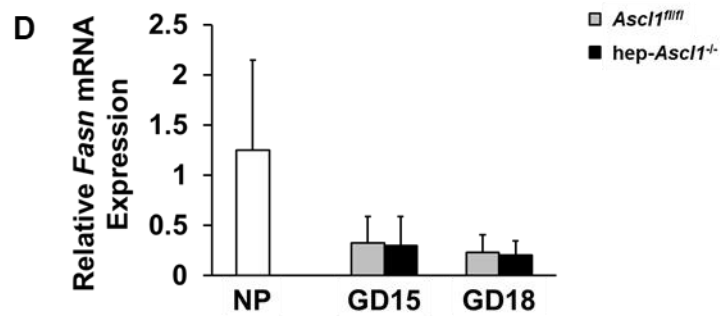
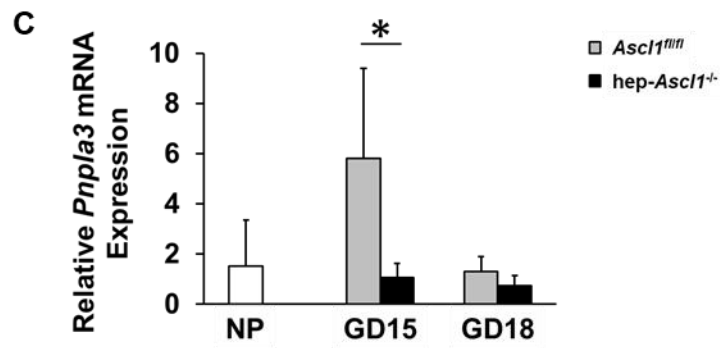
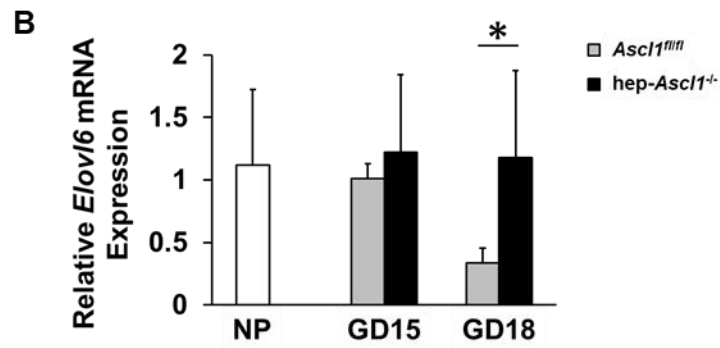
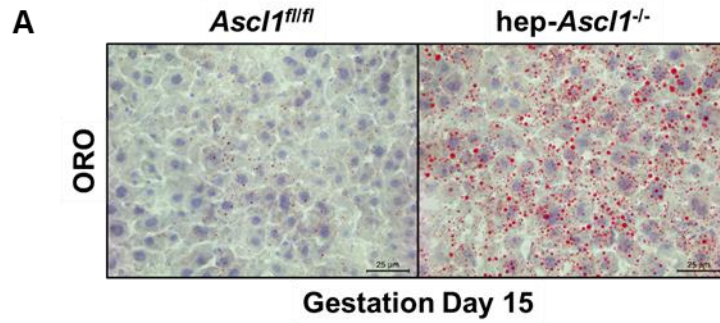
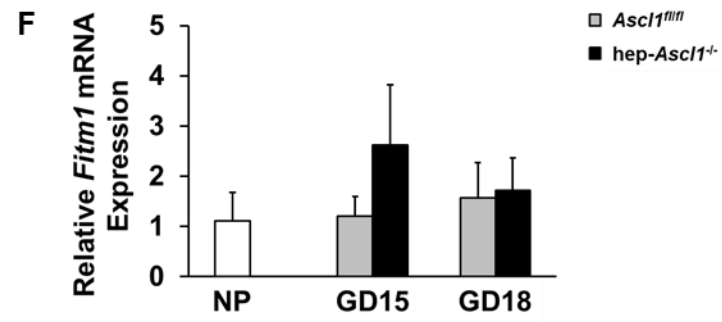
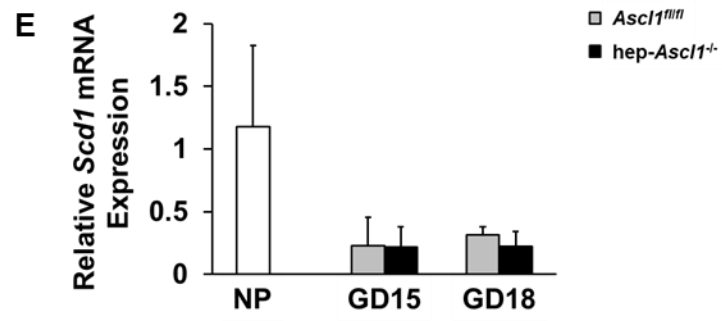


Figure 16, continued.



**Figure 17. Hepatocyte-specific *Ascl1* ablation phenotypes in the maternal pancreas.** The maternal pancreas was collected and weighed from *Ascl1<sup>fl/fl</sup>* and hep-*Ascl1<sup>-/-</sup>* mice (described in **Fig. 9**). **(A)** Morphology of the *Ascl1<sup>fl/fl</sup>* and hep-*Ascl1<sup>-/-</sup>* pancreas on gestation day (GD) 18. **(B)** The maternal pancreas-to-body weight ratios of *Ascl1<sup>fl/fl</sup>* and hep-*Ascl1<sup>-/-</sup>* mice are presented. Data are expressed as means  $\pm$  s.d. (n = 4-5). \*\*,  $P < 0.01$ , between *Ascl1<sup>fl/fl</sup>* and hep-*Ascl1<sup>-/-</sup>* mice. **(C)** Glucose tolerance test (GTT). Pregnant *Ascl1<sup>fl/fl</sup>* and hep-*Ascl1<sup>-/-</sup>* mice on GD18 were fasted for 6 hrs and injected with glucose (2 g of glucose/kg of body weight) via intraperitoneally. Blood glucose levels were measured using a glucometer (OneTouch Ultra 2) before and 30 min after the glucose injection. **(D-E)** Pancreatic islet analysis. Maternal pancreatic sections of *Ascl1<sup>fl/fl</sup>* and hep-*Ascl1<sup>-/-</sup>* mice on GD19 were subjected to  $\beta$ -Catenin staining. The quantification of percent area insulin staining in **(D)** ventral and **(E)** dorsal pancreas was performed by Eli Lilly and Company. Data are expressed as means  $\pm$  s.d. (n = 3-5). \*,  $P < 0.05$ , between *Ascl1<sup>fl/fl</sup>* and hep-*Ascl1<sup>-/-</sup>* mice. **(F-G)** Pancreatic function test. **(F)** Serum glucose was analyzed by Eli Lilly and Company and **(G)** serum insulin was analyzed by the Translation Core at the IU School of Medicine Center for Diabetes and Metabolic Diseases. Data are expressed as means  $\pm$  s.d. (n = 3-6). **(H)** Maternal pancreatic proliferation. Maternal pancreatic sections of *Ascl1<sup>fl/fl</sup>* and hep-*Ascl1<sup>-/-</sup>* mice on GD18 were subjected to Ki67 staining. Ki67-positive cells are stained dark brown in the nucleus. *Ascl1*, achaete-scute homolog 1; Glu, glucose.

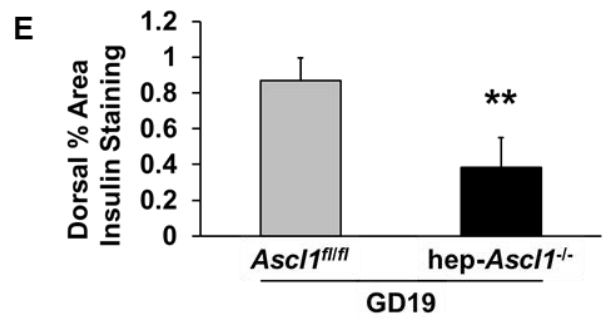
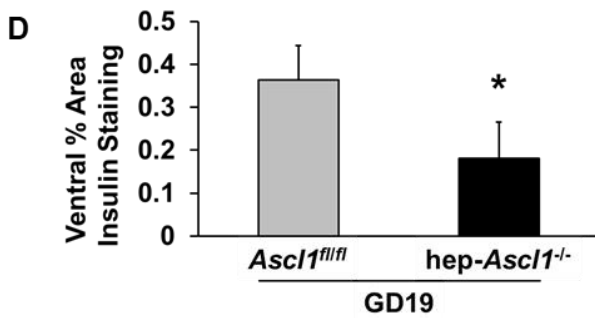
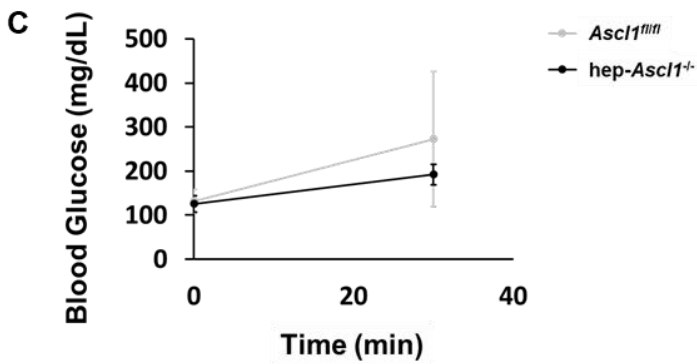
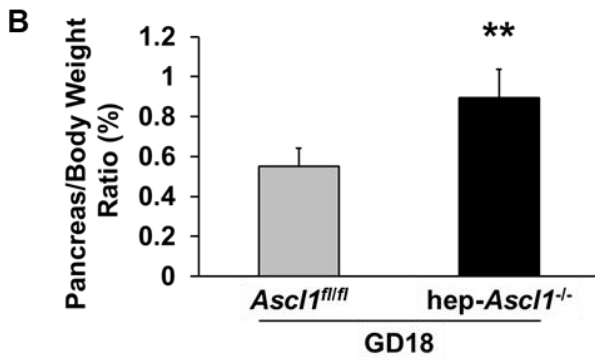
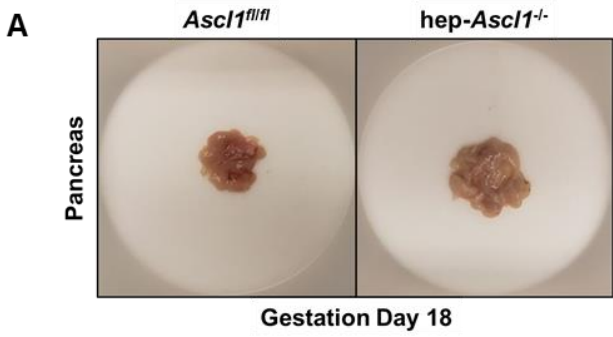
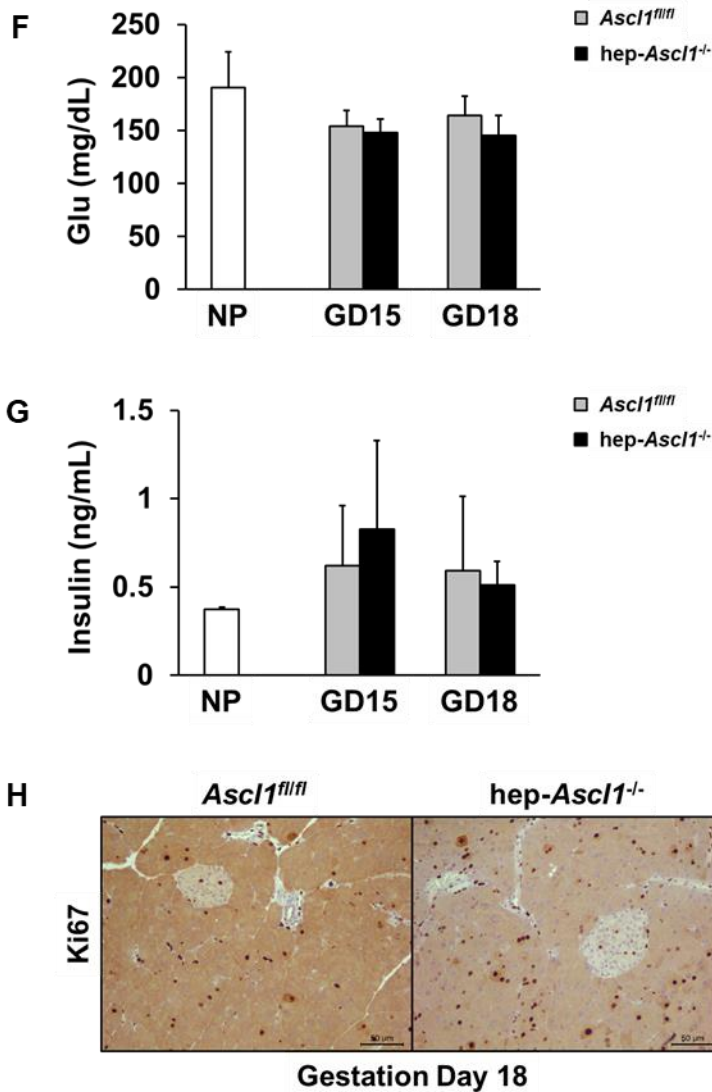


Figure 17, continued.



### 3.4.10 Hepatocyte-Specific *Ascl1* knockout results in abnormalities in maternal compartments

The human maternal spleen enlarges approximately by 50% by the end of pregnancy (108). We have previously shown that the largest splenic growth takes place by the end of gestation in rats and during midgestation in mice due to an increase in the red pulp (177). The maternal spleens in *hep-Ascl1<sup>-/-</sup>* mice were enlarged by 21.4% on GD15 and by 72.3% on GD18 when compared

with the controls (**Fig. 18A-B**). By H&E staining, we were unable to identify overt structural phenotypes in the maternal spleens of hep-*Ascl1*<sup>-/-</sup> mice except that both the red and white pulps enlarged proportionally when compared with the controls (**Fig. 18C**). Interestingly, maternal kidney-to-body weight ratios in hep-*Ascl1*<sup>-/-</sup> mice increased on GD18 by 21% when compared with the controls (**Fig. 18D**). The results revealed that maternal liver crosstalks with other maternal organs via hepatic *Ascl1*.

### 3.4.11 Hepatocyte-specific *Ascl1* knockout results in placental abnormalities

The placental weight in hep-*Ascl1*<sup>-/-</sup> mice had an increase of 26.9% on GD15 and had an increase of 33.0% on GD18 when compared with the controls (**Fig. 19A**). H&E staining showed that the placenta of hep-*Ascl1*<sup>-/-</sup> mice appeared enlarged with an expansion of both the junctional zone and the labyrinth zone (**Fig. 19B**). Periodic acid-Schiff (PAS) staining revealed similar glycogen staining in both genotypes (**Fig. 19C**). *In situ* hybridization showed similar staining in both genotypes for placental lactogen (PL)-I and II on GD15 and GD18, and PL-II on GD18 (**Fig. 19D**). Serum biochemistry analysis revealed that, when compared with the controls, hep-*Ascl1*<sup>-/-</sup> mice had an increase of alkaline phosphatase (ALP) on GD15 and GD18 by 95% and 231%, respectively (**Fig. 19E**). We also analyzed the placental insulin-like growth factor 2 (IGF2) and its downstream proteins by western blotting (**Fig. 19F**). In the hep-*Ascl1*<sup>-/-</sup> placenta, IGF2 decreased by 32% on GD15 and the protein kinase B (AKT) increased in phosphorylation at S473 by 24% on GD18 but not on T308 during pregnancy. Interestingly, the hep-*Ascl1*<sup>-/-</sup> placenta on GD18 had decreased the activities of ERK1 by 80% and ERK2 by 76%. Furthermore, we did not observe significant changes in Janus kinase 2 (p-JAK2) activity and PL-II protein expression. Taken together, we demonstrated that the lack of *Ascl1* in maternal hepatocytes leads to placental overgrowth, accompanied by decreased placental IGF2 production and ERK1/2 activity.

**Figure 18. Hepatocyte-specific *Ascl1* ablation phenotypes in spleen and kidney.** The maternal spleens and kidneys were collected and weighed from *Ascl1<sup>fl/fl</sup>* and hep-*Ascl1<sup>-/-</sup>* mice (described in **Fig. 9**). **(A)** Morphology of the *Ascl1<sup>fl/fl</sup>* and hep-*Ascl1<sup>-/-</sup>* mouse spleens on gestation day (GD) 18. **(B)** The maternal spleen-to-body weight ratios of *Ascl1<sup>fl/fl</sup>* and hep-*Ascl1<sup>-/-</sup>* mice are presented. Data are expressed as means  $\pm$  s.d. (n = 4-10). \*,  $P < 0.05$ , between *Ascl1<sup>fl/fl</sup>* and hep-*Ascl1<sup>-/-</sup>* mice. **(C)** Maternal splenic histology. Maternal splenic sections of *Ascl1<sup>fl/fl</sup>* and hep-*Ascl1<sup>-/-</sup>* mice on GD15 were subjected to hematoxylin and eosin (H&E) staining. **(D)** The maternal kidney-to-body weight ratios of *Ascl1<sup>fl/fl</sup>* and hep-*Ascl1<sup>-/-</sup>* mice are presented. Data are expressed as means  $\pm$  s.d. (n = 4-5). \*\*\*,  $P < 0.001$ , between *Ascl1<sup>fl/fl</sup>* and hep-*Ascl1<sup>-/-</sup>* mice.

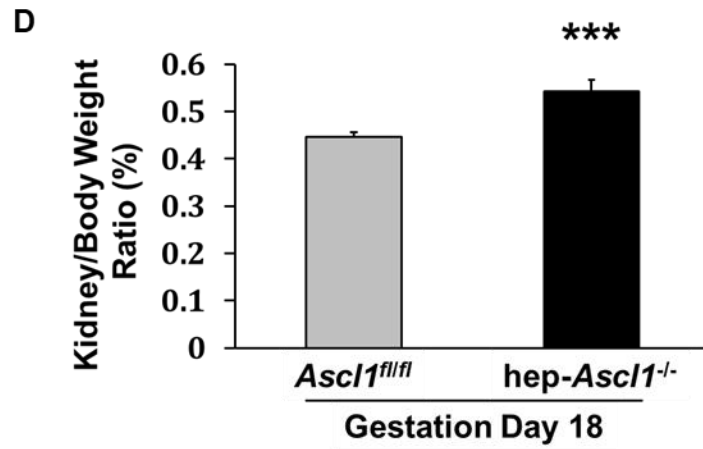
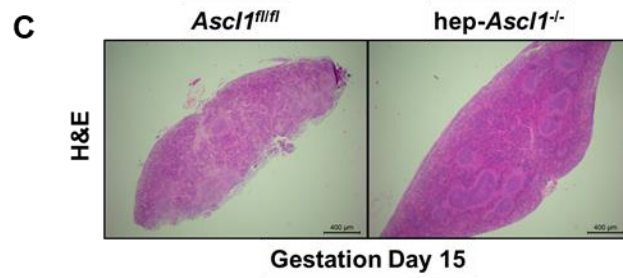
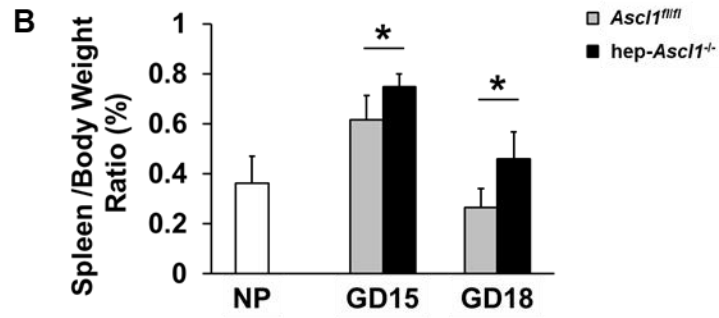
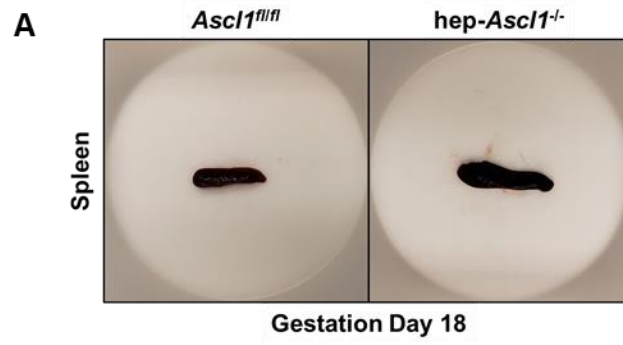


**Figure 19. Hepatocyte-specific *Ascl1* ablation phenotypes in the placenta.** The maternal placenta was collected and weighed from *Ascl1<sup>fl/fl</sup>* and hep-*Ascl1<sup>-/-</sup>* mice (described in **Fig. 9**). **(A)** Placental weights of *Ascl1<sup>fl/fl</sup>* and hep-*Ascl1<sup>-/-</sup>* mice are presented. Data are expressed as means  $\pm$  s.d. (n = 4-9). \*,  $P < 0.05$ ; \*\*,  $P < 0.01$ , between *Ascl1<sup>fl/fl</sup>* and hep-*Ascl1<sup>-/-</sup>* mice. **(B-D)** Maternal placental histology. Placental sections of *Ascl1<sup>fl/fl</sup>* and hep-*Ascl1<sup>-/-</sup>* mice on gestation day (GD) 15 were subjected to **(B)** hematoxylin and eosin (H&E) and **(C)** periodic acid-Schiff (PAS) staining. The glycogen is stained red to purple. **(D)** Placental sections were also subjected to PL-I and PL-II *in situ* hybridization staining using RNAscope 2.5 HD Assay-BROWN kit. The PL-I and PL-II mRNAs are stained dark brown. **(E)** Maternal serum analysis. Maternal serum was collected from *Ascl1<sup>fl/fl</sup>* and hep-*Ascl1<sup>-/-</sup>* mice (described in **Fig. 9**). Maternal serum alkaline phosphatase (ALP) from *Ascl1<sup>fl/fl</sup>* and hep-*Ascl1<sup>-/-</sup>* mice was analyzed by Eli Lilly and Company. **(F)** Placental protein expression. Western blotting was performed on GD15 and GD18 placental homogenates from *Ascl1<sup>fl/fl</sup>* and hep-*Ascl1<sup>-/-</sup>* mice using antibodies against the proteins listed. GAPDH protein levels were used as loading controls. **(G)** Quantification of the placental protein expression. Placental protein levels from **Fig. 19F** were measured using ImageJ and expressed as the mean fold changes relative to GD15 controls ( $\pm$  s.d.; n = 3 for each group). \*,  $P < 0.05$ , between *Ascl1<sup>fl/fl</sup>* and hep-*Ascl1<sup>-/-</sup>* mice. *Ascl1*, achaete-scute homolog 1; IGF2, insulin-like growth factor; ERK1/2, extracellular signal-regulated kinase 1/2; JAK2, Janus kinase 2; PL-II, placental lactogen II; GAPDH, glyceraldehyde 3-phosphate dehydrogenase.

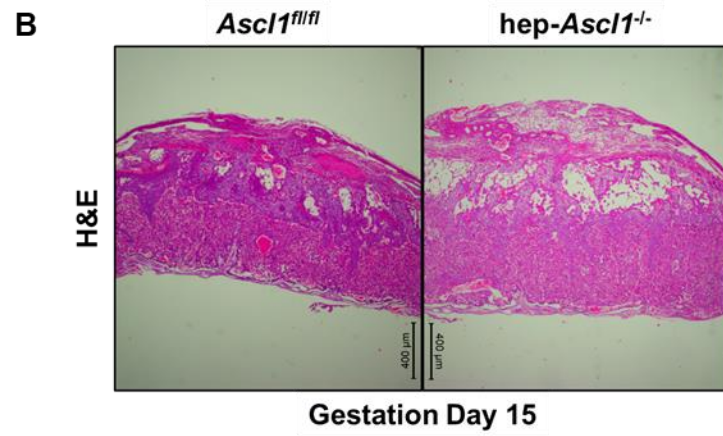
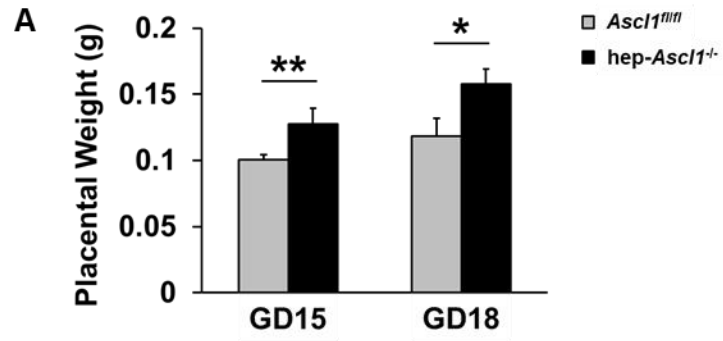


Figure 19, continued.

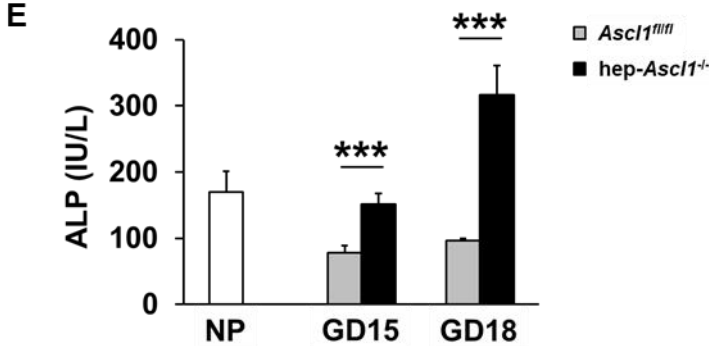
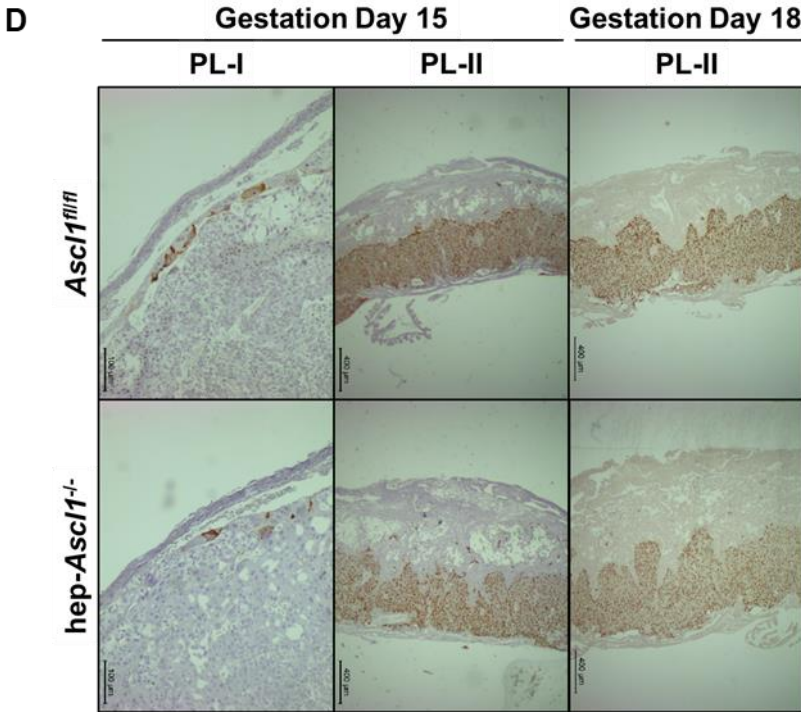


Figure 19, continued.

F

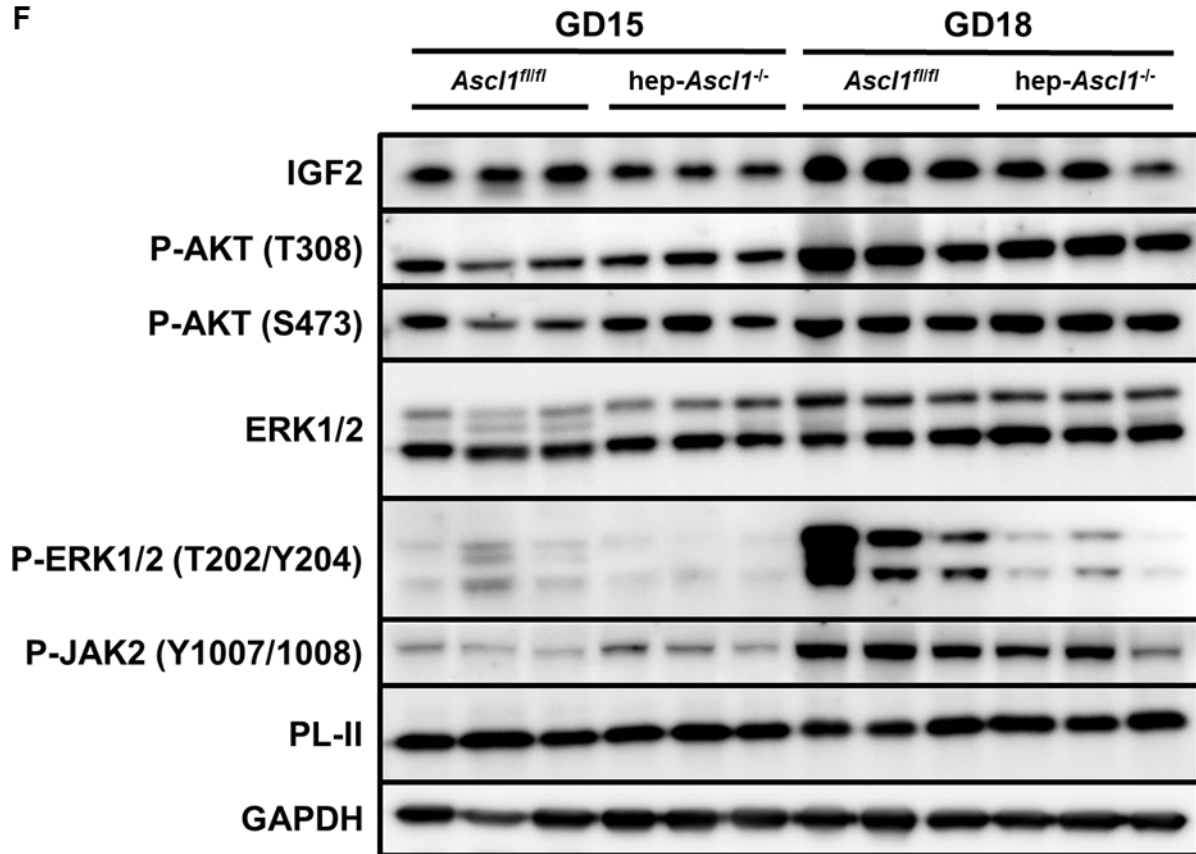
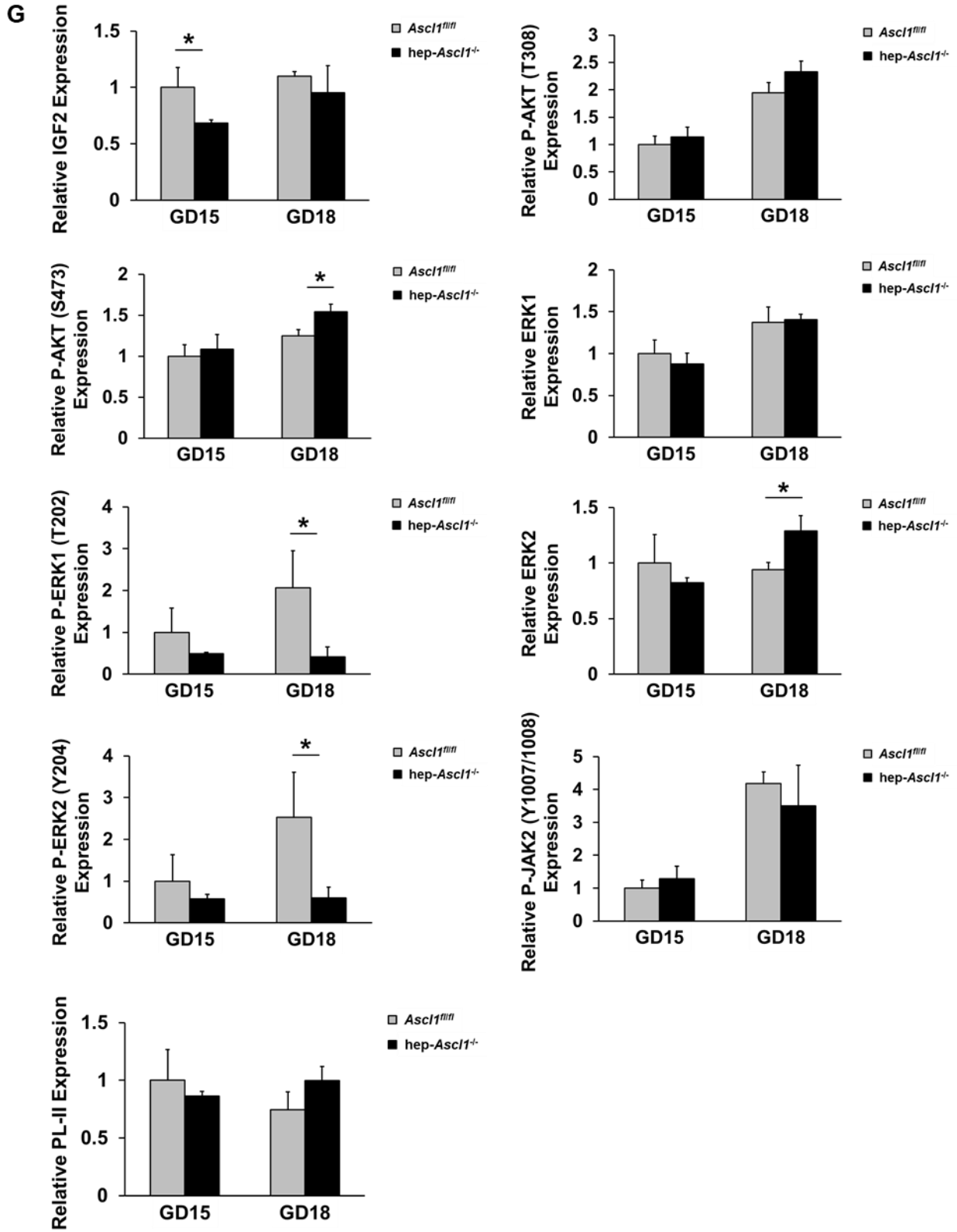


Figure 19, continued.



### 3.4.12 Hepatocyte-specific *Ascl1* knockout results in fetal growth abnormalities

There were no differences in fetal weight and number between hep-*Ascl1*<sup>-/-</sup> and control mice on GD15 and GD18 (**Fig. 20A-B**). However, the bodyweight of pups born from hep-*Ascl1*<sup>-/-</sup> mice was heavier, when compared with the controls, on week 1 by 9%, 2 by 5%, and 5 by 5% after weaning for males and weeks 1 by 10% and 2 by 5% after weaning for females (**Fig. 20C-D**). The body weight changes of the pups born from hep-*Ascl1*<sup>-/-</sup> mice, when compared with the controls, increased on week 1 by 16% but decreased on week 2 by 41% in males and increased on weeks 1 by 32% and 5 by 43% but decreased on week 2 by 35% and 3 by 38% in females (**Fig. 20E-F**). We also tested the blood glucose on the pups born from both genotypes but observed no differences in both males and females (**Fig. 20G**). Therefore, the ablation of maternal hepatic *Ascl1* during pregnancy affects postnatal growth.

### 3.4.13 Hepatocyte-Specific *Ascl1* knockout results in changes in subpopulations of cecal microbiota

We submitted cecal samples of both genotypes to Zymo Research Corporation (Irvine, CA) for sequencing analysis of 16s rRNA on gestation day (GD) 18. We observed changes in several subpopulations of cecal microbiota. *Pseudobutyrvibrio-Roseburia intestinalis*, *Helicobacter hepaticus*, *Clostridiales vadinBB60* were present greater in the control cecal samples whereas *Desulfovibrio oxamicus-vulgaris*, *Candidatus*, *Lactobacillus johnsonii*, *Eubacterium*, and *Bacteroides acidifaciens* were more present in the hep-*Ascl1*<sup>-/-</sup> cecal samples (**Fig. 21A**). Notably, *Pseudobutyrvibrio-Roseburia intestinalis* was absent in the hep-*Ascl1*<sup>-/-</sup> cecal whereas *Desulfovibrio oxamicus-vulgaris* was absent in the control cecal. By qRT-PCR, we observed that a hepatic gene called hepcidin antimicrobial peptide 2 (*Hamp2*) silenced by 99% on GD15 and by

100% GD18 due to the *Ascl1* deficiency in maternal hepatocytes (**Fig. 21B**). Therefore, we demonstrated that maternal hepatic *Ascl1* regulates maternal microbiota at least partly via *Hamp2*.

**Figure 20. Hepatocyte-specific *Ascl1* ablation phenotypes in the fetus and postnatal growth.** Fetuses and weaned pups were collected and weighed from *Ascl1<sup>fl/fl</sup>* and hep-*Ascl1<sup>-/-</sup>* dams (described in **Fig. 9**). Fetal weight (**A**) and numbers (**B**) were recorded. (**C-F**) Postnatal pups were weighed after weaning. (**G**) Fetal glucose measurement. Fetal blood glucose was measured using a glucometer (OneTouch Ultra 2) 5 weeks after weaning. ( $\pm$  SEM; n = 13-31). \*,  $P < 0.05$ ; \*\*,  $P < 0.01$ ; \*\*\*,  $P < 0.001$ , between pups born from *Ascl1<sup>fl/fl</sup>* and hep-*Ascl1<sup>-/-</sup>* dams. *Ascl1*, achaete-scute homolog 1.

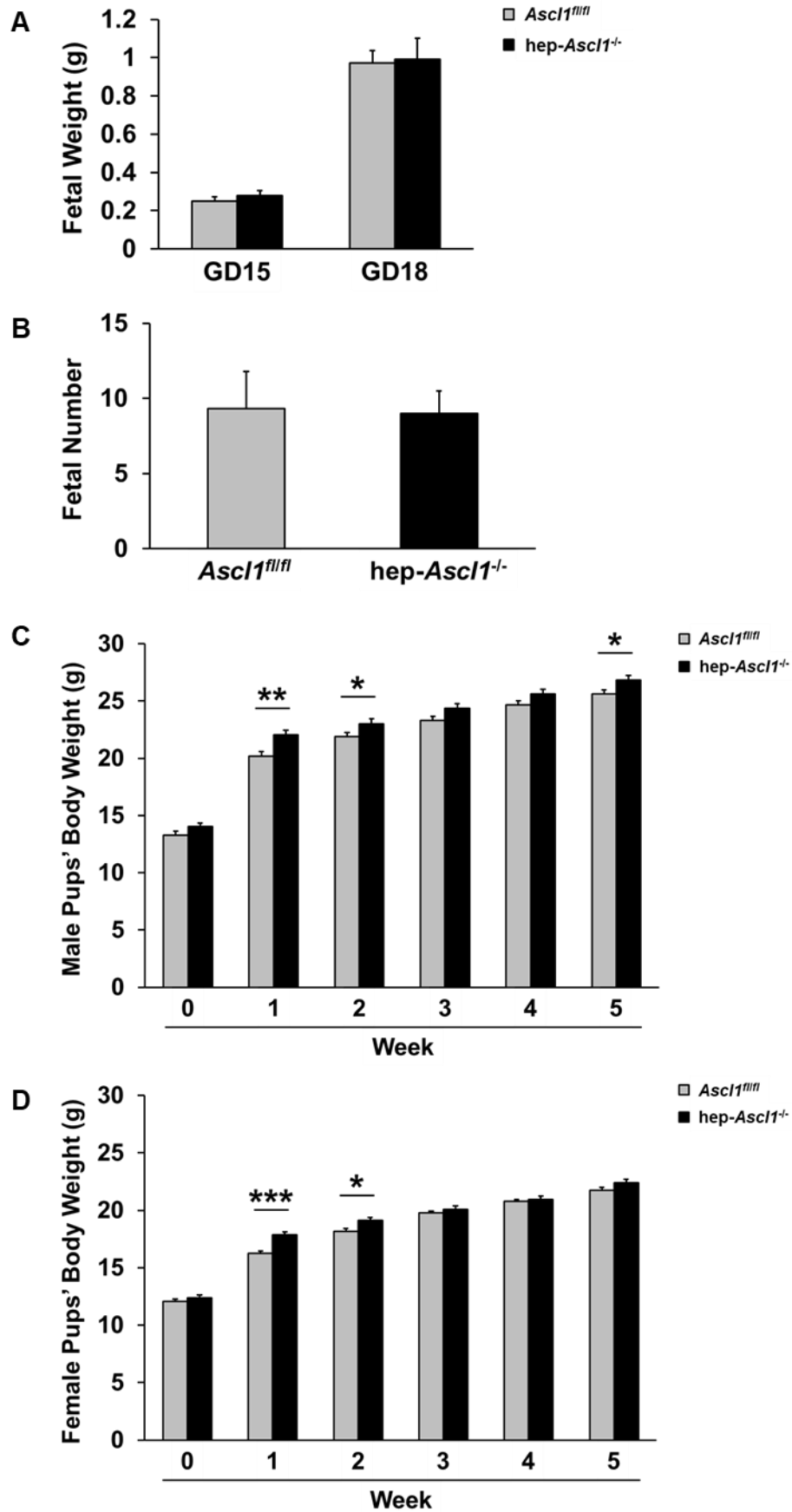
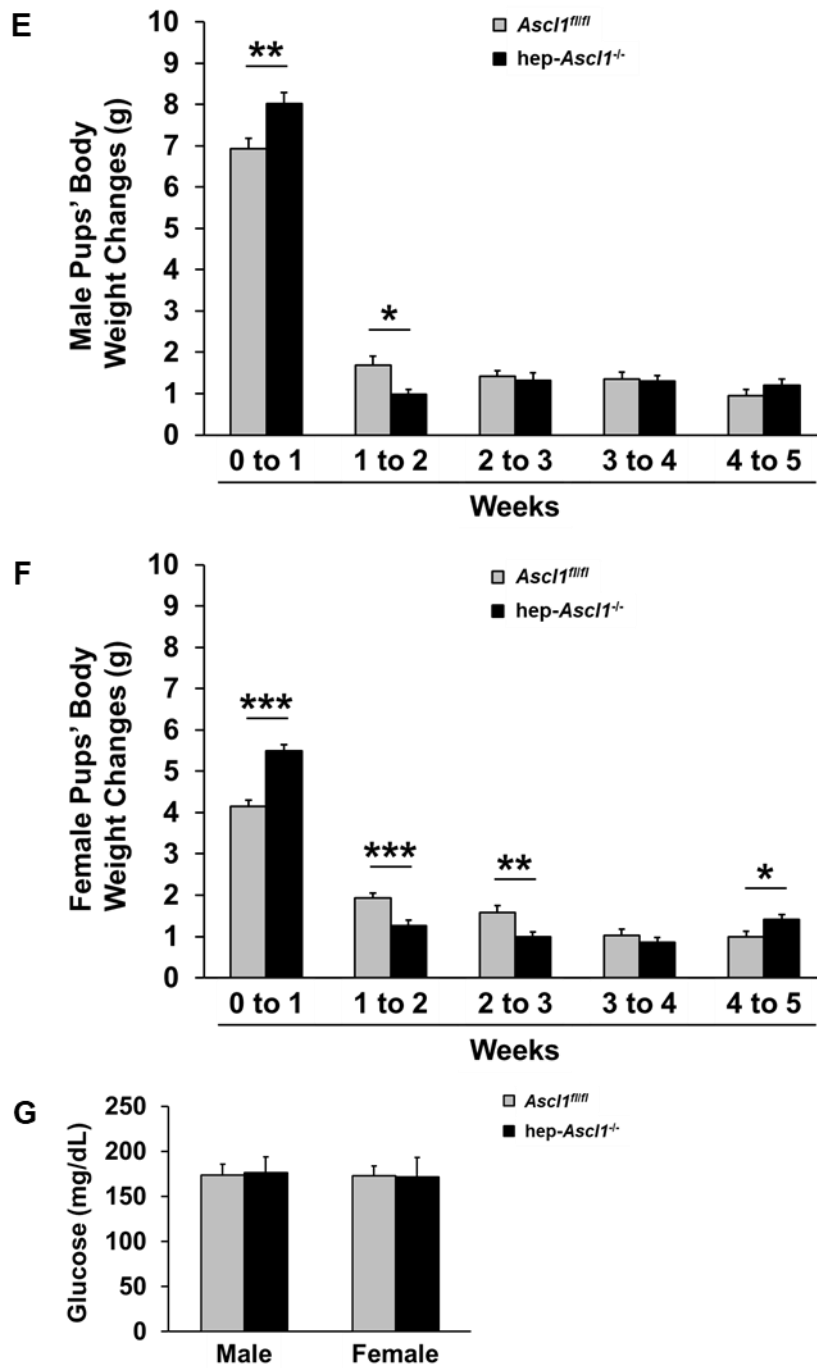
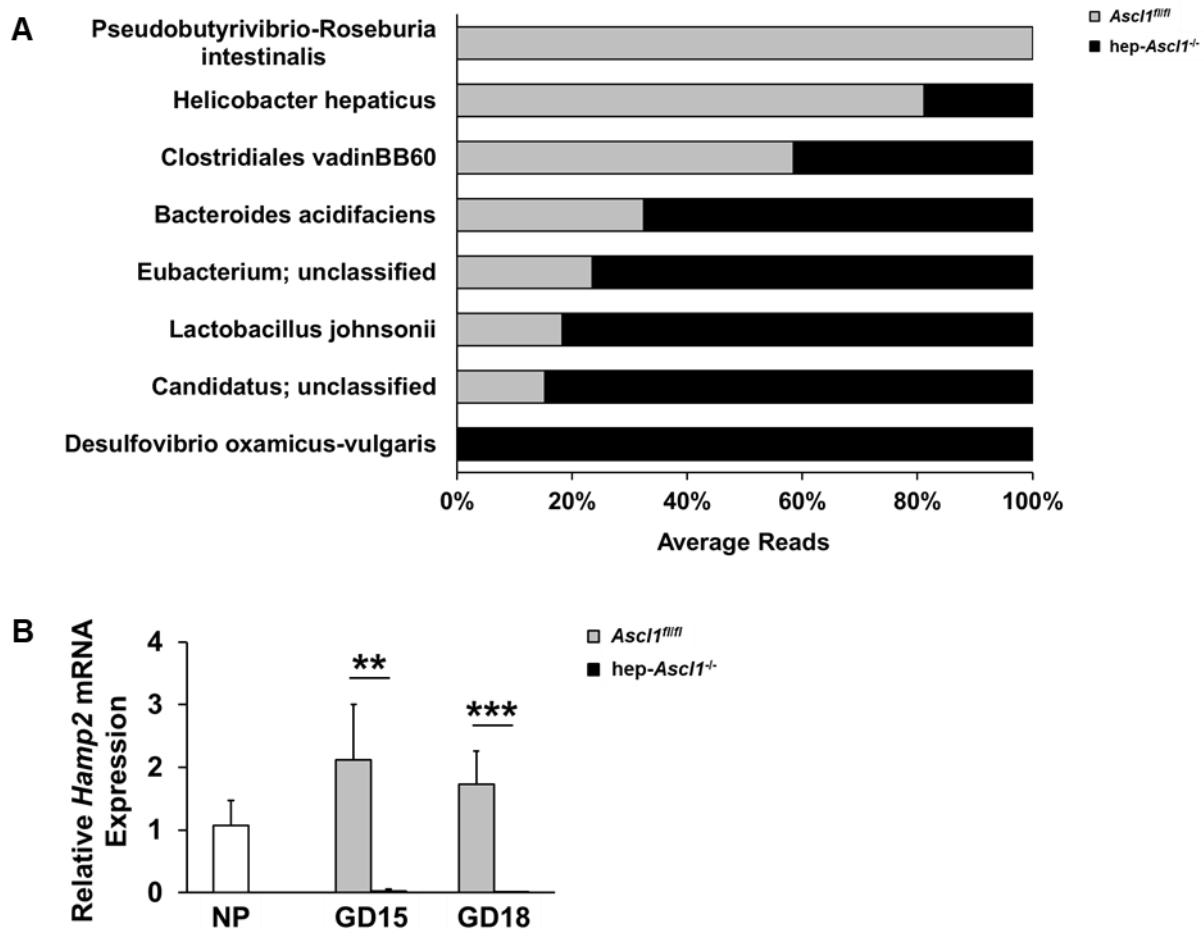


Figure 20, continued.





**Figure 21. Hepatocyte-specific *Ascl1* ablation phenotypes in maternal cecal microbiota.** The maternal cecal samples were collected from *Ascl1<sup>fl/fl</sup>* and hep-*Ascl1*<sup>-/-</sup> mice on gestation day (GD) 18 (described in Fig. 9). (A) DNA was isolated from maternal cecal microbiota of *Ascl1<sup>fl/fl</sup>* and hep-*Ascl1*<sup>-/-</sup> mice on GD18 using the PureLink Microbiome DNA Purification Kit. Maternal cecal microbiota changes with  $P < 0.05$  analyzed by Zymo Research Corporation. (B) Total RNA was isolated from livers of nonpregnant (NP) and pregnant (GD15 and GD18) *Ascl1<sup>fl/fl</sup>* and hep-*Ascl1*<sup>-/-</sup> mice. Hepatic hepcidin antimicrobial peptide 2 (*Hamp2*) mRNA levels were measured using quantitative real-time polymerase chain reaction (qRT-PCR) and expressed as the mean fold changes relative to nonpregnant (NP) controls ( $\pm$  s.d.;  $n = 3-4$ ). \*\*,  $P < 0.01$ ; \*\*\*,  $P < 0.001$ , between *Ascl1<sup>fl/fl</sup>* and hep-*Ascl1*<sup>-/-</sup> mice. *18S* ribosomal RNA (rRNA) levels were used as endogenous controls. *Ascl1*, achaete-scute homolog 1.

## CHAPTER 4. DISCUSSION

### 4.1 Introduction

The liver maintains its size proportional to body weight under homeostasis (28). Many studies revealed the mechanisms of liver growth under injury and stress (1). The maternal liver is unique in that it increases in size and weight to accommodate the increased metabolic needs of the developing placenta and fetus (27). However, the current knowledge of maternal liver growth is lacking. Here, we identified achaete-scute homolog 1 (*Ascl1*), a proneural gene that is quiescent under homeostasis in the liver, highly activated in maternal hepatocytes during mid to late gestation. By establishing three distinct *in vivo* *Ascl1* knockout mouse models, we demonstrated that hepatic *Ascl1* affects the hepatocyte size and identity, numerous hepatic gene expressions, and many signaling pathways. Furthermore, hepatic *Ascl1* influences multiple nonreproductive maternal organs as well as the placenta and fetus, which further illustrates the importance of this gene. Therefore, by elucidating the function of *Ascl1* in the maternal liver, we may partially fill in the knowledge gap of the mechanisms behind the maternal liver adaptations, and help clarify the cause and develop novel therapies on pregnancy-related liver diseases.

### 4.2 Mouse model

We observed that the maternal hepatocytes activate and increase the expression of *Ascl1* in most of the hepatocytes starting from midgestation until the end of pregnancy. Traditional knockout mouse studies cannot be applied to *Ascl1* because pups born with *Ascl1* deficiency die at birth due to respiratory and eating problems. To study the function of *Ascl1* in adults and especially during pregnancy, we generated three independent inducible mouse lines that delete *Ascl1* globally, cell-specifically, and hepatocyte-specifically using doxycycline, tamoxifen, and

virus, respectively (130). Confirmed by quantitative real-time polymerase chain reaction (qRT-PCR), all mouse models effectively deleted *Ascl1* in the maternal liver.

To delete *Ascl1* globally during pregnancy, we generated the *Ascl1*<sup>-/-</sup> (*Ascl1*<sup>fl/fl</sup>;*R26*<sup>rtTA/rtTA</sup>;*tetO*<sup>Cre/-</sup>) mouse model and administered doxycycline before the activation of hepatic *Ascl1*. Doxycycline is a derivative of tetracycline, an antibiotic categorized as a class D drug, that is effective against various infectious diseases in adult and pregnant women such as Lyme disease, anthrax, cholera, and malaria by inhibiting bacterial protein synthesis (182). Additionally, unlike tetracycline, prior research revealed no evidence of doxycycline causing adverse effects such as teratogenicity or hepatotoxicity (183, 184). The use of the doxycycline-induced global knockout mouse model is prevalent in studying the function of a gene in various tissues and organs during development, adult, and pregnancy (185-188). By administering doxycycline during pregnancy as described in other studies, we were able to successfully delete *Ascl1* and analyze *Ascl1*-dependent phenotypes in the maternal liver and fetal outcomes (185, 186). However, we were unable to continue the study due to the reduced fetal numbers and weights, and the inability for the females to become pregnant. As a result, we used two different mouse models to delete *Ascl1* in a cell-specific and hepatocyte-specific manner.

To delete *Ascl1* and trace the *Ascl1*-expressing cells during pregnancy, we generated the cell-*Ascl1*<sup>-/-</sup> (*Ascl1*<sup>Cre/fl</sup>;*R26*<sup>EYFP/EYFP</sup>) mouse model and administered tamoxifen before the peak activation of hepatic *Ascl1*. Tamoxifen is a nonsteroidal selective estrogen receptor modulator that has both estrogen antagonist and agonist effect in breast cancer cells and other tissues, respectively (189). Prior studies thoroughly investigated the use of tamoxifen to treat breast cancer; however, its use during pregnancy has adverse effects on the mother, placenta, and the fetus due to its tissue-specific estrogenic and anti-estrogenic effects (179). Based on the dose and the timing of the

administration, tamoxifen may stabilize and increase the number of estrogen receptors, inhibit the secretion of placental hormones, and result in fetal toxicity and abortions (190-192). Nevertheless, differed from other published studies, we identified the optimal dose and volume of tamoxifen to minimize the deleterious effects in the embryo while at the same time ablating and labeling *Ascl1* in the maternal liver to identify and trace these *Ascl1*-expressing hepatic cells (193, 194).

To delete *Ascl1* in the maternal liver, we generated the hep-*Ascl1*<sup>-/-</sup> (*Ascl1*<sup>fl/fl</sup>;R26<sup>EYFP/EYFP</sup>) mouse model and administered AAV8 viruses before the activation of hepatic *Ascl1*. AAV8 and other AAV vectors are tissue and receptor-specific and can deliver recombinant DNA effectively as a form of gene therapy; however, since the introduced recombinant DNA not being able to integrate into the host genome, its expression dilutes over time due to cell division and turnover rate (195). Introduction of AAV vectors, which have a clearance time in the blood of 2 days, may develop a T-cell response, albeit lower than other viruses such as adenovirus, is not clearly understood (196, 197). Here, we used hepatocyte-specific AAV vector, AAV8, and hepatocyte-specific promoter thyroxine-binding globulin promoter (TBG) at a dosage similar to previously published studies to induce the deletion of hepatic *Ascl1* while using a null AAV8 virus as a control to offset any immunological response (198-200).

### **4.3 Maternal liver and other organ growth**

One of the most noticeable physical phenotypes after deleting *Ascl1* was the enlarged maternal livers. All three *Ascl1* knockout animal models, global, cell-specific, and hepatocyte-specific, manifested in the maternal liver-to-body weight increase. Two possibilities may contribute to the enlargement of the maternal liver: hepatic hyperplasia and hypertrophy. In a neural stem cell, sustained expression of *Ascl1* results in cell cycle exit and differentiation (127). The expression of Ki67, a cell cycle marker, increased in the *Ascl1* knockout maternal livers during

mid to late gestation, suggesting that the maternal hepatocytes are undergoing proliferation; however, we were unable to detect maternal hepatocytes in mitotic phase. Ki67 is present during G1, S, G2, and M phases, and does not indicate whether the cell completes cytokinesis. Additional candidates for liver growth by hyperplasia are hepatocyte growth factor (HGF) and insulin-like growth factor 2 (IGF2), in which we observed the increased expressions after deleting hepatic *Ascl1*. HGF is a potent hepatocyte mitogen, an essential growth factor for the development of multiple organs during embryogenesis, facilitates liver and other organ repairs after injury, and activates anti-apoptotic and anti-inflammatory signals (201). During liver growth and repair, sinusoidal cells and Kupffer cells produce HGF, which promotes hepatocyte cell cycle and protects from organ failure (201, 202). Another vital gene for liver growth is IGF2. IGF2 production not only occurs in the placenta but also in fetal organs such as the pancreas and liver (203, 204). IGF2 binds to multiple variants of the insulin receptors during embryogenesis to induce metabolism, proliferation, differentiation, and anti-apoptosis (205). The increased concentration of serum IGF2 directs increased growth rate and weights in the heart, kidney, and liver (206). Therefore, increased HGF and IGF2 may explain the enlarged maternal liver and other nonreproductive organs, such as the pancreas, spleen, and kidney, which we perceived after hepatic *Ascl1* deletion. Taken together, hepatic *Ascl1* may downregulate HGF, IGF2, and thereby cell proliferation to prevent abnormal organ overgrowth. However, our cell-specific lineage-tracing model did not demonstrate differences in GFP-positive hepatocytes, suggesting that deleting *Ascl1* in the *Ascl1*-expressing hepatocytes does not result in cell proliferation. The other mode of liver enlargement is hepatic hypertrophy. *Ascl1* ablation resulted in maternal hepatocytes increasing their cell size and decreasing their cell density during late gestation by 20% and, if we assume that there was no increase in hepatocyte numbers, may account for the increase in liver-to-body weight ratio on

gestation day (GD) 18 by 14%. The difference in percentage may be due to the cellular contents, especially fat deposition, in the *Ascl1* knockout hepatocytes.

#### **4.4 Maternal hepatocyte identity**

We also identified that the hepatic *Ascl1* controls the maternal hepatocyte identity by affecting the expression of CD133, *EpCAM*, and albumin. Hepatic CD133 and *EpCAM* result in the “stemness” of the liver (207). CD133 localizes in the plasma membrane and, while its function is unknown, is a marker for cancer stem cells (208). Not only does CD133 express in various tumors such as prostate, colon, and ovary, liver cancer stem cells also express CD133 that results in proliferation and reduced expression of mature hepatocyte markers (209-212). We discovered that the expression of hepatic CD133 increased in *Ascl1* knockout livers during pregnancy. On the other hand, CD133 expression is dynamically changed in pregnant livers, where the previous study illustrates that reduced levels of CD133 results in loss of tumor incidence (213). *EpCAM* is a transmembrane glycoprotein with various functions such as cell adhesion, proliferation, differentiation, and migration (214). During development, hepatoblasts and ductal plate cells express *EpCAM* whereas mature hepatocytes lack its expression (215). Furthermore, in addition to CD133, *EpCAM* is also a surface marker for liver cancer stem cells (213). We observed that the lack of hepatic *Ascl1* results in maintenance of the *EpCAM* expression whereas its expression reduces in normal maternal livers. Albumin, constituting around half of the plasma proteins and 2/3 of the plasma oncotic pressure, is a globular transport protein produced by the hepatocytes (216). Not only does albumin transport cholesterol, nitric oxide, fatty acids, and metals, it also interacts with drugs, antibiotics, and reactive species (217-219). The deletion of hepatic *Ascl1* resulted in lower levels of serum albumin. Low serum albumin associated with liver damage, such as cirrhosis, and higher mortality and morbidity (216, 220, 221). Additionally, albumin regulates

fat metabolism by binding to fatty acids in the blood; therefore, low levels of serum albumin may result in increased concentrations of lipids in the blood (219). Thus, *Ascl1* expression in maternal liver may have a protective role against possible liver damage and formation of liver cancer cells, and proper productions and concentrations of albumin and lipids.

#### **4.5 Fatty liver**

In *Ascl1* knockout maternal livers, we observed the abnormally reduced staining of eosin in the cytoplasm, which may be due to the abundant deposition of fat droplets detected by Oil Red O staining. This phenotype is similar to an acute fatty liver of pregnancy (AFLP), a maternal liver disease during pregnancy where current information is lacking (33). Accumulation of fat or triglyceride in the liver can damage the organ that can result in abnormal liver function and even cirrhosis, liver cancer, and mortality (222, 223). In this study, we presented evidences that *Ascl1* governs maternal liver health and fat by serum biochemistry such as alanine aminotransferase (ALT), aspartate aminotransferase (AST), blood nitrogen urea (BUN), creatinine, creatine kinase (CK), cholesterol, including high- and low-density lipoprotein (HDL) cholesterols, and triglyceride. Additionally, we presented data on significantly up- and down-regulating genes and pathways associated with hepatosteatosis such as *Elovl6*, *Pnpla3*, fatty acid binding protein 4 (FABP4), IGF2, Janus kinase 2 (JAK2), and mammalian target of rapamycin (mTOR). We also determined that hepatic *Ascl1* does not regulate selective genes and pathways associated with lipid metabolisms such as fatty acid synthase (*Fasn*), stearyl-CoA desaturase 1 (*Scd1*), fat storage inducing transmembrane protein 1 (*Fitm1*), extracellular signal-regulated kinase 1/2 (ERK1/2), and protein kinase B (AKT).

The liver has high concentrations of both ALT and AST, and, therefore, their secretion into the blood correlates to liver metabolic dysfunction and liver injury from hepatic cell membrane

damage due to hepatitis, drugs, and fatty liver (224, 225). Interestingly, low serum calcium levels correlate with high levels of serum AST (226). Since an increase in serum ALT and AST levels mark steatohepatitis, without hepatic *Ascl1*, the maternal liver amasses fat, resulting in liver injury and ALT and AST release (227, 228).

Elevated levels of serum CK reflects striated skeletal muscle damages and muscle-associated diseases (229, 230) On the other hand, low levels of serum CK associates with alcoholic liver disease due to reduced muscle mass (231, 232). As we also observed decreased levels of serum CK in the hepatic *Ascl1* knockout mice, it will be also interesting to see whether fatty livers caused by the absence of *Ascl1* result in muscle reduction.

Urea and creatinine, which are metabolic products from liver and muscle, respectively, are an indication of kidney function (233, 234). Increased BUN levels may be due to inappropriate activation of the renin-angiotensin-aldosterone system and increased reabsorption of urea (233). BUN levels also increase due to diets with high protein, bleeding of the gastrointestinal tract, infection, and drugs (234). Furthermore, increased creatinine levels may be due to acute kidney injury or hemoconcentration (235). Nevertheless, after hepatic *Ascl1* deletion, we observed both serum BUN and creatinine decrease. Decrease in BUN and creatinine production may be attributed to dysfunction of the liver such as parenchymal liver disease for reduced BUN production and alcoholic liver disease for reduced creatinine production (234, 236). This indicates that hepatic *Ascl1* protects the maternal liver from impaired hepatic metabolic activity and injury.

*Elovl6* is an enzyme in lipogenesis that elongates saturated and monounsaturated fatty acids. *Elovl6* activation modulates hepatic inflammation, oxidative stress, fibrosis, and steatosis (237, 238). We detected that the *Elovl6* expression in *Ascl1* knockout maternal livers did not change while the normal maternal liver decreased in its expression. Reduced expression of *Elovl6* results

in decreased lipid accumulation in the liver (239). Furthermore, in hepatocellular carcinoma (HCC), the absence of *Elavl6* causes decreased proliferation, AKT activation, and growth (240). Thus, *Ascl1* may downregulate *Elavl6* to ameliorate lipid deposition in maternal hepatocytes.

*Pnpla3* hydrolyze triglycerides in hepatic stellate cells and hepatocytes (241). The loss-of-function of *Pnpla3* results in the accumulation and retention of hepatic triglycerides and many liver diseases such as fibrosis and steatosis. We found that ablation of hepatic *Ascl1* results in the inability to activate *Pnpla3* in maternal livers, and, therefore, may inhibit the gene's lipase activity.

FABP4 is a lipid-binding chaperone expressed in adipocyte and macrophages that plays an important role in insulin resistance and type 2 diabetes (242-244). Although the predominant hepatic form is fatty acid binding protein 1 (FABP1), we observed an increased level of hepatic FABP4 expression after the deletion of hepatic *Ascl1* (245). Since elevated hepatic FABP4 expression associates with hepatic steatosis, we conjecture that hepatic *Ascl1* protects the liver from fat accumulation by downregulating FABP4.

We analyzed lipid profiles in the *Ascl1* knockout mice such as cholesterol, HDL cholesterol, LDL cholesterol, triglyceride, phospholipid, and FFA. The liver metabolizes, synthesizes, and transports lipids, which are essential in controlling cellular functions and homeostasis (246). Generally, lipid contents in the blood decrease depending on the cause and progression of the liver disease. For example, alcoholic and nonalcoholic cirrhotic livers result in lower concentrations of blood cholesterol, HDL and LDL cholesterols, and triglyceride levels whereas HCV-induced hepatic steatosis results in lower levels of blood lipids but not triglyceride (247-249). We found decreased levels of cholesterol, HDL and LDL cholesterols, and phospholipids while FFA levels increased in the absence of hepatic *Ascl1* in maternal serum. While increased levels of serum FFA may be due to the imbalance of uptake and release of triglycerides, we did not observe any changes

to the blood triglyceride levels (250, 251). Increased serum FFA levels also cause insulin resistance; however, blood insulin and glucose levels, in addition to glucose tolerance test, of the *Ascl1* knockout animals did not differ from the controls (252, 253). It will be interesting to see whether *Ascl1* null hepatocytes exposed to high levels of FFA result in FFA-induced oxidative stress and inflammation (254). Taken together, the deletion of hepatic *Ascl1* during pregnancy results in the imbalance of lipid metabolism and presents similar phenotypes as hepatic steatosis.

IGF2 is not only a potent mitogen for organ growth, but also its overexpression results in hepatic steatosis by activating AKT and increasing serum cholesterol and hepatic lipid droplets, including free cholesterol, and obesity (255, 256). However, although we observed activation of hepatic IGF2, there was a disconnection in the signaling pathway since we were unable to detect AKT activation. Therefore, hepatic *Ascl1* may downregulate IGF2 to control maternal liver growth and, potentially, hepatic fat deposition.

JAK2 is a signal transducer activated by growth hormones and regulates many liver physiology (257). Expression levels of JAK2 increase in genes associated with fibrosis due to myofibroblastic hepatic stellate cells activation while deletion of JAK2 is lethal during fetal development (258, 259). The phenotypes of hepatocyte-specific deletion of JAK2 are smaller body, fatty liver, where the hepatic triglycerides increased significantly without inhibiting secretion or increasing fatty acid synthesis and increased serum free fatty acid (260). We observed similar properties where the absence of hepatic *Ascl1* also resulted in reduced level of JAK2, increased liver fat content and serum free fatty acid. Thus, hepatic *Ascl1* appears to have a partially similar role as hepatic JAK2 in lipid metabolism.

mTOR is a signaling pathway that involves various metabolism and physiology in the body (261). mTOR activation and activation of its downstream targets such as p70S6K result in

inhibiting lipophagy and activates lipogenesis. However, hepatic *Ascl1* resulted in reduced activation of mTOR while maintaining similar levels of p70S6K. Furthermore, we observed another disconnection to the mTOR signaling pathway, 4E-BP1. *Ascl1* knockout resulted in increased activation of 4E-BP1, another downstream effector of mTOR, and may have a protective role against fatty liver since the ablation of 4E-BP1 results in obesity (262). Therefore, there is a disconnection between mTOR, p70S6K, and 4E-BP1 due to an unknown mechanism with the absence of hepatic *Ascl1* expression.

#### **4.6 Pancreatic function test**

During pregnancy, the preexisting maternal  $\beta$ -cells proliferates and increases insulin production to maintain maternal blood glucose levels (95, 96). We found that, after hepatic *Ascl1* deletion, the maternal pancreas increased in size and weight, which may be due to the increased expression of IGF2. Furthermore, IGF2 overexpression causes  $\beta$ -cell dysfunction and damage by cell dedifferentiation and endoplasmic reticulum stress, resulting in type 2 diabetic phenotypes including increased blood insulin and glucose, and abnormal insulin and glucose tolerance tests (263, 264). Additionally, hepatic *Elovl6* upregulation associates with insulin resistance and hepatic ERK1/2 promotes insulin resistance, weight gain, and obesity (240, 265, 266). Finally, circulating hepatic HGF may bind to the pancreas and act in metabolic homeostasis by stimulating mitosis and regulating insulin production of the  $\beta$ -cells, and maintain blood glucose levels (267). Nevertheless, we were unable to observe any differences in pancreatic cell proliferation, blood glucose or insulin levels, and glucose tolerance test. Since the pancreatic islet sizes were similar even without hepatic *Ascl1*, we postulate that the increase in the organ size may be due to an increase in the pancreatic exocrine cells.

#### 4.7 *Ascl1*-associated canonical pathway

RNA sequencing analysis revealed that hepatic *Ascl1* regulates multiple canonical pathways in the liver. We received two different significantly up- or down-regulated canonical pathways using two independent mouse lines: cell-specific and hepatocyte-specific. The difference may stem from the timing of the *Ascl1* deletion and the type of cells involved. In cell-specific *Ascl1* deletion, many of the death signaling pathways and cell cycle regulations were upregulated whereas the prothrombin activation pathway was downregulated. On the other hand, in hepatocyte-specific *Ascl1* deletion, many of neurotransmitter signaling molecule degradation pathways were downregulated while amyotrophic lateral sclerosis signaling, the degeneration of muscle neurons, and immune response were upregulated. Both the afferent and efferent neurons innervate the liver and, while the hepatic vagus nerve has been studied recently, to our knowledge, there is no current knowledge in the degradation pathways presented in our studies (268). Thus, hepatic *Ascl1* regulates the neurotransmitters in an unknown mechanism.

#### 4.8 Microbiota dysfunction

Maternal microbiota plays an essential role in inoculating the baby during birth, which may affect the health of the baby (70, 73, 74). We observed the dysbiosis of the microbiota in the maternal cecal samples such as *Pseudobutyrvibrio-Roseburia intestinalis*, *Helicobacter hepaticus*, *Clostridiales vadinBB60*, *Bacteroides acidifaciens*, Eubacterium, *Lactobacillus johnsonii*, Candidatus, and *Desulfovibrio oxamicus-vulgaris*.

*Roseburia intestinalis* is one of the most abundant bacteria in the body and helps in protecting colonic mucosa against inflammatory bowel disease (IBD) (269). *Helicobacter hepaticus* infection results in hepatic oxidative stress and may play a role in liver cancer (270). *Bacteroides acidifaciens*-fed mice display less weight and fat gain while having increased serum

insulin levels (271). The genus *Eubacterium* produces butyrate, which helps in the proliferation of colonic epithelial cells (272). *Lactobacillus johnsonii* is a lactic acid bacterium and functions as a probiotic as well as produces antibiotic against certain bacterial species (273). *Candidatus* designates bacteria that are unable to grow in culture plates (274). *Desulfovibrio oxamicus-vulgaris* uses nitrate and reduces it to ammonium, and incompletely oxidizes lactate, alcohol, pyruvate, and more (275).

One of the genes that may be the cause of dysbiosis is *Hamp2*. *Hamp2* is an antimicrobial peptide that expresses primarily in the liver and plays an important role in the immune response against bacterial pathogens (276, 277). In the absence of hepatic *Ascl1*, hepatic *Hamp2* expression decreased markedly, which may have caused changes in the populations of these cecal bacterial strains. Although the function of these bacteria needs to be more elucidated, it will be of interest to see whether the imbalance of microbiome may result in future health problems for the pups born from hepatic *Ascl1*-null dams.

#### **4.9 Pregnancy outcomes**

We postulate that activation of IGF2 in the absence of hepatic *Ascl1* causes both the placental and postnatal growth. For the placenta, we analyzed the disrupted expression levels of IGF2, AKT, ERK1/2, serum alkaline phosphatases (ALP), and placental lactogen I (PL-I) and placental lactogen II (PL-II), which are hormones produced by the placenta during gestation, in the absence of hepatic *Ascl1*; however, JAK2 expression did not differ between genotypes. In addition, we measured the postnatal growth of the pups born from hepatic *Ascl1* knockout dams and observed increased growth rate in both males and females.

IGF2, an imprinted gene where only the paternal allele expresses and the maternal allele silenced, is essential for the growth and development of the embryos (278, 279). In the placenta,

IGF2 is also necessary for the development and function of the trophoblast (280). We detected lower levels of placental IGF2 production in the hepatic *Ascl1* knockout mice, which may be due to the compensation of the activation of IGF2 in the maternal liver. We also observed activation of placental AKT, which is downstream of the IGF2 signaling pathway, that was absent in the maternal liver without *Ascl1*. Thus, hepatic *Ascl1* may regulate hepatic IGF2 production, which then downregulates placental IGF2 production.

In homeostasis, ALP production occurs in the liver; however, during pregnancy, the placenta takes over the production and reaches its peak until the end of pregnancy (281). We observed an increased level of serum ALP in hepatic *Ascl1* knockout pregnant mice, which may be due to liver, kidney, and pregnancy-related diseases (282). High levels of ALP may also associate with premature birth, placental insufficiency, and decreased birth weight; however, we were unable to observe any of these phenotypes in our studies (283, 284). Thus, hepatic *Ascl1* ablation results in an increased size of the placenta in an unknown mechanism.

PL-I production occurs in trophoblast giant cells in the placenta from gestation day (GD) 6 until GD13 whereas PL-II production occurs from the same giant cells from GD10 until the end of pregnancy (285, 286). The concentration of the maternal serum PL-I correlates with litter size (287). We observed an increased placental size in hepatic-specific *Ascl1* knockout mice; however, this increase did not affect the production or distribution of both placental lactogens. Thus, hepatic *Ascl1* does not affect the endocrine production of PL-I and PL-II in the placenta.

ERK1/2 plays an important role in trophoblast differentiation while a mutation in JAK2 results in pregnancy complications (288, 289). Inhibition of ERK1/2 constrains trophoblast differentiation (288). In hepatic *Ascl1* deleted mice, the placenta suppressed the activation of

ERK1/2 while JAK2 expression levels did not differ from the control placenta. Therefore, hepatic *Ascl1* may control the maturation of trophoblast but not JAK2 expression in the placenta.

The deletion of *Ascl1* in the maternal liver also results in increased growth in pups after weaning. Whereas the deletion of IGF2 results in much smaller fetuses, an increase in IGF2 expression causes increase fetal overgrowth (278, 290). Furthermore, IGF2 is sex-dependent where overexpression of fetal IGF2 during pregnancy shows increased weight of fetus, stomach, intestine, liver, and pancreas in males and increased fetal stomach weight in females (291). Although we did not observe fetal overgrowth before parturition, we hypothesize that the overproduction of IGF2 during pregnancy may have caused the increased body weight and growth rate of the pups born from *Ascl1* knockout dams.

#### **4.10 Summary of the findings**

The maternal liver adapts to pregnancy to accommodate the growing placenta and fetus. However, how the maternal liver adjusts metabolically and physiologically to pregnancy is largely unknown. We found that *Ascl1* is the most activated gene in the maternal liver starting from midgestation. Hepatic *Ascl1* *in vivo* lineage tracing and knockout mice showed the wide distribution of *Ascl1*-positive hepatocytes in the maternal liver and hepatic lipid accumulation in the absence of hepatic *Ascl1* (**Fig. 21**). In addition, hepatic *Ascl1* mediates crosstalk between the maternal liver with other maternal organs, such as the pancreas, spleen, and kidney, microbiome, and placenta, which may influence postnatal growth possibly via IGF2 or HGF. Hence, hepatic *Ascl1* plays an important role in regulating other maternal organ adaptations and normal placental and fetal growth.

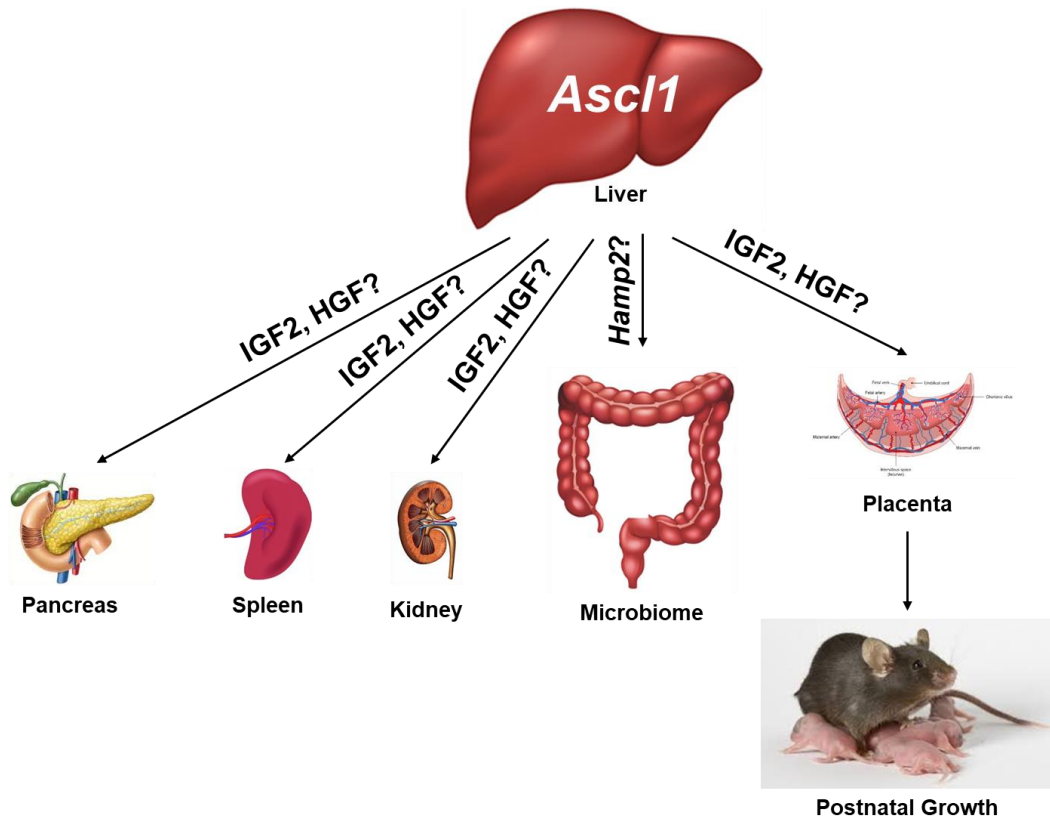


**Figure 22. Summary of hepatic *Ascl1* functions during pregnancy.** *Ascl1*, achaete-scute homolog 1; IGF2, insulin-like growth factor 2; Hamp2, hepcidin antimicrobial peptide 2; HGF, hepatocyte growth factor.

#### 4.11 Future directions of the study

The major follow up study is to determine (1) human relevance and (2) mechanism of hepatic *Ascl1* in maternal organs and pregnancy outcomes. Additionally, we planned to overexpress hepatic IGF2 using a virus in normal pregnant mice to attempt to duplicate the hepatic *Ascl1* knockout phenotypes. However, after numerous attempts, we were unable to overexpress hepatic IGF2. Therefore, we plan to use a different viral construct. If our hypothesis regarding organ growth due to increased expression of IGF2 is correct, the maternal organs, placenta, and fetus should result in overgrowth. However, if the phenotypes from IGF2 overexpression do not match

the phenotypes of *Asc11* deletion in the liver, then an unknown factor or pathway may be the cause of the increased size of maternal organs and pregnancy outcomes.

## CHAPTER 5. REFERENCES

1. Michalopoulos GK. Hepatostat: Liver regeneration and normal liver tissue maintenance. *Hepatology* (Baltimore, Md). 2017;65(4):1384-92. Epub 2016/12/21. doi: 10.1002/hep.28988. PubMed PMID: 27997988.
2. Hata S, Namae M, Nishina H. Liver development and regeneration: from laboratory study to clinical therapy. *Development, growth & differentiation*. 2007;49(2):163-70. Epub 2007/03/06. doi: 10.1111/j.1440-169X.2007.00910.x. PubMed PMID: 17335437.
3. Denson LA, McClure MH, Bogue CW, Karpen SJ, Jacobs HC. HNF3beta and GATA-4 transactivate the liver-enriched homeobox gene, Hex. *Gene*. 2000;246(1-2):311-20. Epub 2000/04/18. PubMed PMID: 10767553.
4. Li Z, White P, Tuteja G, Rubins N, Sackett S, Kaestner KH. Foxa1 and Foxa2 regulate bile duct development in mice. *The Journal of clinical investigation*. 2009;119(6):1537-45. Epub 2009/05/14. doi: 10.1172/jci38201. PubMed PMID: 19436110; PubMed Central PMCID: PMCPMC2689124.
5. Rossi JM, Dunn NR, Hogan BL, Zaret KS. Distinct mesodermal signals, including BMPs from the septum transversum mesenchyme, are required in combination for hepatogenesis from the endoderm. *Genes & development*. 2001;15(15):1998-2009. Epub 2001/08/04. doi: 10.1101/gad.904601. PubMed PMID: 11485993; PubMed Central PMCID: PMCPMC312750.
6. Jung J, Zheng M, Goldfarb M, Zaret KS. Initiation of mammalian liver development from endoderm by fibroblast growth factors. *Science (New York, NY)*. 1999;284(5422):1998-2003. Epub 1999/06/18. PubMed PMID: 10373120.
7. Wandzioch E, Zaret KS. Dynamic signaling network for the specification of embryonic pancreas and liver progenitors. *Science (New York, NY)*. 2009;324(5935):1707-10. Epub 2009/06/27. doi: 10.1126/science.1174497. PubMed PMID: 19556507; PubMed Central PMCID: PMCPMC2771431.
8. Zaret KS. Genetic programming of liver and pancreas progenitors: lessons for stem-cell differentiation. *Nat Rev Genet*. 2008;9(5):329-40. Epub 2008/04/10. doi: 10.1038/nrg2318. PubMed PMID: 18398419.
9. Shafritz DA, Dabeva MD. Liver stem cells and model systems for liver repopulation. *Journal of hepatology*. 2002;36(4):552-64. Epub 2002/04/12. PubMed PMID: 11943430.
10. Bort R, Signore M, Tremblay K, Martinez Barbera JP, Zaret KS. Hex homeobox gene controls the transition of the endoderm to a pseudostratified, cell emergent epithelium for liver bud development. *Developmental biology*. 2006;290(1):44-56. Epub 2005/12/21. doi: 10.1016/j.ydbio.2005.11.006. PubMed PMID: 16364283.
11. Margagliotti S, Clotman F, Pierreux CE, Beaudry JB, Jacquemin P, Rousseau GG, et al. The Onecut transcription factors HNF-6/OC-1 and OC-2 regulate early liver expansion by controlling hepatoblast migration. *Developmental biology*. 2007;311(2):579-89. Epub 2007/10/16. doi: 10.1016/j.ydbio.2007.09.013. PubMed PMID: 17936262.
12. Si-Tayeb K, Lemaigre FP, Duncan SA. Organogenesis and development of the liver. *Developmental cell*. 2010;18(2):175-89. Epub 2010/02/18. doi: 10.1016/j.devcel.2010.01.011. PubMed PMID: 20159590.
13. Lopez-Luque J, Fabregat I. Revisiting the liver: from development to regeneration - what we ought to know! *The International journal of developmental biology*. 2018;62(6-7-8):441-51. Epub 2018/06/26. doi: 10.1387/ijdb.170264JL. PubMed PMID: 29938756.

14. Grijalva J, Vakili K. Neonatal liver physiology. *Seminars in pediatric surgery*. 2013;22(4):185-9. Epub 2013/12/18. doi: 10.1053/j.sempedsurg.2013.10.006. PubMed PMID: 24331092.
15. Gebhardt R, Matz-Soja M. Liver zonation: Novel aspects of its regulation and its impact on homeostasis. *World journal of gastroenterology : WJG*. 2014;20(26):8491-504. Epub 2014/07/16. doi: 10.3748/wjg.v20.i26.8491. PubMed PMID: 25024605; PubMed Central PMCID: PMC4093700.
16. Jungermann K, Katz N. Functional specialization of different hepatocyte populations. *Physiological reviews*. 1989;69(3):708-64. Epub 1989/07/01. doi: 10.1152/physrev.1989.69.3.708. PubMed PMID: 2664826.
17. Parker GA, Picut CA. Immune functioning in non lymphoid organs: the liver. *Toxicologic pathology*. 2012;40(2):237-47. Epub 2011/11/18. doi: 10.1177/0192623311428475. PubMed PMID: 22089842.
18. Elias H, Sokol A. Dependence of the lobular architecture of the liver on the porto-hepatic blood pressure gradient. *Anat Rec*. 1953;115(1):71-85. Epub 1953/01/01. PubMed PMID: 13016996.
19. Sasse D, Spornitz UM, Maly IP. Liver architecture. *Enzyme*. 1992;46(1-3):8-32. Epub 1992/01/01. PubMed PMID: 1289084.
20. Gaspar-Maia A, Alajem A, Polesso F, Sridharan R, Mason MJ, Heidersbach A, et al. Chd1 regulates open chromatin and pluripotency of embryonic stem cells. *Nature*. England2009. p. 863-8.
21. Jungermann K, Sasse D. Heterogeneity of liver parenchymal cells. *Trends in Biochemical Sciences*. 1978;3(3):198-202. doi: [https://doi.org/10.1016/S0968-0004\(78\)91764-4](https://doi.org/10.1016/S0968-0004(78)91764-4).
22. Jungermann K, Thurman RG. Hepatocyte heterogeneity in the metabolism of carbohydrates. *Enzyme*. 1992;46(1-3):33-58. Epub 1992/01/01. PubMed PMID: 1289081.
23. Jungermann K, Kietzmann T. Zonation of parenchymal and nonparenchymal metabolism in liver. *Annual review of nutrition*. 1996;16:179-203. Epub 1996/01/01. doi: 10.1146/annurev.nu.16.070196.001143. PubMed PMID: 8839925.
24. Kietzmann T. Metabolic zonation of the liver: The oxygen gradient revisited. *Redox biology*. 2017;11:622-30. Epub 2017/01/28. doi: 10.1016/j.redox.2017.01.012. PubMed PMID: 28126520; PubMed Central PMCID: PMC45257182.
25. Hollister A, Okubara P, Watson JG, Chaykin S. Reproduction in mice: liver enlargement in mice during pregnancy and lactation. *Life sciences*. 1987;40(1):11-8. Epub 1987/01/05. PubMed PMID: 3796209.
26. Murray SA, Morgan JL, Kane C, Sharma Y, Heffner CS, Lake J, et al. Mouse gestation length is genetically determined. *PloS one*. 2010;5(8):e12418. Epub 2010/09/03. doi: 10.1371/journal.pone.0012418. PubMed PMID: 20811634; PubMed Central PMCID: PMC2928290.
27. Dai G, Bustamante JJ, Zou Y, Myronovych A, Bao Q, Kumar S, et al. Maternal hepatic growth response to pregnancy in the mouse. *Experimental biology and medicine (Maywood, NJ)*. 2011;236(11):1322-32. Epub 2011/10/05. doi: 10.1258/ebm.2011.011076. PubMed PMID: 21969712.
28. Bustamante JJ, Copple BL, Soares MJ, Dai G. Gene profiling of maternal hepatic adaptations to pregnancy. *Liver International*. 2010;30(3):406-15. doi: 10.1111/j.1478-3231.2009.02183.x.

29. Ryan JM, Heneghan MA. Pregnancy and the liver. *Clinical Liver Disease*. 2014;4(3):51-4. doi: 10.1002/cld.361.
30. Knox TA, Olans LB. Liver disease in pregnancy. *N Engl J Med*. 1996;335(8):569-76. Epub 1996/08/22. doi: 10.1056/nejm199608223350807. PubMed PMID: 8678935.
31. Frederiksen MC. Physiologic changes in pregnancy and their effect on drug disposition. *Seminars in perinatology*. 2001;25(3):120-3. Epub 2001/07/17. PubMed PMID: 11453606.
32. Tracy TS, Venkataramanan R, Glover DD, Caritis SN. Temporal changes in drug metabolism (CYP1A2, CYP2D6 and CYP3A Activity) during pregnancy. *American journal of obstetrics and gynecology*. 2005;192(2):633-9. Epub 2005/02/08. doi: 10.1016/j.ajog.2004.08.030. PubMed PMID: 15696014.
33. Ma K, Berger D, Reau N. Liver Diseases During Pregnancy. *Clinics in liver disease*. 2019;23(2):345-61. Epub 2019/04/06. doi: 10.1016/j.cld.2018.12.013. PubMed PMID: 30947881.
34. Mikolasevic I, Filipec-Kanizaj T, Jakopic I, Majurec I, Brncic-Fischer A, Sobocan N, et al. Liver Disease During Pregnancy: A Challenging Clinical Issue. *Medical science monitor : international medical journal of experimental and clinical research*. 2018;24:4080-90. Epub 2018/06/16. doi: 10.12659/msm.907723. PubMed PMID: 29905165; PubMed Central PMCID: PMC6034557.
35. Herrera E. Lipid metabolism in pregnancy and its consequences in the fetus and newborn. *Endocrine*. 2002;19(1):43-55. Epub 2003/02/14. doi: 10.1385/endo:19:1:43. PubMed PMID: 12583601.
36. Wang Q, Liu C, Zhang Z. Transthyretin and Normal Human Pregnancy: Mini Review. *Critical reviews in eukaryotic gene expression*. 2016;26(3):273-7. Epub 2016/09/22. doi: 10.1615/CritRevEukaryotGeneExpr.2016017323. PubMed PMID: 27650990.
37. Villar J, Cogswell M, Kestler E, Castillo P, Menendez R, Repke JT. Effect of fat and fat-free mass deposition during pregnancy on birth weight. *American journal of obstetrics and gynecology*. 1992;167(5):1344-52. Epub 1992/11/01. PubMed PMID: 1442988.
38. Palacin M, Lasuncion MA, Asuncion M, Herrera E. Circulating metabolite utilization by periuterine adipose tissue in situ in the pregnant rat. *Metabolism: clinical and experimental*. 1991;40(5):534-9. Epub 1991/05/01. PubMed PMID: 2023540.
39. Martineau MG, Raker C, Dixon PH, Chambers J, Machirori M, King NM, et al. The metabolic profile of intrahepatic cholestasis of pregnancy is associated with impaired glucose tolerance, dyslipidemia, and increased fetal growth. *Diabetes care*. 2015;38(2):243-8. Epub 2014/12/17. doi: 10.2337/dc14-2143. PubMed PMID: 25504029.
40. Mueckler M, Thorens B. The SLC2 (GLUT) family of membrane transporters. *Molecular aspects of medicine*. 2013;34(2-3):121-38. Epub 2013/03/20. doi: 10.1016/j.mam.2012.07.001. PubMed PMID: 23506862; PubMed Central PMCID: PMC4104978.
41. Mennitti LV, Oliveira JL, Morais CA, Estadella D, Oyama LM, Oller do Nascimento CM, et al. Type of fatty acids in maternal diets during pregnancy and/or lactation and metabolic consequences of the offspring. *The Journal of nutritional biochemistry*. 2015;26(2):99-111. Epub 2014/12/03. doi: 10.1016/j.jnutbio.2014.10.001. PubMed PMID: 25459884.
42. Zeng Z, Liu F, Li S. Metabolic Adaptations in Pregnancy: A Review. *Annals of nutrition & metabolism*. 2017;70(1):59-65. Epub 2017/03/16. doi: 10.1159/000459633. PubMed PMID: 28297696.
43. Ville D, Chiron C, Laschet J, Dulac O. The ketogenic diet can be used successfully in combination with corticosteroids for epileptic encephalopathies. *Epilepsy & behavior : E&B*. 2015;48:61-5. Epub 2015/06/10. doi: 10.1016/j.yebeh.2015.03.003. PubMed PMID: 26057351.

44. Tatone EH, Duffield TF, Capel MB, DeVries TJ, LeBlanc SJ, Gordon JL. A randomized controlled trial of dexamethasone as an adjunctive therapy to propylene glycol for treatment of hyperketonemia in postpartum dairy cattle. *Journal of dairy science*. 2016;99(11):8991-9000. Epub 2016/10/21. doi: 10.3168/jds.2016-11358. PubMed PMID: 27638258.
45. Basit H, Kashou AH, Kashou HE, Chhabra L. *Physiology, Sinoatrial Node (SA Node)*. StatPearls. Treasure Island FL: StatPearls Publishing LLC.; 2019.
46. Buckberg GD, Nanda NC, Nguyen C, Kocica MJ. What Is the Heart? Anatomy, Function, Pathophysiology, and Misconceptions. *Journal of cardiovascular development and disease*. 2018;5(2). Epub 2018/06/06. doi: 10.3390/jcdd5020033. PubMed PMID: 29867011; PubMed Central PMCID: PMC6023278.
47. Boselli F, Freund JB, Vermot J. Blood flow mechanics in cardiovascular development. *Cellular and molecular life sciences : CMLS*. 2015;72(13):2545-59. Epub 2015/03/25. doi: 10.1007/s00018-015-1885-3. PubMed PMID: 25801176; PubMed Central PMCID: PMC6023278.
48. Powers KA, Dharmoon AS. *Physiology, Pulmonary, Ventilation and Perfusion*. StatPearls. Treasure Island FL: StatPearls Publishing LLC.; 2019.
49. Theunissen IM, Parer JT. Fluid and electrolytes in pregnancy. *Clinical obstetrics and gynecology*. 1994;37(1):3-15. Epub 1994/03/01. PubMed PMID: 8194213.
50. Duvekot JJ, Peeters LL. Renal hemodynamics and volume homeostasis in pregnancy. *Obstetrical & gynecological survey*. 1994;49(12):830-9. Epub 1994/12/01. PubMed PMID: 7885660.
51. Thornburg KL, Jacobson SL, Giraud GD, Morton MJ. Hemodynamic changes in pregnancy. *Seminars in perinatology*. 2000;24(1):11-4. Epub 2000/03/10. PubMed PMID: 10709851.
52. Clark SL, Cotton DB, Lee W, Bishop C, Hill T, Southwick J, et al. Central hemodynamic assessment of normal term pregnancy. *American journal of obstetrics and gynecology*. 1989;161(6 Pt 1):1439-42. Epub 1989/12/01. PubMed PMID: 2603895.
53. Bader RA, Bader ME, Rose DF, Braunwald E. Hemodynamics at rest and during exercise in normal pregnancy as studied by cardiac catheterization. *The Journal of clinical investigation*. 1955;34(10):1524-36. Epub 1955/10/01. doi: 10.1172/jci103205. PubMed PMID: 13263433; PubMed Central PMCID: PMC6023278.
54. Suresh L, Radfar L. *Pregnancy and lactation. Oral surgery, oral medicine, oral pathology, oral radiology, and endodontics*. 2004;97(6):672-82. Epub 2004/06/09. doi: 10.1016/s1079210404000861. PubMed PMID: 15184848.
55. Lund CJ, Donovan JC. Blood volume during pregnancy. Significance of plasma and red cell volumes. *American journal of obstetrics and gynecology*. 1967;98(3):394-403. Epub 1967/06/01. PubMed PMID: 5621454.
56. O'Day MP. Cardio-respiratory physiological adaptation of pregnancy. *Seminars in perinatology*. 1997;21(4):268-75. Epub 1997/08/01. PubMed PMID: 9298715.
57. Clapp JF, 3rd, Seaward BL, Sleamaker RH, Hiser J. Maternal physiologic adaptations to early human pregnancy. *American journal of obstetrics and gynecology*. 1988;159(6):1456-60. Epub 1988/12/01. PubMed PMID: 3207124.
58. Contreras G, Gutierrez M, Beroiza T, Fantin A, Oddo H, Villarroel L, et al. Ventilatory drive and respiratory muscle function in pregnancy. *The American review of respiratory disease*. 1991;144(4):837-41. Epub 1991/10/01. doi: 10.1164/ajrccm/144.4.837. PubMed PMID: 1928958.

59. Garcia-Rio F, Pino JM, Gomez L, Alvarez-Sala R, Villasante C, Villamor J. Regulation of breathing and perception of dyspnea in healthy pregnant women. *Chest*. 1996;110(2):446-53. Epub 1996/08/01. doi: 10.1378/chest.110.2.446. PubMed PMID: 8697850.
60. Duvekot JJ, Peeters LL. Maternal cardiovascular hemodynamic adaptation to pregnancy. *Obstetrical & gynecological survey*. 1994;49(12 Suppl):S1-14. Epub 1994/12/01. PubMed PMID: 7877788.
61. Bhagwat AR, Engel PJ. Heart disease and pregnancy. *Cardiology clinics*. 1995;13(2):163-78. Epub 1995/05/01. PubMed PMID: 7614509.
62. Cantor EJ, Babick AP, Vasanji Z, Dhalla NS, Netticadan T. A comparative serial echocardiographic analysis of cardiac structure and function in rats subjected to pressure or volume overload. *Journal of molecular and cellular cardiology*. 2005;38(5):777-86. Epub 2005/04/27. doi: 10.1016/j.yjmcc.2005.02.012. PubMed PMID: 15850571.
63. Dorn GW, 2nd, Mann DL. Signaling pathways involved in left ventricular remodeling: summation. *Journal of cardiac failure*. 2002;8(6 Suppl):S387-8. Epub 2003/01/30. doi: 10.1054/jcaf.2002.129266. PubMed PMID: 12555150.
64. Li J, Umar S, Amjedi M, Iorga A, Sharma S, Nadadur RD, et al. New frontiers in heart hypertrophy during pregnancy. *American journal of cardiovascular disease*. 2012;2(3):192-207. Epub 2012/09/01. PubMed PMID: 22937489; PubMed Central PMCID: PMC3427979.
65. Ogobuiro I, Tuma F. *Physiology, Gastrointestinal*. StatPearls. Treasure Island FL: StatPearls Publishing LLC.; 2019.
66. Koch KL. Gastrointestinal factors in nausea and vomiting of pregnancy. *American journal of obstetrics and gynecology*. 2002;186(5 Suppl Understanding):S198-203. Epub 2002/05/16. PubMed PMID: 12011886.
67. Sherman PW, Flaxman SM. Nausea and vomiting of pregnancy in an evolutionary perspective. *American journal of obstetrics and gynecology*. 2002;186(5 Suppl Understanding):S190-7. Epub 2002/05/16. PubMed PMID: 12011885.
68. ACOG Practice Bulletin #52: Nausea and Vomiting of Pregnancy. *Obstetrics & Gynecology*. 2004;103(4):803-16. PubMed PMID: 00006250-200404000-00045.
69. Laukens D, Brinkman BM, Raes J, De Vos M, Vandenabeele P. Heterogeneity of the gut microbiome in mice: guidelines for optimizing experimental design. *FEMS microbiology reviews*. 2016;40(1):117-32. Epub 2015/09/02. doi: 10.1093/femsre/fuv036. PubMed PMID: 26323480; PubMed Central PMCID: PMC4703068.
70. Schroeder BO, Backhed F. Signals from the gut microbiota to distant organs in physiology and disease. *Nature medicine*. 2016;22(10):1079-89. Epub 2016/10/07. doi: 10.1038/nm.4185. PubMed PMID: 27711063.
71. Sender R, Fuchs S, Milo R. Are We Really Vastly Outnumbered? Revisiting the Ratio of Bacterial to Host Cells in Humans. *Cell*. 2016;164(3):337-40. Epub 2016/01/30. doi: 10.1016/j.cell.2016.01.013. PubMed PMID: 26824647.
72. Tamburini S, Shen N, Wu HC, Clemente JC. The microbiome in early life: implications for health outcomes. *Nature medicine*. 2016;22(7):713-22. Epub 2016/07/09. doi: 10.1038/nm.4142. PubMed PMID: 27387886.
73. Dominguez-Bello MG, Costello EK, Contreras M, Magris M, Hidalgo G, Fierer N, et al. Delivery mode shapes the acquisition and structure of the initial microbiota across multiple body habitats in newborns. *Proceedings of the National Academy of Sciences*. 2010;107(26):11971-5. doi: 10.1073/pnas.1002601107.

74. Wang J, Jia H. Metagenome-wide association studies: fine-mining the microbiome. *Nature reviews Microbiology*. 2016;14(8):508-22. Epub 2016/07/12. doi: 10.1038/nrmicro.2016.83. PubMed PMID: 27396567.
75. Konstantinov SR, van der Woude CJ, Peppelenbosch MP. Do pregnancy-related changes in the microbiome stimulate innate immunity? *Trends in molecular medicine*. 2013;19(8):454-9. Epub 2013/07/13. doi: 10.1016/j.molmed.2013.06.002. PubMed PMID: 23845284.
76. Koren O, Goodrich JK, Cullender TC, Spor A, Laitinen K, Backhed HK, et al. Host remodeling of the gut microbiome and metabolic changes during pregnancy. *Cell*. 2012;150(3):470-80. Epub 2012/08/07. doi: 10.1016/j.cell.2012.07.008. PubMed PMID: 22863002; PubMed Central PMCID: PMC3505857.
77. Aagaard K, Riehle K, Ma J, Segata N, Mistretta TA, Coarfa C, et al. A metagenomic approach to characterization of the vaginal microbiome signature in pregnancy. *PloS one*. 2012;7(6):e36466. Epub 2012/06/22. doi: 10.1371/journal.pone.0036466. PubMed PMID: 22719832; PubMed Central PMCID: PMC3374618.
78. Witkin SS, Linhares IM. Why do lactobacilli dominate the human vaginal microbiota? *BJOG : an international journal of obstetrics and gynaecology*. 2017;124(4):606-11. Epub 2017/02/23. doi: 10.1111/1471-0528.14390. PubMed PMID: 28224747.
79. Jalanka J, Hillamaa A, Satokari R, Mattila E, Anttila VJ, Arkkila P. The long-term effects of faecal microbiota transplantation for gastrointestinal symptoms and general health in patients with recurrent *Clostridium difficile* infection. *Alimentary pharmacology & therapeutics*. 2018;47(3):371-9. Epub 2017/12/12. doi: 10.1111/apt.14443. PubMed PMID: 29226561.
80. Zitomersky NL, Coyne MJ, Comstock LE. Longitudinal analysis of the prevalence, maintenance, and IgA response to species of the order Bacteroidales in the human gut. *Infection and immunity*. 2011;79(5):2012-20. Epub 2011/03/16. doi: 10.1128/iai.01348-10. PubMed PMID: 21402766; PubMed Central PMCID: PMC3088145.
81. Barka EA, Vatsa P, Sanchez L, Gaveau-Vaillant N, Jacquard C, Meier-Kolthoff JP, et al. Taxonomy, Physiology, and Natural Products of Actinobacteria. *Microbiology and molecular biology reviews : MMBR*. 2016;80(1):1-43. Epub 2015/11/27. doi: 10.1128/mnbr.00019-15. PubMed PMID: 26609051; PubMed Central PMCID: PMC4711186.
82. Cherpes TL, Meyn LA, Krohn MA, Lurie JG, Hillier SL. Association between acquisition of herpes simplex virus type 2 in women and bacterial vaginosis. *Clinical infectious diseases : an official publication of the Infectious Diseases Society of America*. 2003;37(3):319-25. Epub 2003/07/29. doi: 10.1086/375819. PubMed PMID: 12884154.
83. Turnbaugh PJ, Hamady M, Yatsunencko T, Cantarel BL, Duncan A, Ley RE, et al. A core gut microbiome in obese and lean twins. *Nature*. 2009;457(7228):480-4. Epub 2008/12/02. doi: 10.1038/nature07540. PubMed PMID: 19043404; PubMed Central PMCID: PMC32677729.
84. Mulligan CM, Friedman JE. Maternal modifiers of the infant gut microbiota: metabolic consequences. *The Journal of endocrinology*. 2017;235(1):R1-R12. Epub 2017/07/29. doi: 10.1530/joe-17-0303. PubMed PMID: 28751453; PubMed Central PMCID: PMC5568816.
85. Cukrowska B. Microbial and Nutritional Programming-The Importance of the Microbiome and Early Exposure to Potential Food Allergens in the Development of Allergies. *Nutrients*. 2018;10(10). Epub 2018/10/21. doi: 10.3390/nu10101541. PubMed PMID: 30340391; PubMed Central PMCID: PMC6212882.
86. Codagnone MG, Spichak S, O'Mahony SM, O'Leary OF, Clarke G, Stanton C, et al. Programming Bugs: Microbiota and the Developmental Origins of Brain Health and Disease.

- Biological psychiatry. 2019;85(2):150-63. Epub 2018/08/02. doi: 10.1016/j.biopsych.2018.06.014. PubMed PMID: 30064690.
87. Al Khodor S, Reichert B, Shatat IF. The Microbiome and Blood Pressure: Can Microbes Regulate Our Blood Pressure? *Frontiers in pediatrics*. 2017;5:138. Epub 2017/07/05. doi: 10.3389/fped.2017.00138. PubMed PMID: 28674682; PubMed Central PMCID: PMC5474689.
88. ElSayed SA, Mukherjee S. *Physiology, Pancreas*. StatPearls. Treasure Island FL: StatPearls Publishing LLC.; 2019.
89. Zhou Q, Melton DA. Pancreas regeneration. *Nature*. 2018;557(7705):351-8. Epub 2018/05/18. doi: 10.1038/s41586-018-0088-0. PubMed PMID: 29769672; PubMed Central PMCID: PMC6168194.
90. Roder PV, Wu B, Liu Y, Han W. Pancreatic regulation of glucose homeostasis. *Experimental & molecular medicine*. 2016;48:e219. Epub 2016/03/12. doi: 10.1038/emm.2016.6. PubMed PMID: 26964835; PubMed Central PMCID: PMC4892884.
91. Baumann MU, Deborde S, Illsley NP. Placental glucose transfer and fetal growth. *Endocrine*. 2002;19(1):13-22. Epub 2003/02/14. doi: 10.1385/endo:19:1:13. PubMed PMID: 12583599.
92. Asplund K, Westman S, Hellerstrom C. Glucose stimulation of insulin secretion from the isolated pancreas of foetal and newborn rats. *Diabetologia*. 1969;5(4):260-2. Epub 1969/08/01. PubMed PMID: 4902721.
93. Espinosa de los M, Driscoll SG, Steinke J. Insulin release from isolated human fetal pancreatic islets. *Science (New York, NY)*. 1970;168(3935):1111-2. Epub 1970/05/29. PubMed PMID: 4909765.
94. Nolan CJ, Proietto J. The feto-placental glucose steal phenomenon is a major cause of maternal metabolic adaptation during late pregnancy in the rat. *Diabetologia*. 1994;37(10):976-84. Epub 1994/10/01. PubMed PMID: 7851692.
95. Toselli C, Hyslop CM, Hughes M, Natale DR, Santamaria P, Huang CT. Contribution of a non-beta-cell source to beta-cell mass during pregnancy. *PloS one*. 2014;9(6):e100398. Epub 2014/06/19. doi: 10.1371/journal.pone.0100398. PubMed PMID: 24940737; PubMed Central PMCID: PMC4062500.
96. Teta M, Rankin MM, Long SY, Stein GM, Kushner JA. Growth and regeneration of adult beta cells does not involve specialized progenitors. *Developmental cell*. 2007;12(5):817-26. Epub 2007/05/10. doi: 10.1016/j.devcel.2007.04.011. PubMed PMID: 17488631.
97. Sorenson RL, Brelje TC. Adaptation of islets of Langerhans to pregnancy: beta-cell growth, enhanced insulin secretion and the role of lactogenic hormones. *Hormone and metabolic research = Hormon- und Stoffwechselforschung = Hormones et metabolisme*. 1997;29(6):301-7. Epub 1997/06/01. doi: 10.1055/s-2007-979040. PubMed PMID: 9230352.
98. Brelje TC, Scharp DW, Lacy PE, Ogren L, Talamantes F, Robertson M, et al. Effect of homologous placental lactogens, prolactins, and growth hormones on islet B-cell division and insulin secretion in rat, mouse, and human islets: implication for placental lactogen regulation of islet function during pregnancy. *Endocrinology*. 1993;132(2):879-87. Epub 1993/02/01. doi: 10.1210/endo.132.2.8425500. PubMed PMID: 8425500.
99. Lain KY, Catalano PM. Metabolic changes in pregnancy. *Clinical obstetrics and gynecology*. 2007;50(4):938-48. Epub 2007/11/06. doi: 10.1097/GRF.0b013e31815a5494. PubMed PMID: 17982337.

100. Kim H, Toyofuku Y, Lynn FC, Chak E, Uchida T, Mizukami H, et al. Serotonin regulates pancreatic beta cell mass during pregnancy. *Nature medicine*. 2010;16(7):804-8. Epub 2010/06/29. doi: 10.1038/nm.2173. PubMed PMID: 20581837; PubMed Central PMCID: PMC2921604.
101. Scaglia L, Smith FE, Bonner-Weir S. Apoptosis contributes to the involution of beta cell mass in the post partum rat pancreas. *Endocrinology*. 1995;136(12):5461-8. Epub 1995/12/01. doi: 10.1210/endo.136.12.7588296. PubMed PMID: 7588296.
102. Sorenson RL, Brelje TC, Roth C. Effects of steroid and lactogenic hormones on islets of Langerhans: a new hypothesis for the role of pregnancy steroids in the adaptation of islets to pregnancy. *Endocrinology*. 1993;133(5):2227-34. Epub 1993/11/01. doi: 10.1210/endo.133.5.8404674. PubMed PMID: 8404674.
103. Mebius RE, Kraal G. Structure and function of the spleen. *Nature reviews Immunology*. 2005;5(8):606-16. Epub 2005/08/02. doi: 10.1038/nri1669. PubMed PMID: 16056254.
104. Fowler JH, Nash DJ. Erythropoiesis in the spleen and bone marrow of the pregnant mouse. *Developmental biology*. 1968;18(4):331-53. doi: [https://doi.org/10.1016/0012-1606\(68\)90045-6](https://doi.org/10.1016/0012-1606(68)90045-6).
105. Mattsson R, Mattsson A, Lindahl-Kiessling K. Anemia causes erythropoiesis and increased antibody synthesis in the spleen of the pregnant mouse. *Developmental and comparative immunology*. 1984;8(1):169-78. Epub 1984/01/01. PubMed PMID: 6539258.
106. Bustamante JJ, Dai G, Soares MJ. Pregnancy and lactation modulate maternal splenic growth and development of the erythroid lineage in the rat and mouse. *Reproduction, fertility, and development*. 2008;20(2):303-10. Epub 2008/02/08. PubMed PMID: 18255020.
107. Maymon R, Strauss S, Vaknin Z, Weinraub Z, Herman A, Gayer G. Normal sonographic values of maternal spleen size throughout pregnancy. *Ultrasound in medicine & biology*. 2006;32(12):1827-31. Epub 2006/12/16. doi: 10.1016/j.ultrasmedbio.2006.06.017. PubMed PMID: 17169694.
108. Maymon R, Zimmerman AL, Strauss S, Gayer G. Maternal Spleen Size Throughout Normal Pregnancy. *Seminars in Ultrasound, CT and MRI*. 2007;28(1):64-6. doi: <https://doi.org/10.1053/j.sult.2006.10.005>.
109. Ogobuiro I, Tuma F. *Physiology, Renal*. StatPearls. Treasure Island FL: StatPearls Publishing LLC.; 2019.
110. Soriano RM, Leslie SW. *Anatomy, Abdomen and Pelvis, Kidneys*. StatPearls. Treasure Island FL: StatPearls Publishing LLC.; 2019.
111. Bailey RR, Rolleston GL. Kidney length and ureteric dilatation in the puerperium. *The Journal of obstetrics and gynaecology of the British Commonwealth*. 1971;78(1):55-61. Epub 1971/01/01. PubMed PMID: 5557675.
112. Roy C, Saussine C, Jahn C, Le Bras Y, Steichen G, Delepaul B, et al. Fast imaging MR assessment of ureterohydronephrosis during pregnancy. *Magnetic resonance imaging*. 1995;13(6):767-72. Epub 1995/01/01. PubMed PMID: 8544647.
113. Beydoun SN. Morphologic changes in the renal tract in pregnancy. *Clinical obstetrics and gynecology*. 1985;28(2):249-56. Epub 1985/06/01. PubMed PMID: 4017319.
114. Dunlop W. Serial changes in renal haemodynamics during normal human pregnancy. *British journal of obstetrics and gynaecology*. 1981;88(1):1-9. Epub 1981/01/01. PubMed PMID: 7459285.
115. Walker JJ. Pre-eclampsia. *Lancet (London, England)*. 2000;356(9237):1260-5. Epub 2000/11/10. doi: 10.1016/s0140-6736(00)02800-2. PubMed PMID: 11072961.
116. Davison JM, Shiells EA, Philips PR, Lindheimer MD. Serial evaluation of vasopressin release and thirst in human pregnancy. Role of human chorionic gonadotrophin in the

- osmoregulatory changes of gestation. *The Journal of clinical investigation*. 1988;81(3):798-806. Epub 1988/03/01. doi: 10.1172/jci113386. PubMed PMID: 3343339; PubMed Central PMCID: PMC442528.
117. Dafnis E, Sabatini S. The effect of pregnancy on renal function: physiology and pathophysiology. *The American journal of the medical sciences*. 1992;303(3):184-205. Epub 1992/03/01. PubMed PMID: 1595782.
118. Renault B, Lieman J, Ward D, Krauter K, Kucherlapati R. Localization of the human achaete-scute homolog gene (ASCL1) distal to phenylalanine hydroxylase (PAH) and proximal to tumor rejection antigen (TRA1) on chromosome 12q22-q23. *Genomics*. 1995;30(1):81-3. Epub 1995/11/01. doi: 10.1006/geno.1995.0012. PubMed PMID: 8595908.
119. Bertrand N, Castro DS, Guillemot F. Proneural genes and the specification of neural cell types. *Nature reviews Neuroscience*. 2002;3(7):517-30. Epub 2002/07/03. doi: 10.1038/nrn874. PubMed PMID: 12094208.
120. Casarosa S, Fode C, Guillemot F. Mash1 regulates neurogenesis in the ventral telencephalon. *Development (Cambridge, England)*. 1999;126(3):525-34. Epub 1999/01/07. PubMed PMID: 9876181.
121. de Pontual L, Nepote V, Attie-Bitach T, Al Halabiah H, Trang H, Elghouzzi V, et al. Noradrenergic neuronal development is impaired by mutation of the proneural HASH-1 gene in congenital central hypoventilation syndrome (Ondine's curse). *Human molecular genetics*. 2003;12(23):3173-80. Epub 2003/10/09. doi: 10.1093/hmg/ddg339. PubMed PMID: 14532329.
122. Tomycz ND, Haynes RL, Schmidt EF, Ackerson K, Kinney HC. Novel neuropathologic findings in the Haddad syndrome. *Acta neuropathologica*. 2010;119(2):261-9. Epub 2009/10/22. doi: 10.1007/s00401-009-0599-8. PubMed PMID: 19844731; PubMed Central PMCID: PMC442528.
123. Wu C, Jin X, Tsueng G, Afrasiabi C, Su AI. BioGPS: building your own mash-up of gene annotations and expression profiles. *Nucleic acids research*. 2016;44(D1):D313-6. Epub 2015/11/19. doi: 10.1093/nar/gkv1104. PubMed PMID: 26578587; PubMed Central PMCID: PMC4702805.
124. Nakada Y, Hunsaker TL, Henke RM, Johnson JE. Distinct domains within Mash1 and Math1 are required for function in neuronal differentiation versus neuronal cell-type specification. *Development (Cambridge, England)*. 2004;131(6):1319-30. Epub 2004/03/03. doi: 10.1242/dev.01008. PubMed PMID: 14993186.
125. Imayoshi I, Isomura A, Harima Y, Kawaguchi K, Kori H, Miyachi H, et al. Oscillatory control of factors determining multipotency and fate in mouse neural progenitors. *Science (New York, NY)*. 2013;342(6163):1203-8. Epub 2013/11/02. doi: 10.1126/science.1242366. PubMed PMID: 24179156.
126. Hirata H, Yoshiura S, Ohtsuka T, Bessho Y, Harada T, Yoshikawa K, et al. Oscillatory expression of the bHLH factor Hes1 regulated by a negative feedback loop. *Science (New York, NY)*. 2002;298(5594):840-3. Epub 2002/10/26. doi: 10.1126/science.1074560. PubMed PMID: 12399594.
127. Shimojo H, Ohtsuka T, Kageyama R. Oscillations in notch signaling regulate maintenance of neural progenitors. *Neuron*. 2008;58(1):52-64. Epub 2008/04/11. doi: 10.1016/j.neuron.2008.02.014. PubMed PMID: 18400163.
128. Kageyama R, Shimojo H, Ohtsuka T. Dynamic control of neural stem cells by bHLH factors. *Neuroscience research*. 2019;138:12-8. Epub 2018/09/19. doi: 10.1016/j.neures.2018.09.005. PubMed PMID: 30227160.

129. Kageyama R, Ohtsuka T, Shimojo H, Imayoshi I. Dynamic Notch signaling in neural progenitor cells and a revised view of lateral inhibition. *Nature neuroscience*. 2008;11(11):1247-51. Epub 2008/10/29. doi: 10.1038/nn.2208. PubMed PMID: 18956012.
130. Guillemot F, Lo LC, Johnson JE, Auerbach A, Anderson DJ, Joyner AL. Mammalian achaete-scute homolog 1 is required for the early development of olfactory and autonomic neurons. *Cell*. 1993;75(3):463-76. Epub 1993/11/05. PubMed PMID: 8221886.
131. Cau E, Gradwohl G, Fode C, Guillemot F. Mash1 activates a cascade of bHLH regulators in olfactory neuron progenitors. *Development (Cambridge, England)*. 1997;124(8):1611-21. Epub 1997/04/01. PubMed PMID: 9108377.
132. Borges M, Linnoila RI, van de Velde HJ, Chen H, Nelkin BD, Mabry M, et al. An achaete-scute homologue essential for neuroendocrine differentiation in the lung. *Nature*. 1997;386(6627):852-5. Epub 1997/04/24. doi: 10.1038/386852a0. PubMed PMID: 9126746.
133. Ito T, Udaka N, Yazawa T, Okudela K, Hayashi H, Sudo T, et al. Basic helix-loop-helix transcription factors regulate the neuroendocrine differentiation of fetal mouse pulmonary epithelium. *Development (Cambridge, England)*. 2000;127(18):3913-21. Epub 2000/08/23. PubMed PMID: 10952889.
134. Lanigan TM, DeRaad SK, Russo AF. Requirement of the MASH-1 transcription factor for neuroendocrine differentiation of thyroid C cells. *Journal of neurobiology*. 1998;34(2):126-34. Epub 1998/02/19. PubMed PMID: 9468384.
135. Huber K, Bruhl B, Guillemot F, Olson EN, Ernsberger U, Unsicker K. Development of chromaffin cells depends on MASH1 function. *Development (Cambridge, England)*. 2002;129(20):4729-38. Epub 2002/10/04. PubMed PMID: 12361965.
136. Petryniak MA, Potter GB, Rowitch DH, Rubenstein JL. Dlx1 and Dlx2 control neuronal versus oligodendroglial cell fate acquisition in the developing forebrain. *Neuron*. 2007;55(3):417-33. Epub 2007/08/07. doi: 10.1016/j.neuron.2007.06.036. PubMed PMID: 17678855; PubMed Central PMCID: PMCPMC2039927.
137. Kameda Y. Mash1 is required for glomus cell formation in the mouse carotid body. *Developmental biology*. 2005;283(1):128-39. Epub 2005/05/10. doi: 10.1016/j.ydbio.2005.04.004. PubMed PMID: 15878769.
138. Ball DW, Azzoli CG, Baylin SB, Chi D, Dou S, Donis-Keller H, et al. Identification of a human achaete-scute homolog highly expressed in neuroendocrine tumors. *Proceedings of the National Academy of Sciences of the United States of America*. 1993;90(12):5648-52. Epub 1993/06/15. PubMed PMID: 8390674; PubMed Central PMCID: PMCPMC46778.
139. Ito T, Kudoh S, Ichimura T, Fujino K, Hassan WA, Udaka N. Small cell lung cancer, an epithelial to mesenchymal transition (EMT)-like cancer: significance of inactive Notch signaling and expression of achaete-scute complex homologue 1. *Human cell*. 2017;30(1):1-10. Epub 2016/10/28. doi: 10.1007/s13577-016-0149-3. PubMed PMID: 27785690.
140. Berninger B, Costa MR, Koch U, Schroeder T, Sutor B, Grothe B, et al. Functional properties of neurons derived from in vitro reprogrammed postnatal astroglia. *The Journal of neuroscience : the official journal of the Society for Neuroscience*. 2007;27(32):8654-64. Epub 2007/08/10. doi: 10.1523/jneurosci.1615-07.2007. PubMed PMID: 17687043.
141. Heinrich C, Blum R, Gascon S, Masserdotti G, Tripathi P, Sanchez R, et al. Directing astroglia from the cerebral cortex into subtype specific functional neurons. *PLoS biology*. 2010;8(5):e1000373. Epub 2010/05/27. doi: 10.1371/journal.pbio.1000373. PubMed PMID: 20502524; PubMed Central PMCID: PMCPMC2872647.

142. Vierbuchen T, Ostermeier A, Pang ZP, Kokubu Y, Sudhof TC, Wernig M. Direct conversion of fibroblasts to functional neurons by defined factors. *Nature*. 2010;463(7284):1035-41. Epub 2010/01/29. doi: 10.1038/nature08797. PubMed PMID: 20107439; PubMed Central PMCID: PMCPMC2829121.
143. Marro S, Pang ZP, Yang N, Tsai MC, Qu K, Chang HY, et al. Direct lineage conversion of terminally differentiated hepatocytes to functional neurons. *Cell stem cell*. 2011;9(4):374-82. Epub 2011/10/04. doi: 10.1016/j.stem.2011.09.002. PubMed PMID: 21962918; PubMed Central PMCID: PMCPMC3218088.
144. Karow M, Sanchez R, Schichor C, Masserdotti G, Ortega F, Heinrich C, et al. Reprogramming of pericyte-derived cells of the adult human brain into induced neuronal cells. *Cell stem cell*. 2012;11(4):471-6. Epub 2012/10/09. doi: 10.1016/j.stem.2012.07.007. PubMed PMID: 23040476.
145. Alders M, Hodges M, Hadjantonakis AK, Postmus J, van Wijk I, Blik J, et al. The human Achaete-Scute homologue 2 (ASCL2, HASH2) maps to chromosome 11p15.5, close to IGF2 and is expressed in extravillous trophoblasts. *Human molecular genetics*. 1997;6(6):859-67. Epub 1997/06/01. doi: 10.1093/hmg/6.6.859. PubMed PMID: 9175731.
146. Rossant J, Guillemot F, Tanaka M, Latham K, Gertenstein M, Nagy A. Mash2 is expressed in oogenesis and preimplantation development but is not required for blastocyst formation. *Mechanisms of development*. 1998;73(2):183-91. Epub 1998/06/12. PubMed PMID: 9622625.
147. van der Flier LG, van Gijn ME, Hatzis P, Kujala P, Haegebarth A, Stange DE, et al. Transcription factor achaete scute-like 2 controls intestinal stem cell fate. *Cell*. 2009;136(5):903-12. Epub 2009/03/10. doi: 10.1016/j.cell.2009.01.031. PubMed PMID: 19269367.
148. Lefebvre L. The placental imprintome and imprinted gene function in the trophoblast glycogen cell lineage. *Reproductive biomedicine online*. 2012;25(1):44-57. Epub 2012/05/09. doi: 10.1016/j.rbmo.2012.03.019. PubMed PMID: 22560119; PubMed Central PMCID: PMCPMC3819294.
149. Hu XG, Chen L, Wang QL, Zhao XL, Tan J, Cui YH, et al. Elevated expression of ASCL2 is an independent prognostic indicator in lung squamous cell carcinoma. *Journal of clinical pathology*. 2016;69(4):313-8. Epub 2015/10/21. doi: 10.1136/jclinpath-2015-203025. PubMed PMID: 26483561.
150. Wang C, Wang M, Arrington J, Shan T, Yue F, Nie Y, et al. Ascl2 inhibits myogenesis by antagonizing the transcriptional activity of myogenic regulatory factors. *Development (Cambridge, England)*. 2017;144(2):235-47. Epub 2016/12/21. doi: 10.1242/dev.138099. PubMed PMID: 27993983; PubMed Central PMCID: PMCPMC5394758.
151. Gude NM, Roberts CT, Kalionis B, King RG. Growth and function of the normal human placenta. *Thrombosis research*. 2004;114(5-6):397-407. Epub 2004/10/28. doi: 10.1016/j.thromres.2004.06.038. PubMed PMID: 15507270.
152. Guillemot F, Nagy A, Auerbach A, Rossant J, Joyner AL. Essential role of Mash-2 in extraembryonic development. *Nature*. 1994;371(6495):333-6. Epub 1994/09/22. doi: 10.1038/371333a0. PubMed PMID: 8090202.
153. Azzouz LL, Sharma S. *Physiology, Large Intestine*. StatPearls. Treasure Island FL: StatPearls Publishing LLC.; 2019.
154. Stevens CE, Leblond CP. Rate of renewal of the cells of the intestinal epithelium in the rat. *Anat Rec*. 1947;97(3):373. Epub 1947/03/01. PubMed PMID: 20341868.
155. Park JH, Kotani T, Konno T, Setiawan J, Kitamura Y, Imada S, et al. Promotion of Intestinal Epithelial Cell Turnover by Commensal Bacteria: Role of Short-Chain Fatty Acids. *PLoS*

- one. 2016;11(5):e0156334. Epub 2016/05/28. doi: 10.1371/journal.pone.0156334. PubMed PMID: 27232601; PubMed Central PMCID: PMC4883796.
156. Reed KR, Tunster SJ, Young M, Carrico A, John RM, Clarke AR. Entopic overexpression of *Ascl2* does not accelerate tumorigenesis in *ApcMin* mice. *Gut*. 2012;61(10):1435-8. Epub 2011/12/06. doi: 10.1136/gutjnl-2011-300842. PubMed PMID: 22138533.
157. Mauro A. Satellite cell of skeletal muscle fibers. *The Journal of biophysical and biochemical cytology*. 1961;9:493-5. Epub 1961/02/01. doi: 10.1083/jcb.9.2.493. PubMed PMID: 13768451; PubMed Central PMCID: PMC2225012.
158. Kuang S, Rudnicki MA. The emerging biology of satellite cells and their therapeutic potential. *Trends in molecular medicine*. 2008;14(2):82-91. Epub 2008/01/26. doi: 10.1016/j.molmed.2007.12.004. PubMed PMID: 18218339.
159. Liu X, Chen X, Zhong B, Wang A, Wang X, Chu F, et al. Transcription factor achaete-scute homologue 2 initiates follicular T-helper-cell development. *Nature*. 2014;507(7493):513-8. Epub 2014/01/28. doi: 10.1038/nature12910. PubMed PMID: 24463518; PubMed Central PMCID: PMC4012617.
160. Crotty S. T follicular helper cell differentiation, function, and roles in disease. *Immunity*. 2014;41(4):529-42. Epub 2014/11/05. doi: 10.1016/j.immuni.2014.10.004. PubMed PMID: 25367570; PubMed Central PMCID: PMC4223692.
161. Torre LA, Bray F, Siegel RL, Ferlay J, Lortet-Tieulent J, Jemal A. Global cancer statistics, 2012. *CA: a cancer journal for clinicians*. 2015;65(2):87-108. Epub 2015/02/06. doi: 10.3322/caac.21262. PubMed PMID: 25651787.
162. Bartis D, Csongei V, Weich A, Kiss E, Barko S, Kovacs T, et al. Down-regulation of canonical and up-regulation of non-canonical Wnt signalling in the carcinogenic process of squamous cell lung carcinoma. *PloS one*. 2013;8(3):e57393. Epub 2013/03/19. doi: 10.1371/journal.pone.0057393. PubMed PMID: 23505429; PubMed Central PMCID: PMC3591434.
163. Zhu R, Yang Y, Tian Y, Bai J, Zhang X, Li X, et al. *Ascl2* knockdown results in tumor growth arrest by miRNA-302b-related inhibition of colon cancer progenitor cells. *PloS one*. 2012;7(2):e32170. Epub 2012/03/03. doi: 10.1371/journal.pone.0032170. PubMed PMID: 22384170; PubMed Central PMCID: PMC3285660.
164. Tian Y, Pan Q, Shang Y, Zhu R, Ye J, Liu Y, et al. MicroRNA-200 (miR-200) cluster regulation by achaete scute-like 2 (*Ascl2*): impact on the epithelial-mesenchymal transition in colon cancer cells. *The Journal of biological chemistry*. 2014;289(52):36101-15. Epub 2014/11/06. doi: 10.1074/jbc.M114.598383. PubMed PMID: 25371200; PubMed Central PMCID: PMC4276874.
165. Zuo Q, Wang J, Chen C, Zhang Y, Feng DX, Zhao R, et al. *ASCL2* expression contributes to gastric tumor migration and invasion by downregulating miR223 and inducing EMT. *Molecular medicine reports*. 2018;18(4):3751-9. Epub 2018/08/15. doi: 10.3892/mmr.2018.9363. PubMed PMID: 30106147; PubMed Central PMCID: PMC6131580.
166. Amid C, Bahr A, Mujica A, Sampson N, Bikar SE, Winterpacht A, et al. Comparative genomic sequencing reveals a strikingly similar architecture of a conserved syntenic region on human chromosome 11p15.3 (including gene *ST5*) and mouse chromosome 7. *Cytogenetics and cell genetics*. 2001;93(3-4):284-90. Epub 2001/08/31. doi: 10.1159/000056999. PubMed PMID: 11528127.
167. Yoshida S, Ohbo K, Takakura A, Takebayashi H, Okada T, Abe K, et al. *Sgn1*, a basic helix-loop-helix transcription factor delineates the salivary gland duct cell lineage in mice.

- Developmental biology. 2001;240(2):517-30. Epub 2002/01/11. doi: 10.1006/dbio.2001.0473. PubMed PMID: 11784080.
168. Aure MH, Arany S, Ovitt CE. Salivary Glands: Stem Cells, Self-duplication, or Both? *J Dent Res*. 2015;94(11):1502-7. Epub 08/18. doi: 10.1177/0022034515599770. PubMed PMID: 26285812.
169. Bullard T, Koek L, Roztocil E, Kingsley PD, Mirels L, Ovitt CE. Ascl3 expression marks a progenitor population of both acinar and ductal cells in mouse salivary glands. *Developmental biology*. 2008;320(1):72-8. Epub 2008/06/24. doi: 10.1016/j.ydbio.2008.04.018. PubMed PMID: 18572159; PubMed Central PMCID: PMCPMC2570651.
170. Rugel-Stahl A, Elliott ME, Ovitt CE. Ascl3 marks adult progenitor cells of the mouse salivary gland. *Stem cell research*. 2012;8(3):379-87. Epub 2012/03/01. doi: 10.1016/j.scr.2012.01.002. PubMed PMID: 22370009; PubMed Central PMCID: PMCPMC3319487.
171. Arany S, Catalan MA, Roztocil E, Ovitt CE. Ascl3 knockout and cell ablation models reveal complexity of salivary gland maintenance and regeneration. *Developmental biology*. 2011;353(2):186-93. Epub 2011/03/08. doi: 10.1016/j.ydbio.2011.02.025. PubMed PMID: 21377457; PubMed Central PMCID: PMCPMC3093111.
172. Weng PL, Vinjamuri M, Ovitt CE. Ascl3 transcription factor marks a distinct progenitor lineage for non-neuronal support cells in the olfactory epithelium. *Scientific reports*. 2016;6:38199. Epub 2016/12/03. doi: 10.1038/srep38199. PubMed PMID: 27910949; PubMed Central PMCID: PMCPMC5133605.
173. Truett GE, Heeger P, Mynatt RL, Truett AA, Walker JA, Warman ML. Preparation of PCR-quality mouse genomic DNA with hot sodium hydroxide and tris (HotSHOT). *BioTechniques*. 2000;29(1):52, 4. Epub 2000/07/25. doi: 10.2144/00291bm09. PubMed PMID: 10907076.
174. Pacary E, Heng J, Azzarelli R, Riou P, Castro D, Lebel-Potter M, et al. Proneural Transcription Factors Regulate Different Steps of Cortical Neuron Migration through Rnd-Mediated Inhibition of RhoA Signaling. *Neuron*. 2011;69(6):1069-84. doi: <http://dx.doi.org/10.1016/j.neuron.2011.02.018>.
175. Schneider CA, Rasband WS, Eliceiri KW. NIH Image to ImageJ: 25 years of image analysis. *Nature methods*. 2012;9(7):671-5. Epub 2012/08/30. PubMed PMID: 22930834; PubMed Central PMCID: PMCPMC5554542.
176. Yang P, Wang Y, Hoang D, Tinkham M, Patel A, Sun M-A, et al. A placental growth factor is silenced in mouse embryos by the zinc finger protein ZFP568. *Science (New York, NY)*. 2017;356(6339):757-9. doi: 10.1126/science.aah6895.
177. Bustamante JJ, Copple BL, Soares MJ, Dai G. Gene profiling of maternal hepatic adaptations to pregnancy. *Liver international : official journal of the International Association for the Study of the Liver*. 2010;30(3):406-15. Epub 2009/12/31. doi: 10.1111/j.1478-3231.2009.02183.x. PubMed PMID: 20040050; PubMed Central PMCID: PMCPMC4356012.
178. Hochedlinger K, Yamada Y, Beard C, Jaenisch R. Ectopic expression of Oct-4 blocks progenitor-cell differentiation and causes dysplasia in epithelial tissues. *Cell*. 2005;121(3):465-77. Epub 2005/05/11. doi: 10.1016/j.cell.2005.02.018. PubMed PMID: 15882627.
179. Braems G, Denys H, De Wever O, Cocquyt V, Van den Broecke R. Use of tamoxifen before and during pregnancy. *The oncologist*. 2011;16(11):1547-51. Epub 2011/10/25. doi: 10.1634/theoncologist.2011-0121. PubMed PMID: 22020212; PubMed Central PMCID: PMCPMC3233288.

180. Sun J-H, Luo Q, Liu L-L, Song G-B. Liver cancer stem cell markers: Progression and therapeutic implications. *World journal of gastroenterology*. 2016;22(13):3547-57. doi: 10.3748/wjg.v22.i13.3547. PubMed PMID: 27053846.
181. Lui JC, Baron J. Evidence that Igf2 down-regulation in postnatal tissues and up-regulation in malignancies is driven by transcription factor E2f3. *Proceedings of the National Academy of Sciences of the United States of America*. 2013;110(15):6181-6. Epub 03/25. doi: 10.1073/pnas.1219079110. PubMed PMID: 23530192.
182. Cross R, Ling C, Day NPJ, McGready R, Paris DH. Revisiting doxycycline in pregnancy and early childhood--time to rebuild its reputation? *Expert Opin Drug Saf*. 2016;15(3):367-82. Epub 01/25. doi: 10.1517/14740338.2016.1133584. PubMed PMID: 26680308.
183. Heaton PC, Fenwick SR, Brewer DE. Association between tetracycline or doxycycline and hepatotoxicity: a population based case-control study. *Journal of clinical pharmacy and therapeutics*. 2007;32(5):483-7. Epub 2007/09/19. doi: 10.1111/j.1365-2710.2007.00853.x. PubMed PMID: 17875115.
184. Czeizel AE, Rockenbauer M. Teratogenic study of doxycycline. *Obstetrics and gynecology*. 1997;89(4):524-8. Epub 1997/04/01. doi: 10.1016/s0029-7844(97)00005-7. PubMed PMID: 9083306.
185. Chu M, Wang L, Wang H, Shen T, Yang Y, Sun Y, et al. A novel role of CDX1 in embryonic epicardial development. *PloS one*. 2014;9(7):e103271. Epub 2014/07/30. doi: 10.1371/journal.pone.0103271. PubMed PMID: 25068460; PubMed Central PMCID: PMC4113346.
186. van Amerongen R, Fuerer C, Mizutani M, Nusse R. Wnt5a can both activate and repress Wnt/beta-catenin signaling during mouse embryonic development. *Developmental biology*. 2012;369(1):101-14. Epub 2012/07/10. doi: 10.1016/j.ydbio.2012.06.020. PubMed PMID: 22771246; PubMed Central PMCID: PMC435145.
187. Perdigoto CN, Dauber KL, Bar C, Tsai PC, Valdes VJ, Cohen I, et al. Polycomb-Mediated Repression and Sonic Hedgehog Signaling Interact to Regulate Merkel Cell Specification during Skin Development. *PLoS genetics*. 2016;12(7):e1006151. Epub 2016/07/16. doi: 10.1371/journal.pgen.1006151. PubMed PMID: 27414999; PubMed Central PMCID: PMC4944976.
188. Gonzalez-Loyola A, Fernandez-Miranda G, Trakala M, Partida D, Samejima K, Ogawa H, et al. Aurora B Overexpression Causes Aneuploidy and p21Cip1 Repression during Tumor Development. *Molecular and cellular biology*. 2015;35(20):3566-78. Epub 2015/08/05. doi: 10.1128/mcb.01286-14. PubMed PMID: 26240282; PubMed Central PMCID: PMC4573715.
189. Schuurman TN, Witteveen PO, van der Wall E, Passier JLM, Huitema ADR, Amant F, et al. Tamoxifen and pregnancy: an absolute contraindication? *Breast Cancer Research and Treatment*. 2019;175(1):17-25. doi: 10.1007/s10549-019-05154-7.
190. Isaacs RJ, Hunter W, Clark K. Tamoxifen as systemic treatment of advanced breast cancer during pregnancy--case report and literature review. *Gynecologic oncology*. 2001;80(3):405-8. Epub 2001/03/27. doi: 10.1006/gyno.2000.6080. PubMed PMID: 11263941.
191. Zhou MH, Han GZ, Chu YH. [Effects of antiestrogenic drug tamoxifen on human placental secretion of progesterone and human chorionic gonadotropin during early gestation]. *Yao xue xue bao = Acta pharmaceutica Sinica*. 1991;26(11):801-4. Epub 1991/01/01. PubMed PMID: 1823973.
192. Furukawa S, Hayashi S, Usuda K, Abe M, Ogawa I. The impairment of metrial gland development in tamoxifen exposed rats. *Experimental and toxicologic pathology : official journal*

- of the Gesellschaft für Toxikologische Pathologie. 2012;64(1-2):121-6. Epub 2010/08/10. doi: 10.1016/j.etp.2010.07.004. PubMed PMID: 20692139.
193. Brzezinski JA, Kim EJ, Johnson JE, Reh TA. Ascl1 expression defines a subpopulation of lineage-restricted progenitors in the mammalian retina. *Development (Cambridge, England)*. 2011;138(16):3519-31. Epub 2011/07/21. doi: 10.1242/dev.064006. PubMed PMID: 21771810; PubMed Central PMCID: PMC3143566.
194. Dyachuk V, Furlan A, Shahidi MK, Giovenco M, Kaukua N, Konstantinidou C, et al. Neurodevelopment. Parasympathetic neurons originate from nerve-associated peripheral glial progenitors. *Science (New York, NY)*. 2014;345(6192):82-7. Epub 2014/06/14. doi: 10.1126/science.1253281. PubMed PMID: 24925909.
195. Hastie E, Samulski RJ. Adeno-associated virus at 50: a golden anniversary of discovery, research, and gene therapy success--a personal perspective. *Human gene therapy*. 2015;26(5):257-65. Epub 2015/03/27. doi: 10.1089/hum.2015.025. PubMed PMID: 25807962; PubMed Central PMCID: PMC4442590.
196. Basner-Tschakarjan E, Mingozzi F. Cell-Mediated Immunity to AAV Vectors, Evolving Concepts and Potential Solutions. *Frontiers in immunology*. 2014;5:350. Epub 2014/08/08. doi: 10.3389/fimmu.2014.00350. PubMed PMID: 25101090; PubMed Central PMCID: PMC4107954.
197. van Gestel MA, Boender AJ, de Vrind VAJ, Garner KM, Luijendijk MCM, Adan RAH. Recombinant adeno-associated virus: efficient transduction of the rat VMH and clearance from blood. *PloS one*. 2014;9(5):e97639-e. doi: 10.1371/journal.pone.0097639. PubMed PMID: 24858547.
198. Chen S-J, Sanmiguel J, Lock M, McMenemy D, Draper C, Limberis MP, et al. Biodistribution of AAV8 vectors expressing human low-density lipoprotein receptor in a mouse model of homozygous familial hypercholesterolemia. *Hum Gene Ther Clin Dev*. 2013;24(4):154-60. Epub 11/09. doi: 10.1089/humc.2013.082. PubMed PMID: 24070336.
199. Sarkar R, Tetreault R, Gao G, Wang L, Bell P, Chandler R, et al. Total correction of hemophilia A mice with canine FVIII using an AAV 8 serotype. *Blood*. 2004;103(4):1253-60. Epub 2003/10/11. doi: 10.1182/blood-2003-08-2954. PubMed PMID: 14551134.
200. Greig JA, Nordin JML, Draper C, McMenemy D, Chroschinski EA, Bell P, et al. Determining the Minimally Effective Dose of a Clinical Candidate AAV Vector in a Mouse Model of Crigler-Najjar Syndrome. *Molecular therapy Methods & clinical development*. 2018;10:237-44. Epub 2018/08/17. doi: 10.1016/j.omtm.2018.07.008. PubMed PMID: 30112420; PubMed Central PMCID: PMC6090885.
201. Nakamura T, Mizuno S. The discovery of hepatocyte growth factor (HGF) and its significance for cell biology, life sciences and clinical medicine. *Proc Jpn Acad Ser B Phys Biol Sci*. 2010;86(6):588-610. doi: 10.2183/pjab.86.588. PubMed PMID: 20551596.
202. Burr AW, Toole K, Chapman C, Hines JE, Burt AD. Anti-hepatocyte growth factor antibody inhibits hepatocyte proliferation during liver regeneration. *The Journal of pathology*. 1998;185(3):298-302. Epub 1998/10/15. doi: 10.1002/(sici)1096-9896(199807)185:3<298::aid-path88>3.0.co;2-b. PubMed PMID: 9771484.
203. Hill DJ. Relative abundance and molecular size of immunoreactive insulin-like growth factors I and II in human fetal tissues. *Early human development*. 1990;21(1):49-58. Epub 1990/01/01. PubMed PMID: 2311550.
204. Sacks DA. Determinants of fetal growth. *Current diabetes reports*. 2004;4(4):281-7. Epub 2004/07/22. PubMed PMID: 15265471.

205. Chao W, D'Amore PA. IGF2: epigenetic regulation and role in development and disease. *Cytokine Growth Factor Rev.* 2008;19(2):111-20. Epub 03/04. doi: 10.1016/j.cytogfr.2008.01.005. PubMed PMID: 18308616.
206. Younis S, Schönke M, Massart J, Hjortebjerg R, Sundström E, Gustafson U, et al. The ZBED6-IGF2 axis has a major effect on growth of skeletal muscle and internal organs in placental mammals. *Proceedings of the National Academy of Sciences of the United States of America.* 2018;115(9):E2048-E57. Epub 02/12. doi: 10.1073/pnas.1719278115. PubMed PMID: 29440408.
207. Uehara T, Ainslie GR, Kutanzi K, Pogribny IP, Muskhelishvili L, Izawa T, et al. Molecular mechanisms of fibrosis-associated promotion of liver carcinogenesis. *Toxicological sciences : an official journal of the Society of Toxicology.* 2013;132(1):53-63. Epub 2013/01/05. doi: 10.1093/toxsci/kfs342. PubMed PMID: 23288052; PubMed Central PMCID: PMC3576012.
208. Ma S. Biology and clinical implications of CD133(+) liver cancer stem cells. *Experimental cell research.* 2013;319(2):126-32. Epub 2012/09/25. doi: 10.1016/j.yexcr.2012.09.007. PubMed PMID: 22999864.
209. Vander Griend DJ, Karthaus WL, Dalrymple S, Meeker A, DeMarzo AM, Isaacs JT. The role of CD133 in normal human prostate stem cells and malignant cancer-initiating cells. *Cancer research.* 2008;68(23):9703-11. Epub 2008/12/03. doi: 10.1158/0008-5472.can-08-3084. PubMed PMID: 19047148; PubMed Central PMCID: PMC3072758.
210. Shmelkov SV, Butler JM, Hooper AT, Hormigo A, Kushner J, Milde T, et al. CD133 expression is not restricted to stem cells, and both CD133+ and CD133- metastatic colon cancer cells initiate tumors. *The Journal of clinical investigation.* 2008;118(6):2111-20. Epub 2008/05/24. doi: 10.1172/jci34401. PubMed PMID: 18497886; PubMed Central PMCID: PMC2391278.
211. Qin Q, Sun Y, Fei M, Zhang J, Jia Y, Gu M, et al. Expression of putative stem marker nestin and CD133 in advanced serous ovarian cancer. *Neoplasma.* 2012;59(3):310-5. Epub 2012/02/03. doi: 10.4149/neo\_2012\_040. PubMed PMID: 22296500.
212. Suetsugu A, Nagaki M, Aoki H, Motohashi T, Kunisada T, Moriwaki H. Characterization of CD133+ hepatocellular carcinoma cells as cancer stem/progenitor cells. *Biochemical and biophysical research communications.* 2006;351(4):820-4. Epub 2006/11/14. doi: 10.1016/j.bbrc.2006.10.128. PubMed PMID: 17097610.
213. Galizia G, Gemei M, Del Vecchio L, Zamboli A, Di Noto R, Mirabelli P, et al. Combined CD133/CD44 expression as a prognostic indicator of disease-free survival in patients with colorectal cancer. *Archives of surgery (Chicago, Ill : 1960).* 2012;147(1):18-24. Epub 2012/01/18. doi: 10.1001/archsurg.2011.795. PubMed PMID: 22250106.
214. Dolle L, Theise ND, Schmelzer E, Boulter L, Gires O, van Grunsven LA. EpCAM and the biology of hepatic stem/progenitor cells. *American journal of physiology Gastrointestinal and liver physiology.* 2015;308(4):G233-50. Epub 2014/12/06. doi: 10.1152/ajpgi.00069.2014. PubMed PMID: 25477371; PubMed Central PMCID: PMC4329473.
215. Zhang L, Theise N, Chua M, Reid LM. The stem cell niche of human livers: symmetry between development and regeneration. *Hepatology (Baltimore, Md).* 2008;48(5):1598-607. Epub 2008/10/31. doi: 10.1002/hep.22516. PubMed PMID: 18972441.
216. Walayat S, Martin D, Patel J, Ahmed U, N Asghar M, Pai AU, et al. Role of albumin in cirrhosis: from a hospitalist's perspective. *J Community Hosp Intern Med Perspect.* 2017;7(1):8-14. doi: 10.1080/20009666.2017.1302704. PubMed PMID: 28634518.
217. Evans TW. Review article: albumin as a drug--biological effects of albumin unrelated to oncotic pressure. *Alimentary pharmacology & therapeutics.* 2002;16 Suppl 5:6-11. Epub 2002/11/09. PubMed PMID: 12423448.

218. Vincent JL. Relevance of albumin in modern critical care medicine. *Best practice & research Clinical anaesthesiology*. 2009;23(2):183-91. Epub 2009/08/06. PubMed PMID: 19653438.
219. Quinlan GJ, Martin GS, Evans TW. Albumin: biochemical properties and therapeutic potential. *Hepatology (Baltimore, Md)*. 2005;41(6):1211-9. Epub 2005/05/26. doi: 10.1002/hep.20720. PubMed PMID: 15915465.
220. Henriksen JH, Siemssen O, Krintel JJ, Malchow-Moller A, Bendtsen F, Ring-Larsen H. Dynamics of albumin in plasma and ascitic fluid in patients with cirrhosis. *Journal of hepatology*. 2001;34(1):53-60. Epub 2001/02/24. doi: 10.1016/s0168-8278(00)00009-x. PubMed PMID: 11211908.
221. Vincent JL, Dubois MJ, Navickis RJ, Wilkes MM. Hypoalbuminemia in acute illness: is there a rationale for intervention? A meta-analysis of cohort studies and controlled trials. *Annals of surgery*. 2003;237(3):319-34. Epub 2003/03/05. doi: 10.1097/01.sla.0000055547.93484.87. PubMed PMID: 12616115; PubMed Central PMCID: PMCPMC1514323.
222. Cohen JC, Horton JD, Hobbs HH. Human fatty liver disease: old questions and new insights. *Science (New York, NY)*. 2011;332(6037):1519-23. Epub 2011/06/28. doi: 10.1126/science.1204265. PubMed PMID: 21700865; PubMed Central PMCID: PMCPMC3229276.
223. Jemal A, Bray F, Center MM, Ferlay J, Ward E, Forman D. Global cancer statistics. *CA: a cancer journal for clinicians*. 2011;61(2):69-90. Epub 2011/02/08. doi: 10.3322/caac.20107. PubMed PMID: 21296855.
224. Pratt DS, Kaplan MM. Evaluation of abnormal liver-enzyme results in asymptomatic patients. *N Engl J Med*. 2000;342(17):1266-71. Epub 2000/04/27. doi: 10.1056/nejm200004273421707. PubMed PMID: 10781624.
225. Sookoian S, Pirola CJ. Alanine and aspartate aminotransferase and glutamine-cycling pathway: their roles in pathogenesis of metabolic syndrome. *World journal of gastroenterology : WJG*. 2012;18(29):3775-81. Epub 2012/08/10. doi: 10.3748/wjg.v18.i29.3775. PubMed PMID: 22876026; PubMed Central PMCID: PMCPMC3413046.
226. Meyer MS, Wexler S, Jedwab M, Spirer Z, Keysar N, Shibolet S. Low levels of serum calcium, phosphorus and plasma 25-hydroxy vitamin D in cirrhosis of the liver. *Israel journal of medical sciences*. 1978;14(7):725-30. Epub 1978/07/01. PubMed PMID: 681162.
227. Hanley AJ, Williams K, Festa A, Wagenknecht LE, D'Agostino RB, Jr., Kempf J, et al. Elevations in markers of liver injury and risk of type 2 diabetes: the insulin resistance atherosclerosis study. *Diabetes*. 2004;53(10):2623-32. Epub 2004/09/28. doi: 10.2337/diabetes.53.10.2623. PubMed PMID: 15448093.
228. Hadizadeh F, Faghihimani E, Adibi P. Nonalcoholic fatty liver disease: Diagnostic biomarkers. *World J Gastrointest Pathophysiol*. 2017;8(2):11-26. doi: 10.4291/wjgp.v8.i2.11. PubMed PMID: 28573064.
229. Stollwerck PL, Namdar T, Stang FH, Lange T, Mailander P, Siemers F. Rhabdomyolysis and acute renal failure in severely burned patients. *Burns : journal of the International Society for Burn Injuries*. 2011;37(2):240-8. Epub 2010/10/23. doi: 10.1016/j.burns.2010.09.009. PubMed PMID: 20965664.
230. Clarkson PM, Kearns AK, Rouzier P, Rubin R, Thompson PD. Serum creatine kinase levels and renal function measures in exertional muscle damage. *Medicine and science in sports and exercise*. 2006;38(4):623-7. Epub 2006/05/09. doi: 10.1249/01.mss.0000210192.49210.fc. PubMed PMID: 16679975.

231. Barnert J, Behr W. Acute viral hepatitis and low values for serum creatine kinase. *Clinical chemistry*. 1985;31(11):1909-10. Epub 1985/11/01. PubMed PMID: 4053364.
232. Nanji AA, Blank D. Low serum creatine kinase activity in patients with alcoholic liver disease. *Clinical chemistry*. 1981;27(11):1954. Epub 1981/11/01. PubMed PMID: 7296863.
233. Nunez J, Minana G, Santas E, Bertomeu-Gonzalez V. Cardiorenal Syndrome in Acute Heart Failure: Revisiting Paradigms. *Revista espanola de cardiologia (English ed)*. 2015;68(5):426-35. Epub 2015/03/12. doi: 10.1016/j.rec.2014.10.016. PubMed PMID: 25758162.
234. Hosten AO. BUN and Creatinine. In: rd, Walker HK, Hall WD, Hurst JW, editors. *Clinical Methods: The History, Physical, and Laboratory Examinations*. Boston: Butterworth Publishers, a division of Reed Publishing.; 1990.
235. Metra M, Davison B, Bettari L, Sun H, Edwards C, Lazzarini V, et al. Is worsening renal function an ominous prognostic sign in patients with acute heart failure? The role of congestion and its interaction with renal function. *Circulation Heart failure*. 2012;5(1):54-62. Epub 2011/12/15. doi: 10.1161/circheartfailure.111.963413. PubMed PMID: 22167320.
236. MacAulay J, Thompson K, Kiberd BA, Barnes DC, Peltekian KM. Serum creatinine in patients with advanced liver disease is of limited value for identification of moderate renal dysfunction: are the equations for estimating renal function better? *Canadian journal of gastroenterology = Journal canadien de gastroenterologie*. 2006;20(8):521-6. doi: 10.1155/2006/858053. PubMed PMID: 16955148.
237. Moon YA, Shah NA, Mohapatra S, Warrington JA, Horton JD. Identification of a mammalian long chain fatty acyl elongase regulated by sterol regulatory element-binding proteins. *The Journal of biological chemistry*. 2001;276(48):45358-66. Epub 2001/09/22. doi: 10.1074/jbc.M108413200. PubMed PMID: 11567032.
238. Matsuzaka T, Atsumi A, Matsumori R, Nie T, Shinozaki H, Suzuki-Kemuriyama N, et al. Elovl6 promotes nonalcoholic steatohepatitis. *Hepatology (Baltimore, Md)*. 2012;56(6):2199-208. Epub 2012/07/04. doi: 10.1002/hep.25932. PubMed PMID: 22753171.
239. Kuba M, Matsuzaka T, Matsumori R, Saito R, Kaga N, Taka H, et al. Absence of Elovl6 attenuates steatohepatitis but promotes gallstone formation in a lithogenic diet-fed Ldlr<sup>-/-</sup> mouse model. *Scientific reports*. 2015;5:17604. doi: 10.1038/srep17604  
<https://www.nature.com/articles/srep17604#supplementary-information>.
240. Su Y-C, Feng Y-H, Wu H-T, Huang Y-S, Tung C-L, Wu P, et al. Elovl6 is a negative clinical predictor for liver cancer and knockdown of Elovl6 reduces murine liver cancer progression. *Scientific reports*. 2018;8(1):6586-. doi: 10.1038/s41598-018-24633-3. PubMed PMID: 29700319.
241. Trepo E, Romeo S, Zucman-Rossi J, Nahon P. PNPLA3 gene in liver diseases. *Journal of hepatology*. 2016;65(2):399-412. Epub 2016/04/04. doi: 10.1016/j.jhep.2016.03.011. PubMed PMID: 27038645.
242. Kazemi MR, McDonald CM, Shigenaga JK, Grunfeld C, Feingold KR. Adipocyte fatty acid-binding protein expression and lipid accumulation are increased during activation of murine macrophages by toll-like receptor agonists. *Arteriosclerosis, thrombosis, and vascular biology*. 2005;25(6):1220-4. Epub 2005/02/12. doi: 10.1161/01.ATV.0000159163.52632.1b. PubMed PMID: 15705927.
243. Boord JB, Maeda K, Makowski L, Babaev VR, Fazio S, Linton MF, et al. Combined adipocyte-macrophage fatty acid-binding protein deficiency improves metabolism, atherosclerosis, and survival in apolipoprotein E-deficient mice. *Circulation*. 2004;110(11):1492-8. Epub

- 2004/09/09. doi: 10.1161/01.cir.0000141735.13202.b6. PubMed PMID: 15353487; PubMed Central PMCID: PMC4027050.
244. Hotamisligil GS, Johnson RS, Distel RJ, Ellis R, Papaioannou VE, Spiegelman BM. Uncoupling of obesity from insulin resistance through a targeted mutation in aP2, the adipocyte fatty acid binding protein. *Science (New York, NY)*. 1996;274(5291):1377-9. Epub 1996/11/22. doi: 10.1126/science.274.5291.1377. PubMed PMID: 8910278.
245. Thompson KJ, Austin RG, Nazari SS, Gersin KS, Iannitti DA, McKillop IH. Altered fatty acid-binding protein 4 (FABP4) expression and function in human and animal models of hepatocellular carcinoma. *Liver international : official journal of the International Association for the Study of the Liver*. 2018;38(6):1074-83. Epub 2017/11/25. doi: 10.1111/liv.13639. PubMed PMID: 29171144.
246. Halsted CH. Nutrition and alcoholic liver disease. *Seminars in liver disease*. 2004;24(3):289-304. Epub 2004/09/07. doi: 10.1055/s-2004-832941. PubMed PMID: 15349806.
247. Chrostek L, Supronowicz L, Panasiuk A, Cylwik B, Gruszewska E, Flisiak R. The effect of the severity of liver cirrhosis on the level of lipids and lipoproteins. *Clin Exp Med*. 2014;14(4):417-21. doi: 10.1007/s10238-013-0262-5. PubMed PMID: 24122348.
248. Ramcharran D, Wahed AS, Conjeevaram HS, Evans RW, Wang T, Belle SH, et al. Serum lipids and their associations with viral levels and liver disease severity in a treatment-naive chronic hepatitis C type 1-infected cohort. *Journal of viral hepatitis*. 2011;18(4):e144-52. Epub 2010/11/13. doi: 10.1111/j.1365-2893.2010.01394.x. PubMed PMID: 21070504.
249. Ghadir MR, Riahin AA, Havaspour A, Nooranipour M, Habibinejad AA. The relationship between lipid profile and severity of liver damage in cirrhotic patients. *Hepat Mon*. 2010;10(4):285-8. Epub 12/01. PubMed PMID: 22312394.
250. Lewis GF, Carpentier A, Adeli K, Giacca A. Disordered fat storage and mobilization in the pathogenesis of insulin resistance and type 2 diabetes. *Endocrine reviews*. 2002;23(2):201-29. Epub 2002/04/12. doi: 10.1210/edrv.23.2.0461. PubMed PMID: 11943743.
251. Karjalainen L, Pihlajamaki J, Karhapaa P, Laakso M. Impaired insulin-stimulated glucose oxidation and free fatty acid suppression in patients with familial combined hyperlipidemia: a precursor defect for dyslipidemia? *Arteriosclerosis, thrombosis, and vascular biology*. 1998;18(10):1548-53. Epub 1998/10/09. doi: 10.1161/01.atv.18.10.1548. PubMed PMID: 9763525.
252. Laws A, Hoen HM, Selby JV, Saad MF, Haffner SM, Howard BV. Differences in insulin suppression of free fatty acid levels by gender and glucose tolerance status. Relation to plasma triglyceride and apolipoprotein B concentrations. *Insulin Resistance Atherosclerosis Study (IRAS) Investigators. Arteriosclerosis, thrombosis, and vascular biology*. 1997;17(1):64-71. Epub 1997/01/01. doi: 10.1161/01.atv.17.1.64. PubMed PMID: 9012639.
253. Boden G. Obesity, insulin resistance and free fatty acids. *Current opinion in endocrinology, diabetes, and obesity*. 2011;18(2):139-43. Epub 2011/02/08. doi: 10.1097/MED.0b013e3283444b09. PubMed PMID: 21297467; PubMed Central PMCID: PMC3169796.
254. Liu J, Han L, Zhu L, Yu Y. Free fatty acids, not triglycerides, are associated with non-alcoholic liver injury progression in high fat diet induced obese rats. *Lipids Health Dis*. 2016;15:27-. doi: 10.1186/s12944-016-0194-7. PubMed PMID: 26868515.
255. Kessler SM, Laggai S, Van Wonterg E, Gemperlein K, Müller R, Haybaeck J, et al. Transient Hepatic Overexpression of Insulin-Like Growth Factor 2 Induces Free Cholesterol and

Lipid Droplet Formation. *Front Physiol.* 2016;7:147-. doi: 10.3389/fphys.2016.00147. PubMed PMID: 27199763.

256. Faienza MF, Santoro N, Lauciello R, Calabro R, Giordani L, Di Salvo G, et al. IGF2 gene variants and risk of hypertension in obese children and adolescents. *Pediatric research.* 2010;67(4):340-4. Epub 2010/01/09. doi: 10.1203/PDR.0b013e3181d22757. PubMed PMID: 20057340.

257. Mueller KM, Themanns M, Friedbichler K, Kornfeld JW, Esterbauer H, Tuckermann JP, et al. Hepatic growth hormone and glucocorticoid receptor signaling in body growth, steatosis and metabolic liver cancer development. *Molecular and cellular endocrinology.* 2012;361(1-2):1-11. Epub 2012/05/09. doi: 10.1016/j.mce.2012.03.026. PubMed PMID: 22564914; PubMed Central PMCID: PMCPMC3419266.

258. Granzow M, Schierwagen R, Klein S, Kowallick B, Huss S, Linhart M, et al. Angiotensin-II type 1 receptor-mediated Janus kinase 2 activation induces liver fibrosis. *Hepatology (Baltimore, Md).* 2014;60(1):334-48. Epub 2014/03/13. doi: 10.1002/hep.27117. PubMed PMID: 24619965; PubMed Central PMCID: PMCPMC5512562.

259. Neubauer H, Cumano A, Muller M, Wu H, Huffstadt U, Pfeffer K. Jak2 deficiency defines an essential developmental checkpoint in definitive hematopoiesis. *Cell.* 1998;93(3):397-409. Epub 1998/05/20. doi: 10.1016/s0092-8674(00)81168-x. PubMed PMID: 9590174.

260. Sos BC, Harris C, Nordstrom SM, Tran JL, Balázs M, Caplazi P, et al. Abrogation of growth hormone secretion rescues fatty liver in mice with hepatocyte-specific deletion of JAK2. *The Journal of clinical investigation.* 2011;121(4):1412-23. doi: 10.1172/JCI42894. PubMed PMID: 21364286.

261. Han J, Wang Y. mTORC1 signaling in hepatic lipid metabolism. *Protein Cell.* 2018;9(2):145-51. Epub 04/22. doi: 10.1007/s13238-017-0409-3. PubMed PMID: 28434145.

262. Le Bacquer O, Petroulakis E, Pagliarunga S, Poulin F, Richard D, Cianflone K, et al. Elevated sensitivity to diet-induced obesity and insulin resistance in mice lacking 4E-BP1 and 4E-BP2. *The Journal of clinical investigation.* 2007;117(2):387-96. Epub 2007/02/03. doi: 10.1172/jci29528. PubMed PMID: 17273556; PubMed Central PMCID: PMCPMC1783830.

263. Casellas A, Mallol C, Salavert A, Jimenez V, Garcia M, Agudo J, et al. Insulin-like Growth Factor 2 Overexpression Induces  $\beta$ -Cell Dysfunction and Increases Beta-cell Susceptibility to Damage. *The Journal of biological chemistry.* 2015;290(27):16772-85. Epub 05/13. doi: 10.1074/jbc.M115.642041. PubMed PMID: 25971976.

264. Devedjian JC, George M, Casellas A, Pujol A, Visa J, Pelegrin M, et al. Transgenic mice overexpressing insulin-like growth factor-II in beta cells develop type 2 diabetes. *The Journal of clinical investigation.* 2000;105(6):731-40. Epub 2000/03/23. doi: 10.1172/jci5656. PubMed PMID: 10727441; PubMed Central PMCID: PMCPMC377454.

265. Bost F, Aouadi M, Caron L, Binetruy B. The role of MAPKs in adipocyte differentiation and obesity. *Biochimie.* 2005;87(1):51-6. Epub 2005/03/01. doi: 10.1016/j.biochi.2004.10.018. PubMed PMID: 15733737.

266. Khan AS, Subramaniam S, Dramane G, Khelifi D, Khan NA. ERK1 and ERK2 activation modulates diet-induced obesity in mice. *Biochimie.* 2017;137:78-87. Epub 2017/03/18. doi: 10.1016/j.biochi.2017.03.004. PubMed PMID: 28302472.

267. Dai C, Li Y, Yang J, Liu Y. Hepatocyte growth factor preserves beta cell mass and mitigates hyperglycemia in streptozotocin-induced diabetic mice. *The Journal of biological chemistry.* 2003;278(29):27080-7. Epub 2003/05/15. doi: 10.1074/jbc.M211947200. PubMed PMID: 12746445.

268. Jensen KJ, Alpini G, Glaser S. Hepatic nervous system and neurobiology of the liver. *Comprehensive Physiology*. 2013;3(2):655-65. Epub 2013/05/31. doi: 10.1002/cphy.c120018. PubMed PMID: 23720325; PubMed Central PMCID: PMC3733049.
269. Zhu C, Song K, Shen Z, Quan Y, Tan B, Luo W, et al. Roseburia intestinalis inhibits interleukin-17 excretion and promotes regulatory T cells differentiation in colitis. *Molecular medicine reports*. 2018;17(6):7567-74. Epub 03/29. doi: 10.3892/mmr.2018.8833. PubMed PMID: 29620246.
270. Fox JG, Dewhirst FE, Tully JG, Paster BJ, Yan L, Taylor NS, et al. *Helicobacter hepaticus* sp. nov., a microaerophilic bacterium isolated from livers and intestinal mucosal scrapings from mice. *Journal of clinical microbiology*. 1994;32(5):1238-45. Epub 1994/05/01. PubMed PMID: 8051250; PubMed Central PMCID: PMC3733049.
271. Yang JY, Lee YS, Kim Y, Lee SH, Ryu S, Fukuda S, et al. Gut commensal *Bacteroides acidifaciens* prevents obesity and improves insulin sensitivity in mice. *Mucosal immunology*. 2017;10(1):104-16. Epub 2016/04/28. doi: 10.1038/mi.2016.42. PubMed PMID: 27118489.
272. Kanauchi O, Fujiyama Y, Mitsuyama K, Araki Y, Ishii T, Nakamura T, et al. Increased growth of *Bifidobacterium* and *Eubacterium* by germinated barley foodstuff, accompanied by enhanced butyrate production in healthy volunteers. *International journal of molecular medicine*. 1999;3(2):175-9. Epub 1999/01/26. doi: 10.3892/ijmm.3.2.175. PubMed PMID: 9917526.
273. Bereswill S, Ekmekci I, Escher U, Fiebiger U, Stingl K, Heimesaat MM. *Lactobacillus johnsonii* ameliorates intestinal, extra-intestinal and systemic pro-inflammatory immune responses following murine *Campylobacter jejuni* infection. *Scientific reports*. 2017;7(1):2138-. doi: 10.1038/s41598-017-02436-2. PubMed PMID: 28522817.
274. Stackebrandt E, Frederiksen W, Garrity GM, Grimont PA, Kampfer P, Maiden MC, et al. Report of the ad hoc committee for the re-evaluation of the species definition in bacteriology. *International journal of systematic and evolutionary microbiology*. 2002;52(Pt 3):1043-7. Epub 2002/06/11. doi: 10.1099/00207713-52-3-1043. PubMed PMID: 12054223.
275. López-Cortés A, Fardeau M-L, Fauque G, Joulain C, Ollivier B. Reclassification of the sulfate- and nitrate-reducing bacterium *Desulfovibrio vulgaris* subsp. *oxamicus* as *Desulfovibrio oxamicus* sp. nov., comb. nov. *International journal of systematic and evolutionary microbiology*. 2006;56(7):1495-9. doi: <https://doi.org/10.1099/ijms.0.64074-0>.
276. Lu S, Seravalli J, Harrison-Findik D. Inductively coupled mass spectrometry analysis of biometals in conditional *Hamp1* and *Hamp1* and *Hamp2* transgenic mouse models. *Transgenic Res*. 2015;24(4):765-73. Epub 04/23. doi: 10.1007/s11248-015-9879-3. PubMed PMID: 25904410.
277. Pigeon C, Ilyin G, Courselaud B, Leroyer P, Turlin B, Brissot P, et al. A new mouse liver-specific gene, encoding a protein homologous to human antimicrobial peptide hepcidin, is overexpressed during iron overload. *The Journal of biological chemistry*. 2001;276(11):7811-9. Epub 2000/12/13. doi: 10.1074/jbc.M008923200. PubMed PMID: 11113132.
278. DeChiara TM, Robertson EJ, Efstratiadis A. Parental imprinting of the mouse insulin-like growth factor II gene. *Cell*. 1991;64(4):849-59. Epub 1991/02/22. doi: 10.1016/0092-8674(91)90513-x. PubMed PMID: 1997210.
279. Paulsen M, Davies KR, Bowden LM, Villar AJ, Franck O, Fuermann M, et al. Syntenic organization of the mouse distal chromosome 7 imprinting cluster and the Beckwith-Wiedemann syndrome region in chromosome 11p15.5. *Human molecular genetics*. 1998;7(7):1149-59. Epub 1998/06/09. doi: 10.1093/hmg/7.7.1149. PubMed PMID: 9618174.

280. Reik W, Constancia M, Dean W, Davies K, Bowden L, Murrell A, et al. Igf2 imprinting in development and disease. *The International journal of developmental biology*. 2000;44(1):145-50. Epub 2000/04/13. PubMed PMID: 10761859.
281. Okamoto T, Seo H, Mano H, Furuhashi M, Goto S, Tomoda Y, et al. Expression of human placenta alkaline phosphatase in placenta during pregnancy. *Placenta*. 1990;11(4):319-27. Epub 1990/07/01. PubMed PMID: 2235914.
282. Boronkai A, Than NG, Magenheimer R, Bellyei S, Szigeti A, Deres P, et al. Extremely high maternal alkaline phosphatase serum concentration with syncytiotrophoblastic origin. *Journal of clinical pathology*. 2005;58(1):72-6. doi: 10.1136/jcp.2003.015362. PubMed PMID: 15623487.
283. Meyer RE, Thompson SJ, Addy CL, Garrison CZ, Best RG. Maternal serum placental alkaline phosphatase level and risk for preterm delivery. *American journal of obstetrics and gynecology*. 1995;173(1):181-6. Epub 1995/07/01. doi: 10.1016/0002-9378(95)90187-6. PubMed PMID: 7631677.
284. Ferianec V, Linhartova L. Extreme elevation of placental alkaline phosphatase as a marker of preterm delivery, placental insufficiency and low birth weight. *Neuro endocrinology letters*. 2011;32(2):154-7. Epub 2011/05/10. PubMed PMID: 21552196.
285. Yamaguchi M, Ogren L, Endo H, Thordarson G, Bigsby RM, Talamantes F. Production of mouse placental lactogen-I and placental lactogen-II by the same giant cell. *Endocrinology*. 1992;131(4):1595-602. Epub 1992/10/01. doi: 10.1210/endo.131.4.1396305. PubMed PMID: 1396305.
286. Faria TN, Deb S, Kwok SC, Talamantes F, Soares MJ. Ontogeny of placental lactogen-I and placental lactogen-II expression in the developing rat placenta. *Developmental biology*. 1990;141(2):279-91. Epub 1990/10/01. doi: 10.1016/0012-1606(90)90384-u. PubMed PMID: 2210037.
287. Ogren L, Southard JN, Colosi P, Linzer DI, Talamantes F. Mouse placental lactogen-I: RIA and gestational profile in maternal serum. *Endocrinology*. 1989;125(5):2253-7. Epub 1989/11/01. doi: 10.1210/endo-125-5-2253. PubMed PMID: 2791990.
288. Daoud G, Amyot M, Rassart E, Masse A, Simoneau L, Lafond J. ERK1/2 and p38 regulate trophoblasts differentiation in human term placenta. *The Journal of physiology*. 2005;566(Pt 2):409-23. Epub 05/12. doi: 10.1113/jphysiol.2005.089326. PubMed PMID: 15890698.
289. Passamonti F, Randi ML, Rumi E, Pungolino E, Elena C, Pietra D, et al. Increased risk of pregnancy complications in patients with essential thrombocythemia carrying the JAK2 (617V>F) mutation. *Blood*. 2007;110(2):485-9. Epub 2007/04/12. doi: 10.1182/blood-2007-01-071068. PubMed PMID: 17426257.
290. Eggenschwiler J, Ludwig T, Fisher P, Leighton PA, Tilghman SM, Efstratiadis A. Mouse mutant embryos overexpressing IGF-II exhibit phenotypic features of the Beckwith-Wiedemann and Simpson-Golabi-Behmel syndromes. *Genes & development*. 1997;11(23):3128-42. Epub 1998/02/12. doi: 10.1101/gad.11.23.3128. PubMed PMID: 9389646; PubMed Central PMCID: PMC316748.
291. White V, Jawerbaum A, Mazzucco MB, Gauster M, Desoye G, Hiden U. IGF2 stimulates fetal growth in a sex- and organ-dependent manner. *Pediatric research*. 2018;83(1-1):183-9. Epub 2017/09/15. doi: 10.1038/pr.2017.221. PubMed PMID: 28910276.